Trafficking of N-type voltage-gated Ca^{2+} channels and their regulation by alternative splicing

Natsuko Macabuag

Doctor of Philosophy

UCL

2015

Department of Neuroscience, Physiology and Pharmacology

Division of Biosciences

Andrew Huxley Building

University College London

Gower Street

London WC1E 6BT

I, Natsuko Macabuag confirm that the work presented in this thesis is my own. Where information is derived from other sources, I confirm that this has been indicated in this thesis.

Natsuko Macabuag

Abstract

N-type voltage-gated calcium (Ca$_V$2.2) channels are expressed predominantly in the central and peripheral nervous systems and play a crucial role in neurotransmitter release. Expression of these channels at the plasma membrane and in the membrane of presynaptic terminals is key for their function, however, how they are trafficked from the subcellular organelles is still poorly understood. In this study, trafficking of mutually-exclusive alternative splice variants of Ca$_V$2.2, containing either exon 37a or 37b at the proximal C-terminus and its mechanisms were examined. Ca$_V$2.2 with exon 37a (selectively expressed in nociceptors) reveals a significantly greater intracellular trafficking to the axons and plasma membrane of DRG neurons than Ca$_V$2.2 with exon 37b. Further examination of the amino acid sequence in exon 37 uncovers that the canonical binding motifs for adaptor protein 1 (AP-1), YxxΦ and [DE]xxxL[LI], present only in exon 37a are accountable for mediating the enhanced channel trafficking from the trans-Golgi network to the plasma membrane. Finally, the dopamine-2 receptor (D2R) and its agonist-induced activation, reveal differential effects on trafficking of these Ca$_V$2.2 isoforms. D2R slowed the endocytosis of Ca$_V$2.2 containing exon 37b but not exon 37a, and activation by the D2R-selective agonist quinpirole reversed the effect of the D2R. Disrupting the interaction between adaptor proteins and YxxΦ or [DE]xxxL[LI] in Ca$_V$2.2 perturbed these effects, suggesting that the interaction of adaptor proteins with Ca$_V$2.2 channels may also be key underlying mechanisms for differential trafficking of Ca$_V$2.2 splice variants, mediated by D2R. This study thus reveals key mechanisms involved in the trafficking of N-type calcium channels.

Acknowledgement

First and foremost, I would like to thank my supervisor Professor Annette Dolphin who has been very supportive throughout my PhD, and given me scientific advice and guidance by providing me tremendous insight and knowledge into the subject. I would also like to thank all the present and past Dolphin lab members for giving me practical and technical advice whenever I needed it. All the scientific and non-scientific discussions we shared in the lab and during lunchtimes will always be fond memories of my PhD that will stay with me. Last but not least, I would like to thank my family for supporting me throughout the PhD, especially my loving husband Josh Macabuag for encouraging me to study for my PhD. Without him, I might not be writing this acknowledgement of my PhD thesis – so thank you.

Dolphin lab members (present and past)

Annette Dolphin, Laurent Ferron, Manuela Nieto-Rostro, Karen Page, Ivan Kadurin, Marianna D'Arco, Shehrazade Dahimene, Wendy Pratt, Kanchan Chaggar, Wojciech Margas, Simon Rothwell, Stuart Martin, Beatrice Lana, John Cassidy, Otto Mayer, Susy Senatore, Claudia Bauer

Natsuko Macabuag

Publication

Macabuag, N. and Dolphin, A.C. (2015). Alternative splicing in Ca$_V$2.2 regulates neuronal trafficking via adaptor protein complex-1 adaptor protein motifs. The Journal of Neuroscience. 2015 Oct 28; 35(43):14636-52. doi: 10.1523/JNEUROSCI.3034-15.2015.

Table of Contents

List of Figures

List of Tables

Abbreviations

5-HT	5-hydroxytryptamine
ADBE	Activity-dependent bulk endocytosis
AID	α interaction domain
AMPA	α-amino-3-hydroxy-5-metheyl-4-isoxazolepropionic acid
ANOVA	Analysis of variance
AP	Adaptor protein complex
AP-1	Adaptor protein 1 complex
AP-2	Adaptor protein 2 complex
Arf1	ADP ribosylation factor-1
BBS	Bungarotoxin binding site
BFA	Brefeldin A
BID	β interaction domain
BSA	Bovine Serum Albumin
BTX	α-bungarotoxin
BTX-488	α-bungarotoxin Alexa Fluor® 488 conjugate
cAMP	Cyclic AMP
CIP	Calf-intestinal alkaline phosphatase
D1R	Dopamine-1 receptor
D2R	Dopamine-2 receptor
DH	Dorsal horn
DMEM	Dulbecco's modified Eagle's medium
DMSO	Dimethyl sulfoxide
DNA	Deoxyribonucleic acid
cDNA	Complementary deoxyribonucleic acid
DRG	Dorsal root ganglion
DTT	Dithiothreitol
epsinR	Epsin-related protein

ER	Endoplasmic reticulum
EtBr	Ethidium bromide
GABA	γ-aminobutyric acid
GFP	Green fluorescent protein
GGAs	Golgi-localised γ-ear containing Arf-binding proteins
GK	Guanylate kinase
G_{max}	Conductance
GPCR	G protein-coupled receptor
GPI	Glycosylphosphatidylinositol
GTP	Guanosine triphosphate
HA	Haemagglutinin
HBSS	Hank's Balanced Salt Solution
HRP	Horseradish peroxide
IV	Current-voltage
LB	Luria-Bertani
MAP1A	Microtubule-associated protein 1A
MEDNIK	mental retardation, enteropathy, deafness, neuropathy, ichthyosis and keratodermia
mEos2	Monomeric Eos2
MIDAS	Metal ion-dependent adhesion site
mRNA	Messenger ribonucleic acid
Na_V	Voltage-gated sodium channel
NEM	N-ethylmaleimide
NGF	Nerve growth factor
NMDA	*N*-methyl-*D*-aspartate
ORL1	Opioid-receptor like receptor-1
P10	Postnatal Day 10
PCR	Polymerase-chain reaction
PFA	Paraformaldehyde
PI	Complete Protease Inhibitor Cocktail
$PtdIns4,5P_2$	Phosphatidylinositol-4,5-bisphosphate
PtdIns4P	Phosphatidylinositol 4-phosphate

PTX	Pertussis toxin
PVDF	Polyvinylidene fluoride
RNA	Ribonucleic acid
RIM	Rab3-interacting molecule
RIM-BP	RIM-Binding Protein
RT-PCR	Reverse transcriptase PCR
SCA6	Spinocerebellar ataxia 6
SDS	Sodium dodecyl sulfate
SDS-PAGE	Sodium dodecyl sulfate polyacrylamide gel electrophoresis
SEM	Standard error of mean
SH3	*Src* homology 3
siRNA	Small interfering ribonucleic acid
shRNA	Short hairpin ribonucleic acid
SNARE	Soluble N-ethylmaleimide-sensitive factor attachment receptor
SV	Synaptic vesicle
Syt	Synaptotagmin
TAE	Tris-Acetate-EDTA
TARP	Transmembrane AMPA regulatory protein
TBE	Tris-Borate-EDTA
TBS	Tris-buffered saline
TGN	Trans-Golgi network
TTX	Tetrodotoxin
$V_{50,act}$	Half maximal activation voltage
$V_{50,inact}$	Half maximal inactivation voltage
VGCC / Ca_V	Voltage-gated calcium channel
vGpH	VGlut1-pHluorin
V_{rev}	Reversal potential
VWA	Von Willebrand factor A
WT	Wild type

Chapter 1 Introduction

1.1 Background

1.1.1 Neurons

Neurons are excitable cells, and in human more than 86 billion neurons comprise the central and peripheral nervous systems (Herculano-Houzel, 2009). The neuronal plasma membrane contains transporters and channels that establish the resting potential of approximately -70 mV. Neurons differentiate to adapt highly polarised morphologies for their specialised functions: signalling and transmitting information. Typically, a neuron in the central nervous system has an axon, a cell body (soma) and dendrites (Figure 1.1). These compartments differ from each other in the composition of their proteins to mediate their designated functions. These special morphologies are established in response to the extracellular signals as well as the intracellular mechanisms (reviewed in Arimura and Kaibuchi, 2007).

1.1.2 Plasma membrane and membrane potential

In mammalian cells, the intracellular compartment is separated from the extracellular environment by the plasma membrane (Alberts et al., 2002). The plasma membrane consists of a phospholipid bilayer, which forms an impermeable barrier to ions while allowing diffusion of nonpolar molecules such as O_2, CO_2 and water. The only route for ions to cross the lipid bilayer is via transporter proteins or ion channels, which allow the controlled movement of ions across the plasma membrane, thus establishing different ionic solute compositions inside from outside the cell. The difference in electrochemical gradient across the plasma membrane creates the membrane potential. This property is crucial for the physiological function of the cells, especially for
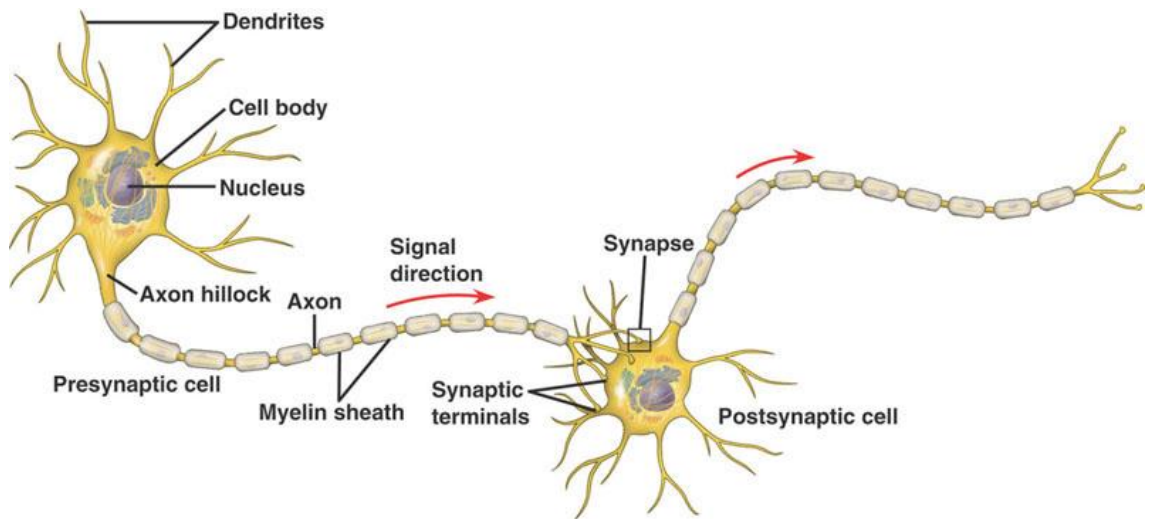
Figure 1.1 Schematic diagram of neurons.

Diagram of a presynaptic neuron shows a cell body containing a nucleus, and projections from the cell body such as dendrites and an axon which is surrounded by electrically insulating myelin sheath. At presynaptic terminals, the presynaptic neuron makes a connection with a postsynaptic neuron via synapses for signal transmission. (http://science.kennesaw.edu/)

excitable cells such as neurons for transmitting signals in the form of potential changes.

1.1.3 Ion channels

Ion channels exist as the selective pores in the plasma membrane for inorganic ions such as Na^+, K^+, Ca^{2+} and Cl^- (Hille, 2001). Ion channels are different from transporters such that their fast conductance (10^5 times faster than transporters) does not require energy input, and they mediate passive transport of specific ions down the electrochemical gradient. Ion channels interchange between open (active) and closed (inactive or desensitised) states, a process known as gating, in response to a change in their environment. There are mainly two types of ion channels: voltage-gated and ligand-gated. Voltage-gated ion channels are activated and deactivated by membrane potential changes, while ligand-gated ion channels are activated by binding of small molecules or peptides.

1.1.4 Action potential

An action potential is a large rise and fall in membrane potential from the resting membrane potential. It occurs in excitable cells such as neurons, muscle cells and endocrine cells, and is crucial for the communication between multiple cells. Action potentials in neurons were first measured by Hodgkin and Huxley in 1952. In their study, they determined the time and voltage-dependence of inward Na^+ current and outward K^+ current in the squid giant axon, and deduced that these changes in conductance cause the action potential (Hodgkin and Huxley, 1952). Indeed, later it was discovered that activation of voltage-gated sodium (Na_V) channels is fully accountable for the influx of Na^+ (Narahashi et al., 1964), as a result of small depolarization that was propagated by the neighbouring region and activates the channels when it reaches the threshold, which leads to a large depolarization (Figure 1.2). Action potentials are typically initiated by Na_V channel activation and are self-propagating. Action potentials are automatically triggered once this threshold is surpassed, thus they are said to be "all-or-none".

1.1.5 Neurotransmitter release

Neurotransmitters are endogenous chemicals that transmit signals from a neuron to another neuron or its targets such as muscle and endocrine cells. Junctions between multiple neurons are called synapses, in which an electrical signal in a neuron is converted into a chemical signal by release of neurotransmitters, which then activate the neighbouring neuron(s) by diffusing across the synapse. Neurotransmitter release from presynaptic terminals are tightly regulated by multiple events, however, the most crucial event is the Ca^{2+} influx into the synapses via calcium ion channels (Katz and Miledi, 1965). When the action potential reaches the presynaptic terminal, the depolarisation activates voltage-gated calcium ion channels (VGCCs) and Ca^{2+} in the presynaptic terminal triggers the exocytosis of vesicles containing neurotransmitter to be released into the synaptic cleft (Reynolds et al., 1986). The region of presynaptic terminals dense with vesicles and release machinery is known as the active zone (reviewed in Südhof, 2012).
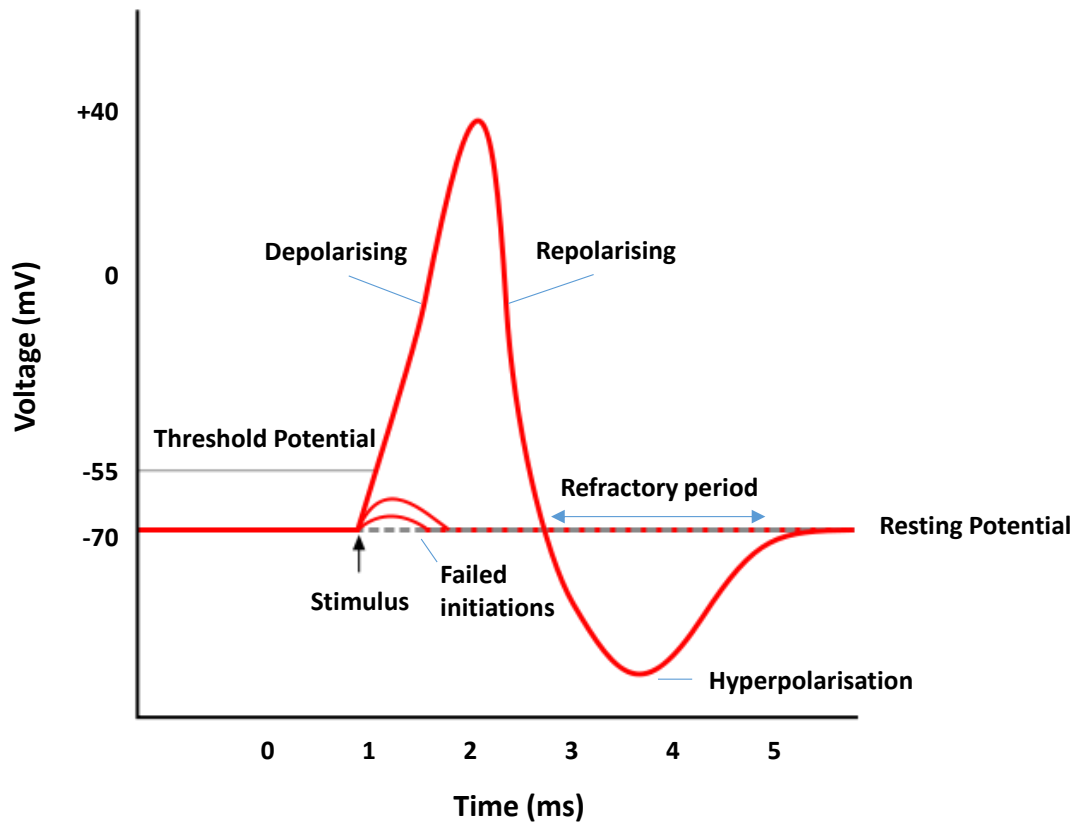
Figure 1.2 Action potential.

At resting state, the plasma membrane of neurons is at around -70 mV (known as resting potential). Electrical stimulation of a neuron raises the membrane potential, and when the stimulus is large enough for the membrane potential to rise above the threshold potential (~ -55 mV), a burst of depolarisation occurs where the membrane potential rises to ~ +40 mV by opening of Na_V channels. At this potential, potassium channels are activated and cause repolarisation of the membrane potential. After a small overshoot (hyperpolarisation), the membrane potential returns to the resting potential, ready for the next action potential.

Neurotransmitter release from the vesicles at the active zone is tightly regulated by numerous proteins which compose the presynaptic release machinery (reviewed in Südhof, 2013). First, synaptobrevin (also known as VAMP) on the synaptic vesicle forms a complex with the SNARE (soluble NSF attachment receptor) proteins, syntaxin-1 and SNAP-25 on the plasma membrane in the active zone (Söllner et al., 1993). Munc18 also interacts with syntaxin-1 to form a part of a SNARE protein complex to complete the initial stage of the vesicle priming (Hata et al., 1993; Dulubova, 1999). The zippering of the four-helical SNARE complexes forces the vesicle membrane and the plasma membrane to a close proximity for fusion (Hanson et al., 1997). Complexin then binds to the SNARE protein complex (McMahon et al., 1995), which engages the Ca^{2+}-binding transmembrane protein synaptotagmin on the synaptic vesicle (Perin et al., 1990; Brose et al., 1992) to the SNARE complex by acting as a cofactor of synaptotagmin, and completes the priming. Synaptotagmin is thought to act as a Ca^{2+} sensor in the SNARE protein complex, and its interaction with Ca^{2+} is necessary for triggering fast vesicle exocytosis (Geppert et al., 1994; Fernández-Chacón et al., 2001; Sørensen et al., 2003; Pang et al., 2006). For a fast vesicle fusion in response to the action potential, the VGCC needs to be in a close proximity to the vesicle fusion site to allow Ca^{2+} influx. Another cytosolic protein complex, which consists of Rab3-interacting molecule (RIM), RIM-Binding Protein (RIM-BP) and Munc-13, binds to Rab3 on the vesicle and mediates the docking and priming of the synaptic vesicle, and recruits VGCC to the primed vesicle in the active site (Kaeser et al., 2011). VGCCs are generally positioned within 100 nm away from the docked vesicle to ensure the fast coupling of the action potential to Ca^{2+}-triggered neurotransmitter release (Eggermann et al., 2012).

1.2 Voltage-gated calcium ion channels (VGCCs)

VGCCs are expressed in all excitable cells such as neurons, skeletal muscle cells, heart cells and endocrine cells and play an important role in the physiological function of these cells. VGCCs consist of 3 subfamilies, comprised of 10 members in total (Figure 1.3); the Ca_V1 and Ca_V2 families are

activated by high voltage, whereas the Ca_V3 family is activated by low voltage. All members contain a pore forming α_1 subunit, which allow influx of Ca^{2+} upon activation. The majority of these interact with auxiliary subunits $\alpha_2\delta$, β and γ, which modulate the activity of the α_1 subunit. Tissue distribution, specific blockers and association with auxiliary subunits of each VGCC are summarised in Table 1.1.
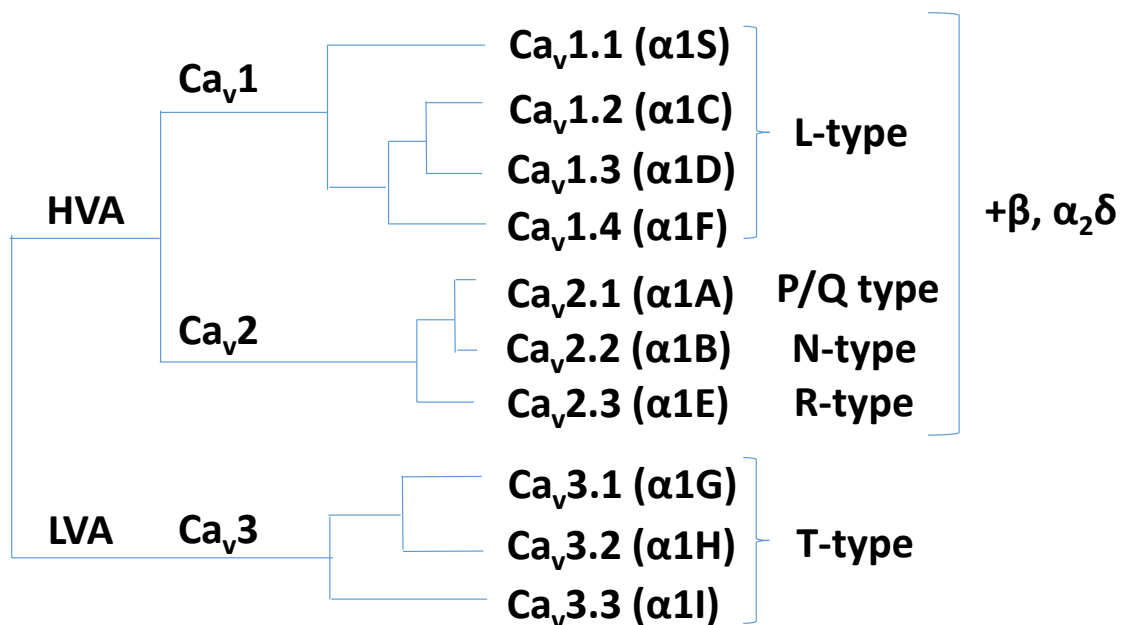
Figure 1.3 Subtypes of VGCCs.

VGCC family consists of 10 members (previous nomenclatures in brackets). Ca_V1 and Ca_V2 are high-voltage activated (HVA) channels and associated with auxiliary subunits β and $\alpha_2\delta$. Ca_V3 are low-voltage activated (LVA) and their function is not dependent on the auxiliary subunits.

Table 1.1 Characteristics of VGCCs.

Type	VGCC	Tissues	Specific blockers	Functions
L	Ca$_V$1.1	Skeletal muscle	DHPs	Excitation-contraction coupling Calcium homeostasis Gene regulation
	Ca$_V$1.2	Cardiac muscle Endocrine cells Neurons	DHPs	Excitation-contraction coupling Calcium homeostasis Gene regulation
	Ca$_V$1.3	Endocrine cells Neurons	DHPs	Hormone secretion Gene regulation
	Ca$_V$1.4	Retina	DHPs	Tonic neurotransmitter release
P/Q	Ca$_V$2.1	Nerve terminals Dendrites	ω-Agatoxin IVA	Neurotransmitter release Dendritic Ca^{2+} transients
N	Ca$_V$2.2	Nerve terminals dendrites	ω-Conotoxin GVIA	Neurotransmitter release Dendritic Ca^{2+} transients
R	Ca$_V$2.3	Cell bodies Nerve terminals dendrites	SNX-482*	Neurotransmitter release
T	Ca$_V$3.1	Cardiac muscle Skeletal muscle Neurons	TTA-A2 TTA-P2 block all Ca$_V$3	Pacemaking and repetitive firing of action potential
	Ca$_V$3.2	Cardiac muscle Neurons	None **	
	Ca$_V$3.3	Neurons	None	

*only in some cell types. ** Ni has some selectivity. Adapted from Catterall (2000).

1.2.1 Ca$_V$2.2 (N-type)

The N-type VGCC (Ca$_V$2.2) encoded by the *CACNA1b* gene is widely expressed in the central and peripheral nervous system, and plays an important role in neurotransmission. Ca$_V$2.2 was first distinguished from other calcium channels, such as L-type and T-type channels, present in isolated chick dorsal root ganglions (DRGs) by observation of its different voltage-dependence and rate of inactivation (Nowycky et al., 1985). Ca$_V$2.2 is also pharmacologically distinguishable. Ca$_V$2.2 is persistently blocked by ω-conotoxin GVIA, but is insensitive to the L-type calcium channel blockers, 1,4-dyhydropyridines (McCleskey et al., 1987). The function of Ca$_V$2.2 channels is particularly important at presynaptic terminals where they are recruited to the active zone where they are activated upon the arrival of action potentials, triggering influx of Ca^{2+} through the pore-forming α1 subunit and causing neurotransmitter release (Reynolds et al., 1986; Hirning et al., 1988; Maximov and Bezprozvanny, 2002; Han et al., 2011). The recruitment of the channels to the vicinity of the docked synaptic vesicle in the active site is mediated by the binding of RIM and RIM-BP to the C-terminus (Hibino et al., 2002; Kaeser et al., 2011). Ca$_V$2.2 is thought to be important in neurotransmission particularly in the development of neuropathic pain, as treatments with selective Ca$_V$2.2 antagonists and Ca$_V$2.2 α$_1$ subunit knockout mice show markedly reduced response to painful stimuli (Bowersox et al., 1996; Chaplan et al., 1994; Hatakeyama et al., 2001; Kim et al., 2001; Saegusa et al., 2001).

1.2.2 Structure of Ca$_V$2.2

Ca$_V$2.2 was first purified using ^{125}I ω-conotoxin GVIA from rat brain, which co-purified with auxiliary subunits β and α$_2$δ (McEnery et al., 1991), at a molecular weight of 230 kDa (α$_1$), 60-70 kDa (β) and 175 kDa (α$_2$δ). Traditionally, these auxiliary subunits are thought to play a key role in modulating the biophysical properties and trafficking of Ca$_V$2.2. Ca$_V$2.2 consists of 4 repeated domains (I-IV) (Figure 1.4). Each domain contains 6 transmembrane α helices (S1-S6) (Dubel et al., 1992). S4 is a voltage-sensing transmembrane segment. The intracellular linkers between these domains, as well as the N-terminal and C-terminal domains interact with a number of

cytosolic proteins including Ca$_V$ auxiliary β subunits, and these interactions are thought to play important role in modulating channel properties and cell surface expression (Catterall, 2000; Dolphin, 2012).
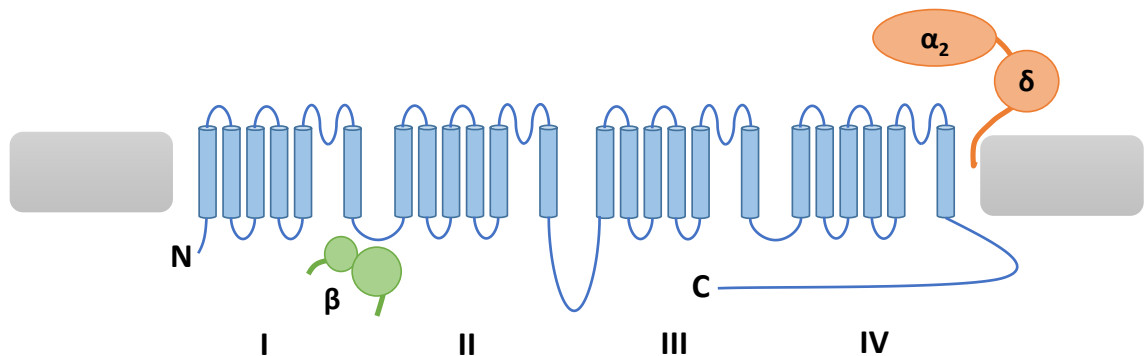
Figure 1.4 Structure of Ca$_V$2.2 and auxiliary subunits β and α$_2$δ.

The pore forming α$_1$ subunit (blue) consists of domain I-IV, each containing 6 transmembrane α helices (S1-S6). Auxiliary subunits β (green) binds to the intracellular I-II loop, while α$_2$δ (orange) is a GPI-anchored protein which associates with the extracellular region of α$_1$.

1.2.2.1 α$_2$δ subunits

There are 4 genes encoding α$_2$δ proteins, *CACNA2D1 - 4*, which encode for α$_2$δ-1, -2, -3 and -4. α$_2$δ-1, α$_2$δ-2 and α$_2$δ-3 are expressed widely in the central and peripheral nervous system. In particular, α$_2$δ-1 is found in many neuronal cell types, including DRGs (Dolphin, 2012). α$_2$δ subunits are glycosylphosphatidylinositol (GPI)-anchored extracellular proteins (Davies et al., 2010) and are thought to interact weakly with the extracellular loops of α$_1$ subunits (Gurnett et al., 1997), and increase the Ca^{2+} current density and modulate voltage dependency (Cantí et al., 2003). α$_2$δ increases Ca^{2+} current

density at least in part by increasing the trafficking of VGCCs to the cell surface (Cassidy et al., 2014). The trafficking mechanism of α2δ is still unknown, but the metal ion-dependent adhesion site (MIDAS) motif found within a Von Willebrand factor A (VWA) domain may be crucial (Cantí et al., 2005). The proteolytic cleavage and formation of the disulphide bond between α2 and δ are also important for α1 subunit functions (Figure 1.5) (Jay et al., 1991; Davies et al., 2010; Calderón-Rivera et al., 2012).   In addition, antiepileptic and neuropathic pain treatment drug gabapentin which binds to α2δ reduces the cell surface expression of Cav2.2 when applied chronically, leading to reduction in Cav2.2 current (Field et al., 2006; Hendrich et al., 2008; Cassidy et al., 2014).
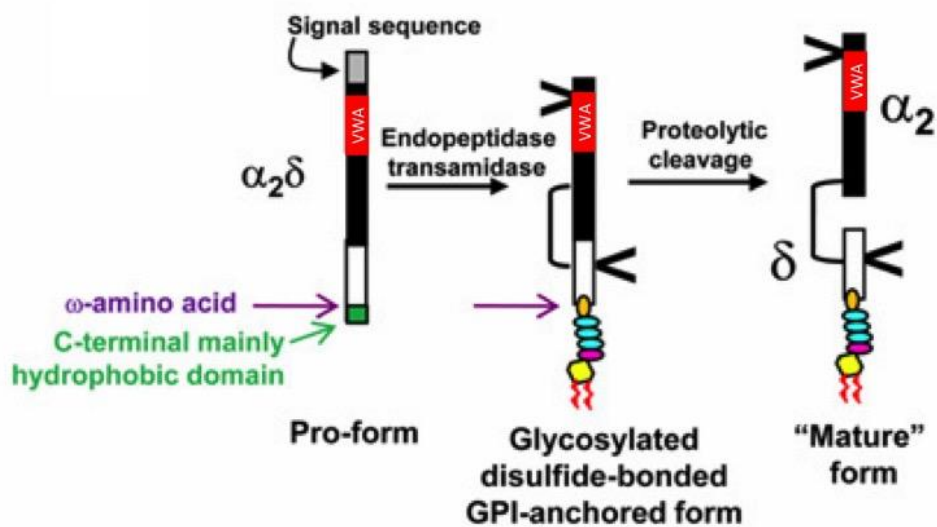
Figure 1.5 Formation of α2δ subunits.

α2δ is encoded as a single gene to be expressed as a pro-form protein. The VWA domain is indicated in red. Its C-terminus end of the protein is GPI-anchored, and glycosylation (denoted as V) takes place on both α2 and δ proteins. The GPI-anchor consists of ethanolamine (orange), three mannose rings (blue), glucosamine (pink), and inositol (yellow). Disulphide bridge is thought to form between α2 and δ before the pro-form is proteolytically cleaved by an unknown protease (Davies et al., 2010).

1.2.2.2 β subunits

There are four β subunit genes encoding β1, β2, β3, and β4. A splice variant form of β1, β1b is also identified in neuronal cells (reviewed in Buraei and Yang, 2010; Dolphin, 2003a, 2012). Crystal structures have been solved for β2, β3, and β4 by three groups, showing two highly conserved domains: a guanylate kinase (GK) domain and *src* homology 3 (SH3) domain (Chen et al., 2004; Opatowsky et al., 2004; Van Petegem et al., 2004). From these studies it was found that the α interaction domain (AID) motif in the I-II loop of $α_1$ subunit interacts with the GK domain, not the β interaction domain (BID) motif where it was originally predicted to bind (Figure 1.6). The increased Ca^{2+} current density due to co-expression of β subunits with Ca_V channels has been demonstrated in a number of electrophysiological and immunocytochemistry studies in heterologous expression systems. It was originally thought that β subunits mask an endoplasmic reticulum (ER) retention signal and increase the trafficking of the $α_1$ subunit to the cell membrane (Bichet et al., 2000; Cornet et al., 2002), however, no such motifs have been identified in the I-II loop of $α_1$ subunit. Instead, it is likely that β subunits increase the cell surface expression of the $α_1$ subunit by protecting it from proteasomal degradation (Altier et al., 2011; Waithe et al., 2011).
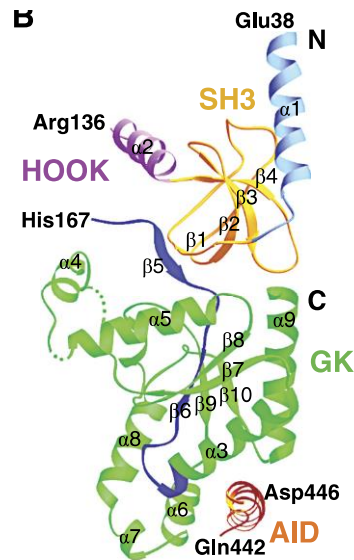
Figure 1.6 Crystal structure of a Ca$_V$ β subunit.

Cytosolic protein Ca$_V$ β consists of SH3 domain (yellow) and GK domain (green), connected by a HOOK region (purple). AID motif in the I-II loop of Ca$_V$ α subunit (red) is modelled in this structure, showing its interaction with GK domain. BID motif of β$_3$ (dark blue) modelled in the crystal structure shows a very little interaction with AID (Buraei and Yang, 2010).

1.2.2.3 γ subunits

γ subunits were originally identified by co-purification with then skeletal muscle isoform of VGCCs from dihydropyridine labelling (Takahashi et al., 1987). Association of γ subunits with VGCCs in the brain is still unclear, since the purification and immunoprecipitation of N-type and P/Q-type channels from the brain membrane preparation did not reveal γ subunits, despite the fact that several forms of γ subunit-like proteins, including stargazin are expressed in the brain (Catterall, 2011). These γ subunit-like proteins are also known as transmembrane α-amino-3-hydroxy-5-metheyl-4-isoxazolepropionic acid (AMPA) regulatory proteins (TARPs), which interact with AMPA receptors and stabilise their lateral diffusion at the post-synaptic cell surface (Bats et al., 2007).

1.2.3 G-protein-mediated regulation of VGCCs

Activities of VGCCs are regulated by the action of G protein-coupled receptors (GPCRs) that are activated by extracellular signals such as neurotransmitters and hormones that act as agonists (for reviews see Dolphin, 2003b; Tedford and Zamponi, 2006). GPCR activation causes activation of heterotrimeric G protein ($G\alpha\beta\gamma$), which dissociates into $G\alpha$ and $G\beta\gamma$ that act as signalling molecules, and can either enhance or inhibit the activity of VGCCs. G-protein mediated inhibition of VGCCs was first described in chick DRG neurons, in which the action potential was reduced in response to the γ-aminobutyric acid (GABA), 5-hydroxytryptamine (5-HT) and noradrenaline. It was revealed that inhibition of VGCCs leads to the reduction in the action potential (Dunlap and Fischbach, 1981).

The subtypes of GPCRs that are involved in inhibition of VGCCs are typically the G_i/G_o subtypes that couple to and activate pertussis toxin-sensitive G_i/G_o G proteins. Examples of these receptors are α_2 adrenergic, $GABA_B$, δ and μ-opioid, adenosine A1 receptors (Dolphin and Scott, 1987; Scott and Dolphin, 1987). The tonic inhibition by the activation of these GPCRs can be removed by a depolarising prepulse immediately prior to the channel activation pulse (Ikeda, 1991).

$G\beta\gamma$ directly modulates the biophysical properties of VGCCs, predominantly N- and P/Q-type VGCCs, whereas the $G\alpha$ species do not. This mode of direct G-protein modulation was first reported from transfection of neurons or cell lines with $G\beta\gamma$, which led to inhibition of the calcium current that could be transiently reversed by a depolarising pulse, similarly to the activation of GPCRs by neurotransmitters, whereas transfection with different $G\alpha$ species had no effect (Herlitze et al., 1996; Ikeda, 1996). The exact mechanism of how $G\beta\gamma$ modulates $Ca_V2.1$ and $Ca_V2.2$ channels is still unclear, however, binding of $G\beta\gamma$ to the N-terminus, I-II loops and C-terminus of $Ca_V2.2$ is considered to play a crucial role (De Waard et al., 1994; Zamponi et al., 1997; Page et al., 1998; Cantí et al., 1999; Li et al., 2004). G-protein mediated inhibition of $Ca_V2.2$ is due to the slowed rate of activation and the shift of activation voltage to a more depolarised potential. In addition, the gating of $Ca_V2.2$ is accelerated by

prolonged depolarisation to a more positive potential, which indicates that the movement of S4 voltage-sensor is impaired (Jones et al., 1997).

Different Gα subunits can also modulate VGCCs indirectly via activation of intracellular signalling cascades. Activated Gαs activates adenylyl cyclase which increases cyclic AMP (cAMP) level, and activates cyclic AMP-dependent protein kinase, protein kinase A, whereas protein kinase C is mainly activated indirectly by Gq-coupled receptors. Phosphorylation by these kinases enhances activity of VGCCs, particularly for L-type VGCCs (for review see Catterall, 2000).

1.3 Alternative splicing

During pre-mRNA splicing, introns are removed and appropriate exons are joined by spliceosomes. Alternative splicing occurs in > 80 % of genes, and enables formation of multiple isoform proteins from a single gene, thereby generating complex proteomes (Matlin et al., 2005). Different splice sites can be joined together (Figure 1.7). This process is regulated by *cis* (sequences in pre-mRNA) and *trans* (protein or RNA) components of splicing.

1.3.1 Alternative splicing in VGCCs

There are a number of studies on various alternative splicing in VGCCs, reporting its effects on biophysical properties, tissue distributions, and expression at different developmental stages. The VGCC splice variants discussed here are summarised in Table 1.2.

1.3.1.1 P/Q-type

A number of alternative splicing variants of $Ca_V2.1$ are reported to occur in the C-terminus. Exon 37 of $Ca_V2.1$ contains exon 37a and 37b, which are alternatively spliced in a mutual exclusive manner (Krovetz et al., 2000). In rat hippocampus, $Ca_V2.1e37b$ is expressed throughout the developmental stages,
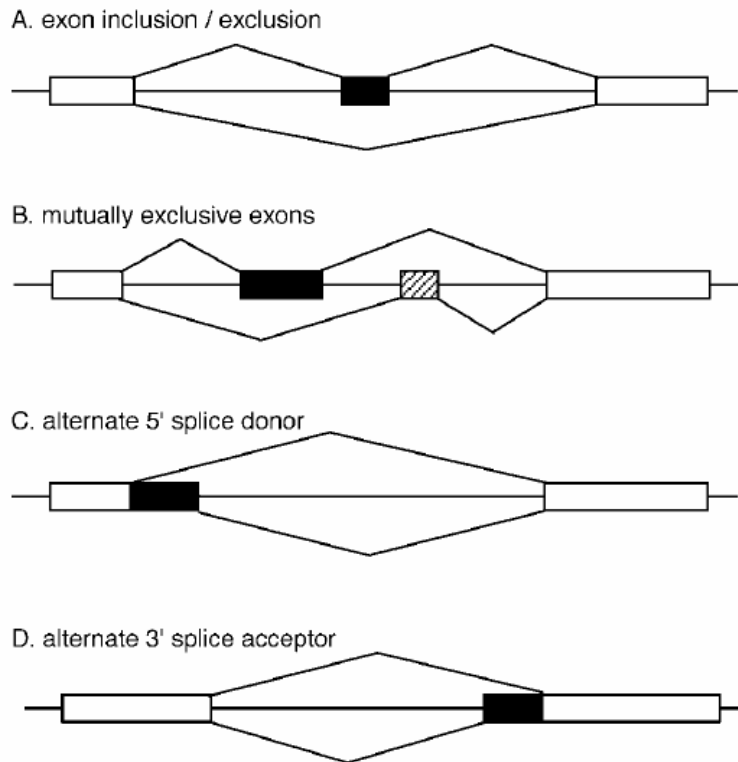
Figure 1.7 Different modes of alternative splicing.

A schematic diagram showing different modes of alternative splicing of exons. (A) Exon inclusion / exclusion, in which the alternative exon (black) is included or excluded. (B) Mutually exclusive exons (black and shaded), in which the final mRNA sequence can contain one of the exons, but not the other simultaneously. (C) The alternate 5' splice donor can include or exclude the 3' end of the sequence (black) of the first exon. (D) The alternate 3' splice acceptor can include or exclude the 5' end of the sequence (black) of the second exon. (Kaneko, 2003)

whereas $Ca_V2.1e37a$ is not expressed in embryonic rat hippocampus (Vigues et al., 2002). Exon 37 of Cav2.1 overlaps with a EF hand-like region where calmodulin binds, and the channels containing e37 give rise to a larger current that show calcium-dependent facilitation, and the PCR of the human cDNA library shows that $Ca_V2.1e37a$ is upregulated during development (Chaudhuri et al., 2004). Furthermore, immunocytochemistry with specific antibodies against e37a and 37b show enhanced localisation of $Ca_V2.1e37b$ channels in dendrites of Purkinje neurons (Chaudhuri et al., 2005). In addition, this splice isoform

Ca$_V$2.1e37b shows a ~30% increase in its expression in the cerebellum of ducky (du^{2J}/du^{2J}) mice, which contain mutations in α$_2$δ-2, compared to the wild-type without changing the total expression level of Ca$_V$2.1 (Donato et al., 2006). Another Ca$_V$2.1 splice variant which is missing exon 44 shows inactivation which is 3 times slower than Ca$_V$2.1 with exon 44 (Krovetz et al. 2000). An insertion in exon 46 in the distal C-terminus of Ca$_V$2.1 creates a stop codon, resulting in a Ca$_V$2.1 splice variant with a C-terminus that is 151-amino acids shorter (BI-1) than the longer form (BI-2). BI-2 has a more hyperpolarised activation voltage in the presence of β3 and β4, as well as a significantly larger whole-cell current with β4. On the other hand, the biophysical properties of BI-1 are not significantly affected by these β subunits (Mori et al., 1991; Sandoz et al., 2001). In patients with spinocerebellar ataxia 6 (SCA6), inclusion of exon 47 leads to expression of an expanded CAG repeat sequence, which generates Ca$_V$2.1 channels with an extended poly-glutamine repeat that correlates with the severity of SCA6 (Zhuchenko et al., 1997).

Another site of Ca$_V$2.1 splice variation occurs in S3-S4 loop in Domain IV, as an insertion of two amino acids (NP) exhibits 10 times less selective-antagonist agatoxin IVA inhibition compared to Ca$_V$2.1 without the NP insertion (Bourinet et al. 1999). There are a number of other short isoforms identified by western blot and in-situ hybridization, which could arise from an exon inclusion or exclusion during splicing events which causes a frame shift and termination of a coding sequence, but it is unclear whether these truncated channels arise as a result of alternative splicing (Sakurai et al., 1995; Scott et al., 1998), and require further confirmation by pre-mRNA analysis such as reverse transcriptase PCR (RT-PCR).

1.3.1.2 N-type

Tissue specific expression of Ca$_V$2.2 splice variants has been reported, for example the rat brain isoform contains an alternative exon 24a, which leads to an insertion of four amino acids (SMGF) in the S3-S4 loop in Domain III, whereas the sympathetic neuronal isoform contains an alternative exon 31a, which causes an insertion of two amino acids (ET) in the S3-S4 loop in Domain IV, and shifts the activation voltage to a more hyperpolarized potential and

slows the opening of the channel (Lin et al., 1997, 1999; Lipscombe et al., 2002). Alternative splicing at exon 18 of Ca$_V$2.2 leads to an insertion of 21 amino acids and causes a shift in the steady-state inactivation to a more depolarised state (Pan and Lipscombe, 2000; Lipscombe et al., 2002). Furthermore, Ca$_V$2.2 splice variants that omit exon 18 to 21 (Δ1) and exon 18 to 19 (Δ2) in the II-III loop are identified in human brain (Kaneko et al., 2002). These splice variants do not interact with syntaxin 1A, and interestingly, Δ1 shows 10-30 times less affinity towards the selective antagonist ω-conotoxin GVIA.

Exon 37 in the C-terminus of Ca$_V$2.2 is also alternatively spliced in a mutually exclusive manner, similarly to Ca$_V$2.1, which will be discussed in detail below. In addition, at the distal end of Ca$_V$2.2 C-terminus a splice variant from the rabbit brain that is 187-amino acid shorter, due to the loss of the 3' acceptor splice site at exon 46 has been reported (Williams et al., 1992). The long splice variant appears to be trafficked to the axons and presynaptic terminals of mature cultured hippocampal neurons and excluded from the somatodendritic compartments, whereas the short splice variant is expressed throughout the neurons (Maximov and Bezprozvanny, 2002).

1.3.1.3 L-type

Alternative splicing in L-type VGCCs has been extensively studied, especially in the context of diseases (for reviews, see Liao et al., 2009; Lipscombe et al., 2013). Ca$_V$1.2 in Timothy syndrome patients contains a gain-of-function mutation (often G406R) in an alternative spliced mutually exclusive exon 8a within the S6 transmembrane of Domain I, which exhibits a more severe phenotype than when the same mutation is in exon 8 (Splawski et al., 2004). Mutually-exclusive alternative splicing occurs in exon 8 of Ca$_V$1.3 as well, and a loss-of-function mutation in exon 8b is found in patients with hereditary hearing loss and bradycardia (Baig et al., 2011). Somatic gain of function mutations, including in exon 8a have been identified in adrenal zona glomerulosa cells, leading to hyperaldosteronism (Azizan et al., 2013).

Table 1.2 Summary of VGCC alternative splice variants.

VGCC	Exon	Consequences of splicing	References
$Ca_V1.2$	8	Severe phenotype with exon 8a when gain-of-function mutation (often G406R) is found in Timothy syndrome patients	Splawski et al., 2004
$Ca_V1.3$	8	Loss-of-function mutation in exon 8b in patients with hereditary hearing loss and bradycardia	Baig et al., 2011
	8	Somatic gain of function mutations in exon 8a in adrenal zona glomerulosa cells lead to hyperaldosteronism	Azizan et al., 2013
$Ca_V2.1$	37a/37b	• Channels containing exon 37 give rise to a larger current that show calcium-dependent facilitation • Exon 37b is expressed throughout the developmental stages • Exon 37a is upregulated during development to adult • Enhanced localisation of exon 37b containing channels in dendrites of Purkinje neurons • Exon 37b shows a ~30% increase in its expression in the cerebellum of ducky (du^{2J}/du^{2J}) mice	Vigues et al., 2002, Chaudhuri et al., 2004, Chaudhuri et al., 2005, Donato et al., 2006
	44	3 times slower inactivation in channels missing exon 44	Krovetz et al., 2000
	46	Insertion in exon 46 creates a stop codon, resulting in a shorter form (BI-1) and a longer form (BI-2). BI-2 has a more hyperpolarised activation voltage with β3 and β4, and a significantly larger whole-cell current with β4, compared to BI-1	Mori et al., 1991; Sandoz et al., 2001
	47	Inclusion of exon 47 leads to an expanded CAG (ploy-glutamine) repeat expression which correlates with the severity of SCA6	Zhuchenko et al., 1997
$Ca_V2.2$	18	Exon18a leads to 21-amino acids insertion, causes a shift in the steady-state inactivation to a more depolarised state	Pan and Lipscombe, 2000; Lipscombe et al., 2002

Ca$_V$2.2	24	Exon 24a leads to an insertion of four amino acids (SMGF) in the S3-S4 loop in Domain III, shifts the activation voltage to a more hyperpolarized potential and slows the opening of the channel	Lin et al., 1997, 1999; Lipscombe et al., 2002
	31	Exon 31a leads to an insertion of two amino acids (ET) in the S3-S4 loop in Domain IV, shifts the activation voltage to a more hyperpolarized potential and slows the opening of the channel	Lin et al., 1997, 1999; Lipscombe et al., 2002
	omitted exon 18-21 (Δ1),18-19 (Δ2)	Identified in human brain, do not interact with syntaxin 1A. Δ1 shows 10-30 times less affinity towards the selective antagonist ω-conotoxin GVIA	Kaneko et al., 2002
	37a/37b	• Exon 37b is expressed in all neuronal cells • Exon 37a expression is found in nociceptive DRG neurons, coexpressed with TRPV1 and Na$_V$1.8, and down-regulated in DRGs of neuropathic pain models • Exon 37a conducts larger Ca^{2+} current, opens for longer and shows greater gating charges than 37b • Exon 37a is important in thermal hyperalgesia, both isoforms contribute to mechanical allodynia • Exon 37a is voltage-independently inhibited by GABA and μ-opioid receptor activation, and important for morphine analgesia	Bell et al., 2004, Castiglioni et al., 2006, Altier et al., 2007, Raingo et al., 2007, Andrade et al., 2010, Jiang et al., 2013
	46	The loss of the 3' acceptor splice site at exon 46 leads to a short form which is187-amino acid shorter. The long form is trafficked to the axons and presynaptic terminals and excluded from the somatodendritic compartments. The short form is expressed throughout the neurons	Williams et al., 1992, Maximov and Bezprozvanny, 2002

1.3.2 Expression of Ca$_V$2.2e37a/b

Ca$_V$2.2e37a/b splice variants arise from the alternative splicing of two mutually-exclusive exons 37a (e37a) and 37b (e37b) in the *CACNA1B* gene. Both exon 37 variants code for 32 amino acids, and 14 of those are different between e37a and e37b (Figure 1.8). Ca$_V$2.2 containing e37b is expressed abundantly in the central and peripheral nerves, whereas Ca$_V$2.2 containing e37a is only detected in DRGs, and at very low levels in brain (Bell et al., 2004; Castiglioni et al., 2006). The RNA level of Ca$_V$2.2e37a determined by RNase protection assay is approximately 6 % of the total Ca$_V$2.2 RNA in DRGs, on the other hand it is less than 2 % in brain. Whether or not these RNA levels reflect the protein expression of the isoforms has not been determined, due to the lack of specific antibodies against these splice variants.

Despite the low level of Ca$_V$2.2e37a RNA, it is thought to have a significant role in modulating nociception. Bell et al. (2004) determined the level of Ca$_V$2.2 from individual DRG neurons by single-cell RT-PCR using e37a- and e37b- specific primers after testing for capsaicin responsiveness. Interestingly, Ca$_V$2.2e37a is preferentially expressed in small-diameter DRG neurons that are responsive to capsaicin. In addition, all of the DRG neurons expressing e37a also express the tetrodotoxin (TTX)-resistant sodium ion channel Na$_V$1.8 (Bell et al., 2004). Taken together, from these single cell RT-PCR experiments, approximately 75 % of DRG neurons expressing Ca$_V$2.2e37a are nociceptive small-diameter neurons (Bell et al., 2004). These small diameter neurons are likely to be unmyelinated C-fibre neurons, which project into laminae I and II of the dorsal horn of the spinal cord (Snider and McMahon, 1998; Basbaum et al., 2009). It is estimated that at least 20% of total DRG neurons express Ca$_V$2.2e37a (Castiglioni et al., 2006), whereas Ca$_V$2.2e37b was expressed ubiquitously in all types of DRG neurons.

In another study where the RNA levels of e37a and e37b were determined in rat DRGs after spinal nerve ligation as an animal model of neuropathic pain, surprisingly transcription of e37a was significantly down-regulated from 7 % to 3 % while the mRNA level of e37b remained the same (Altier et al., 2007).

In summary, these studies indicate that Ca$_V$2.2e37a is highly expressed in the small nociceptive DRGs and serves an important role in nociception, and may be down-regulated following sensory nerve injury, as a part of endogenous anti-nociceptive mechanism.

a

b


```
      *  * *  *  * *       *       * *  * * * *  * *  *  * * *
37a   C C R I H Y K D M Y S L L R C I A P P V G L G K N C P R R L A Y K
37b   C G R I S Y N D M F E M L K H M S P P L G L G K K C P A R V A Y K
      |                                                           |
      1766                                                        1798
```

Figure 1.8 Mutually exclusive alternative splicing in Ca$_V$2.2 exon 37

(**a**) Exon 37 (yellow) is located in the proximal C-terminus of Ca$_V$2.2, close to the S6 of Domain IV and the plasma membrane. (**b**) Schematic diagram of mutually-exclusive exons 37a and 37b, and their amino acid alignment. The conserved residues are highlighted.

1.3.3 Ca$_V$2.2e37a channels conduct more Ca^{2+} current than e37b

The capsaicin-responsive DRGs expressing both Ca$_V$2.2e37a and e37b have shown a significantly larger N-type Ca^{2+} current than those expressing only Ca$_V$2.2e37b (Bell et al., 2004). A number of studies have also demonstrated that the e37a isoform has greater current density than e37b when it is co-expressed with β and α$_2$δ subunits in heterologous expression systems such as tsA-201 cell line and *Xenopus* oocytes (Bell et al., 2004; Castiglioni et al., 2006; Raingo et al., 2007). The factors that contribute to an increase in current density could be a combination of more than one property of the channel. Castiglioni et al. studied this in detail, and concluded that; 1) e37a opens for longer duration due to the slower deactivation and inactivation of the channel, 2) the gating charge of e37a was greater than that of e37b when they were expressed in tsA-201 cells, and 3) The open probabilities of these isoforms are the same (Castiglioni et al., 2006). This greater gating charge suggests that functional Ca$_V$2.2 channels containing e37a may be expressed at a higher density than e37b.

1.3.4 Ca$_V$2.2e37a/b undergo different modes of inhibition upon GPCR activation

GPCRs such as GABA$_B$, μ-opioid and endocannabinoid receptors are activated by binding to the endogenous neurotransmitters and agonists for signal transduction in both central and peripheral neurons. G protein-mediated inhibition of Ca$_V$2.2 has been extensively studied, and there are mainly two types of inhibition. The first type is the voltage-dependent inhibition where Gβγ (downstream of G$_i$- and G$_o$- class of G proteins) binds directly to Ca$_V$2.2 to stabilise the closed state of the channel, which is often ineffective during intense neuronal firing as the inhibition is removed by depolarisation (Herlitze et al., 1996; Ikeda, 1996). The second type is the voltage-independent inactivation mediated by second messengers, including phosholipase C (PLC) activation, which is often downstream of G$_{q/11}$- class G-proteins, to cause slow inhibition that is not relieved by depolarisation in sympathetic neurons (Bernheim et al., 1991; Delmas et al., 2005). In DRGs, voltage-independent inhibition of Ca$_V$2.2

has been suggested to occur through phosphorylation of tyrosine residues as a result of crosstalk between G protein and tyrosine kinase pathways, although the mechanism underlying this is unknown (Wijetunge et al., 2002).

Raingo et al. (2007) revealed that $Ca_V2.2e37a$ undergoes voltage-independent inhibition as well as voltage-dependent inhibition upon G_i/G_o activation, while the majority of $Ca_V2.2e37b$ inhibition was voltage-dependent in tsA-201 cells (Raingo et al., 2007). They found that the voltage-independent inhibition of e37a does not involve $G\beta\gamma$, but requires phosphorylation of Y1747 by tyrosine kinase. This amino acid is widely conserved in different species, which indicates the evolutionary importance of its role in $Ca_V2.2$ function. This finding was further investigated in transgenic mice which were generated to express only $Ca_V2.2e37a$ by replacing exon 37b with 37a (aa*), and to express only $Ca_V2.2e37b$ by replacing exon 37a with 37b (b*b) in the *CACNA1B* gene (Andrade et al., 2010). Surprisingly, the DRG current density from the aa* mice was smaller than the b*b or wild-type (WT) mice, due to the specific down-regulation of $Ca_V2.2$ protein expression in the brain and DRGs of the aa* mice, compared to the b*b and WT mice. Nevertheless, the small diameter DRG neurons of aa* mice exhibited voltage-independent inhibition upon μ-opioid receptor activation, relative to that in b*b mice. This finding is in agreement with the initial studies in tsA-201 cells, and shows the importance of voltage-independent inhibition through $Ca_V2.2e37a$ in modulating the nociception.

1.3.5 Roles of $Ca_V2.2e37a/b$ in neuropathic pain

To address the question of whether Cav2.2e37a and e37b are equally effective in mediating transmission of nociceptive signals, Altier et al. (2007) used RNA interference approaches to knockdown these isoforms in cultured DRG neurons and in rat neuropathic pain models (Altier et al., 2007). Small interfering RNAs (siRNAs) against $Ca_V2.2e37a$ and e37b reduce the Substance P release from cultured DRG neurons, which implies that these channels are effective in modulating the nociception. Silencing $Ca_V2.2e37a$ by intrathecal injection of the siRNA in the naïve rats reduces both the basal mechanical and thermal nociception, while silencing $Ca_V2.2e37b$ does not. $Ca_V2.2e37a$ siRNA also prevents formalin-induced thermal and mechanical hyperalgesia, and

reverses the thermal hyperalgesia in the neuropathic pain model with a chronic constriction injury in the sciatic nerve. On the other hand, Ca$_v$2.2e37b siRNA appears to be only effective in reducing the nociceptive score in the mechanical hyperalgesia model.   Therefore, Ca$_v$2.2e37a is the predominant channel isoform in thermal hyperalgesia, whereas both isoforms contribute to the tactile allodynia.

Transgenic mice that express only Ca$_v$2.2e37a (aa*) or e37b (b*b) by exon substitution show no effect on the basal nociception (Andrade et al., 2010), unlike the previous report in the intrathecal Ca$_v$2.2e37a siRNA-treated rats (Altier et al., 2007).   Upon intrathecal morphine injection, the paw withdrawal latency is increased for the aa* and WT mice against thermal noxious stimuli, whereas the b*b mice show a reduced latency score, indicating that Ca$_v$2.2e37a plays a predominant role in morphine-mediated analgesic effect at spinal level (Andrade et al., 2010). Subsequently, comparing maximal possible effect of intrathecal morphine on the b*b and WT mice in thermal hyperalgesia confirmed the important role of e37a in morphine analgesia (Jiang et al., 2013). Although both e37a and e37b contributed to the development of the thermal and mechanical hypersensitivity in this study, it is clear that e37a plays a key role in the analgesic action of intrathecal morphine.

1.4 Protein sorting to and from plasma membrane

The plasma membrane is a fluid structure, and the functional integral components of the membrane such as transmembrane proteins are able to move within the membrane laterally, but also in and out of the membrane, to maintain the homeostatic regulations of the components, as well as to increase or decrease the components at the cell surface in response to cell signalling (Maxfield and McGraw, 2004). Ca$_v$2.2 is no exception and its overall cell surface level is regulated by a number of cellular events (Figure 1.9). Ca$_v$2.2 is translated in association with the ER, and is then translocated across the Golgi stack. At the trans-Golgi network (TGN), Ca$_v$2.2 is thought to be packaged into an exocytic vesicle, and inserted into the plasma membrane where it is functional.   At the cell surface, Ca$_v$2.2 channels are internalised into

endosomes, which can either be recycled back to the plasma membrane (recycling endosomes), or degraded in the lysosomes.
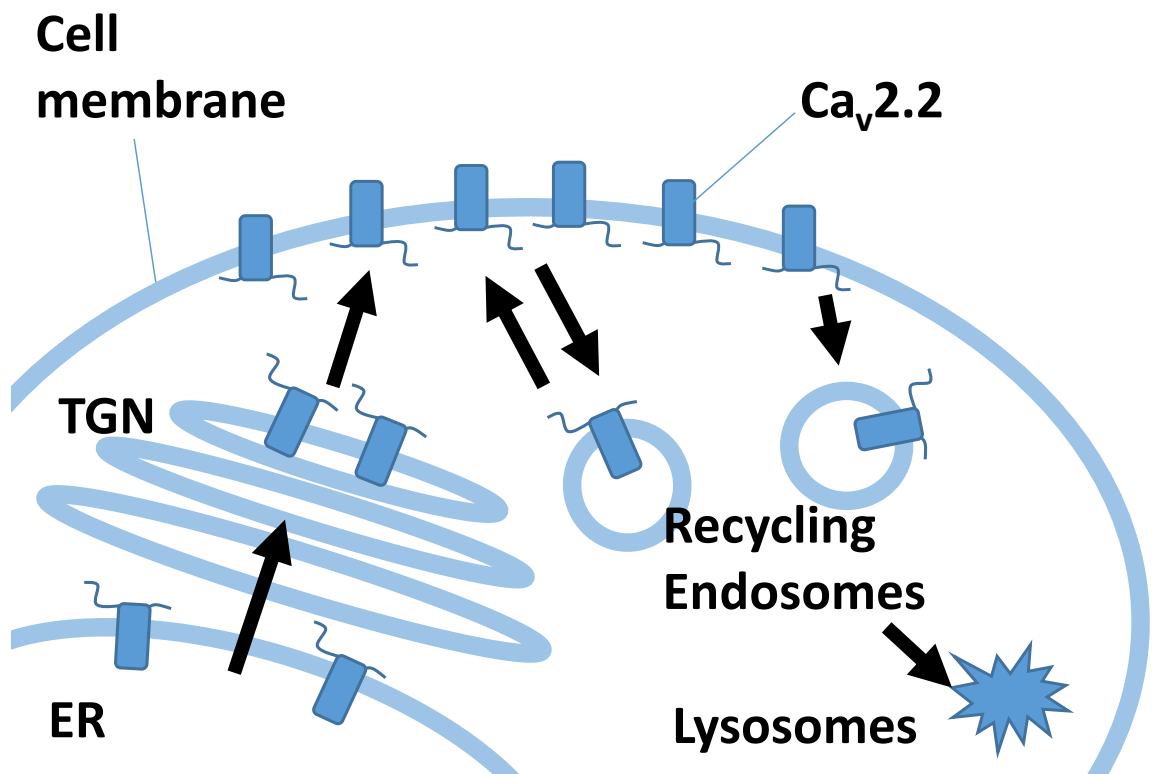
Figure 1.9 Pathways of intracellular protein sorting.

$Ca_V2.2$ is transcribed in the nucleus and translated in association with the endoplasmic reticulum (ER) and translocated across the stack of Golgi. At the trans-Golgi network (TGN) it is sorted and packaged into vesicles to be trafficked to the plasma membrane. The cell surface $Ca_V2.2$ is endocytosed into recycling endosomes and then to endosomal recycling compartment, where it is repackaged into vesicles to return to the plasma membrane, or degraded via late endosomes and lysosomes.

1.4.1 Trans-Golgi Network (TGN) to plasma membrane

Newly synthesised proteins are translocated into the TGN from ER via the Golgi stack, where they are sorted into carrier vesicles for their destinations. The majority of the cargo containing vesicles from the TGN are clathrin-coated. Coatomer Protein Complex I (COPI)-coated buds are also found on the TGN, but at a much lower frequency, as it is thought that their main function is to mediate vesicle trafficking from the ER to Golgi (reviewed in Klumperman, 2011). Cytosolic cargo adaptors play a key role in cargo sorting by directly or indirectly interacting via sorting signal in the cytosolic domains of transmembrane proteins at the TGN (reviewed in Guo et al., 2014).

1.4.1.1 Adaptor protein complexes (APs)

The AP family is the most studied cargo adaptor proteins (APs) for clathrin-mediated protein sorting (Table 1.3) (Boehm and Bonifacino, 2001; Owen et al., 2004; Robinson, 2004; Hirst et al., 2011). There are 5 members (AP-1 to 5) in this family of hetero-tetrameric proteins, and so far AP-1, AP-3 and AP-4 have been implicated in cargo sorting at TGN. Recruitment of AP-1 and AP-3 to the cargo in the membrane of the TGN is regulated by the ADP-ribosylation factor (Arf) family of small GTP proteins, in particular Arf1 and Arf3. The protein cargo binds to μ and σ subunits of APs via its signalling motifs, $Yxx\Phi$ and $[DE]xxxL[LI]$ respectively, with a exception of AP-5 for which the mechanism of cargo interaction is still unknown (Bonifacino and Traub, 2003). AP-1, 2 and 3 mediates interaction with clathrin via the ear-domain of the β subunits.

Table 1.3 Adaptor binding protein family.

	Subunits	Cargo motif	Clathrin dependent	Location
AP-1	μ1, σ1, β1, γ	YxxΦ [DE]xxxL[LI]	Yes	Trans-Golgi network Endosomes
AP-2	μ2, σ2, β2, α	YxxΦ [DE]xxxL[LI] NPXY	Yes	Plasma membrane
AP-3	μ3, σ3, β3, δ	YxxΦ [DE]xxxL[LI]	Yes	Endosomes Trans-Golgi network Lysosomes
AP-4	μ4, σ4, β4, ε	YxxΦ	No	Trans-Golgi network
AP-5	μ5, σ5, β5, ζ	Unknown	No	Late endosomes Lysosomes
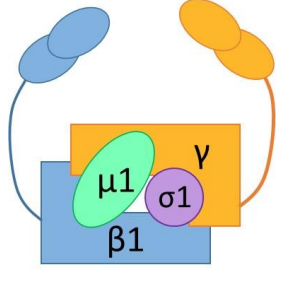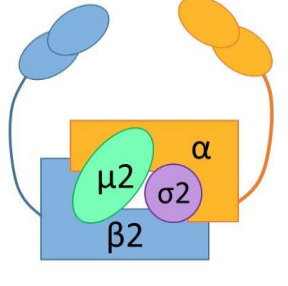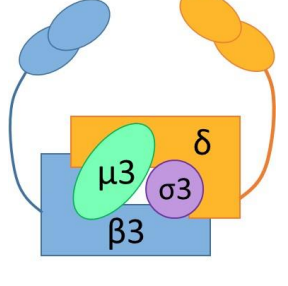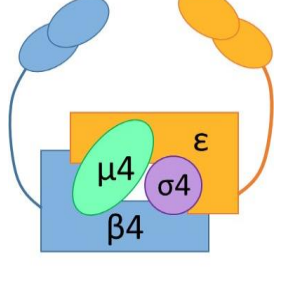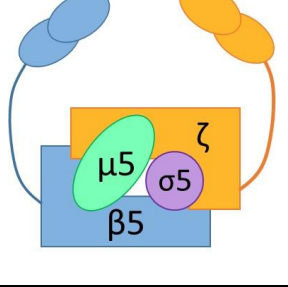
1.4.1.2 Golgi-localised γ-ear containing Arf-binding proteins (GGAs)

GGAs are another class of clathrin adaptors, which interact with a cargo through the DxxLL motif and mediate trafficking between TGN and endosomes (Guo et al., 2014). GGAs are thought to be targeted to the membrane of the TGN via ADP ribosylation factor-1 (Arf1) and phosphatidylinositol 4-phosphate (PtdIns4P). Some reports suggest that GGAs and AP-1 are involved in a cooperative protein sorting at TGN, while other evidence indicates that these proteins can function independently of each other (Hirst et al., 2009, 2012).

1.4.1.3 Epsin-related proteins (epsinR)

EpsinR is a class of monomeric clathrin adaptors that regulates cargo trafficking between TGN and endosomes (Guo et al., 2014). EpsinR contains binding sites for AP-1 and GGAs, which indicates that these protein may either function together or regulate each other in mediating trafficking between TGN and endosomes (Owen et al., 2004).

1.4.1.4 Exomer

Exomer is a heteromeric cargo adaptor protein that mediates trafficking directly from TGN and the cell surface (Guo et al., 2014). Exomer binds directly to a novel sorting signal (IXTPK) on a cargo, a fusion protein Fus1p, and mediate its trafficking from the TGN to the plasma membrane (Barfield et al., 2009). The cell surface membrane recruitment of exomer is mediated by Arf1-GTP, but requires other proteins to deform lipid membranes for vesicle budding (Wang et al., 2006).

1.4.2 Plasma membrane to endosomes

1.4.2.1 Clathrin-dependent pathways

Clathrin in the cytoplasm is recruited to the plasma membrane to mediate endocytosis in the classical clathrin-dependent pathway (Kirchhausen, 2000). The soluble clathrin molecule in a shape of a three-legged triskelion forms a lattice at the plasma membrane which invaginates and pinches off to

form a coated vesicle. The adaptor protein 2 complex (AP-2) binds both to the cargo protein and clathrin to mediate this process (Kirchhausen, 1999). Binding of AP-2 to the cargo in the plasma membrane is regulated by phosphatidylinositol-4,5-bisphosphate (PtdIns4,5P$_2$) in the membrane and AP-binding motifs in the cytosolic domain of the cargo protein. The proportion of total endocytosis mediated by the clathrin-dependent pathway is unknown; however, some studies report as much as 95 % of endocytosis is mediated by clathrin-dependent pathway in certain cell types such as a HeLa cell line (Bitsikas et al., 2014).

1.4.2.2 Clathrin-independent pathways

Clathrin-independent endocytosis is sensitive to cholesterol-depletion, and may be further subdivided into dynamin-GTPase-dependent and dynamin-GTPase-independent for pinching off vesicles (Figure 1.10) (for reviews, see Le Roy and Wrana, 2005; Mayor and Pagano, 2007). Caveolae are small (50-100 nm diameter) invaginations, and their scission at the plasma membrane is mediated by dynamin-GTPase. Cargo selection for clathrin-independent endocytosis is not as well-defined as the clathrin-dependent pathway; however, mechanisms such as ubiquitination and interaction with integral transmembrane proteins flotillin-1 and flotillin-2 are implicated in clathrin-independent pathways (Glebov et al., 2006).
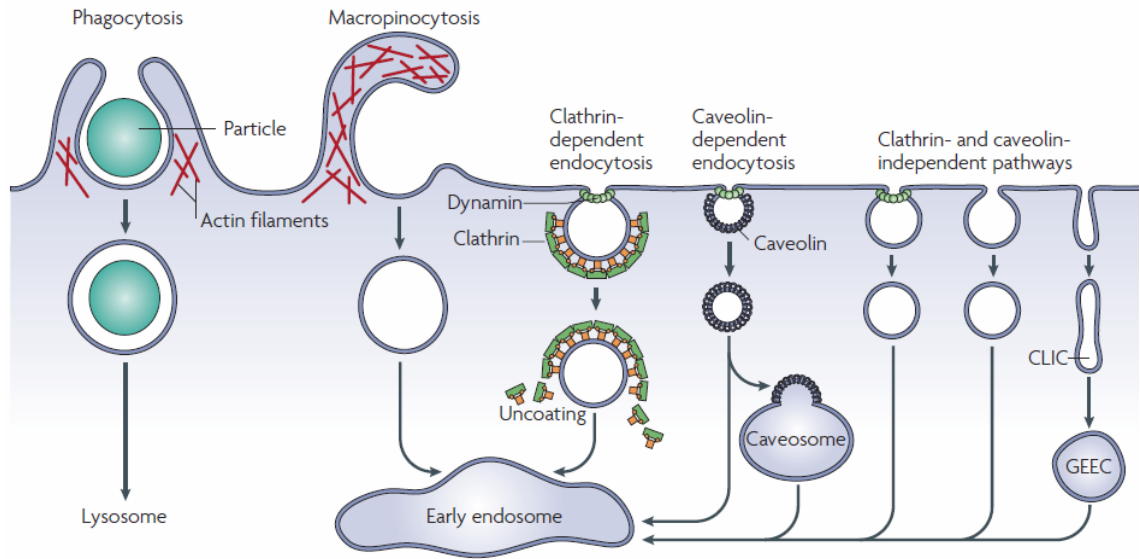
Figure 1.10 Different modes of endocytosis.

Small scale (50-100nm) endocytosis events are divided into clathrin-dependent endocytosis, caveolin-dependent endocytosis, and clathrin- and caveolin-independent pathways (Mayor and Pagano, 2007). CLIC, clathrin- and dynamin-independent carrier. GEEC, glycosyl phosphatidylinositol-anchored protein enriched early endosomal compartment.

1.4.2.3 Activity-dependent bulk endocytosis (ADBE)

Endocytosis of synaptic vesicles after exocytosis is essential for neuronal activity. Activity-dependent bulk endocytosis (ADBE) is an effective way to retrieve a large area of plasma membrane by forming a large invagination into an endosome-like structure known as a bulk endosome, from which synaptic vesicles bud off to join the recycling synaptic vesicle pool (Richards et al., 2000). This budding of synaptic vesicles from the bulk endosome is clathrin-dependent, which is mediated by AP-1 and AP-3 (Cheung and Cousin, 2012).

1.4.2.4 Ultrafast Endocytosis

Watanabe et al. (2013) demonstrated another mode of synaptic vesicle membrane recycling called ultrafast endocytosis (Watanabe et al., 2013), occurring between 50-100 ms after the neuronal terminal stimulation, which is much faster than previous models of synaptic vesicle recycling, kiss-and-run (Fesce et al., 1994) and clathrin-mediated endocytosis (Miller and Heuser, 1984). This fast endocytosis in active nerve terminals occurs independently of clathrin and generates recycling endosomes, followed by a clathrin-dependent process in which the new synaptic vesicles bud off from the endosomes (Watanabe et al., 2014). The ultrafast endocytosis was observed at 34 °C, which is close to the physiological temperature, whereas it collapsed when the experiment was conducted at room temperature (22 °C), at which many experiments demonstrating the clathrin-mediated endocytosis in synaptic vesicle recycling commonly take place. This type of endocytosis may provide a fast clearance of the fusion site, and allows for other vesicles to fuse in rapid succession (Watanabe, 2015).

1.4.3 Recycling endosome pathways

After endocytosis, most of the proteins and lipids return to the plasma membrane with a relatively fast rate ($\tau_{1/2}$~2 min) (Maxfield and McGraw, 2004). The endocytosed vesicles are pooled into the endocytic recycling compartment, where proteins are repackaged into vesicles (clathrin-dependent and clathrin-independent) and return to the plasma membrane. This is regulated by sorting motifs on the cargo proteins and regulatory molecules such as Rab proteins, particularly Rab 4, 5 and 11, which are a family of more than 60 small GTPase regulatory proteins, and play important roles in vesicle sorting (Stenmark, 2009).

1.5 VGCC trafficking mechanisms and regulations

1.5.1 Auxiliary subunits

The role of α2δ and β auxiliary subunits in trafficking of VGCCs is well-established. β subunits are likely to promote the channel cell surface expression by preventing the interaction between E3 ubiquitin ligase and the I-II loop of the channels that leads to proteasomal degradation, which has been demonstrated for $Ca_V1.2$ (Altier et al., 2011) and $Ca_V2.2$ (Waithe et al., 2011). On the other hand, although the vital role of $α_2δ$ in $Ca_V2.2$ trafficking is shown in both expression system and *in vivo* models (Bauer et al., 2009; Tran-Van-Minh and Dolphin, 2010; Cassidy et al., 2014), the precise mechanism(s) of how $α_2δ$ mediates $Ca_V2.2$ trafficking is poorly understood. Gabapentinoids such as gabapentin and pregabalin bind to α2δ and reduce trafficking of $Ca_V2.2$ to the cell surface and leads to a reduction in Ca^{2+} influx through $Ca_V2.2$ upon chronic application (Hendrich et al., 2008; Cassidy et al., 2014). Furthermore, gabapentin has been shown to reduce the Rab11-dependent recycling of $Ca_V2.2$ (Tran-Van-Minh and Dolphin, 2010).

1.5.2 Cytosolic proteins

VGCCs interact with numerous cytosolic proteins that regulate intracellular localisation of the channels. $Ca_V2.2$ requires protein kinase C activation for interaction with actin and membrane insertion of the channels (Zhang et al., 2008). Collapsin response mediator protein, CRMP-2 binds to dynein to link transport vesicles to microtubules and is important for long distance axonal transport (Arimura et al., 2009; Rahajeng et al., 2010). CRMP-2 co-localises with $Ca_V2.2$ in the growth cones of immature sensory neurons and in presynaptic terminals of hippocampal neurons, by directly binding to the I-II loop and distal C-terminus of $Ca_V2.2$, and thus enhances Ca^{2+} current (Brittain et al., 2009; Chi et al., 2009). However, whether CRMP-2 increases $Ca_V2.2$ trafficking to the cell surface or retains $Ca_V2.2$ at the cell surface is not clear. The light chain (LC2) of microtubule-associated protein (MAP1A) interacts with the distal C-terminus of $Ca_V2.2$ and enhances retention of the channel at the presynaptic terminal membrane (Leenders et al., 2008). On the other hand, $Ca_V2.2$/LC1-MAP1B complex is bound by ubiquitin conjugase

UBE2L3, which may regulate proteasomal degradation of Ca$_V$2.2 and reduces the cell surface expression of the channels (Gandini et al., 2014). Moreover, α-actinin directly binds to the C-terminus to increase surface expression of L-type (Ca$_V$1.2) channels by stabilising the channels at the cell surface, but its function in other type of VGCCs have not been explored. The regulation of Ca$_V$1.2 trafficking via α-actinin is channel activity-based, since it requires calmodulin to bind to Ca^{2+} and the activated calmodulin competes with α-actinin for its shared binding site, which leads to Ca$_V$1.2 internalisation (Hall et al., 2013). At presynaptic terminals, Ca$_V$2.2 channels are recruited to the active zone, and allow neurotransmitter release upon activation. Presynaptic protein interactions at the C-terminus of the channels are also important for their recruitment to the presynaptic terminals. RIM and RIM-BP have been shown to directly interact with Ca$_V$1.3 and Ca$_V$2 channels at the distal C-terminus (Hibino et al., 2002; Kaeser et al., 2011).

1.5.3 GPCRs

Another way in which GPCRs can modulate the function of VGCCs is through regulation of channel trafficking. GPCRs such as dopamine-1 (D1R) and -2 (D2R) receptor interact directly with Ca$_V$2.2 and increase the channel cell surface expression (Kisilevsky and Zamponi, 2008; Kisilevsky et al., 2008). Upon receptor activation, D1R and D2R internalise together with Ca$_V$2.2, and reduce the cell surface presence of the channels. Another example is opioid-receptor like receptor-1 (ORL1) which also co-localises with Ca$_V$2.2 in expression systems; furthermore ORL1 activation by nociceptin leads to Ca$_V$2.2 internalisation in DRG neurons (Altier et al., 2006). Mechanisms regarding how Ca$_V$2.2 is endocytosed have not been reported, but AP-2 binds to the synprint site in the II-III loop of Ca$_V$2.2, which is originally described as an interaction site for syntaxin, synaptotagmin (Syt) and SNAP25 (Watanabe et al., 2010). AP-2 and Syt compete for the synprint site in a Ca^{2+}-dependent manner, therefore clathrin-mediated endocytosis may be important for Ca$_V$2.2 function.

1.6 Hypothesis

Mutually exclusive alternative splice variants, $Ca_V2.2e37a$ and e37b are differentially expressed in small nociceptive DRG neurons where their function is also differentially modulated by GPCR activation. However, whether these two splice isoforms are trafficked equally to the cell surface where their function is vital in mediating Ca^{2+} influx upon activation by action potentials is still unknown.

I hypothesised that $Ca_V2.2$ channels containing e37a may be more readily trafficked to the cell membrane compared to $Ca_V2.2e37b$, and remain at the cell surface which leads to greater cell surface expression. This greater cell surface presence of $Ca_V2.2e37a$ could be the source of the larger whole-cell Ca^{2+} current and gating charges which have been reported previously (Castiglioni et al., 2006). If this is the case, the underlying mechanism(s) for $Ca_V2.2$ trafficking may be due to the difference in a relatively small number of amino acids in the C-terminus between the two isoforms. As indicated in the discussion of Raingo et al. (2007), one of the possible key amino residue could be Y1773, which is a part of the AP-binding motif YxxΦ. Although there are other potential AP-binding motifs identified in the $Ca_V2.2$ sequence (Figure 1.11), the interaction between VGCCs and AP has not been reported so far.

In addition, the differential GPCR control of $Ca_V2.2e37$ splice variants could also be a result of differences in the intracellular trafficking between $Ca_V2.2e37$ splice variants. Studying the effects on Cav2.2 isoform trafficking mediated by the action of GPCRs may elucidate further mechanisms of GPCR-mediated regulation of $Ca_V2.2$.
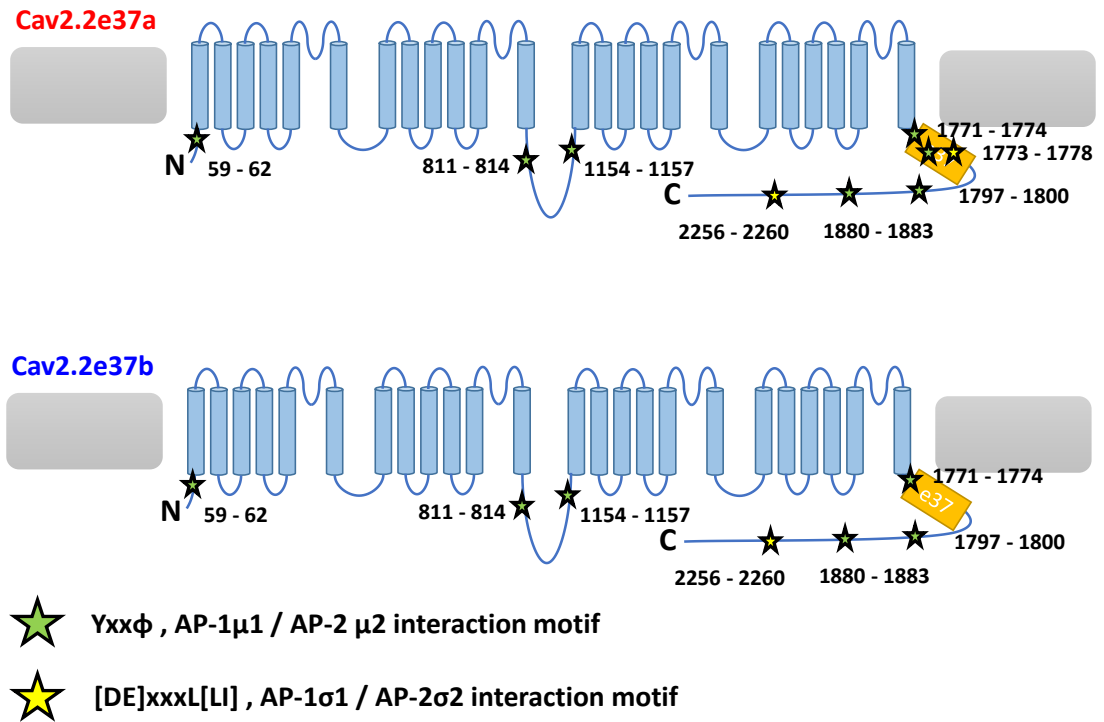
Figure 1.11 Adaptor protein interaction sites in Ca$_V$2.2e37a/b.

Schematic diagrams of Ca$_V$2.2e37 isoforms and the locations of YxxΦ (green) and [DE]xxxL[LI] (yellow) motifs. The start- and the end-amino acid residue numbers of the motifs are indicated.

1.7 Aim

The aim of this study is to investigate the mechanism of Ca$_V$2.2 splice variant trafficking by developing and critically assessing the molecular tools, in the expression systems and neuronal cells (Chapter 3). One important point of this study is to examine whether Ca$_V$2.2e37 splice variants are differentially trafficked to the cell surface (Chapter 4). If the trafficking of the Ca$_V$2.2e37 isoforms is found to be different, then the underlying mechanism(s) mediating this trafficking will be investigated. Furthermore, the amino acid sequence that is vital for the Ca$_V$2.2 trafficking will also be determined.

In addition, how the activation of GPCRs such as D2R may regulate the trafficking of Ca$_V$2.2 splice variants will also be investigated (Chapter 5). Further understanding of interactions between GPCRs and Cav2.2, and the modulation by Ca$_V$2.2 alternative splicing could be important for elucidating the physiological and pathological observations related to GPCR activities, as well as for discovering novel pharmacological targets in treating neurodegenerative diseases.

Chapter 2   Materials and Methods

2.1   cDNA constructs

Table 2.1 and Table 2.2 list the information on all the cDNA constructs used in the experiments.

Table 2.1 Description of Ca$_V$2.2 e37a and e37b cDNA constructs

Name	Tag	Vector	Species / GenBank association number	Source
mEos2-Ca$_V$2.2 37b	mEos2 at N-terminus	pMT2, pRK5	Rabbit / D14157	Created by W.Pratt, subcloned into pMT2 by N.Macabuag
HA-Ca$_V$2.2 37b	2xHA between A566 and V567	pMT2, pcDNA3.0	Rabbit / D14157	(Cassidy et al., 2014)
BBS-Ca$_V$2.2 37b	2xBBS between A566 and V567	pMT2, pcDNA3.0	Rabbit / D14157	(Cassidy et al., 2014)
GFP-Ca$_V$2.2 37b	GFP at N-terminus	pMT2, pcDNA3.0	Rabbit / D14157	(Raghib et al., 2001)
GFP-HA-Ca$_V$2.2 37b	GFP at N-terminus, 2xHA between A566 and V567	pMT2, pcDNA3.0	Rabbit / D14157	Created by N.Macabuag

mEos2-Ca$_V$2.2 37a	mEos2 at N-terminus	pMT2, pRK5	Rabbit	Created by W.Pratt, subcloned into pMT2 by N.Macabuag
HA-Ca$_V$2.2 37a	2xHA between A566 and V567	pMT2, pcDNA3.0	Rabbit	Created by W.Pratt, subcloned into pcDNA3 by N.Macabuag
BBS-Ca$_V$2.2 37a	2xBBS between A566 and V567	pMT2, pcDNA3.0	Rabbit	Created by N.Macabuag
GFP-HA-Ca$_V$2.2 37a	GFP at N-terminus, 2xHA between A566 and V567	pMT2, pcDNA3.0	Rabbit	Created by W.Pratt, subcloned into pcDNA3 by N.Macabuag

Table 2.2 Description of all other cDNA

Name	cDNA	Vector	Species/ GenBank association number	Source
α$_2$δ-1	α$_2$δ-1	pMT2, pcDNA3.0	Rat / M86621	
β1b	β1b	pMT2, pRK5	Rat / X61394	From Dr T.P. Snutch
β3	β3	pMT2	Rat	
CD8	CD8			
mCherry	mCherry	pcDNA3.0		
mut3 GFP	GFP			
D2R	Dopamine 2 receptor (long splice form)	pMT2	Rat	
FLAG-D2R	Dopamine 2 receptor (long splice	pMT2	Rat	Created by N.Macabuag

	form) with a signal sequence and 3xFLAG tag at the N terminus			
AP-2µ2 WT	AP-2µ2 subunit (wild type)	pcDNA3.1	Rat	From Dr M.S. Robinson (Motley et al., 2006)
AP-2µ2 T156A	Dominant-negative mutant of AP-2µ2 subunit with a mutation in the phosphorylation site	pcDNA3.1	Rat	From Dr M.S. Robinson (Motley et al., 2006)
AP-2µ2 F174A /D176S	Dominant-negative mutant of AP-2µ2 subunit with mutations in the YXXΦ interaction site	pcDNA3.1	Rat	From Dr M.S. Robinson (Motley et al., 2006)
AP-1 1a shRNA	shRNA against AP-1γ with mCerulean	mSUPER	Mouse, Human, Rat	From Prof. M.A. Cousin (Cheung and Cousin, 2012)
AP-1 1b shRNA	shRNA against AP-1γ with mCerulean	mSUPER	Rat	From Prof. M.A. Cousin (Cheung and Cousin, 2012)
AP-1σ1 WT	AP-1σ1a subunit (wild type)	pcDNA3.1	Human	From Dr J.S. Bonifacino (Jain et al., 2015)
AP-1σ1 V98S	Dominant-negative mutant of AP-1σ1a subunit with mutations in the [D/E]xxxL[L/I]	pcDNA3.1	Human	From Dr J.S. Bonifacino (Jain et al., 2015)
vGlut1-pHlourin (vGpH)	vGlut1 with the super-ecliptic pHlourin tag	pcDNA3.0		From Prof. T.A. Ryan (Hoppa et al., 2012)

	attached			
Dynamin WT	Dynamin-1	pcDNA3.1	Human	From Dr O.Staub (Ruffieux-Daidié et al., 2008)
Dynamin K44R	Dominant-negative mutant of dynamin-1	pcDNA3.1	Human	From Dr O.Staub (Ruffieux-Daidié et al., 2008)

2.2 Antibodies

Table 2.3 and Table 2.4 list the information on antibodies that were used in the experiments.

Table 2.3: A list of primary antibodies used in experiments.

Name	Epitope	Species	Dilution used	Manufacture / source
$Ca_V2.2$	$Ca_V2.2$ II-III loop	Rabbit	1:500 (immunocytochemistry), 1:1000 (western blot)	In-house (Raghib et al., 2001)
HA	HA (3F10), YPYDVPDYA	Rat	1:500	Roche
Myc	c-myc (9E10), EQKLISEEDL	Mouse (mono-clonal)	1:100	Santa Cruz
FLAG	FLAG, DYKDDDDK	Rabbit	1:500	Sigma
$\alpha_2\delta$-1		Mouse (mono-clonal)	1:1000	Sigma

		Rabbit	1:1000	Cell Signaling Technology
Akt				
GAPDH		Mouse	1:25000	Ambion

Table 2.4: A list of secondary antibodies used in experiments.

Name	Epitope	Species	Dilution	Manufacture / source
Alexa Fluor® 488 anti-rabbit	Rabbit IgG	Goat	1:500	Life Technologies
FITC anti-rat	Rat IgG	Goat	1:500	Sigma
Alexa Fluor® 594 anti-rabbit	Rabbit IgG	Goat	1:500	Life Technologies
Alexa Fluor® 594 anti-rat	Rat IgG	Goat	1:500	Life Technologies
Alexa Fluor® 594 anti-mouse	Mouse IgG	Goat	1:500	Life Technologies
Alexa Fluor® 647 anti-mouse	Mouse IgG	Goat	1:500	Life Technologies
Alexa Fluor® 647 anti-rabbit	Rabbit IgG	Goat	1:500	Life Technologies
Horseradish peroxide (HRP) anti-mouse	Mouse IgG	Goat	1:3000	Life Technologies
Horseradish peroxide (HRP) anti-rabbit	Rabbit IgG	Goat	1:3000	Life Technologies

2.3 Molecular biology

2.3.1 Polymerase-chain reaction (PCR)

In order to introduce point mutations or to insert tags in expression vectors, the following DNA oligonucleotide primers were designed (Table 2.5). Oligonucleotides were purchased from Eurofins Genomics (Ebersberg, Germany) in lyophilised form, which were re-constituted in nuclease-free water to 50 pmol/µl. PCR was performed using a Veriti® thermal cycler (Applied Biosystems) in the following PCR reaction mix and cycle protocol.

Table 2.5: A list of oligonucleotide primers used in experiments.

Primers	Sequence (5' to 3')
pMT2-R	GGTCGAACCATGATGGCAGC
α1B-Kpn21-F	CACAATAACTTCCGGACGTTTCTGCAG
LA-F	GGATATGTACAGTGCGTTGCGTTGTATTGC
LA-R	GCAATACAACGCAACGCACTGTACATATCC
LLAA-F	GGATATGTACAGTGCGGCGCGTTGTATTGC
LLAA-R	GCAATACAACGCGCCGCACTGTACATATCC
YA-F	AGGATATGGCCAGTTTGTTGCGTTG
YA-R	CAACGCAACAAACTGGCCATATCCT
YALLAA-F	AGGATATGGCCAGTGCGGCGCGTTGTATTGC
YALLAA-R	GCAATACAACGCGCCGCACTGGCCATATCCT
AP-1a_ Scrambled-A	GATCCCCGAGACCTTAAGATCCTATTTTCAAGAGAAATAGGATCTTAAGGTCTCTTTTTA
AP-1a_ Scrambled-B	AGCTTAAAAAGAGACCTTAAGATCCTATTTCTCTTGAAAATAGGATCTTAAGGTCTCGGG
ss_3FLAG_D2_R	TTCAGTGGATCCTTGTCGTCATCGTCTTTGTAGTCGATGTCATGATCTTTATAATCACCGTCATGGTCTTTGTAGTCACCGGTTTCAGCTACG
ss_3FLAG_D2_F2	CAGCTGGTACCGCCACCATGGGCATTCTTCCCAGCCCTGGG

Table 2.6: PCR reaction mix.

	Volume (µl)
Forward primer (50 pmol/µl)	1
Reverse primer (50 pmol/µl)	1
cDNA (1 µg/ml)	2
Pfu DNA polymerase (Promega)	1
10x buffer (Promega)	10
PCR nucleotide mix (Promega)	2
DMSO (Sigma)	5
Nuclease-free water	78
Total	100

Table 2.7: PCR thermal cycle protocol.

98 °C	2 min	x 1
98 °C	1 min	
50 °C	40 s	
73 °C	1 min for every 500 base pair PCR products	x 30
73 °C	10 min	x 1
16 °C	∞	

2.3.1.1 Generating HA-Ca$_V$2.2e37a-pMT2 mutants

In order to generate HA-tagged Ca$_V$2.2e37a mutants in pMT2, the following combination of primers with HA-Ca$_V$2.2e37a-pMT2 cDNA were used in the PCR (Table 2.8). These combinations were used to perform the first PCR using HA-Ca$_V$2.2e37a-pMT2 as a cDNA template in the protocol described in Table 2.6 and Table 2.7. The schematic diagram of the overall PCR strategy to introduce site-directed mutagenesis is described in Figure 2.1.

Table 2.8: Primer combinations for the first PCR.

	Primer combination 1		Primer combination 2	
Mutation	Forward	Reverse	Forward	Reverse
Y1775A (Y/A)	LA-F	pMT2-R	α1B-Kpn21-F	LA-R
L1777A (L/A)	LLAA-F	pMT2-R	α1B-Kpn21-F	LLAA-R
L1777A/L1778A (LL/AA)	YA-F	pMT2-R	α1B-Kpn21-F	YA-R
Y1775A/L1777A/L1778A (YSLL/ASAA)	YALLAA-F	pMT2-R	α1B-Kpn21-F	YALLAA-R

Molecular weights of the PCR products were confirmed on a 1 % agarose gel in TAE buffer containing 0.01 % ethidium bromide (EtBr) by running 8 µl of the product together with the molecular weight marker Hyperladder™ 1kb (Bioline). The rest of the PCR products were then separated on a 1 % agarose gel in Tris-Acetate-EDTA (TAE) buffer, which was post-stained with GelStar™ (Lonza) and visualised on ultra-violet (UV) light using the blue light box. The PCR fragment was extracted from the gel using QIAquick Gel Extraction kit (QIAGEN) following the manufacturer's protocol, and DNA was eluted in 50 µl nuclease-free water from the column. For the second PCR reaction to amplify from the two PCR products (1 and 2) from the two primer combinations (1 and 2) per mutant as described above, the following PCR reaction mix was used.

The unincorporated nucleotides and primers were removed using QIAquick PCR purification kit (QIAGEN) following the manufacture's protocol, and the PCR product was eluted in 50 µl nuclease-free water from the column. The PCR fragment was then digested with restriction enzymes BspEI and SpeI. The host plasmid HA-Ca$_V$2.2e37a-pMT2 was also digested with SpeI and SalI, and SalI and BspEI separately to perform a 3-part ligation (Figure 2.2).
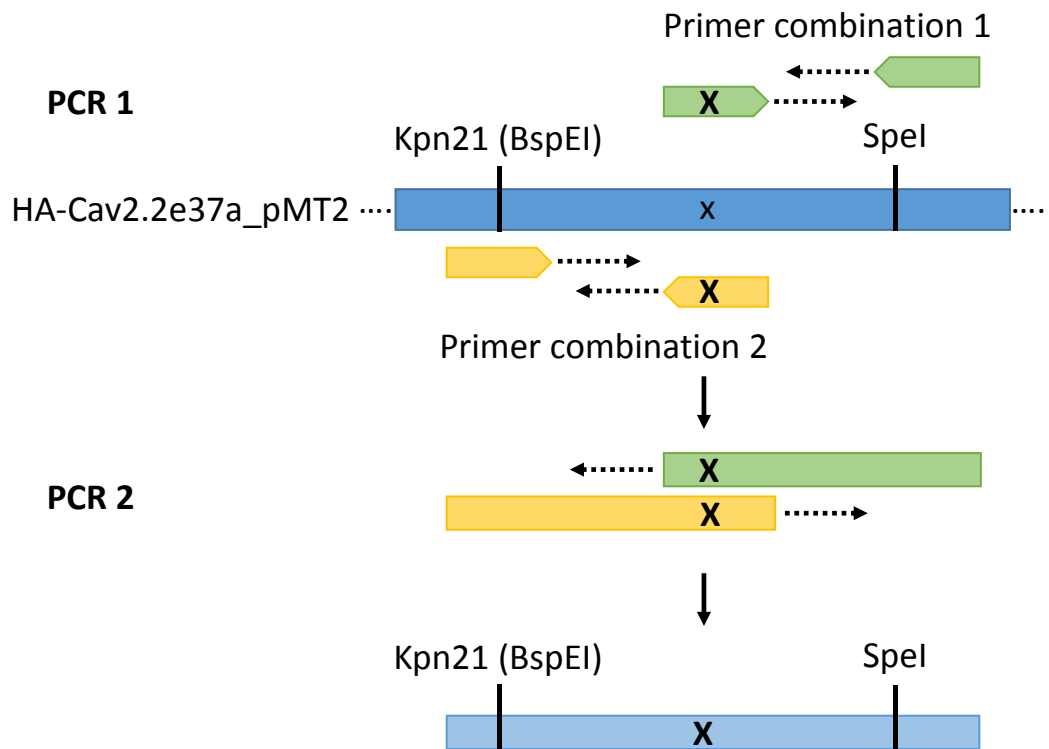
Figure 2.1 Schematic diagram of site-directed mutagenesis protocol.

This protocol was used to generate a fragment (1kb) containing a desired mutation, which is inserted into the original CaV2.2 expression vector using two restriction sites (Kpn21 and SpeI). The first PCR (PCR 1) involves two sets of separate PCRs: with primer combination 1 (green) and 2 (yellow). The template cDNA (dark blue) showing the original amino acid as X, whereas the forward primer from combination 1 and the reverse primer from combination 2 contain a mutated amino acid as X. The second PCR (PCR2) contains the products from PCR1 where the two large primers extend to generate the final DNA fragment containing the mutation and two restriction sites, Kpn21 (also known as BspEI) and SpeI to be inserted into a HA-Ca$_V$2.2e37a-pMT2 plasmid.
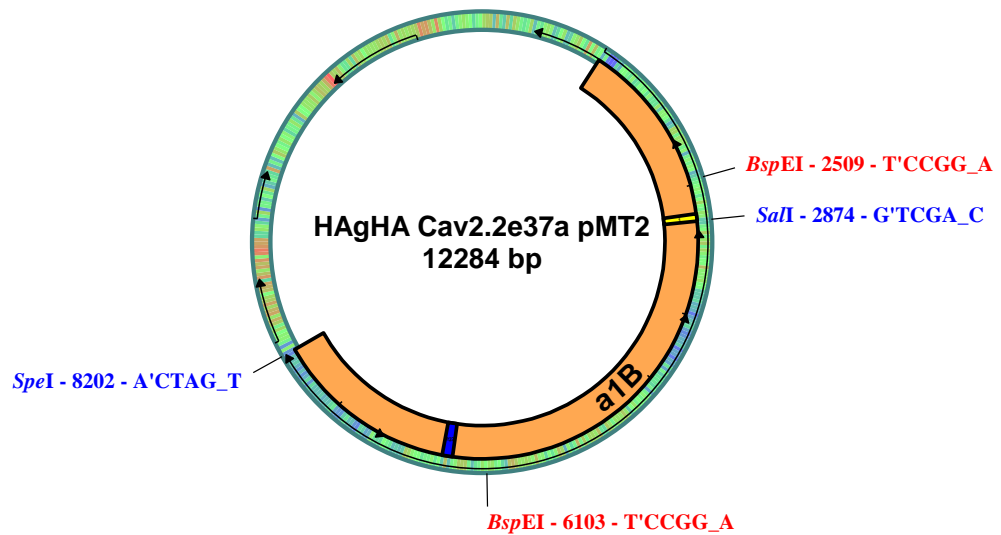
Figure 2.2 Ligation strategy for generating HA-Ca$_V$2.2e37a-pMT2 mutants.

The host plasmid HA-Ca$_V$2.2e37a-pMT2 was digested in order to insert the PCR fragment with appropriate mutations generated by PCR as described above. SpeI-SalI and SalI-BspEI fragments were generated by restriction digest of the host plasmid. 3-part ligation was then performed with these two fragments and the digested PCR fragment.

Table 2.9: PCR reaction mix for the second PCR reaction for generating Ca$_V$2.2e37a mutants

	Volume (µl)
PCR product 1	5
PCR product 2	5
α1B-Kpn21-F	1
pMT2-R	1
Pfu DNA polymerase (Promega)	1
10x buffer (Promega)	10
PCR nucleotide mix (Promega)	2
DMSO (Sigma)	5
Nuclease-free water	70
Total	100

2.3.1.2 Generating scrambled AP-1 shRNA

In order to generate a scrambled AP-1 shRNA expression cDNA vector as a control for AP-1 1a and 1b shRNA_mCerulean_pSUPER (Cheung and Cousin, 2012), DNA oligonucleotides AP-1a_Scrambled-A and AP-1a_Scrambled-B (Table 2.5) were designed using an online software on GenScript (https://www.genscript.com/ssl-bin/app/scramble) from AP-1 1a sequence described in Cheung and Cousin (2012). The oligonucleotides were adjusted to 5 pmol/µl in nuclease-free water. To anneal these oligonucleotides, 1 µl each of the two oligonucleotides were added to 13 µl of ligation buffer (1 mM EDTA pH 8.0, 10 mM Tris, 0.1 mM NaCl) in a PCR tube, and annealed at 95 °C for 5 min. This was inserted into the mCerulean_pSUPER vector which contains BglII and HindIII ends. The following reaction mix was set up for the ligation: 15 µl of the annealed oligonucleaotides in ligation buffer, 2 µl mCerulean_pSUPER vector (BglII, HindIII), 1 µl T4 ligase (Promega), 2 µl 10x T4 ligase buffer (Promega).

2.3.1.3 Generating FLAG-tagged dopamine 2 receptor (D2R)

3xFLAG and an ER signal sequence were added to D2R in pMT2 vector at the N-terminus of the receptor, in order to detect the cell surface expression by anti-FLAG antibody (Figure 2.3). Primers against the signal sequence in the in-house pHLsec construct (based on Aricescu et al., 2006), termed ss_3FLAG_D2_F2 and ss_3FLAG_D2_R were designed (Table 2.5), which contain KpnI and BamHI restriction sites. The PCR protocol was performed as below. To confirm, the PCR products (~ 200 bp) were run on 2.5 % TBE gel with 0.01% EtBr. The unincorporated nucleotides and primers were removed using QIAquick PCR purification kit (QIAGEN) following the manufacture's protocol, and the PCR product was eluted in 50 µl nuclease-free water from the column prior to the restriction digests.

Table 2.10 PCR reaction mix for the second PCR reaction for generating ss_3xFLAG-tagges D2R

	Volume (µl)
ss_3FLAG_D2_F2	1
ss_3FLAG_D2_R	1
CLC2-pHLsec (1 µg/ml)	2
Pfu DNA polymerase (Promega)	1
10x buffer (Promega)	10
PCR nucleotide mix (Promega)	2
DMSO (Sigma)	5
Nuclease-free water	78
Total	100
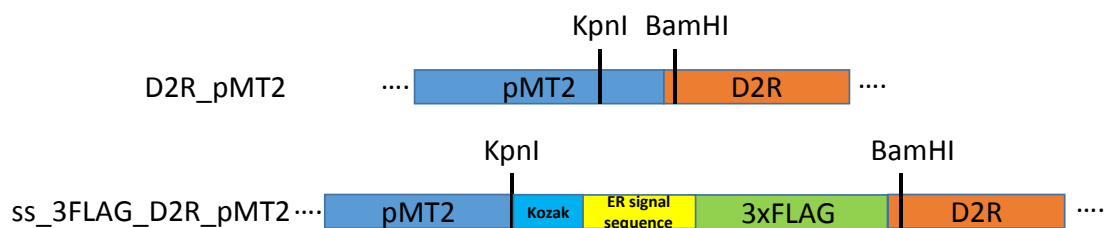
Figure 2.3 3xFLAG-tagged D2R with ER signal sequence.

ER signal sequence (yellow) containing Kozak sequence (blue) and 3xFLAG tag (green) were inserted into 5' end of D2R in pMT2. The start codon of D2R and an additional *BamHI* in the signal sequence were removed in the primer design.

2.3.2 Restriction digests

To subclone a construct into another vector, or to confirm the positive clones after ligation, a restriction digest with appropriate restriction enzymes was performed under the following condition;

Table 2.11: A protocol for restriction digests.

	Vector	PCR product	Miniprep elute
cDNA	3 µg	50 µl elute	2.5 µl
Restriction enzyme	2 µl	2 µl	0.2 µl
Buffer (x10)	4 µl	6 µl	1 µl
H_2O	To 40 µl total	To 60 µl total	To 10 µl total
Reaction condition	2 h at 37 °C	2 h at 37 °C	1 h at 37 °C

In order to avoid self-ligation of the vector after the restriction digest, dephosphorylation of the 5' end was performed using calf-intestinal alkaline phosphatase (CIP) in some cases. Once the vector was digested, the reaction mix was cleaned up to remove enzymes and exchange buffer using QIAquick PCR purification kit (QIAGEN) following the manufacture's protocol. The digested cDNA was eluted from the column with nuclease-free water. The cDNA was incubated with 4 µl Buffer 1 (New England Biolab) and 2 µl CIP for 1 h at 37 ˚C. The reaction mix was cleaned again prior to the ligation.

2.3.2.1 Generating GFP-tagged HAgHA-Ca$_V$2.2

N-terminus cDNA sequence of GFP-Ca$_V$2.2-pMT2 cDNA construct including GFP was digested with BglII and NotI, and inserted into the N-terminus of HAgHA-Ca$_V$2.2-pMT2 (Figure 2.4). Positive clones containing the insert were screened and the sequence was confirmed by sequencing.
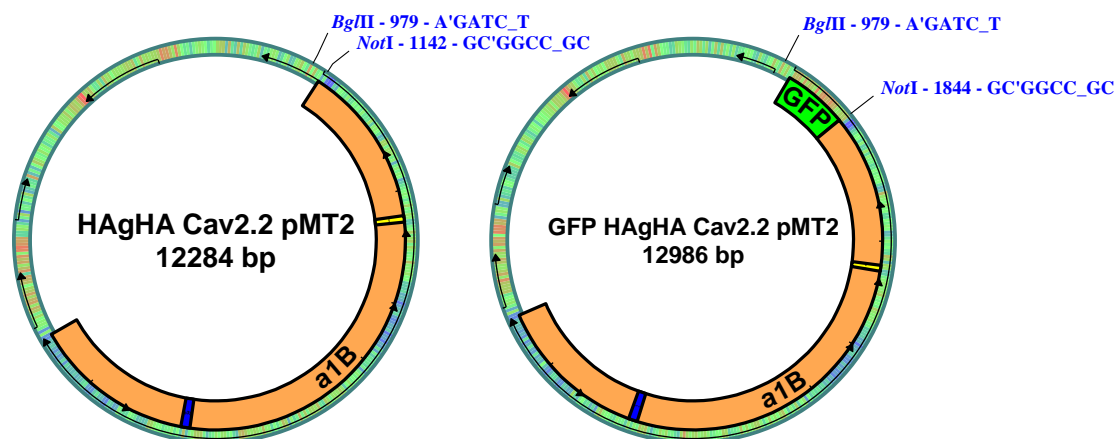
Figure 2.4 Plasmid maps and restriction sites to create GFP-HA-Ca$_V$2.2.

HA-Ca$_V$2.2e37b (left) and GFP-HA-Ca$_V$2.2e37b (right) in pMT2 are shown with BglII and NotI sites. GFP (green) at N-terminus of HA-Ca$_V$2.2 from GFP-Ca$_V$2.2-pMT2 was inserted into HA-Ca$_V$2.2-pMT2 at these restriction sites. HA (yellow), e37b (blue).

2.3.3 Gel electrophoresis

In order to determine the size of the cDNA fragments from PCR or restriction digest, the samples were typically run on 1 % TAE agarose gel (Life Technology). When the fragments of interest are smaller than 200 bp, 2.5-3 % TAE or Tris-Borate-EDTA (TBE) agarose gel was used to resolve the bands with lower molecular weight. To visualise the DNA, the agarose gel contained 0.01 % EtBr. The fragments were separated for 1-2 h at 90V along with appropriate molecular weight markers. If the cDNA fragments were to be used in subsequent cloning, the agarose gel without EtBr was post-stained with GelStar™ in the same buffer as the gel for 30 min on a shaking platform. The bands with correct molecular weights were cut out of the gel on a filtered UV box. The fragments of interest were extracted from the gel using QIAquick Gel Extraction kit (QIAGEN) following the manufacturer's protocol, and DNA was eluted from the column in 30-50 µl nuclease-free water.

2.3.4 Ligation

To ligate DNA fragments with compatible ends, the ligation reaction was performed under the following condition:

Table 2.12: Protocol for ligation.

Vector	6.5 µl
Insert(s)	2 µl (2-part ligation) or 1 µl each (3-part ligation)
T4 ligase	0.5 µl
10x T4 ligase buffer	1 µl
Reaction condition	3 h at room temperature or overnight at 4 °C

2.3.5 Transformation

To transform *E.coli* cells with the ligation mix or diluted plasmid (1 ng/µl), 5 µl of cDNA was added to a vial of OneShot® Chemically Competent *E.coli* (Life Technology), mixed by gentle tapping, and was incubated on ice for 30 min. The cells were heat-shocked at 42 °C for 30 s and incubated on ice for 2 min. 250 µl of S.O.C. medium (Life Technologies) was added to the cells and incubated in the shaking incubator at 225 rpm for 1 h at 37 °C. The cells (200 µl on one plate and 20 µl on the other) were spread on Luria-Bertani (LB, 10 g bacto-tryptone, 5 g bacto-yeast extract, 10 g NaCl, pH 7.0) agar plates containing 15 g/l agar and 50 µg/ml ampicillin in LB medium. The culture plates were incubated at 37 °C overnight.

2.3.6 Clone selection

In order to select an appropriate clone, isolated colonies of transformed *E.coli* cells were picked from the culture plate, and were cultured in 5ml LB medium containing 50 µg/ml ampicillin for 8 -16 h at 37 °C shaking incubator at 225 rpm. Plasmids from these clones was isolated using Miniprep kit (QIAGEN) following manufacture's protocol. Briefly, 2 ml of cell suspension was centrifuged at 7000 g in a tabletop centrifuge for 3 min. The cell pellets were lysed and cDNA was collected in the columns. The cDNA was eluted in 50 µl nuclease-free water. Test digests were performed to select the clones, which

contained the correct insert by determining the size of cDNA fragments after the restriction digest. In some cases, a part of the miniprep construct was sequenced to confirm that the clones contained correct fragments.

2.3.7 Plasmid cDNA purification

300 µl of cell culture of the positive clone from the clone selection was added to 200 ml LB medium containing 50 µg/ml ampicillin, and cultured for 16 h at 37 °C in a shaking incubator at 225 rpm. cDNA from these clones was isolated using QIAGEN Plasmid Maxi or Endofree Plasmid Maxi kit following manufacturer's protocol. The cDNA concentration was determined by DU-800 spectrophotometer (Beckman Coulter) at 260 nm and 280 nm wavelength and adjusted to 1 µg/µl.

2.3.8 Sequencing

All cDNA sequences were confirmed by sequencing. Briefly, the PCR was run with appropriate sequencing primers under the conditions stated in Table 2.13 and Table 2.14.

The PCR products were precipitated by adding 10 µl nuclease-free water, 2 µl 3 M sodium acetate (pH 5.2), 50 µl ethanol, which were incubated on ice for 10 min. The samples were centrifuged at 13000 rpm for 15 min at room temperature. The pellet was washed with 70 % ethanol, centrifuged at 13000 rpm for 5 min, and air-dried. The samples were resuspended in 10 µl Hi-Dye formamide (Life Technology) and analysed on 3100 *Avant* Genetic Analyser (Applied Biosystems) with a NanoPOP-6 polymer (Nimagen).

Table 2.13: Protocol for sequencing PCR.

Sequencing primer (2 pmol/µl)	2 µl
cDNA (1 µg/µl)	0.5 µl
BigDye® Terminator v1.1 (Life Technology)	4 µl
DMSO	0.5 µl
Nuclease-free water	3 µl

Table 2.14: PCR thermal cycle protocol for sequencing.

98 °C	3 min	x 1
98 °C	30 s	
50 °C	15 s	x 25
60 °C	4 min	
16 °C	∞	

2.4 Cell culture and transfection

2.4.1 tsA-201 cell culture

tsA-201 cells (human embryonic kidney 293 cell line, stably expressing SV40 T-antigen) were cultured in Dulbecco's modified Eagle's medium (DMEM) with high glucose and L-glutamine, supplemented with 1 unit/ml penicillin, 1 µg/ml streptomycin, 10 % foetal bovine serum (FBS), and 1 % GlutaMAX (Life Technologes). The cells were cultured to 80 % confluence in a 5 % CO_2 incubator at 37 °C, and passaged every 3 to 4 days.

2.4.2 N2a cell culture

The mouse neuroblastoma cell line Neuro-2a (N2a) was cultured in 50 % DMEM (with high glucose and L-glutamine) and 50 % OPTI-MEM (with L-glutamine), supplemented with 1 unit/ml penicillin, 1 µg/ml streptomycin, 5 % FBS, and 1 % GlutaMAX (Life Technologies). The N2a cells were cultured to 80 % confluence in a 5 % CO_2 incubator at 37 °C, and passaged every 3 to 4 days.

2.4.2.1 tsA-201 and N2a cell transfection

To transiently express recombinant proteins, tsA-201 cells were transfected using either PolyJet™ (SignaGen Laboratories) or Fugene® 6 (Promega) in 1:3 ratio with cDNA mix. tsA-201 cells were plated to 30-60% confluent >3 h prior to a transfection procedure. Typically for a 35 mm cell culture dish, 2 µg cDNA was mixed with 50 µl serum-free DMEM, and 6 µl PolyJet was mixed with 50 µl serum-free DMEM in separate tubes by pipetting. These were then mixed by gentle pipetting, and incubated for 15 min at room temperature before they were added dropwise to the cells. Similarly for a Fugene-transfection in a 35 mm cell culture dish, 6 µl Fugene was mixed with 94 µl serum-free DMEM, and left to incubate for 5 min at room temperature. 2 µg cDNA mix (typically $Ca_V2.2$: β1b: α2δ-1= 3:2:2, in pMT2 vector for tsA-201, in pcDNA3 or pRK5 for N2a) was then gently mixed with the mixture and incubated for further 30 min before they were added dropwise to the cells.

2.4.3 DRG neuronal cell culture

DRGs were extracted in Hank's Balanced Salt Solution (HBSS) without Ca^{2+} and Mg^{2+}, from the spinal column of a male rat in postnatal Day 10 (P10), which were killed under the Schedule 1 procedure. DRGs were then dissociated in 1 ml of a dissociation solution (5 mg/ml Dispase (Life Technologies), 2 mg/ml Collagenase (231 U/mg) and 0.1 mg/ml (or 0.1 U/µl) DNase (Life Technologies) in HBSS without Ca^{2+} and Mg^{2+}) in a 15 ml falcon tube in a shaking water bath at 37 °C for 30 min. The enzymes were inactivated by addition of 10% FBS. The cells were triturated by pipetting and centrifuged at 1000 rpm for 3 min to remove the solution. The cells were re-suspended in the culture medium (DMEM/F12, 10 % FBS, 100 ng/ml nerve growth factor (NGF), 1 unit/ml penicillin, 1 µg/ml streptomycin), which were then plated onto coverslips that were pre-coated with 17.9 µg/ml poly-L-lysine, and cultured at 37 °C in a 5 % CO_2 incubator. The culture medium was changed 2 h after plating.

2.4.3.1 DRG transfection

After the DRGs were dissociated, triturated and centrifuged, the cell pellet was re-suspended in 1 ml HBSS, and split into two Eppendorf tubes (500 µl each) to be further centrifuged at 1000 rpm for 3 min. The cell pellet was re-suspended in 80 µl Nucleofector™ (Lonza) transfection reagent, containing 2 µg of cDNA mix (typically, $Ca_V2.2$-pcDNA3: β1b-pRK5: α2δ-1-pcDNA3: mCherry-pcDNA3= 3:1.5:2:0.5). Following the electroporation protocol in the Nucleofector cuvette, 500 µl of RPMI supplemented with 10 % FBS and 50 ng/ml NGF was added to the cells in the cuvette, which were then transferred into a 1.5 ml Eppendorf tube and incubated in a 5 % CO_2 incubator at 37 °C for 8 min. The cells were plated onto coverslips (250 µl each) that were pre-coated with poly-L-lysine (Sigma), and cultured at 37 °C in a 5 % CO_2 incubator. The culture medium was changed at 2 h after plating.

2.4.4 DRG-dorsal horn (DH) co-culture

DRGs and DH were extracted in ice-cold L15 dissection medium, from a male rat at postnatal day 0 (P0), which was killed under the Schedule 1 procedure. The DH was dissociated in 100 µl 2.5% trypsin in S-MEM at 37 °C for 20-25 min in a dish. The dissociated DH was transferred into a 15 ml tube and was washed twice with warm culture medium (50 % NeuroBasal A (Life Technologies), 2 % B27-supplement (Life Technologies), 100 ng/ml NGF, 1 unit/ml penicillin, 1 µg/ml streptomycin, 1 % Glutamax, 50 % astrocytes-conditioned medium*), and triturated gently using a fire polished glass pipette. DH neurons were plated onto coverslips coated with poly-L-lysine and laminin (Sigma). DRGs were dissociated in 1 ml of 5 mg/ml Dispase at 37 °C for 25-30 min in a dish. The dissociated DRGs were transferred to a 1.5ml Eppendorf tube and triturated with pipettes. The supernatant was removed by centrifuging at 1000 rpm for 3 min. The pellet was washed with 1 ml of warm HBSS and centrifuged again. For DRG transfection, the supernatant was discarded and the cells were resuspended in 80 µl Nucleofector™ (Lonza) transfection reagent, and they were transferred to a fresh tube containing 2 µg of cDNA mix (HA-$Ca_V2.2$-pcDNA3: β1b-pRK5: α2δ-1-pcDNA3: vGpH-pcDNA3= 3:1:1.5:1.5). Following the electroporation protocol in the Nucleofector cuvette, 500 µl of

RPMI supplemented with 10 % FBS and 50 ng/ml NGF was added to the cells in the cuvette, which were then transferred into a 1.5 ml Eppendorf tube and incubated in a 5 % CO_2 incubator at 37 °C for 8 min. The cells were plated on top of the DH neurons. The wells were flooded with warm medium 1 h after the transfected DRG neurons were plated. The growth medium was replaced after 16h, and half of the medium every 3-4 days. Cells were cultured for 7 days before the experiment.

(*Astrocytes-conditioned medium was prepared from growth medium of the astrocytes culture from dissociated cerebral cortex of P0 rat. The growth medium contained DMEM with 10 % horse serum, 2.5 % FBS, 1 unit/ml penicillin, 1 µg/ml streptomycin.)

2.4.5 Hippocampal neuronal cell culture

Hippocampal neurons were isolated from the hippocampus of P0 rats, which were killed under the Schedule 1 procedure. The cerebrum was cut into two, and the hippocampi were extracted from each hemisphere in ice cold HBSS with 10 mM HEPES. The hippocampi were then cut into small segments and digested gently in Papain solution (7 U/ml Papain, 0.2 mg/ml L-Cysteine, 0.2 mg/ml Bovine Serum Albumin (BSA), 5 mg/ml glucose, 10 mM HEPES in HBSS with 200 µl DNase) in a shaking water both for 40 min at 37 °C. The cells were washed twice with the growth medium (NeuroBasal, 2 % B27-supplement, 1 unit/ml penicillin, 1 µg/ml streptomycin, 1 % Glutamax, 0.1% β-marcaptoethanol), and triturated gently. The cells were plated onto the coverslips that are coated with poly-L-lysine and laminin at 750 cell/µl, 100 µl per coverslip. The entire growth medium was changed after 2 h of plating, and half of the medium was then changed every 3-4 days.

2.5 Western Blot

2.5.1 Whole-cell proteins

Cells were transfected with $Ca_V2.2$ with $\alpha_2\delta$-1, β1b subunits and GFP either in T25 or T75 flasks, using PolyJet. Control cells were transfected with GFP only. After 40 h expression, the cell transfection was confirmed by visually examining GFP expression under a fluorescent microscope.

The cells were washed twice with PBS, and harvested in 5 ml PBS containing Complete Protease Inhibitor Cocktail (PI, Roche) using a cell scraper. The cell suspension was centrifuged at 1000 x g for 5 min at 4 °C. The cell pellet was re-suspended with either Lysis Buffer (50 mM Tris pH 7.4, 50 mM NaCl, PI), or in PBS. To prevent the protein aggregation of $Ca_V2.2$, 25 mM N-ethylmaleimide (NEM) was added to the samples to prevent the formation of $Ca_V2.2$ α subunit aggregates in some experiments as stated. The suspension was sonicated for 7 s and 1 % IGEPAL® CA-630 (a detergent from Sigma) was added, which was then left on ice for 45 min to complete the lysis. The lysate was centrifuged at 14000 x g for 20 min. The supernatant was transferred to a fresh Eppendorf tube and the protein concentration was determined by Bradford assay (Bio-Rad). Samples were denatured by heating at 55 °C for 15 min with reducing Laemmli Sample Buffer (2 % SDS, 2 % glycerol, 0.02 % bromophenol blue, 50 mM Tris HCl pH 6.8, 20 mM dithiothreitol (DTT)). Proteins were separated on a 3-8 % Tris-Acetate gel (Life Technologies), and transferred onto a polyvinylidene fluoride (PVDF) membrane. The membrane was blocked in Tris-buffered saline (TBS) solution (10mM Tris pH7.4, 500mM NaCl, 0.5 % IGEPAL CA-630) with 3 % BSA, and was then incubated with the primary antibody (1:1000) in antibody diluent (10% goat serum, 3 % BSA, 0.02 % IGEPAL in TBS) overnight at 4 ℃. The secondary antibody conjugated with horseradish peroxide (HRP) (1:3000) in antibody diluent was incubated with the membrane for 1h at room temperature. The proteins were detected using ECL Plus Western Blotting Detection Reagents (GE Healthcare) according to the manufacturer's protocol and scanned using the fluorescent detection mode on Typhoon 9410 (GE Healthcare).

2.5.2 Biotinylation of plasma membrane proteins

Cells were transfected with $Ca_V2.2$, $\alpha_2\delta$-1, β1b and GFP either in T25 or T75 flasks using PolyJet. Control cells were transfected with GFP only. After 64 h expression, the transfection efficiency was confirmed to be the same in all conditions by visually examining GFP expression under a fluorescent microscope. The culture medium was replenished 1 h before the experiment to increase the cell adhesion during biotinylation. The cells were washed twice in PBS, and incubated with 5 ml of 1mg/ml EZ-Link™ Sulfo-NHS-SS-Biotin (Thermo Fisher) at 4 °C for 30 min. The biotinylated cells were washed once with PBS, and washed twice with 200 mM glycine (pH 8.0) in PBS to quench the biotin. The cells were washed twice with PBS and harvested in 5 ml PBS containing PI using a cell scraper. The cells were centrifuged and lysed in PBS containing 1 % IGEPAL as above. 50 µl of Pierce streptavidin agarose beads (Life technologies) were pre-equilibrated by centrifuging at 500 x g for 2 min, removing the supernatant and adding 800 µl PBS with 1 % IGEPAL. These steps were repeated twice, and 800 µg of lysate was incubated with the beads at 4 °C overnight on a tube rotator. The beads were then washed three times with PBS with 1 % IGEPAL by centrifuging and removing supernatant. The biotinylated proteins were liberated by incubating with 100 mM DTT and 2x SDS sample buffer for 1 h at 37 °C. The supernatant was run on a gel to separate the proteins as described above.

2.6 Visualisation of calcium ion channels

2.6.1 Immunocytochemistry

Cells were plated onto either coverslips or glass-bottomed dishes (MatTek Corporation) which were coated with poly-L-lysine prior to transfection, and cultured in a 5 % CO_2 incubator at 37 °C. After 40-72 h expression, cells were fixed with 4 % paraformaldehyde (PFA) in PBS, pH7.4 at room temperature for 10 min. For labelling the HA epitope on the cell surface in non-permeabilised conditions, the cells were incubated with primary antibody with 2.5% BSA and 10% goat serum in PBS at room temperature for 1 h for N2a cells, or overnight at 4 °C for DRG neurons. The secondary antibody was

added with 2.5% BSA and 10% goat serum in PBS, and incubated for 1 h at room temperature. In experiments in which the D2R was activated, 100nM quinpirole (Quin, Sigma) was added to N2a cells in Krebs-Ringer solution with HEPES (KRH) (in mM; 125 NaCl, 5 KCl, 1.1 $MgCl_2$, 1.2 KH_2PO_4, 2 $CaCl_2$, 6 Glucose, 25 HEPES, 1 $NaHCO_3$) at 37 °C for 30 min. 500 ng/ml pertussis toxin (PTX, Life Technologies) was added to the cells in the culture media overnight. To label intracellular proteins, the cells were permeabilised with 0.2 % Triton X-100 in PBS for 10 min. The primary and secondary antibodies in 2.5 % BSA and 10 % goat serum were added to the cells as above. Cell nuclei were stained with 0.5 µM 4',6'-diamidino-2-phenylindole (DAPI) in PBS for 10 min. The coverslips were mounted onto glass slides using VECTASHIELD® mounting medium (Vector Laboratories).

2.6.2 Endocytosis assay

Transfected cells were plated onto glass-bottomed dishes (MatTek Corporation), coated with poly-L-lysine, and cultured in a 5 % CO_2 incubator at 37 °C. After 40 h expression, N2a cells in glass-bottomed dishes were washed twice with KRH. The cells were incubated with 10 µg/ml α-bungarotoxin Alexa Fluor® 488 conjugate (BTX-488) (Life Technologies) in 100 µl KRH for 30 min at 17 °C. The unbound BTX-488 was removed by washing with KRH, and the labelled cells were returned to 37 °C for the kinetic assay. Endocytosis was terminated by fixing the cells with cold 4 % PFA in PBS. For endocytosis experiments in which the D2R was activated, 100 nM Quin was added to the cells in KRH buffer after the BTX-488 labelling stage. The cells were then permeabilised and intracellular $Ca_V2.2$ and nuclei were labelled as described above. The 13 mm coverslips were mounted onto dishes using VECTASHIELD® mounting medium.

2.6.3 Forward trafficking assay

Transfected cells were plated onto glass-bottomed dishes (MatTek Corporation), coated with poly-L-lysine, and cultured in a 5 % CO_2 incubator at 37 °C. After 40 h expression, N2a cells in glass-bottomed dishes were washed twice with KRH. The cells were incubated with 10 µg/ml unlabelled α-

bungarotoxin (BTX) (Life technologies) for 30 min at 17 °C. The unbound BTX was washed off with KRH, and the cells were then incubated with 10 µg/ml BTX-488 in KRH at 37 °C. To terminate the reaction, cells were washed twice with cold KRH and then fixed with 4 % PFA in PBS at specified times for the kinetic assay. 200 ng/ml (0.713 µM) Brefeldin A (BFA, Sigma) in 0.4 % DMSO was added to the cells in FBS-free N2a cell culture medium for 4 h before and during the experiment in KRH buffer. The cells were then permeabilised and intracellular Ca$_V$2.2 and nuclei were labelled as described above. The 13 mm coverslips were mounted onto dishes using VECTASHIELD® mounting medium.

2.6.4 Confocal microscopy

All images were acquired using either an LSM 510 or LSM 780 Meta scanning confocal microscope (Zeiss), equipped with a Plan-Apochromat 63x/1.4 or 40x/1.3 DICII oil immersion objective lens, in 8- or 16-bit mode. The laser powers, gains and acquisition settings were kept constant for images that were used subsequently for quantification. The region of interest was determined by identifying cells with expression of a transfection marker or intracellular staining of the protein of interest (e.g. GFP, Ca$_V$2.2 II-III loop staining), without selecting for the cell surface immunostaining to avoid bias. In addition, on the LSM 780 confocal microscope, the region of interest was selected as described here, and the tile scan of 3 x 3 (9 tiles including the selected tile) was performed to further remove the bias in selecting cells with high expression. For cell surface expression analysis, images were taken with 0.7 µm optical section. For neurite expression analysis, images were taken with 0.9 µm optical sections in Z-stack, and presented as maximum projection. Confocal images were imported and analysed in ImageJ (National Institutes of Health). The membrane fluorescence was quantified using the freehand brush tool with a selection width of 0.66 µm, and tracing the membrane region manually. Neurite fluorescence was quantified using the freehand brush tool with a selection with of 2 µm and manually tracing the entire neurites using mCherry expression as a marker. Lengths of neurites expressing GFP-Ca$_V$2.2 were quantified using the freehand brush tool with a selection with of 2 µm and manually tracing the neurites expressing GFP as a marker. The measured area

in μm^2 was divided by the width of the selection (2 μm) to derive the length. Intracellular and whole-cell fluorescence was quantified using freehand selection, omitting the signal intensity from the nuclei. The background fluorescence intensity in each channel was also taken from the same image, and subtracted from the signal intensity. In the cell surface expression and trafficking experiments, all cells chosen for analysis contained Ca$_V$2.2 II-III loop immunostaining, confirming the Ca$_V$2.2 α subunit expression. The whole-cell Ca$_V$2.2 expression levels were not significantly different in all experiments. For the endocytosis assay, the normalized membrane fluorescent intensities were fitted to the single exponential decay equation (Equation 1), where x is time, y is intensity, y0 is the initial intensity, A is amplitude, and τ is the time constant.

$$y = y0 + Ae^{-x/\tau} \qquad \text{(Equation 1)}$$

For the forward trafficking assay, the membrane fluorescent intensities were fitted to the single exponential association equation (Equation 2), where x is time, y is intensity, y0 is the initial intensity, A is amplitude, and τ is the time constant.

$$y = y0 + A(1 - e^{-x/\tau}) \qquad \text{(Equation 2)}$$

All experiments were repeated n=3 to n=5, and approximately 30 to 50 cells (N2a) were analysed for each experiment. All data were presented as pooled in the resulting graphs, except for the trafficking rates and time constants, which are averages of separate experiments.

2.7 Electrophysiology

tsA-201 cells were transfected with cDNA mix containing Ca$_V$2.2, α$_2$δ-1, β1b, and CD8 or GFP at a ratio of 3 : 2 : 2 : 0.4 using a Fugene transfection protocol. After 40 h expression, cells were replated in cell culture medium at 1 in 3 or 5 dilution depending on their confluency. Transfected cells were identified by co-expression of either GFP or CD8. CD8 expression was detected with CD8 Dynabeads (Life Technologies). Whole-cell currents were

recorded in voltage-clamp mode in following solutions; intracellular (electrode) solution (mM): 140 Cs-aspartate*, 5 EGTA, 2 $MgCl_2$, 0.1 $CaCl_2$, 2 K_2ATP, 20 HEPES, pH 7.2, 310 mOsm (* 0.5 M stock is made with 6.65 g L-aspartic acid in 50 ml H_2O and 3 M CsOH was added to adjust the pH to 7.2, then H_2O was added to make up to 100 ml). Extracellular solution (mM): 1 $BaCl_2$, 3 KCl, 1 $NaHCO_3$, 1 $MgCl_2$, 10 HEPES, 4 D-glucose, 160 tetraethylammonium bromide, pH 7.4, 320 mOsm. The borosilicate glass electrode resistance was between 1.5 and 4 MΩ. Cell capacitance and series resistance were compensated to 70-80 %. Whole-cell currents were recorded on Axopatch-200B amplifier using pClamp 9 or 10 (Molecular Devices). The cells were held at -90 mV, and 50 ms pulses were applied in +5 mV steps between -30 mV and +70 mV. For D2R activation, Quin was applied by local application through a perfusion system. To correct for the leak current, P/8 leak subtraction protocol was applied. Recordings were made at 20 kHz sampling frequency and filtered at 5 kHz (low-pass 4-pole Bessel filter) in the amplifier. The digital low-pass 8-pole Bessel filter with 1 kHz 3dB cut-off was applied in Clampfit 10.9 (Molecular Devices) before the current amplitudes were determined. Average peak currents were taken between 8–13 ms after the test potentials were applied, and normalized to the cell capacitance to obtain current density. Current-voltage (IV) relationships were fitted to a modified Boltzmann equation (Equation 3) to give V_{50} activation ($V_{50,act}$), conductance (G_{max}), and reversal potential (V_{rev}) using Origin 7.

$$I = \frac{Gmax(V - Vrev)}{1 + e^{\frac{-(V - V50,act)}{k}}}$$ (Equation 3)

2.8 Co-localisation analysis

Co-localisation of two different fluorophores was analysed using ImageJ plugin, Just Another Co-localisation Plugin (JACoP) (Bolte and Cordelières, 2006). Pearson's correlation coefficient (r_P), overlapping coefficient (r), and Manders' co-localisation coefficients (M_1 and M_2) (Manders et al., 1993) were assessed for each set of images. Pearson's coefficient provides the correlation between the distributions of two signals, while overlapping coefficient represents fraction of co-localising objects, if there are an equal number of

components in each channel. Mander's coefficients are independent of the number of objects, and better express the fraction of co-localising objects, however, they are ineffective for comparing images with a very high background noise.

2.9 Sample numbers

The number of samples (n) in most of the experiments in this study is the total number of individual cells analysed, which are pooled from separate experiments (with a minimum of three repeats), and from this the mean and the standard error of mean (SEM) were calculated. The only exception is for the experiments determining the rates of Ca$_V$2.2 trafficking, in which the rate of Ca$_V$2.2 trafficking was determined from each experiment by analysing 20 to 50 cells per data point, and then the mean and SEM were determined from the repeated experiments.

2.10 Statistical analysis

Statistical analysis was performed using Student's t test or one-way ANOVA with Bonferroni post-hoc test as appropriate in GraphPad Prism. All the data were expressed as mean ± SEM.

Chapter 3   Molecular tools to study trafficking of Ca$_V$2.2 splice variants

3.1 Introduction

Cellular localisation of a single VGCC can be visualised by tagging the channel with a fluorescent protein or a tag that can be specifically identified. Such molecular tools for locating calcium channels have been generated and have been used in various studies previously, however not all of these resulted in functional VGCCs. It is essential to ensure that the tagged VGCCs are also functional for the modelling of the channel localisation to be physiologically relevant since the channel activity may modulate its cellular localisation, which has been shown in other channels such as AMPA and *N*-methyl-*D*-aspartate (NMDA) receptors (Ju et al., 2004; Lau and Zukin, 2007).

Here, new molecular tools and methods to study Ca$_V$2.2 trafficking are developed. In addition, expression and trafficking of the exofacial-tagged Ca$_V$2.2 that have been previously developed (Cassidy et al., 2014) have been assessed for Ca$_V$2.2e37 splice variants to compare the difference in their cell surface expression and intracellular trafficking.

3.2 mEos-tagged Ca$_V$2.2

Photoactivatable fluorescent proteins are variants of fluorescent proteins, which can be activated by a specific wavelength to significantly change the excitation and emission wavelengths. Monomeric Eos2 (mEos2) is one of the recently developed photoactivatable proteins, which is functional at physiological temperature (i.e. at 37 °C), and its fluorescence is relatively stable (McKinney et al., 2009), therefore it is a good candidate as a tag to monitor the trafficking of Ca$_V$2.2 splice variants. The advantage of mEos-tagged Ca$_V$2.2 is

two-fold; 1) expression of the channel can be detected in live-cells without the need of immunocytochemistry, 2) green-to-red photoconverting mEos can be used to track the movement of the tagged-channels and monitored quantitatively as a ratio of red to green. mEos-tagged $Ca_V2.2$ splice variants were generated by attaching mEos sequence to the N-terminus of $Ca_V2.2$.

3.2.1 Biophysical properties of mEos-$Ca_V2.2$ splice variants

3.2.1.1 Whole-cell current of mEos-$Ca_V2.2$ splice variants

To determine whether mEos-$Ca_V2.2$ splice variants are functional, and mEos tag does not interfere with the biophysical properties of $Ca_V2.2$, the Ba^{2+} whole-cell current was recorded from these isoforms, which were expressed with $\alpha_2\delta$-1 and β1b in tsA-201. All of the electrophysiological recordings were performed in tsA-201, since the neuronal cell line N2a was not robust enough as an expression system for whole-cell patch clamp recordings (Appendix 1). The current density peak of mEos-Cav2.2e37a was greater than mEos-$Ca_V2.2$e37b (Figure 3.1a). The current density of the untagged $Ca_V2.2$e37b was not significantly different from the mEos-tagged $Ca_V2.2$e37b, suggesting that mEos at the N-terminus does not affect the biophysical properties of the channels. Activation voltage ($V_{50, act}$) was obtained from the fit of the modified Boltzmann equation, and showed that activation of $Ca_V2.2$e37a was significantly more hyperpolarised compared to $Ca_V2.2$e37b (Figure 3.1b). These properties of $Ca_V2.2$e37a and e37b currents are in agreement with the previous reports in expression systems (Bell et al., 2004; Castiglioni et al., 2006; Raingo et al., 2007) and in transgenic mice (Andrade et al., 2010).

a
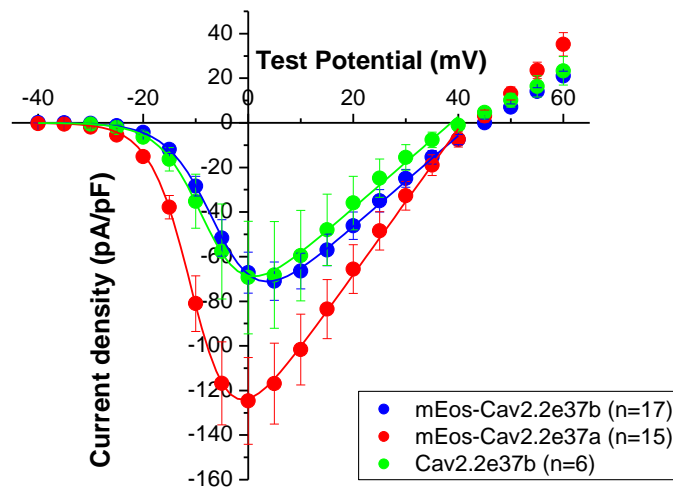
b
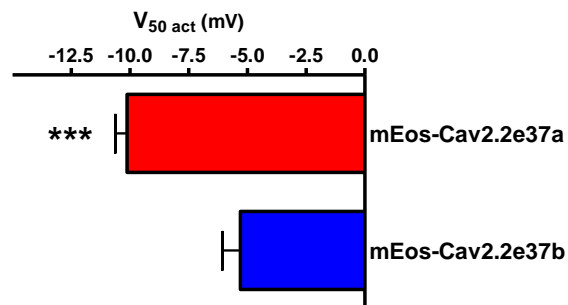
Figure 3.1 Whole-cell current of mEos-Ca$_V$2.2e37 splice variants.

(**a**) Whole-cell current densities of mEos-Ca$_V$2.2e37 isoforms and Ca$_V$2.2e37b control, expressed with β1b and α$_2$δ-1 in tsA-201. Peak current densities were; mEos-Ca$_V$2.2e37a, -124.6 ± 19.5 pA/pF at 0mV (n=15), mEos-Ca$_V$2.2e37b, -71.0 ± 8.6 pA/pF at +5mV (n=17), Ca$_V$2.2e37b, -69.4 ± 25.2 pA/pF at 0mV (n=6). (**b**) Activation voltage (V$_{50,act}$) of mEos-Ca$_V$2.2e37a was significantly more hyperpolarised than e37b. ***$P<0.001$ (Student's unpaired t-test).

3.2.1.2 Steady-state inactivation of mEos-Ca$_V$2.2 splice variants

To compare the inactivation of Ca$_V$2.2 splice variants, steady-state inactivation protocol (Figure 3.2a) was utilised. The normalised current showed that Ca$_V$2.2e37a was inactivated at a more hyperpolarised potential, compared to Ca$_V$2.2e37b (Figure 3.2b). Inactivation voltage (V$_{50, inact}$) determined from the sigmoidal curve fit reveals that the V$_{50, inact}$ of Ca$_V$2.2e37a was modestly but significantly more negative than Ca$_V$2.2e37b (Figure 3.2c).

3.2.1.3 Effect of β subunits on mEos-Ca$_V$2.2 splice variants

β1b (brain isoform of β1) and β3 (neuronal) are the isoforms of β subunits that are likely to be expressed where Ca$_V$2.2 channels are important. To determine whether different β isoforms affect the biophysical properties of the tagged Ca$_V$2.2 splice variants, Ca$_V$2.2e37b was expressed with either β1b or β3 in the presence of α$_2$δ-1, and the whole-cell current was recorded. The current-voltage (IV) relationships of Ca$_V$2.2e37b with β1b and β3 were largely identical. In addition, Ca$_V$2.2e37a with β3 also showed a greater whole-cell current density (Figure 3.3a). V$_{50, act}$ of Ca$_V$2.2e37a was significantly shifted to a more hyperpolarised potential than Ca$_V$2.2e37b in the presence of β3, similarly to the findings with β1b (Figure 3.3b). Therefore, I conclude that the biophysical properties of Ca$_V$2.2e37 isoforms with β1b and β3 are very similar to each other.

a
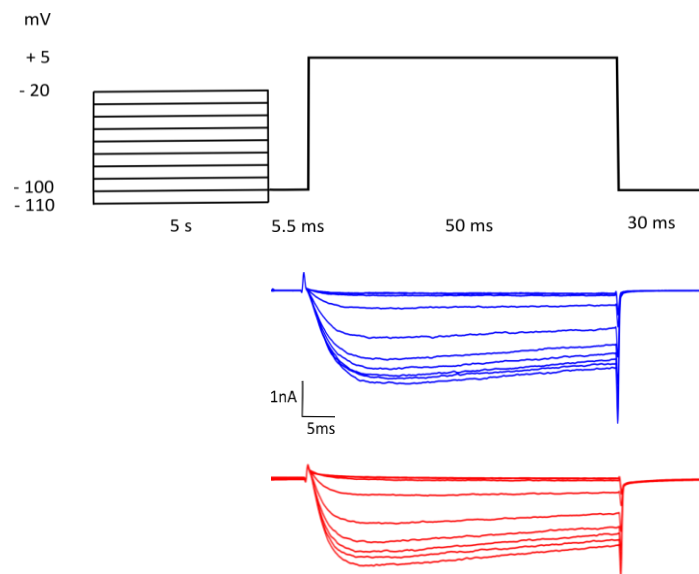
b
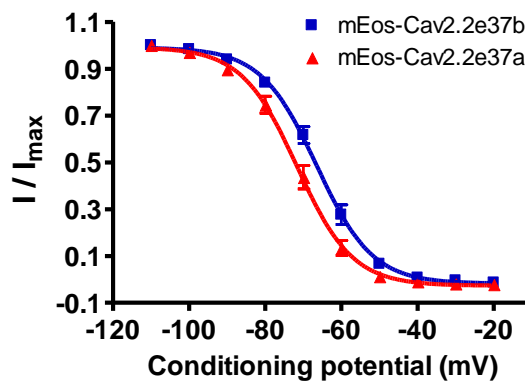
c
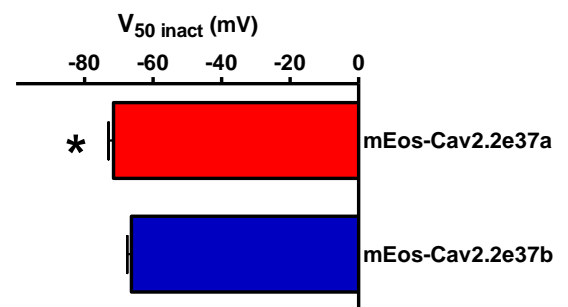
Figure 3.2 Steady-state inactivation of mEos-Ca$_V$2.2e37 isoforms.

(**a**) Schematic diagram of the steady-state inactivation protocol (top), and exemplary whole-cell current traces of mEos-Ca$_V$2.2e37b (blue) and e37a (red), expressed with β1b and α$_2$δ-1 in tsA-201. (**b**) The average relative current from steady-state inactivation of Ca$_V$2.2e37 isoforms. (**c**) Half-maximal inactivation voltage (V$_{50,inact}$) obtained from (b). V$_{50,inact}$ of mEos-Ca$_V$2.2e37a was significantly more hyperpolarised than e37b. *$P<0.05$ (Student's unpaired t-test).

a
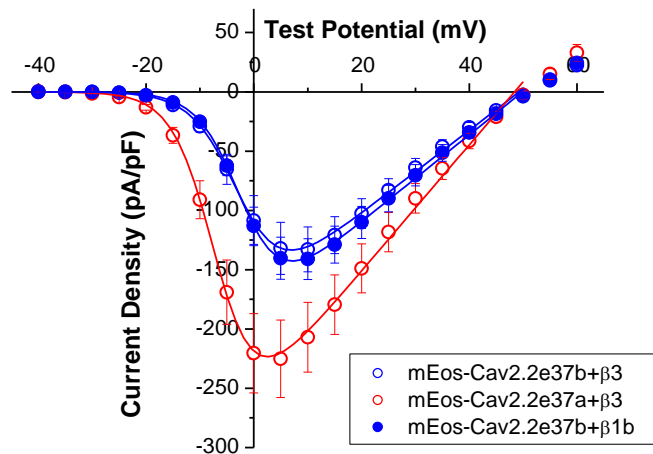
b
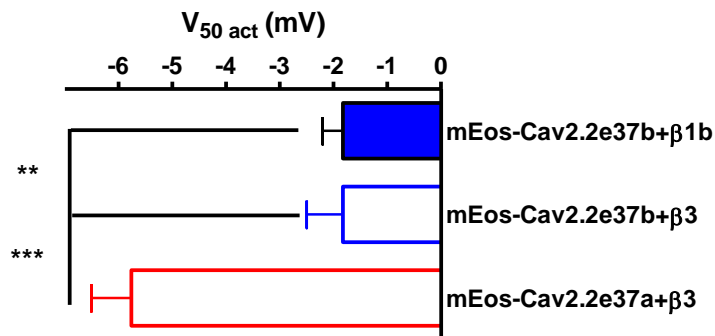
Figure 3.3 Effect of β1b and β3 on mEos-Ca$_V$2.2e37 splice variants.

(**a**) Whole-cell current densities of mEos-Ca$_V$2.2e37 isoforms with β3 and mEos-Ca$_V$2.2e37b with β1b as a control, expressed with $\alpha_2\delta$-1 in tsA-201. Peak current densities were; mEos-Ca$_V$2.2e37a+β3, -225.2 ± 32.7 pA/pF at 5mV (n=14); mEos-Ca$_V$2.2e37b+β3, -132.9 ± 18.3 pA/pF at 10mV (n=12); mEos-Ca$_V$2.2e37b+β1b, -141.1 ± 17.1 pA/pF at 10mV (n=5). (**b**) Activation voltage (V$_{50,act}$) of mEos-Ca$_V$2.2e37a was significantly more hyperpolarised than e37b with β1b or β3. **$P<0.01$, ***$P<0.001$ (one-way ANOVA).

3.2.2 Cellular localisation of mEos-tagged Ca$_V$2.2

To determine the protein expression patterns in N2a cells, mEos-tagged Ca$_V$2.2e37b was transiently expressed with α$_2$δ-1 and β1b (Figure 3.4). Firstly, the fluorescence intensity from mEos-Ca$_V$2.2e37b on average appeared lower in comparison to GFP-tagged Ca$_V$2.2e37b. Secondly, some cells expressed mEos-Ca$_V$2.2 possibly at the plasma membrane, which was exhibited as a ring-like expression pattern, separate from the intracellularly accumulated channels. However, cell surface localisation of the tagged-channels is difficult to determine reliably without a plasma membrane marker, which is essential for comparing the cell surface expression of Ca$_V$2.2 splice variants.

3.2.3 Photoconversion of mEos-Ca$_V$2.2

mEos2 undergoes green-to-red photoconversion when it is exposed to 405 nm wavelengths (McKinney et al., 2009). A small region of N2a cell expressing mEos-Ca$_V$2.2e37b in a glass-bottom dish was photoactivated under a confocal microscope with a localised laser at 405 nm, and the fluorescence signal of both green and red channels were recorded continuously for 100 frames (Figure 3.5). Prior to the photoactivation, there was no fluorescence in the red channel. Immediately after the photoactivation, the red fluorescence appeared in the region of excitation, but it was not localised as weaker red fluorescence was also observed around the region (Figure 3.5, right column). In addition, the green fluorescence was also increased after photoactivation over the entire cell (Figure 3.5, left column). This observation was unexpected and has not been reported in any literature, but this increase in the green fluorescence was observed in all the cells analysed. It is possible that the laser exposure is causing a change in intracellular pH, which alters the fluorescence level temporarily, however, lowering the laser power and exposure length was ineffective in photoactivation. Nonetheless, monitoring the channel movement to and from the plasma membrane could not be achieved with this method, as the photoconversion could not be localised to a sufficiently small region such as plasma membrane, and there were significant signal decay over a long period of time due to photobleaching.
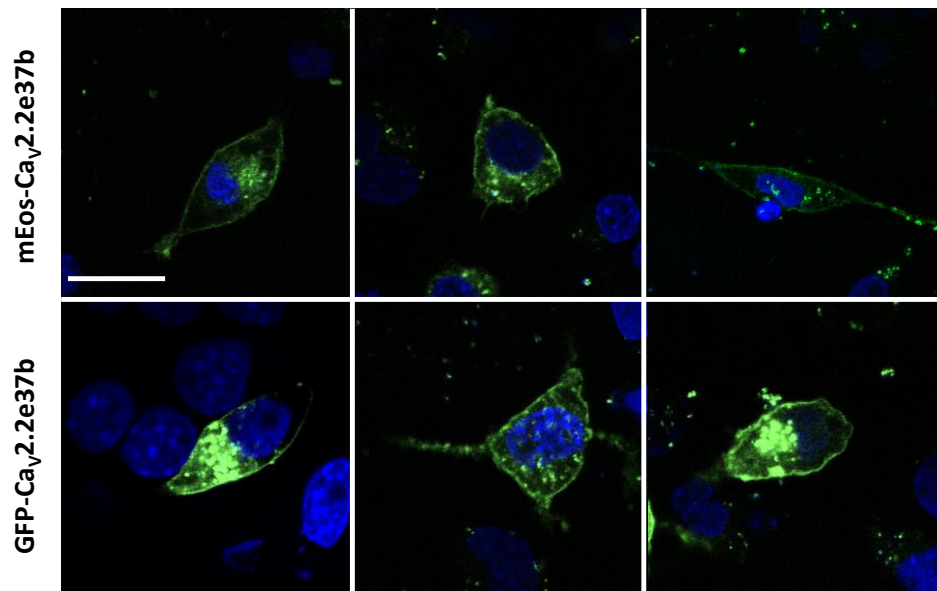
Figure 3.4 mEos- and GFP-tagged Ca$_V$2.2e37b in N2a cells.

Exemplary confocal images of N2a cells expressing mEos- (top) and GFP-(bottom) tagged Cav2.2e37b with β1b and α$_2$δ-1, demonstrating the heterogeneous expression of these constructs.. Plasma membrane-like expression is observed from both constructs, albeit weak in some cells. Most of cells exhibited aggregated expression of the tagged-channels around the nuclei. In general, fluorescence intensity of GFP-Ca$_V$2.2e37b appeared stronger than mEos-Ca$_V$2.2e37b. Scale bar, 20 μm
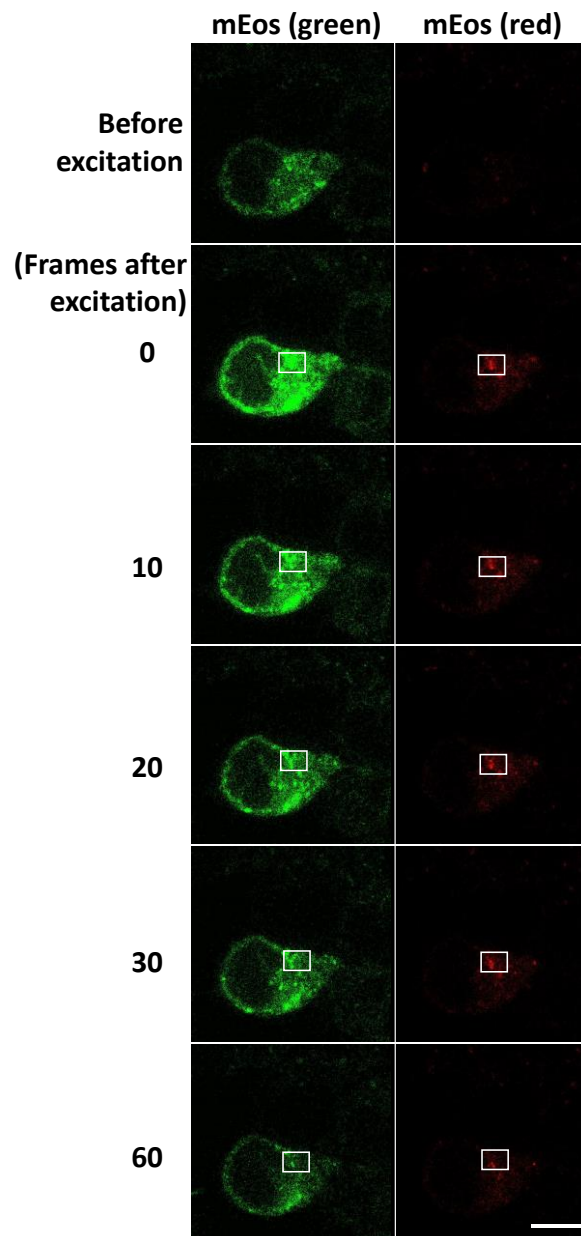
Figure 3.5 Photoconversion of mEos-Ca$_V$2.2.

N2a expressing mEos-Ca$_V$2.2e37b with β1b and α$_2$δ-1 was imaged on a confocal microscope with a temperature-control chamber at 37 °C. The white box indicates the region of excitation at 405 nm for green-to-red photoconversion of mEos2. Green channel (left, excitation 488 nm, emission 490-562 nm), red channel (right, excitation 543 nm, emission 562-650 nm), scale bar, 20 μm.

3.3 Cell surface biotinylation

A high affinity interaction between biotin and avidin is a useful tool in immunocytochemistry and western blot, as the side chain of biotin forms a covalent link with a lysine residue in a protein of interest, which remains conjugated. This is particularly useful and has been used frequently for examining transmembrane proteins. Biotin can be used to selectively label transmembrane proteins by applying biotin to intact cells extracellularly, without detecting the intracellular proteins.

To examine the cell surface expression of Ca$_V$2.2 splice variants in tsA-201, the cell surface proteins including Ca$_V$2.2 were labelled extracellularly with biotin before the cells were lysed. Biotin-conjugated Ca$_V$2.2 was precipitated with streptavidin-coated beads, and detected with a specific antibody against Ca$_V$2.2. Ca$_V$2.2 splice variants were successfully expressed and detected in the cell lysis, however, the biotin-coupled Ca$_V$2.2 was hardly detected, despite that $\alpha_2\delta$-1 co-expressed with Ca$_V$2.2 was successfully detected in both fractions (Figure 3.6). The protein-load for streptavidin-precipitation was therefore doubled, and as a result biotinylated Ca$_V$2.2 splice variants were detected (Figure 3.7). The band intensities for both biotinylated Ca$_V$2.2 and $\alpha_2\delta$-1 from cells expressing Ca$_V$2.2e37a were consistently lower than those expressing Ca$_V$2.2e37b, even though the whole-cell expression of these subunits were similar. The difference in cell surface expression of $\alpha_2\delta$-1 in the cells expressing Ca$_V$2.2e37a and 37b was unexpected, but it is unlikely that cell surface expression of $\alpha_2\delta$-1 is modulated in this expression system, which makes the interpretation of the difference in biotinylated Ca$_V$2.2 splice variants difficult. In addition, untagged Ca$_V$2.2e37b was not detected in the biotinylated fraction in this experiment (Figure 3.7). Overall, this experiment is not robust enough to reliably compare the cell surface expression of Ca$_V$2.2 splice variants and examine the factors that affect Ca$_V$2.2 cell surface expression.
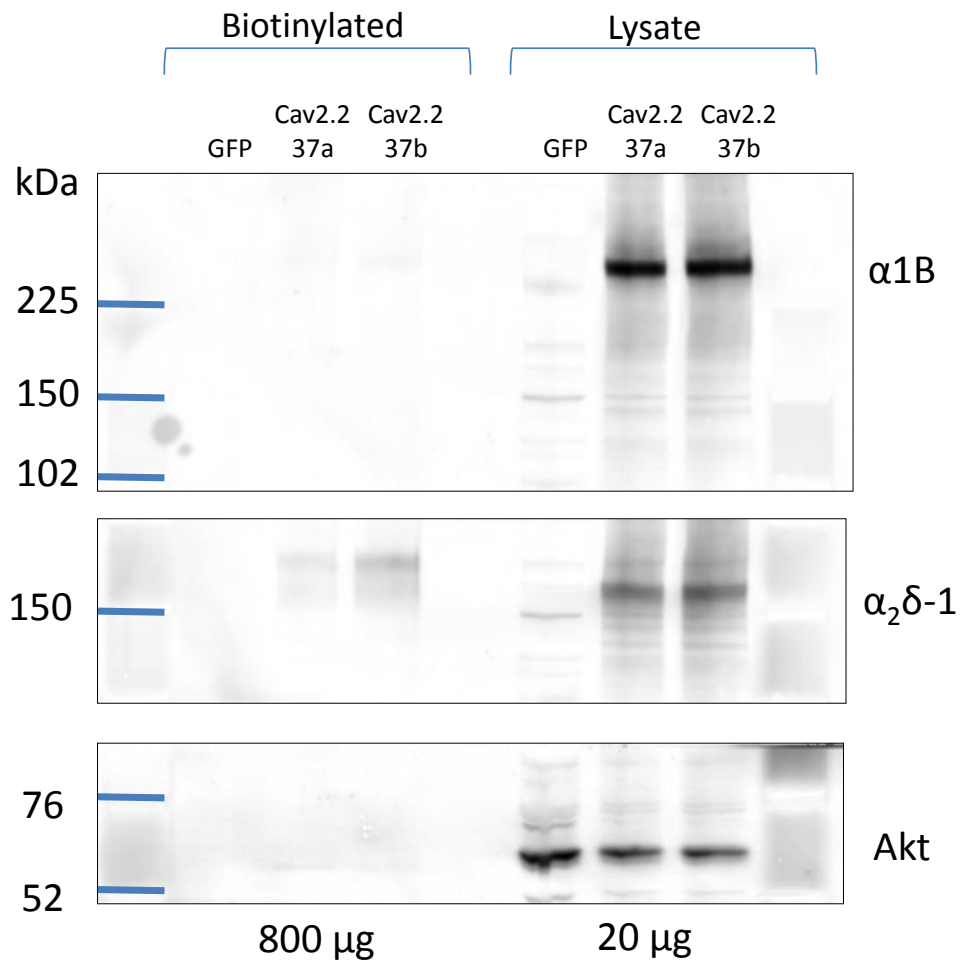
Figure 3.6 Cell surface biotinylation of Ca$_V$2.2 splice variants.

Biotin-labelled Ca$_V$2.2 (top) precipitated with streptavidin (left) and whole-cell lysate (right). $\alpha_2\delta$-1 (middle) was detected as a positive control, showing the glycosylated and non-glycosylated form as separate bands. Soluble protein Akt (bottom) was shown as a negative control for biotinylation, and as a protein loading control in lysate blot. 800 µg lysate was loaded on the streptavidin-coated beads for precipitation. 20 µg lysate per lane was loaded as a protein expression control.

Figure 3.7 Cell surface biotinylation of Ca$_V$2.2 splice variants.

Biotin-labelled Ca$_V$2.2 (top) precipitated with streptavidin (left) and whole-cell lysate (right). α$_2$δ-1 (middle) was detected as a positive control, and soluble protein Akt (bottom) was shown as a negative control. 1600 µg lysate was loaded on the streptavidin-coated beads for precipitation. 15 µg lysate per lane was loaded as a protein expression control.

3.4 BBS-tagged Ca$_V$2.2

Labelling with bungarotoxin (BTX) by inserting a short sequence of the bungarotoxin binding site (BBS) into an extracellular region of transmembrane proteins has proven useful for monitoring intracellular trafficking of a number of receptors and channels in live cells (Sekine-Aizawa and Huganir, 2004; Wilkins et al., 2008; Bogdanov et al., 2006; Tran-Van-Minh and Dolphin, 2010; Cassidy et al., 2014). Taking advantage of the recently developed BBS-tagged Ca$_V$2.2e37b (Cassidy et al., 2014), two BBS sequences in tandem were inserted into the extracellular loop of Ca$_V$2.2e37a to generate BBS-tagged Ca$_V$2.2e37a.

To test the channel function of BBS-Ca$_V$2.2e37a and e37b, the whole-cell current densities were determined by transient expression in tsA-201 with $\alpha_2\delta$-1 and β1b. In order to examine the trafficking of Ca$_V$2.2e37 isoforms to and from the plasma membrane with BTX-labelling, the effect of BTX-binding itself on Ca$_V$2.2 surface expression was also determined by comparing the whole-cell current densities with and without BTX.

Both BBS-Ca$_V$2.2e37a and e37b channels were fully functional as previously described (Figure 3.8). The presence of BTX did not affect the whole-cell current densities of the Ca$_V$2.2e37 isoforms, indicating that BTX itself does not modulate the overall cell surface expression of Ca$_V$2.2.

a
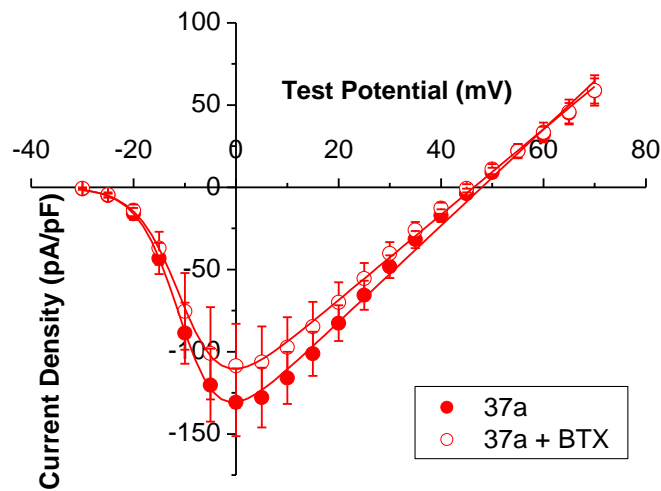
b
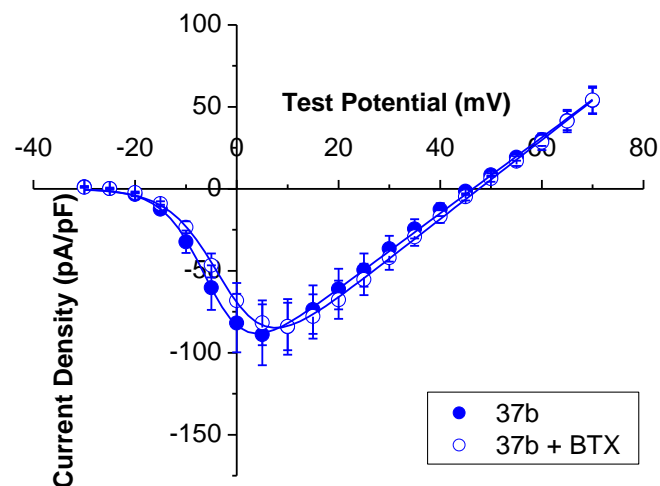
Figure 3.8 Whole-cell current densities of BBS-Ca$_V$2.2e37 splice variants in the presence and absence of BTX.

The whole-cell current densities of BBS-Ca$_V$2.2e37 splice variants expressed with β1b and α$_2$δ-1 in tsA-201 were determined in the presence and absence of 10 µg/ml BTX in the extracellular solution. (**a**) Whole-cell current densities of BBS-Ca$_V$2.2e37a. No BTX (red closed circle), n=14. With BTX (red open circle), n=15. (**b**) Whole-cell current densities of BBS-Ca$_V$2.2e37b. No BTX (blue closed circle), n=11. With BTX (blue open circle), n=8.

3.4.1 Live cell imaging of BBS-Ca$_V$2.2

To compare the intracellular trafficking kinetics of Ca$_V$2.2e37 isoforms, it was necessary to understand the time course at which Ca$_V$2.2 internalises from the cell surface. Turnover durations of VGCCs are poorly understood so far, mainly due to the lack of molecular tools to monitor their trafficking.

Fluorescently labelled BTX, BTX-488 was incubated with N2a cells expressing BBS-Ca$_V$2.2e37 isoforms for 30 min at 17 °C and washed off prior to the start of the imaging in glass-bottom dishes, and fluorescence intensity at the plasma membrane was monitored by taking time-lapse images on a confocal microscope over the 60-min time course in the temperature-controlled chamber at 37 °C and 20 °C to determine the temperature effect on the cell surface Ca$_V$2.2 (Figure 3.9). At 37 °C which is the physiological temperature, a majority of the BTX-labelled cell surface Ca$_V$2.2 was internalised by 15 min after the start of the recording and some intracellular puncta were observed, however, these puncta were not observed as an accumulation, suggesting either that the BTX-488 dissociates from the channels after endocytosis, or the internalised channels are degraded. By the 30 min-time point, there were hardly any labelled channels left at the plasma membrane (Figure 3.9). On the other hand, at 20 °C there was still a considerable amount of labelled Ca$_V$2.2 in the plasma membrane at 30 min after the start of the experiments, as the internalising events were drastically reduced at this temperature compared to 37 °C (Figure 3.9).
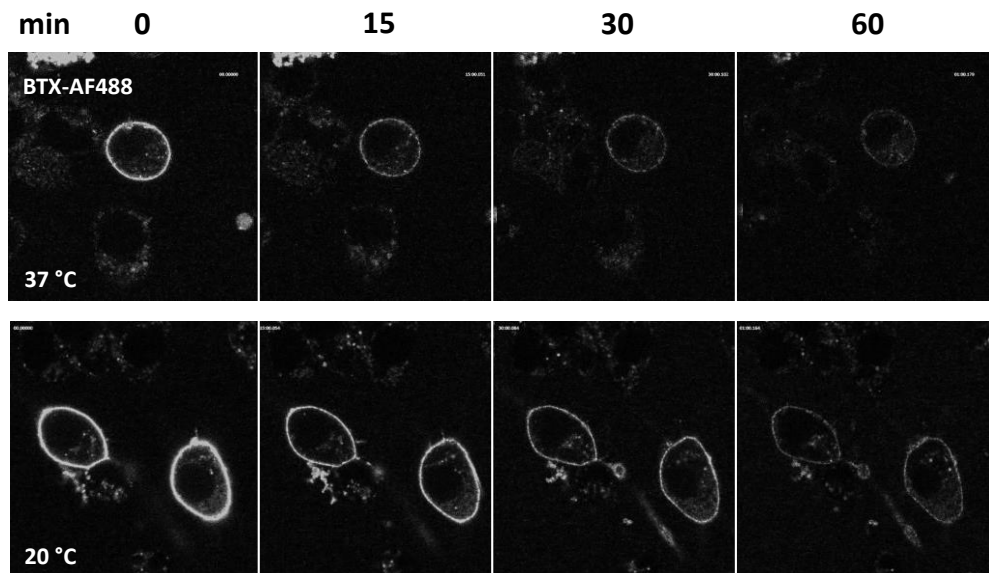
Figure 3.9 Time-lapse images of cell surface BBS-Ca$_V$2.2 in N2a cells at 37 °C and 20 °C.

Live N2a cells expressing BBS-Ca$_V$2.2e37b were labelled with BTX-488 for 30 min at 17 °C and washed off prior to the start of the imaging, and the time-lapse images were taken on a confocal microscope every 5 min at a fixed gain over 60 min. The effect of incubation temperature on cell surface Ca$_V$2.2 were demonstrated at 37 °C (top) and 20 °C (bottom).

3.4.2 Endocytosis and forward trafficking assays of BBS-Ca$_V$2.2

In order to maximise the sampling number per condition in one experiment, N2a cells with BTX-labelled Ca$_V$2.2 were fixed at various times after the start of the experiment. The cells were also post-stained with Ca$_V$2.2 antibodies as an expression marker to aid the selection of the cells expressing Ca$_V$2.2, rather than selecting cells that have cell surface staining to avoid bias.

3.4.2.1 BBS-Ca$_V$2.2 endocytosis assay optimisation

To monitor and compare endocytosis of Ca$_V$2.2 splice variants, the following protocol was established, which is explained in a schematic diagram (Figure 3.10). During the labelling step, BBS-Ca$_V$2.2 was incubated with 10 µg/ml BTX-488 at 17 °C for 30 min to label all of the channels at the cell surface by minimising the internalisation which occurs at faster rate at higher temperature.   All the washes were performed on the bench at room temperature. The endocytosis experiment was performed at 37 °C, and cells were fixed with PFA on ice immediately at various time points to minimise further channel internalisation during fixation. As shown in the initial experiment at 37 °C, the Ca$_V$2.2 internalisation occurs relatively fast during the first 15 min, therefore the cells were sampled at 0, 5, 10, 20 and 40 min after the start of the experiment (Figure 3.11).   The BTX-labelled cell surface BBS-Ca$_V$2.2 was internalised and increasing numbers of intracellular puncta were observed during the experiment. By 20 min after the start of the experiment, most of the cell surface Ca$_V$2.2 was internalised. In this protocol, the cells were exposed to multiple washes and more prone to detachment from the dishes. Therefore, a higher seeding density (1:25-30 cell dilution) was required prior to the transfection, compared to that for the standard immunocytochemistry experiment (1:40-60 cell dilution), for a successful experiment. Quantification of cell surface BBS-Ca$_V$2.2e37 isoforms and their endocytosis rates will be discussed in Chapter 4.

A limitation of this experiment is that 1) internalised BTX-labelled Ca$_V$2.2 can be recycled and re-appear on the cell surface, which cannot be distinguished, 2) there may be a dissociation of BTX from the cell surface Ca$_V$2.2, independent of channel endocytosis.   Association and dissociation

kinetics of BTX at 37 °C have not been reported, although at 20 °C it poses a minor factor in the disappearance of the BTX label (Salvaterra and Mahler, 1976; Cassidy et al., 2014). In addition, when the experiment was carried out at 4 or 20 °C, the majority of the cell surface Ca$_V$2.2 remained at the plasma membrane (Figure 3.12). Diffusion of small molecules such as BTX is less temperature-dependent compared to biological processes such as endocytosis. Therefore, the rate of endocytosis by this method should be relatively representative of the physiological event.
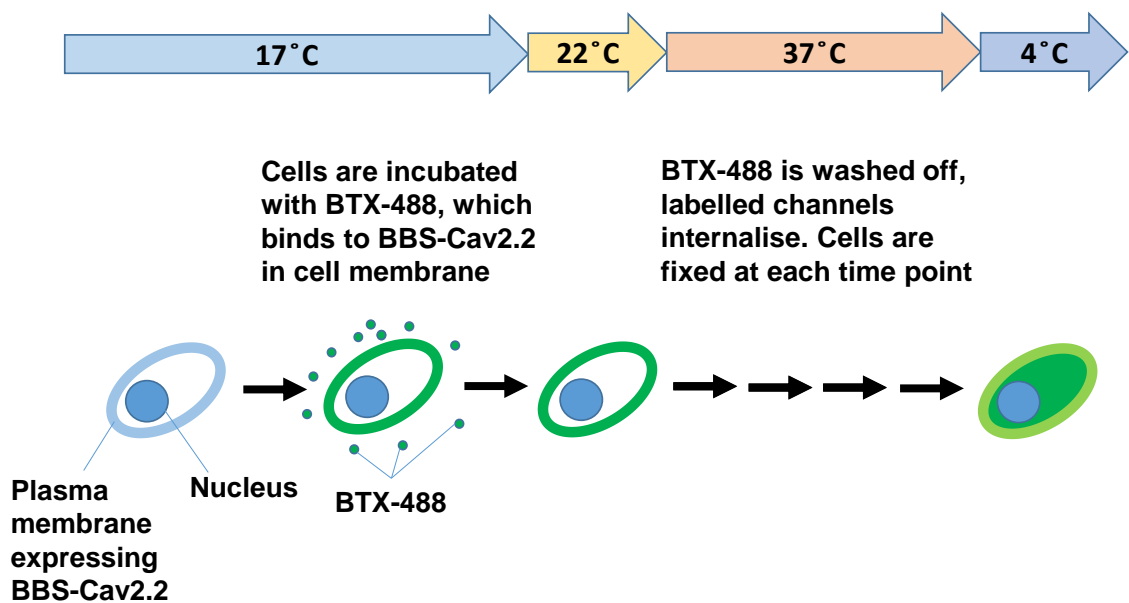
Figure 3.10 BBS-Ca$_V$2.2 endocytosis assay protocol.

During the labelling step, N2a cells expressing BBS-Ca$_V$2.2 with β1b and α$_2$δ-1 was incubated with 10 μg/ml BTX-488 at 17 °C for 30 min to label all of the channels at the cell surface. Unbound BTX-488 was washed off at room temperature. The endocytosis experiment was performed at 37 °C, and cells were fixed with PFA on ice immediately at various time points to minimise further channel internalisation during fixation.
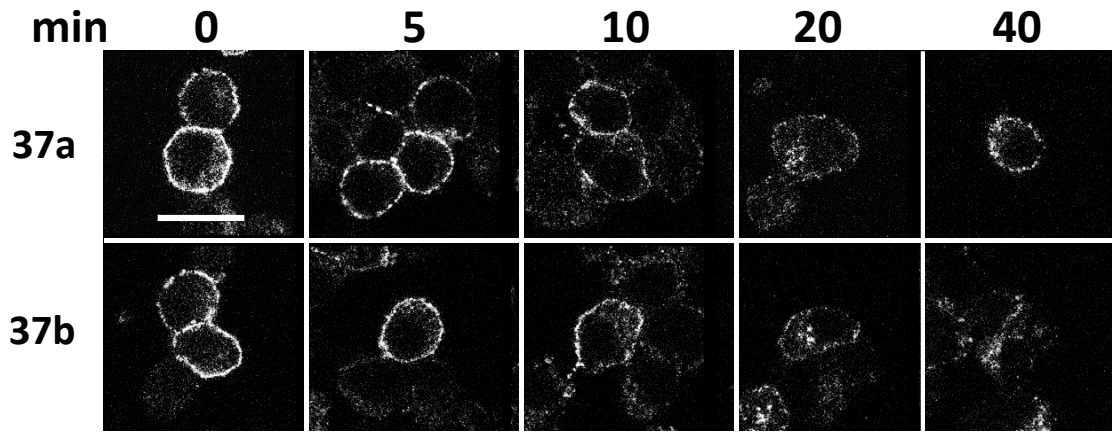
Figure 3.11 Endocytosis of BBS-Ca$_V$2.2 splice variants.

Exemplary confocal images of N2a cells expressing BBS-Ca$_V$2.2e37a (top) and e37b (bottom) with β1b and α$_2$δ-1 from an endocytosis experiment. The cells were fixed with 4 % PFA at 0, 5, 10, 20 and 40 min after the start of the experiment at 37 °C. Reduction of BTX-488 at the cell surface at later time points indicates the Ca$_V$2.2 endocytosis. Scale bar, 20 μm.
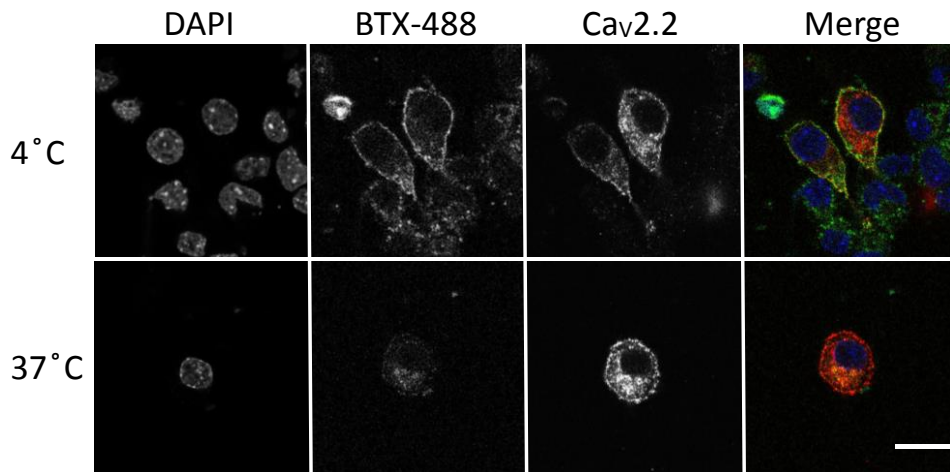
Figure 3.12 BBS-Ca$_V$2.2 endocytosis is blocked at 4 °C.

Exemplary confocal images of N2a cells expressing BBS-Ca$_V$2.2e37b in endocytosis experiments at 4 °C (top) and 37 °C (bottom) at 40 min. BBS-Ca$_V$2.2 remains at cell surface at 4 °C, which indicates that the channel endocytosis is blocked at this temperature, and very little dissociation of BTX from the cell surface Ca$_V$2.2 during this time period. DAPI (blue), BTX-488 (green), Ca$_V$2.2 (red). Scale bar, 20 μm.

3.4.2.2 Forward trafficking (exocytosis) assay optimisation

A forward trafficking experiment to monitor the Ca$_V$2.2 appearance at the cell surface was established in a similar manner to the endocytosis protocol, which was described above (Figure 3.13 and Figure 3.14). The same concentration of unlabelled BTX as the BTX-488 (10 µg/ml) was applied to saturate the entire cell surface Ca$_V$2.2. This concentration was sufficient as there was no Ca$_V$2.2 labelling by BTX-488 when the experiment was carried out at 4 °C to block any movement of the channels in the plasma membrane (Figure 3.15). Quantification of cell surface BBS-Ca$_V$2.2e37 isoforms and their forward trafficking rates will be discussed in Chapter 4.

| 17˚C | 22˚C | 37˚C | 4˚C |

Cells are incubated with BTX, which binds to BBS-Cav2.2 in cell membrane

BTX is washed off, cells are incubated with BTX-488, which binds to unlabelled channels trafficked to cell membrane

BTX-488 is washed off, cells are fixed at each time point

BTX

BTX-488
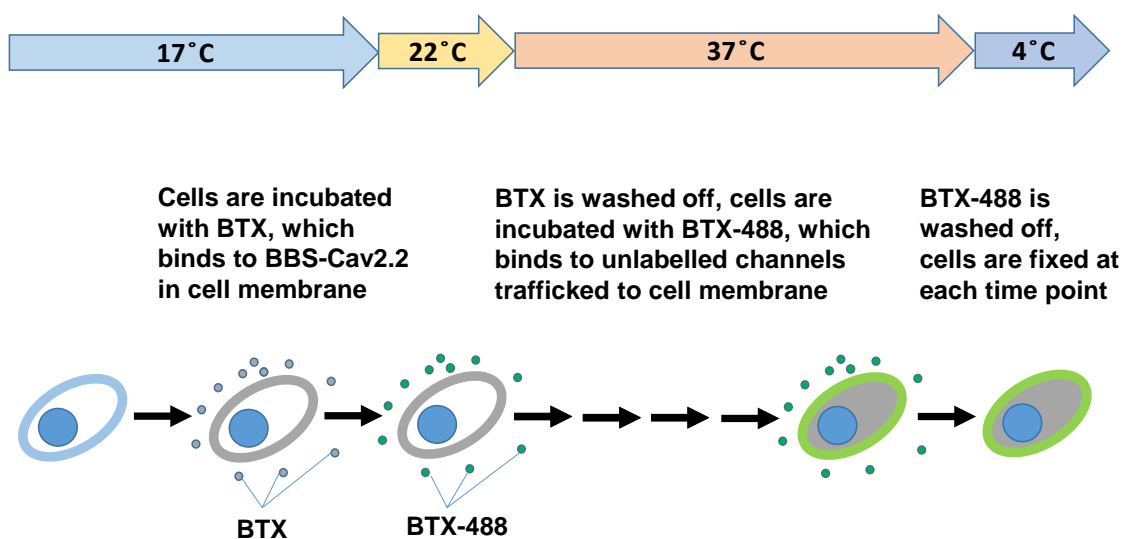
Figure 3.13 BBS-Ca$_V$2.2 forward trafficking protocol.

During the blocking step, N2a cells expressing BBS-Ca$_V$2.2 with β1b and α$_2$δ-1 was incubated with 10 µg/ml unconjugated BTX at 17 °C for 30 min to label all of the channels at the cell surface. Unbound BTX was washed off at room temperature, and 10 µg/ml BTX-488 was added to the cells to label newly inserted channels at the cell surface during the forward trafficking experiment, performed at 37 °C. The cells were fixed with 4 % PFA on ice immediately at various time points to minimise further channel internalisation during fixation.
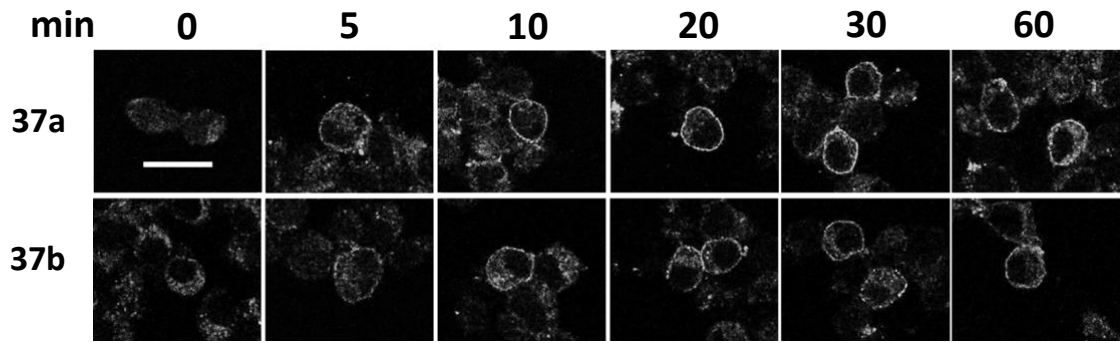
Figure 3.14 Forward trafficking of BBS-Ca$_V$2.2 splice variants.

Exemplary confocal images of N2a cells expressing BBS-Ca$_V$2.2e37a (top) and e37b (bottom) with β1b and α$_2$δ-1 from a forward trafficking experiment. The cells were fixed with 4 % PFA at 0, 5, 10, 20, 40 and 60 min after the start of the experiment at 37 °C. Increase in BTX-488 at the cell surface at later time points indicates an increase in newly inserted Ca$_V$2.2 in the plasma membrane from the forward trafficking. Scale bar, 20 µm.
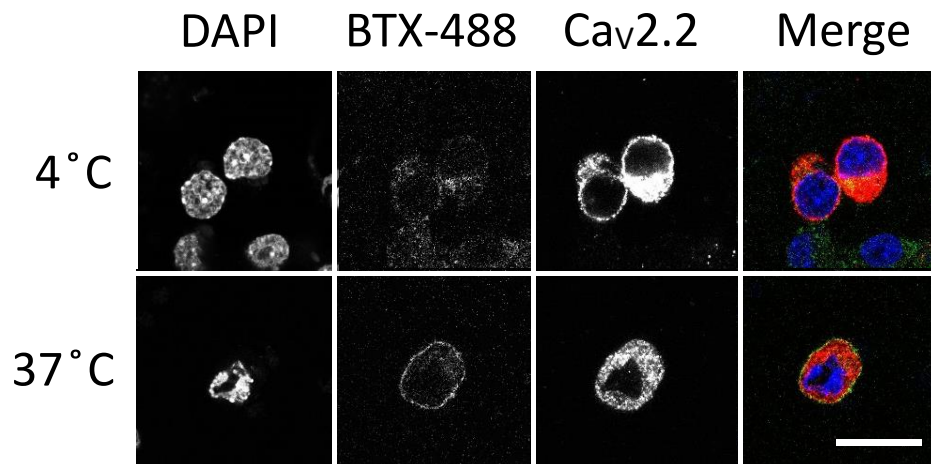
Figure 3.15 No BBS-Ca$_V$2.2 forward trafficking at 4 °C.

Exemplary confocal images of N2a cells expressing BBS-Ca$_V$2.2e37b in forward trafficking experiments at 4 °C (top) and 37 °C (bottom) at 60 min. No surface staining of BBS-Ca$_V$2.2 is observed at 4 °C, indicating the forward trafficking does not occur at this temperature. DAPI (blue), BTX-488 (green), Ca$_V$2.2 (red). Scale bar, 20 µm.

3.4.3 Monitoring BBS-Ca$_V$2.2 trafficking in neurons

In order to examine the trafficking of Ca$_V$2.2 splice variants in neurons using BBS-tagged Ca$_V$2.2 constructs, rat hippocampal neurons were chosen as the most robust expression system, as they provide more tissue per animal, thus more neurons in each experiment to test multiple conditions such as transfection and immunostaining protocols than DRG neurons. Before expressing BBS-Cav2.2 in the hippocampal neurons, the background signal from BTX-488 binding was assessed, as these neurons express a large number of endogenous nicotinic acetylcholine receptors (Salvaterra and Mahler, 1976), and the acetylcholine binding site of these receptors are also bound by BTX with a sub-nM affinity (Tzartos and Changeux, 1983). A competitive antagonist of the nicotinic acetylcholine receptor, tubocurarine was used to block the BTX binding (Wenningmann and Dilger, 2001). 100 µM tubocurarine was sufficient in reducing the background signal from BTX-488 in cultured hippocampal neurons (Figure 3.16).

| | DAPI | BTX-488 | βIII-tubulin | Merge |
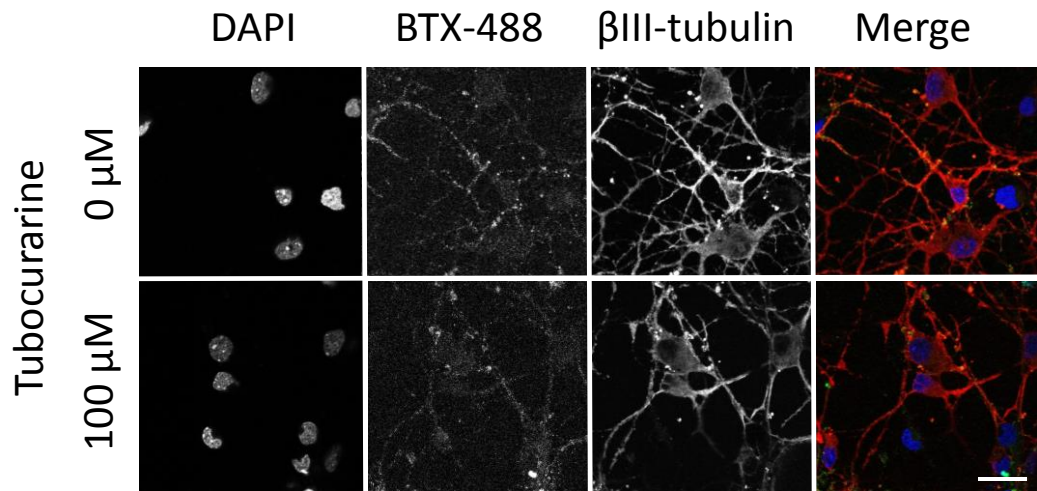
Figure 3.16 Endogenous binding of BTX in rat hippocampal neurons.

Exemplary confocal images of cultured hippocampal neurons labelled with BTX-488 in the presence or absence of tubocurarine. BTX-488 (green) binds to endogenous nicotinic acetylcholine receptors in cultured hippocampal neurons to give a high background signal (top). 100 µM tubocurarine, a competitive antagonist, reduced the background signal from BTX-488 (bottom). βIII-tubulin (red) was used as a neuronal marker. DAPI (blue), scale bar, 20 µm.

3.5 HA-tagged Ca$_V$2.2

To compare the subcellular localisation of Ca$_V$2.2 isoforms containing e37a or e37b, both channels were exofacially-tagged with haemagglutinin (HA) as described previously to generate HA-tagged Ca$_V$2.2e37 splice variants (Cassidy et al., 2014). The advantage of HA-tagged Ca$_V$2.2 is that detection by secondary and possibly tertiary antibodies can amplify the signal. Furthermore, HA-antibody labelling gives more options for confocal microscopy analysis as it allows the use of more than one channel, compared to other tags discussed in this chapter, which is useful in dual labelling with multiple proteins.

3.5.1 Biophysical properties of HA-tagged Ca$_V$2.2 splice variants

3.5.1.1 Whole-cell current density of Ca$_V$2.2e37 isoforms

First, to demonstrate that the exofacial tag does not affect the function of the Ca$_V$2.2 splice variant channels, whole-cell Ba^{2+} currents were recorded from tsA-201 cells that are transiently expressing HA-tagged Ca$_V$2.2e37a and Ca$_V$2.2e37b, together with the auxiliary subunits α$_2$δ-1 and β1b. The average whole-cell current density of Ca$_V$2.2e37a was significantly larger than that of Ca$_V$2.2e37b at test potentials between -25 mV and 15 mV (Figure 3.17), which was in agreement with the previous reports (Bell et al., 2004; Castiglioni et al., 2006; Raingo et al., 2007).

3.5.2 Conductance and activation voltage

The whole-cell conductance (G$_{max}$) and the half-maximal activation voltage (V$_{50,act}$) were determined from fitting the IV curves to the modified Boltzmann equation. The average G$_{max}$ for Ca$_V$2.2e37a currents was approximately 1.5-fold greater than Ca$_V$2.2e37b currents (Figure 3.18a). Furthermore, Ca$_V$2.2e37a channels were activated at a more hyperpolarized potential than those containing e37b (Figure 3.18b). These properties of Ca$_V$2.2e37a and e37b currents are in agreement with the previous reports in expression systems (Bell et al., 2004; Castiglioni et al., 2006; Raingo et al., 2007) and in transgenic mice (Andrade et al., 2010).

a

b
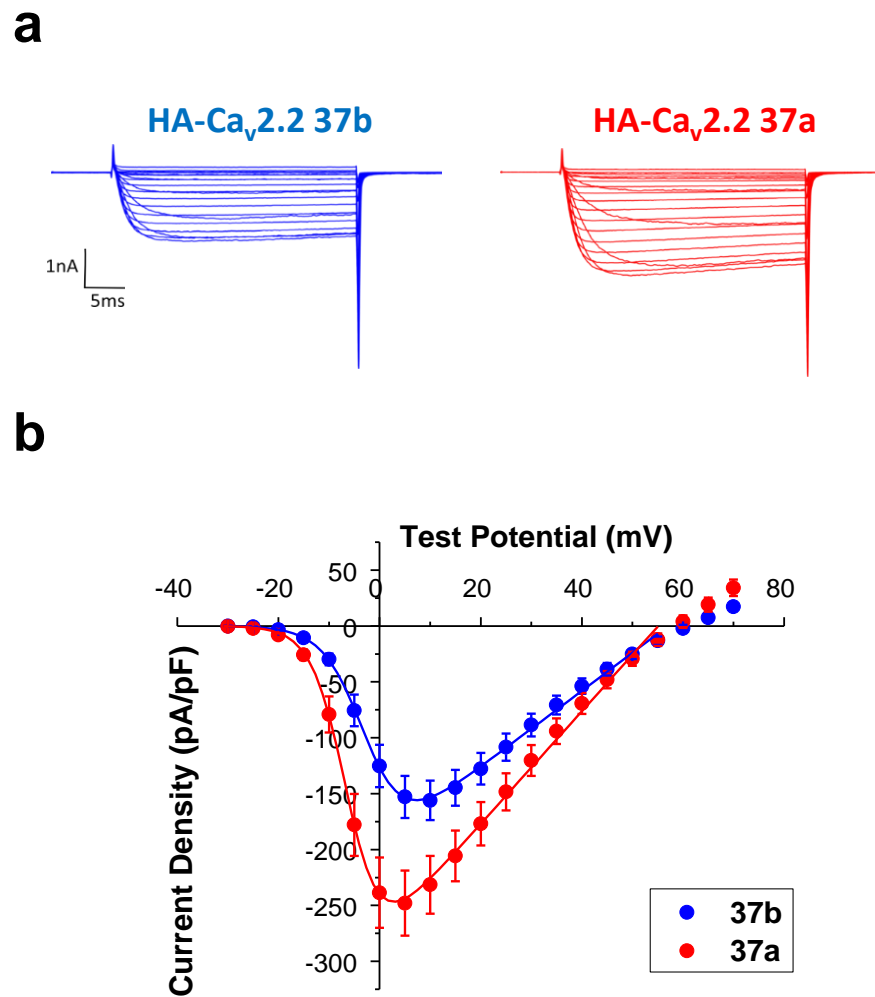
Figure 3.17 Whole-cell current density of HA-tagged Ca$_V$2.2e37 splice variants.

(**a**) Exemplary traces of HA-Ca$_V$2.2e37b (left, blue) and e37a (right, red) whole-cell current in tsA201, expressed with β1b and α$_2$δ-1. (**b**) Average whole-cell current density of HA-tagged Ca$_V$2.2e37a and e37b. The average peak current density was: Ca$_V$2.2e37a (red), -245.0 ± 29.1 pA/pF at +5mV (n=22); Ca$_V$2.2e37b (blue), -156.0 ± 17.7 pA/pF at +10mV (n=24).
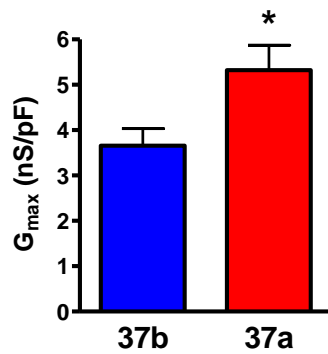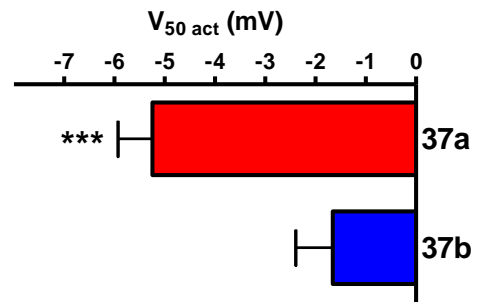
Figure 3.18 Conductance (G_{max}) and activation voltage ($V_{50, act}$) of HA-Ca$_V$2.2e37a and e37b.

The values of G_{max} and $V_{50,act}$ were determined from fitting each IV curve to the modified Boltzmann equation (see method). (**a**) The average G_{max} of Ca$_V$2.2e37a (red, n=22) was significantly larger than Ca$_V$2.2e37b (blue, n=24). (**b**) $V_{50,act}$ of Ca$_V$2.2e37a (red, n=22) was significantly more hyperpolarised compared with Ca$_V$2.2e37b (blue, n=24). *$P<0.05$, ***$P<0.001$, Student's unpaired t-test.

3.5.3 G protein-mediated inhibition of Ca$_V$2.2e37 isoforms

In order to determine whether the exofacial tagged Ca$_V$2.2e37 isoforms also exhibited differential voltage-dependence upon GPCR activation, in a similar manner to that previously reported (Raingo et al., 2007; Andrade et al., 2010), D2R was co-expressed with Ca$_V$2.2 isoforms in the presence of $\alpha_2\delta$-1 and β1b. Using a double pulse protocol (Figure 3.19a), Ca$_V$2.2e37a and Ca$_V$2.2e37b currents (P1) were inhibited by the D2R selective agonist, quipirole (Quin, Tsuruta et al., 1981). When a large depolarising pulse was applied just prior to the second test pulse (P2) in the presence of Quin, Ca$_V$2.2e37a exhibited significantly smaller relative currents (P2/P1), compared to Ca$_V$2.2e37b (Figure 3.19b). This voltage-independent inhibition of Ca$_V$2.2e37a by D2R activation largely agrees with previous findings with GABA$_B$ and μ-opioid receptor activation in expression systems and in transgenic mice (Raingo et al., 2007; Andrade et al., 2010), albeit the difference in voltage dependence between the two splice variants from this study is smaller than these reports. This could be due to the different GPCRs used and/or difference in the β subunits (β3 subunits used in these reports instead of β1b in this study). These results demonstrate that the Ca$_V$2.2e37 isoforms containing exofacial tags function as predicted by previous studies.

a
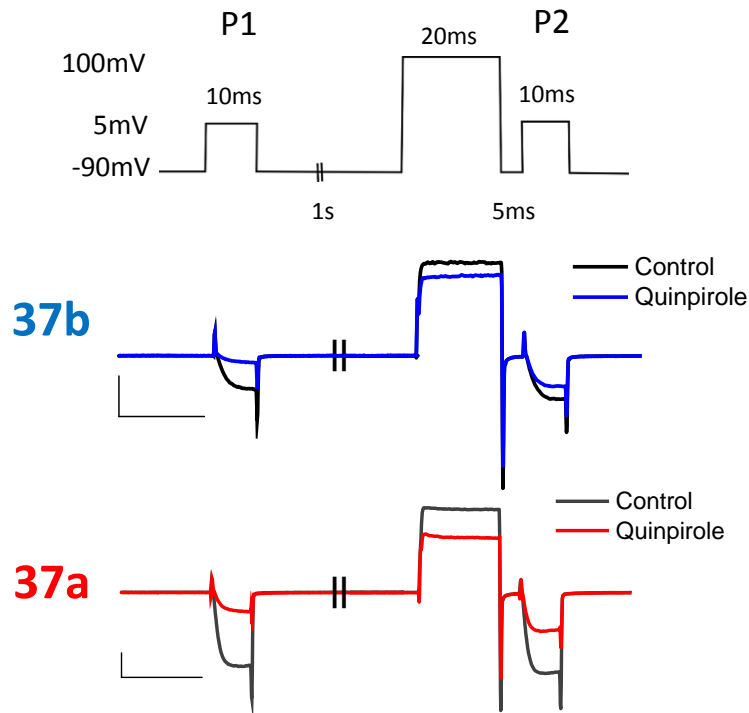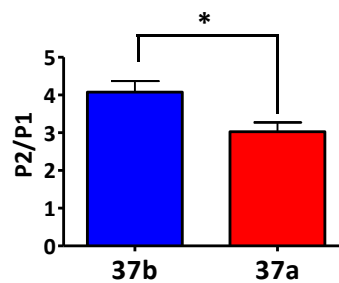
Figure 3.19 D2 receptor-mediated inhibition of Ca$_V$2.2e37 isoforms.

The whole-cell currents of HA-Ca$_V$2.2e37 isoforms expressed with D2R, β1b and α$_2$δ-1 in tsA-201 cells with or without D2R agonist, quinpirole (Quin). (**a**) Whole-cell current was recorded before and after 300nM Quin, applied in a perfusion system. The voltage clamp protocol is shown on the top. The exemplary current traces of Ca$_V$2.2e37b (black for control, blue for 300nM Quin) and Ca$_V$2.2e37a (grey for control, red for 300nM Quin) are also shown. (**b**) The relative current in the presence of 300nM Quin as P2/P1. Ca$_V$2.2e37b (blue, n=22), Ca$_V$2.2e37a (red, n=19). *$P<0.05$ (Student's unpaired t-test).

3.6 GFP-tagged HA-Ca$_V$2.2 (GFP-HA-Ca$_V$2.2)

Green fluorescent protein (GFP) was added to the N-terminus of the Ca$_V$2.2 splice variants containing the exofacial HA tag (Figure 3.20). The advantage of these constructs is that expression of the channel at the plasma membrane can be detected by immunostaining for the cell surface HA epitope in non-permeabilising conditions after fixation, and the total channel localization determined by GFP simultaneously.
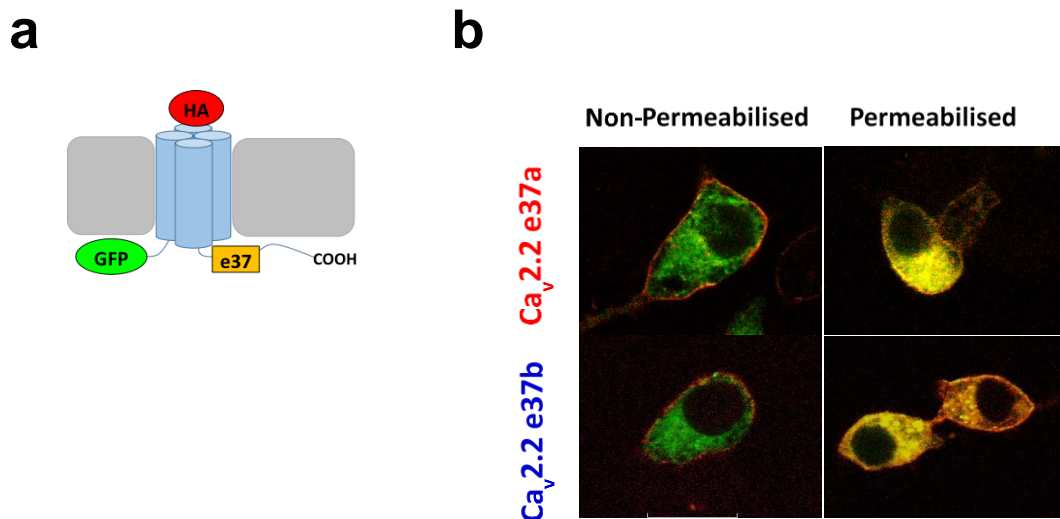
Figure 3.20 GFP-HA-Ca$_V$2.2e37 splice variants.

(**a**) A schematic diagram showing GFP-HA-tagged Ca$_V$2.2, which contains GFP at the N-terminus and HAgHA in the extracellular loop. (**b**) Exemplary confocal images of N2a cells expressing GFP-HA-Ca$_V$2.2e37a and e37b with α$_2$δ-1 and β1b. Non-permeabilised cells are showing Ca$_V$2.2 on the cell surface, which is visualised by extracellular HA labelling (red). All the intracellular GFP (green) co-localises with HA, as shown in the permeabilised cells.

3.6.1 Western blot

Whole-cell protein expression levels of both GFP-HA-tagged $Ca_V2.2e37$ isoforms were at a similar level from the western blot, in which these isoforms were co-expressed with $\alpha_2\delta$-1 and β1b (Figure 3.21). The molecular weights of these isoforms were as expected for full-length channels, and were slightly larger than HA-$Ca_V2.2$ due to the GFP at the N-terminus.
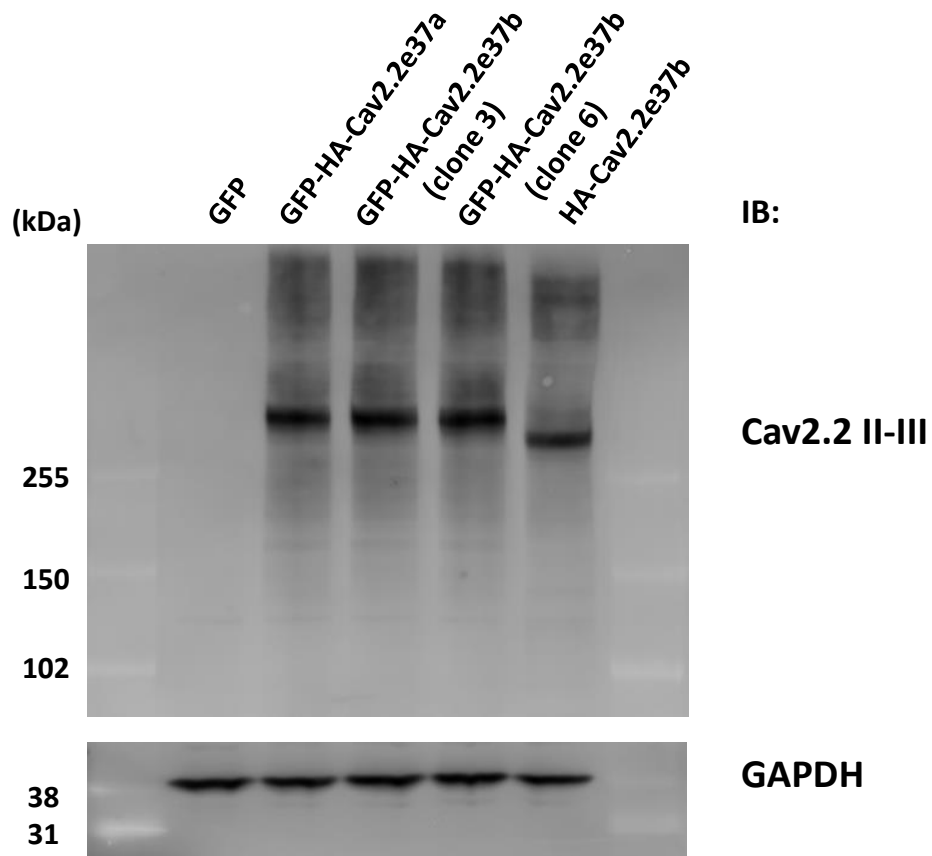
Figure 3.21 Western blot of GFP-HA-CaV2.2e37 splice variants.

(Top panel) GFP-HA-Cav2.2e37a and both clones of GFP-HA-$Ca_V2.2e37b$ were expressed in full-length in the tsA201. Similar whole cell protein expression levels were obtained from all clones. GFP-HA-$Ca_V2.2$ isoforms show a higher molecular weight relative to HA-$Ca_V2.2$ due to the GFP in the N-terminus. (Bottom panel) Glyceraldehyde 3-phosphate dehydrogenease (GAPDH) was shown as a protein loading control.

3.6.2 Whole-cell current

The average whole-cell current density of GFP-HA-Ca$_V$2.2e37a was significantly larger than Ca$_V$2.2e37b between -20 and 0 mV (Figure 3.22a). The V$_{50,act}$ of this Ca$_V$2.2e37a was also shifted to a significantly more hyperpolarised potential compared to Ca$_V$2.2e37b, similarly to the other tagged-channels. These properties were in agreement with those of HA-tagged Ca$_V$2.2 (3.5.1), therefore, GFP at the N-terminus does not affect these biophysical propertised of Ca$_V$2.2e37 splice variants.
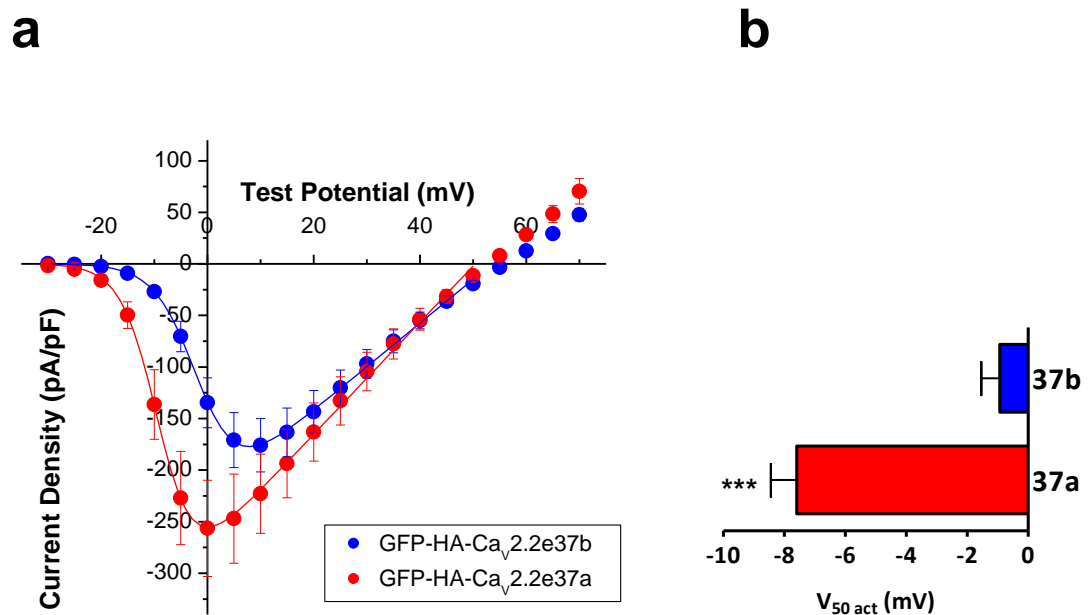
Figure 3.22 Whole-cell current of GFP-HA-Ca$_V$2.2e37 splice variants.

(**a**) Average whole-cell current densities of GFP-HA-Ca$_V$2.2e37 isoforms expressed with β1b and α$_2$δ-1 in tsA-201. The average peak current density was: Ca$_V$2.2e37a (red), -256.5 ± 46.6 pA/pF at +0mV (n=12); Ca$_V$2.2e37b (blue), -175.9 ± 24.2 pA/pF at +10mV (n=8). (**b**) The average activation potential of GFP-HA-Ca$_V$2.2e37a (red) was significantly more hyperpolarised than e37b (blue). ***$P<0.001$, Student's unpaired t-test.

3.7 Ca$_V$2.2 splice variant trafficking in DRG

Taking advantage of the GFP-HA-tagged Ca$_V$2.2 constructs, expression of Ca$_V$2.2 splice variants in different compartment of DRG neurons was visualised. GFP on the N-terminus of Ca$_V$2.2 was observed in DRG soma, as well as the neuronal projections (Figure 3.23). Staining with HA antibody post fixation completely co-localised with GFP in the neurites and on the plasma membrane of the soma. However, in the case of the neurites, the extracellular HA-labelling may be unreliable as an indicator for the neurite plasma membrane expression, since the fixation with PFA can cause permeabilisation of the neurites (from the observation by other members of the laboratory), therefore the cell surface Ca$_V$2.2 is indistinguishable from the intracellular Ca$_V$2.2. To resolve this, the cell surface Ca$_V$2.2 was live-labelled to avoid the neurites being permeabilised. HA antibody was applied to the DRG in serum-free medium for 1 h at 37 °C, before fixation, and the secondary antibody was applied post-fixation, similarly to the standard immunocytochemistry procedure. The limitations of this method is that the cell surface-bound antibodies can be internalised at 37 °C during labelling and requires higher concentration of primary antibodies. The live-labelling was performed at 1:250 dilution of HA antibody which is double the standard immunostaining concentration, however, very small amount of cell surface labelling was observed (Figure 3.23), and this method was not sufficiently robust in comparing Ca$_V$2.2 isoforms. This could be due to the fast turnover of cell surface HA-Ca$_V$2.2 at 37 °C, and the HA antibody is internalised. A greater expression level of GFP-HA-Ca$_V$2.2 may be required to resolve the detection of cell surface Ca$_V$2.2 in the neurites.

| GFP-Ca$_V$2.2 | HA-Ca$_V$2.2 | Merge |
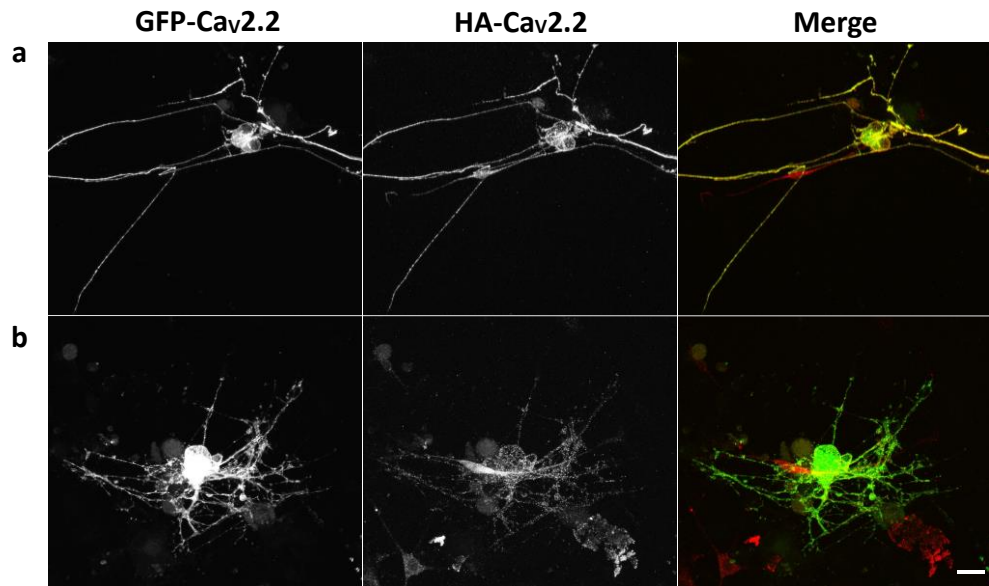
Figure 3.23 GFP-HA-Ca$_V$2.2e37b expressed in DRG neurons.

(**a**) DRG neurons were fixed in 4 % PFA and surface Ca$_V$2.2 was immunostained with HA antibody without permeabilisation. Cell bodies of DRG neurons show cell surface staining of Ca$_V$2.2, but most of the neurites were permeabilised by PFA. (**b**) DRG neurons were live-labelled with HA antibody at 37 °C before fixation with 4 % PFA. Very little immunostaining was observed with this method. GFP (green), HA (red). Scale bar, 20 µm.

3.8 Expression of tagged-Ca$_V$2.2 in DRG-DH co-cultures

VGlut1-pHluorin (vGpH) is expressed at the presynaptic terminals of glutamatergic neurons, and co-localises with a presynaptic protein, synapsin

(Todd et al., 2003; Hoppa et al., 2012; Ferron et al., 2014). DRG and DH neurons in co-culture form functional synapses (Hendrich et al., 2012), therefore the localisation of HA-tagged Ca$_v$2.2 in the presynaptic terminals was examined. Puncta of vGpH and HA-staining were observed in the DRG neurites (Figure 3.24). HA-Ca$_v$2.2 generally co-localised with vGpH along the axons, which indicated that the tagged Ca$_v$2.2 channels were trafficked to the presynaptic terminals. However, visualisation of HA-CaV2.2 in the DRG-DH co-culture was more challenging than it was anticipated, as not many neurons exhibited this pattern of expression. HA-staining was often lacking, probably due to the thick culture that results from this dense co-culture that does not allow sufficient antibody penetration, even with a long permeabilisation with PFA. This unreliable HA staining could be a source of error when comparing the expression of HA-Ca$_v$2.2e37 splice variants and other factors that may influence the synaptic expression of Ca$_v$2.2. Therefore, an appropriate positive control is required for immunostaining at these synaptic terminals.
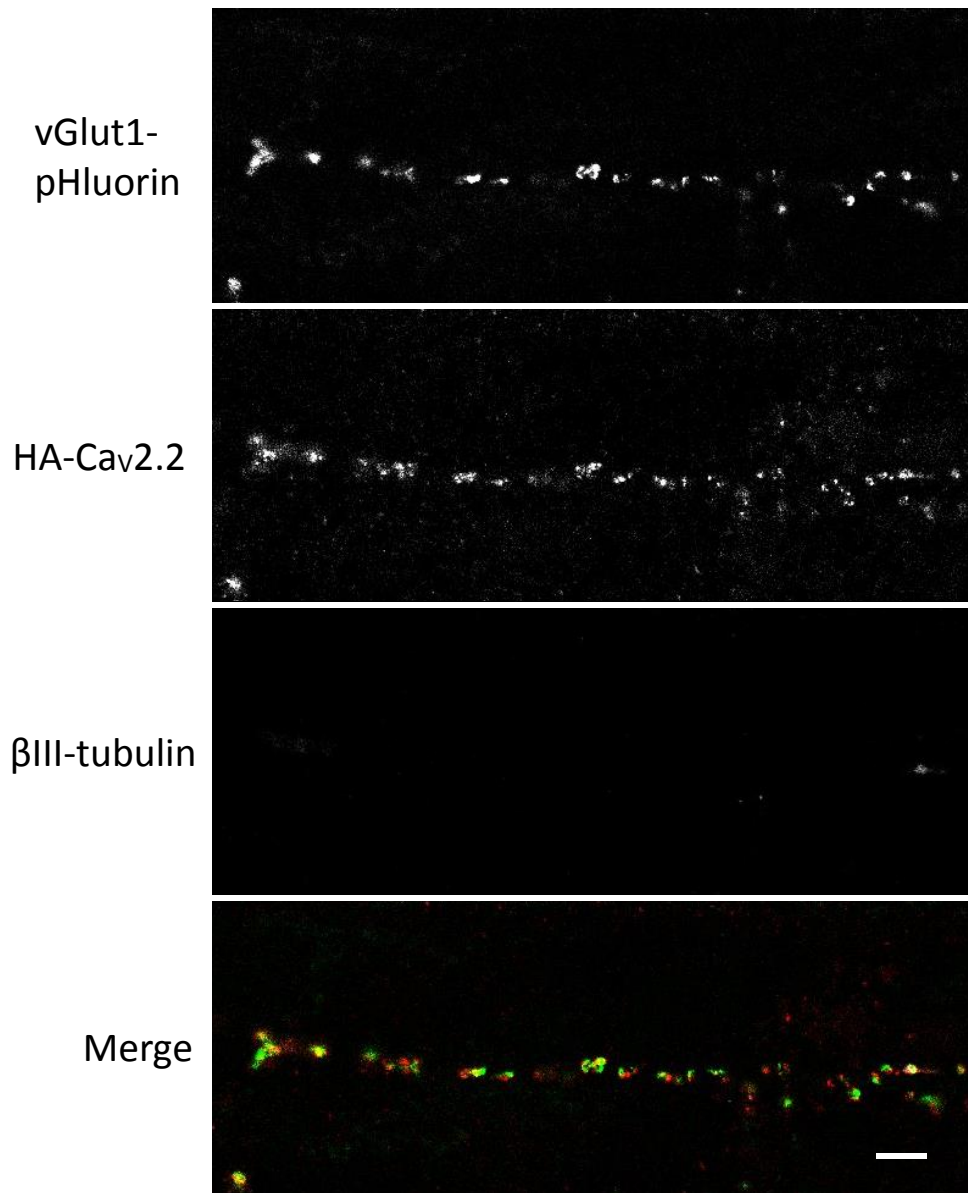
Figure 3.24 Presynaptic expression of HA-Ca$_V$2.2 in DRG-DH co-culture.

Confocal images of the axon of DRG neurons in DRG-DH co-culture. DRG neurons are expressing HA-Ca$_V$2.2e37b (red) and vGpH (green). Immunostaining against HA and βIII-tubulin (grey) was performed without permeabilisation. In this neuron the axon was not permeabilised, as there is no βIII-tubulin staining. After the HA and βIII-tubulin immunostaining protocol, the neurons were permeabilised to reveal the vGpH, which fluoresces in the neutral pH. Ca$_V$2.2 shows punctate immunostaining that co-localise with vGpH along the axon. Scale bar, 5μm.

3.9 Summary and Discussion

In this study, the protein expression and properties of tagged-Ca$_V$2.2 channels such as mEos-Ca$_V$2.2 and GFP-HA-Ca$_V$2.2 were investigated as novel molecular tools for examining the channel cell surface expression and trafficking. All of the tagged Ca$_V$2.2 splice variants containing exon 37a or 37b generated here were expressed sufficiently in the recombinant cells, with electrophysiological properties as expected from the previous studies of these splice variants in the expression systems (Bell et al., 2004; Castiglioni et al., 2006; Raingo et al., 2007) and in the transgenic mice (Andrade et al., 2010). The activation voltage of Ca$_V$2.2e37a is significantly hyperpolarised compared to Ca$_V$2.2e37b, and more importantly, the peak current density of the tagged Ca$_V$2.2e37a is consistently larger than that of Ca$_V$2.2e37b, suggesting that Ca$_V$2.2 channels containing exon 37a are trafficked to the cell surface more readily.   Different β subunits did not alter these properties in this study. Trafficking of these Ca$_V$2.2 splice variants will be further investigated in the next chapter.

mEos-Ca$_V$2.2 constructs could not be visualised reliably at the plasma membrane in N2a cells, although some of the cells exhibited membrane-like localisation of fluorescently tagged channels.   This could be addressed by plasma membrane labelling agents such as fluorescent wheat germ agglutinin, which is a lectin that binds to N-acetyl-D-glucosamine and sialic acid residues found on the surface of the plasma membranes. Although this was used in an attempt to stain the plasma membrane of N2a cells and assess the signal co-localisation with mEos-Ca$_V$2.2, it resulted in considerable non-specific intracellular labelling (result not shown), therefore successful visualisation of Ca$_V$2.2 in the plasma membrane could not be obtained.   The use of the photoconvertible property of the mEos-tag for monitoring intracellular movements of Ca$_V$2.2 channels presents a potential for investigating Ca$_V$2.2 trafficking, however, the excitation of mEos from green to red was not sufficiently localised in my hands to be reliable in subsequent studies to monitor the subtle movement of Ca$_V$2.2 to and from the plasma membrane.   The improved mEos such as mEos3 (Zhang et al., 2012) and mEos4 (Paez-Segala et al., 2015) which are reported to be brighter than mEos2 used in this study might be useful as a tag for Ca$_V$2.2 in the future studies. Furthermore, it was

concluded that biotinylation of the cell surface Ca$_V$2.2 to compare the cell surface expression of the two splice variants was also not robust enough to be used in examination of various factors affecting Ca$_V$2.2 trafficking.

HA-tagged Ca$_V$2.2 constructs are robust and versatile molecular tools to assess the level of cell surface Ca$_V$2.2 splice variants. They were expressed successfully at the presynaptic terminals of DRG neurons in rat DRG-DH co-culture. However, in order to compare the expression Ca$_V$2.2 splice variants, I faced a multitude of challenges. Firstly, reliable and robust quantification methods such as the fluorescent intensity, size of each synapse and number of the synapses with HA-staining present, need to be established to compare different conditions influencing Ca$_V$2.2 trafficking to the synapses. Secondly, the synaptic HA fluorescence intensity is dependent on the total protein expression as well as the efficiency of immunostaining, as these cultures can be thick with multiple layers of cells, and antibody penetration could be insufficient. To overcome these issues, appropriate positive controls should be used to reliably compare the synaptic expression of Ca$_V$2.2 splice variants in the DRG-DH co-cultures.

Addition of GFP to the N-terminus of HA-tagged Ca$_V$2.2 proves to be a useful tool to study the trafficking of Ca$_V$2.2 channels. This construct allows visualisation of cell surface expression by immunostaining for HA extracellularly, as well as intracellular localisation of the channels by GFP simultaneously. Overexpression of GFP-HA-Ca$_V$2.2 resulted in saturation of the channels in all organelles in N2a cells and DRG cell bodies, and it was difficult to distinguish if one of the splice variants was localised more highly than the other in a particular subcellular compartment in this study. Nonetheless, this construct was expressed well in the DRG neurites, therefore it is a useful molecular tool to assess the cell surface expression in the cell body, as well as the trafficking to the neurites simultaneously in the same DRG neuron.

This study showed that the N-terminus GFP does not alter the peak current density of HA-Ca$_V$2.2, which is in agreement with the previous report of current densitied of the untagged Ca$_V$2.2 and Ca$_V$2.2 tagged with GFP at the N-terminus (Raghib et al., 2001), however, the effect of the N-terminus GFP in $V_{50,act}$ and G-protein modulation of Ca$_V$2.2 have not been reported so far. Furthermore, the role of Ca$_V$2.2 N-terminus has been reported in G-protein

modulation (Page et al., 1998). For these reasons, GFP-HA-Ca$_V$2.2 is a good tool to study the channel trafficking, however, HA-Ca$_V$2.2 should be used for investigating its interaction with GPCRs.

BBS-tagged Ca$_V$2.2 constructs were then used to establish protocols to examine the endocytosis and forward trafficking in N2a cells in this study. Live-cell labelling with BTX-488 gives more physiologically relevant information on the intracellular trafficking of Ca$_V$2.2, therefore it is a powerful molecular tool in studying the movement of the channels to and from the plasma membrane.

Monitoring transmembrane protein trafficking in live cells is effective on a confocal microscope with a pre-programmed image acquisition with fixed time intervals. This method is only effective if it does not require a large sampling number per condition due to a small expression variability (e.g. stable cell line). However, transient expression of BBS-Ca$_V$2.2 in N2a cells resulted in a large variability in the expression level of cell surface Ca$_V$2.2. This is due to the fact that in transient expression system, the number of copies of the Ca$_V$2.2 plasmid can vary among the cells, and leads to a large variation in the expression level of Ca$_V$2.2. Furthermore, Ca$_V$2.2 requires co-expression of auxiliary subunits $\alpha_2\delta$ and β for its protein expression and cell surface localisation, however, these subunits had to be transfected in separate plasmids. Moreover, expression of auxiliary subunits is not monitored in individual cells under the assumption that when a cell expresses Ca$_V$2.2, $\alpha_2\delta$ and β subunits are also expressed as these are much smaller in terms of their molecular weights, relative to Ca$_V$2.2. Finally, the repetitive laser exposure for image acquisition during the course of experiment could potentially cause bleaching of the fluorophore, and may lead to a source of error. For these reasons, the best approach to monitor Ca$_V$2.2 trafficking in live cells would be to conduct time-course experiments in which the N2a cells expressing BBS-Ca$_V$2.2 are fixed at various time points after the start of endocytosis / forward trafficking experiment to quantify the average cell surface Ca$_V$2.2 at different time points. This method also allows post-staining of intracellular Ca$_V$2.2 with a specific antibody to ensure that the total protein expression levels were comparable in all time-points.

The only disadvantage of the BBS-tagged construct is that the cell surface staining with BTX-488 is relatively weak compared to HA, despite the insertion of BBSs in tandem. Using different fluorescent BTX such as BTX-555

did not improve the staining (result not shown). As a result, BBS-Ca$_V$2.2 could not be successfully visualised in DRGs and hippocampal neurons. To express this construct in these neurons will require a new strategy, such as using much stronger expression method and/or subcloning BBS-Ca$_V$2.2 into an expression vector with a stronger promoter than pcDNA3. The pCAGGS vector containing the CMV early enhancer/chicken β actin (CAG) promoter drives high protein expression in mammalian cells for proteins that are difficult to express in a large scale, and has been used in a number of expression systems (Aricescu et al., 2006; Alexopoulou et al., 2008). Subcloning BBS-Ca$_V$2.2 into pCAGGS may be a powerful tool for neuronal expression and investigating Ca$_V$2.2 trafficking in neurons.

Chapter 4   Trafficking of Ca$_V$2.2 splice variants

4.1 Introduction

Post-transcriptional modification such as alternative splicing provides Ca$_V$2.2 with further functional variation, which fine-tunes neuronal excitability. To elucidate how Ca$_V$2.2 channels are trafficked to the plasma membrane in neurons, I investigated whether there are differences in trafficking between two Ca$_V$2.2 alternative splice variants of exon 37 in the proximal C-terminus of Ca$_V$2.2, which is alternatively spliced in a mutually exclusive manner to give rise to Ca$_V$2.2 channels that contain either e37a or e37b (Figure 1.8); (Lipscombe et al., 2002; Bell et al., 2004). This introduces a relatively restricted change in the amino acid sequence. Despite this small change in the amino acid sequence, Ca$_V$2.2e37a has a larger whole-cell current compared to Ca$_V$2.2e37b (Bell et al., 2004; Castiglioni et al., 2006; Raingo et al., 2007; Marangoudakis et al., 2012). I noted that the exon 37a sequence introduces two canonical adaptor protein complex binding motifs, YxxΦ and [DE]xxxL[LI], that are absent from exon 37b. Together with several lines of evidence that the C-terminus of Ca$_V$ channels is important in channel targeting (Bourinet et al., 1999; Gao et al., 2000; Kepplinger et al., 2000; Krovetz et al., 2000; Hall et al., 2013), I hypothesised that Ca$_V$2.2 channels containing e37a may be more readily trafficked to the plasma membrane compared to Ca$_V$2.2e37b channels by virtue of these motifs.

To examine whether alternative splicing regulates trafficking of Ca$_V$2.2, functional exofacially-tagged Ca$_V$2.2 channels, HA- and BBS-tagged Ca$_V$2.2 (Cassidy et al., 2014), as well as the newly-developed GFP-tagged HA-Ca$_V$2.2 (3.6), were used to visualise their cellular localisation in both N2a cells and DRG neurons. Electrophysiological, immunocytochemical and live-cell labelling approaches were used to demonstrate the trafficking of Ca$_V$2.2 channels containing e37a and e37b from the subcellular compartments to the plasma

membrane and to the processes of DRG neurons. Furthermore, it was also revealed that this trafficking pathway is indeed dependent on specific motifs in e37a that mediate interaction with AP-1, involved in clathrin-mediated protein sorting (Bonifacino and Traub, 2003).

4.2 Cell surface expression of Ca$_V$2.2 splice variants in N2a cells

To investigate whether the increased current exhibited by Ca$_V$2.2e37a results from an effect on trafficking, mediating altered cellular localisation of the Ca$_V$2.2e37 isoforms, GFP-HA-tagged channels were transiently expressed in the presence of α$_2$δ-1 and β1b (Figure 4.1a). This revealed a larger plasma membrane expression level of Ca$_V$2.2e37a compared to Ca$_V$2.2e37b, without altering the whole-cell expression level of the channels (Figure 4.1b). GFP at the N-terminus did not alter this cellular localisation pattern, as the same observation was validated from cells expressing the HA-tagged Ca$_V$2.2 isoforms, in which the intracellular channels were immunolabelled with anti-Ca$_V$2.2 II-III loop antibody, post-permeabilisation (Figure 4.1c). This confirmed that Ca$_V$2.2 channels containing e37a are preferentially localised in the plasma membrane, and that the increase in the cell surface expression is not due to the overall increase in the protein expression level.

a

GFP
HA
DAPI

b

GFP-HA-Ca$_v$2.2

c
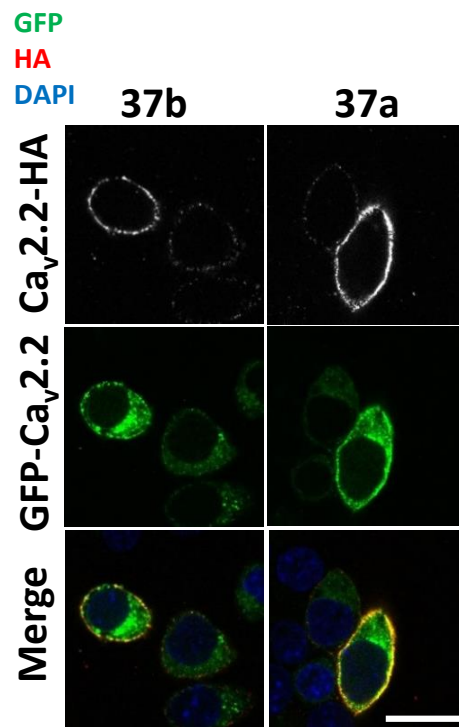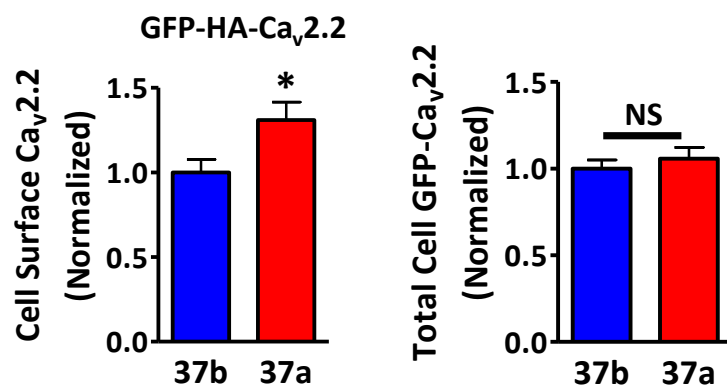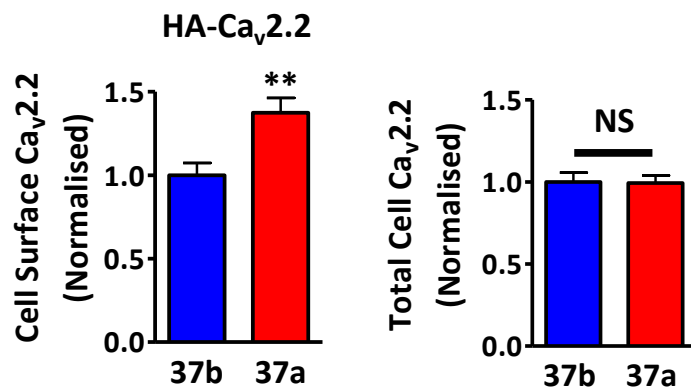
HA-Ca$_v$2.2

Figure 4.1 Localisation of GFP-HA-tagged Ca$_V$2.2 in N2a cells and comparison of GFP-HA-Ca$_V$2.2 splice variants cell surface expression.

(**a**) Confocal images of N2a cells expressing GFP-HA-Ca$_V$2.2e37 isoforms. Ca$_V$2.2 channels were expressed throughout the cells including at the cell surface. Some degree of accumulation in the organelles around the nucleus is also observed. Scale bar, 20 μm. (**b**) Normalised cell surface (left) and total (right) Ca$_V$2.2 of GFP-HA-Ca$_V$2.2e37 isoforms. Cell surface HA and total GFP fluorescence intensities of both Ca$_V$2.2e37a and e37b were quantified and normalised to the average intensity value of Ca$_V$2.2e37b from each experiment. Cell surface: Ca$_V$2.2e37b (blue, n=148); Ca$_V$2.2e37a (red, n=134). Total: Ca$_V$2.2e37b (blue, n=148); Ca$_V$2.2e37a (red, n=134); P=0.49. (**c**) Normalised cell surface (left) and total (right) Ca$_V$2.2 levels for HA-Ca$_V$2.2 isoforms. Cell surface: Ca$_V$2.2e37b (blue, n=83); Ca$_V$2.2e37a (red, n=87). Total: Ca$_V$2.2e37b (blue, n=83); Ca$_V$2.2e37a (red, n=87); P=0.22. Mean ± SEM, *P<0.05, **P<0.01, ***P<0.001 (Student's unpaired t-test).

4.3 Cell surface expression of Ca$_V$2.2 splice variants in DRG neurons

In order to determine whether preferential expression of Ca$_V$2.2e37a at the cell membrane was also exhibited in neurons such as DRG neurons, the localisation of Ca$_V$2.2e37 isoforms was investigated. Immunolabelling in the cell bodies of isolated cultured DRG neurons expressing the HA-tagged GFP-Ca$_V$2.2 isoforms with α$_2$δ-1 and β1b that Ca$_V$2.2e37a surface expression level was significantly greater than Ca$_V$2.2e37b, without altering the whole-cell expression level of the channels (Figure 4.2), similarly to the expression pattern in N2a.
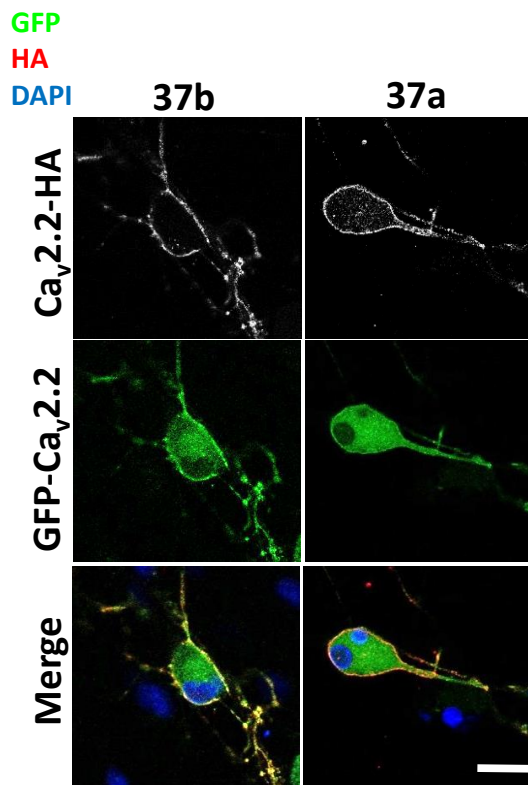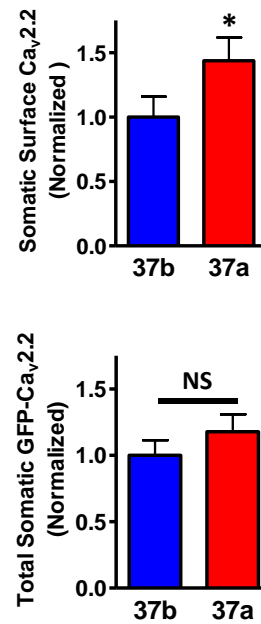
Figure 4.2 Cell surface expression of Ca$_V$2.2 splice variants in DRG cell bodies.

(**a**) Confocal images of DRG cell bodies expressing GFP-HA-Ca$_V$2.2 isoforms with $\alpha_2\delta$-1 and β1b (scale bar, 20 μm). (**b**) Normalised cell surface and total Ca$_V$2.2 in DRG cell bodies. The cell surface HA and total GFP fluorescence densities were quantified and normalised to the average intensity value of Ca$_V$2.2e37b from each experiment. Cell surface: Ca$_V$2.2e37b (blue, n=49); Ca$_V$2.2e37a (red, n=49). Total: Ca$_V$2.2e37b (blue, n=49); Ca$_V$2.2e37a (red, n=49); *P*=0.31.

4.4 Expression of Ca$_V$2.2 splice variants in DRG neurites

To examine whether Ca$_V$2.2e37a was also more highly expressed in the neurites of DRG neurons compared to Ca$_V$2.2e37b, GFP fluorescence in the neurites as a Ca$_V$2.2 expression level was quantified from the same transfected DRG neuron. The amount of tagged Ca$_V$2.2e37a channels in the neurites of these DRG neurons was also significantly higher than Ca$_V$2.2e37b, without altering the level of an expression marker mCherry that was co-transfected to visualise the entire field of neurites (Figure 4.3). Ca$_V$2.2e37a channels in the DRG neurons were trafficked further along the neurites to a significantly greater degree than Ca$_V$2.2e37b channels.
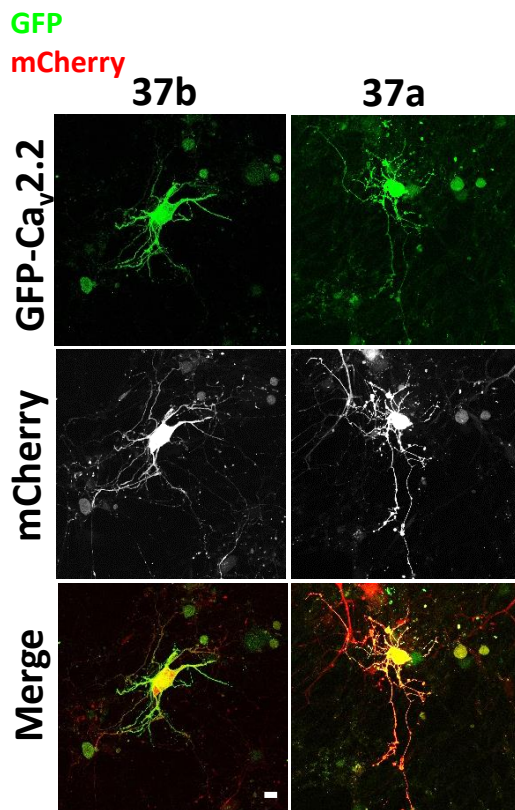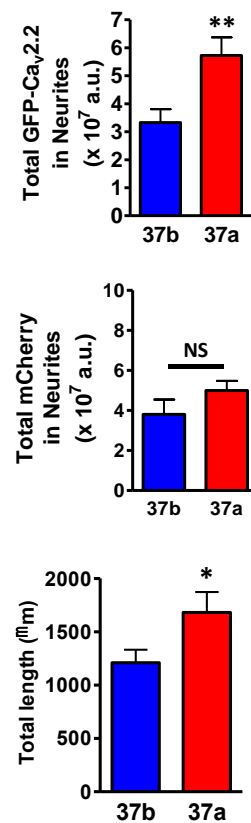
Figure 4.3 Expression of Ca$_V$2.2 splice variants in DRG neurites.

(**a**) Confocal images of DRG neurites expressing GFP-HA-Ca$_V$2.2 isoforms with free mCherry (scale bar, 20 μm). (**b**) (Top) Total fluorescence of Ca$_V$2.2 isoforms and free mCherry in the DRG neurites (in x10^7 a.u.). Total GFP-Ca$_V$2.2: Ca$_V$2.2e37b (blue, n=40); Ca$_V$2.2e37a (red, n=40). (Middle) Total mCherry: Ca$_V$2.2e37b (blue, n=40); Ca$_V$2.2e37a (red, n=40); P=0.18. (Bottom) Total length of neurites with GFP-Ca$_V$2.2: Ca$_V$2.2e37b (blue, n=40); Ca$_V$2.2e37a (red, n=40). Mean ± SEM, *P<0.05, **P<0.01 (Student's unpaired t-test).

4.5 Effect of auxiliary subunits on cell surface expression of Ca$_V$2.2 splice variants

It is well-established that auxiliary subunits play an important role in Ca$_V$2.2 trafficking (Waithe et al., 2011; Dolphin, 2012; Cassidy et al., 2014). To determine whether α$_2$δ-1 and β1b are required for the differential cell surface expression of Ca$_V$2.2e37a and e37b channels, HA-tagged Ca$_V$2.2e37 isoforms were expressed, with or without α$_2$δ-1 and β1b, in the N2a cells to compare the cell localisation of the Ca$_V$2.2 isoforms with both α$_2$δ-1 and β1b.

In the presence of both α$_2$δ-1 and β1b subunits, the Ca$_V$2.2 splice variants were efficiently trafficked to the plasma membrane (Figure 4.4). In the absence of α$_2$δ-1, both Ca$_V$2.2 splice variants are inefficiently trafficked to the cell surface, although a larger amount of Ca$_V$2.2e37b was observed at the plasma membrane compared to Ca$_V$2.2e37a. Without β1b, the whole-cell expression of Ca$_V$2.2 was almost completely diminished for both splice variants, similarly to the previous report of Ca$_V$2.2e37b cell surface expression in the absence of β1b (Cassidy et al., 2014). In addition, the lower expression level of Ca$_V$2.2 and a smaller number of N2a cells expressing Ca$_V$2.2 were also observed in the absence of β1b, which indicates that the pore-forming subunits are degraded in the absence of β1b, which is in agreement with the previous reports (Altier et al., 2011; Waithe et al., 2011).
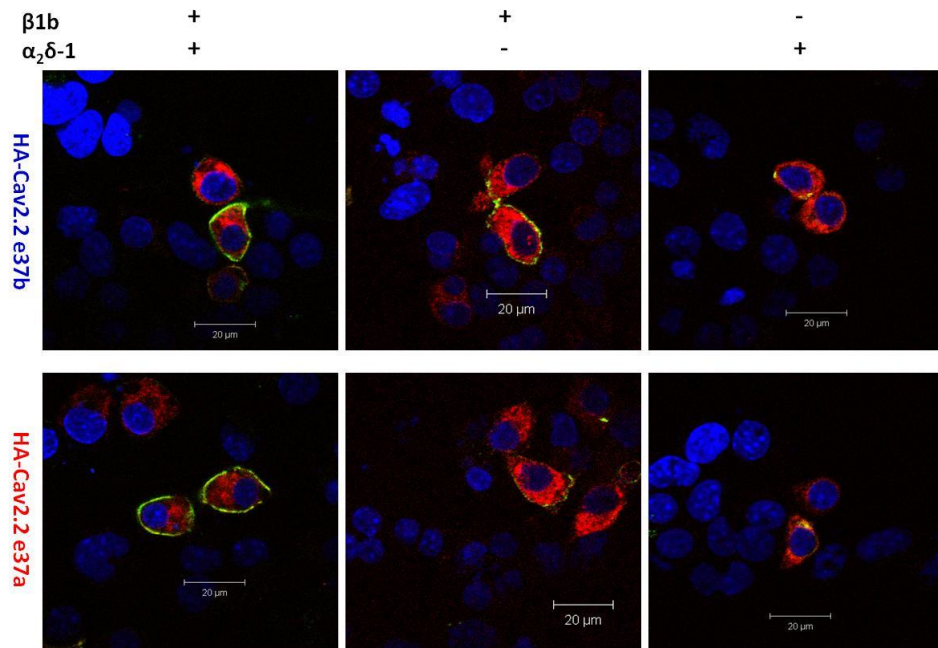
Figure 4.4 Effect of Auxiliary Subunits on Cell Surface Expression of HA-tagged Ca$_V$2.2 Splice Variants.

Exemplary confocal images of HA-Ca$_V$2.2e37 isoforms expressed in N2a cells with or without $\alpha_2\delta$-1 or β1b show extracellular HA (green), intracellular HA (red) and nuclei (blue). Both Ca$_V$2.2 isoforms show reduction in cell surface Ca$_V$2.2 in the absence of $\alpha_2\delta$-1 or β1b. There was a smaller population of cells expressing whole-cell Ca$_V$2.2 in the absence of β1b, compared to conditions with both $\alpha_2\delta$-1 and β1b, or $\alpha_2\delta$-1 only.

4.5.1 Effect of α₂δ-1 on cell surface expression of Caᵥ2.2 splice variants

The effects of $\alpha_2\delta$-1 on the cell surface expression of $Ca_V2.2e37$ isoforms were evaluated. The quantification of immunostaining of the cell surface HA-$Ca_V2.2$ in N2a cells revealed that the increased plasma membrane expression of $Ca_V2.2e37a$ relative to $Ca_V2.2e37b$ was lost in the absence of $\alpha_2\delta$-1 (Figure 4.5), suggesting that $\alpha_2\delta$-1 is required for underlying mechanisms involved in the differential trafficking of $Ca_V2.2$ isoforms. Although it is highly unlikely that $\alpha_2\delta$-1 directly interacts with the C-terminus of $Ca_V2.2$ where the exon 37 alternative splicing occurs, $\alpha_2\delta$-1 may be involved in $Ca_V2.2$ trafficking possibly via interaction through intermediate protein(s) and utilisation of the same pathway(s) involved in transporting the channels to the plasma membrane.
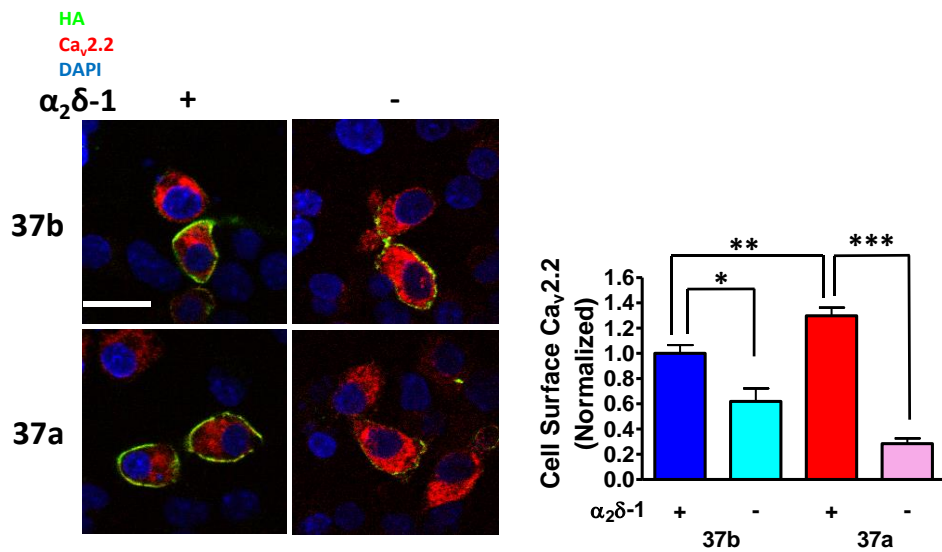
Figure 4.5 Effect of α₂δ-1 on cell surface expression of HA-CaᵥV2.2e37 isoforms.

(Left) Merged confocal images of N2a cells expressing HA-CaV2.2e37 isoforms with or without $\alpha_2\delta$-1. HA (green), $Ca_V2.2$ (red), nucleus (blue), scale bar, 20 µm. (Right) HA fluorescence intensities were normalized to the average intensity of $Ca_V2.2e37b$ with $\alpha_2\delta$-1 in each experiment. Cell surface: $Ca_V2.2e37b+\alpha_2\delta$-1 (blue, n=125); $Ca_V2.2e37b$ (cyan, n=39); $Ca_V2.2e37a+\alpha_2\delta$-1 (red, n=135); $Ca_V2.2e37a$ (pink, n=37). The difference between $Ca_V2.2e37a$ and e37b without $\alpha_2\delta$-1 was not statistically significant. Mean ± SEM, *$P<0.05$, **$P<0.01$, ***$P<0.001$ (one-way ANOVA).

4.5.2 Effect of α2δ-1 on biophysical properties of Cav2.2 splice variants

4.5.2.1 Whole-cell current, conductance and V_{50} activation

The effects of α2δ-1 on the cell surface expression of Cav2.2 splice variants were validated in the whole-cell current recording. In the absence of α2δ subunits, the whole-cell current densities from both Cav2.2e37 isoforms were significantly smaller than that with α2δ-1 (Figure 4.6a), confirming the immunocytochemistry experiment 4.5.1. Interestingly, the average IV curves of Cav2.2e37a and Cav2.2e37b were very similar in the absence of α2δ, unlike those with α2δ-1. The average whole-cell G_{max} for both isoforms in the absence of α2δ-1 was significantly reduced, and the difference in conductance between e37a and e37b was lost (Figure 4.6b). Both Cav2.2 isoforms were activated at slightly more depolarised potential without α2δ-1, although the differences were not statistically significant in one-way ANOVA Bonferroni post-hoc test (Figure 4.6c).

4.5.2.2 Steady-state inactivation

In general, the inactivation voltages of both Cav2.2 isoforms were more depolarised in the absence of α2δ, compared to those in the presence of α2δ-1 (Figure 4.7), in consensus with the previous reports (Dolphin, 2012). The effect on Cav2.2e37a was more prominent, where the voltage-dependence of steady-state inactivation was significantly more depolarised in the absence of α2δ-1.
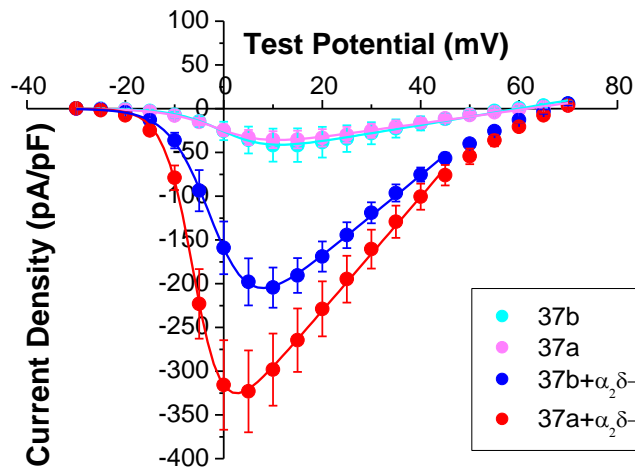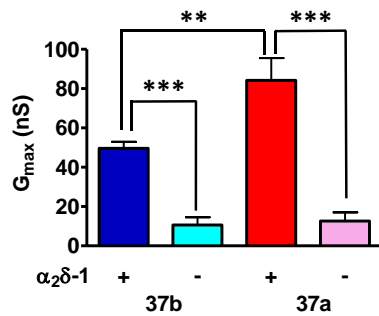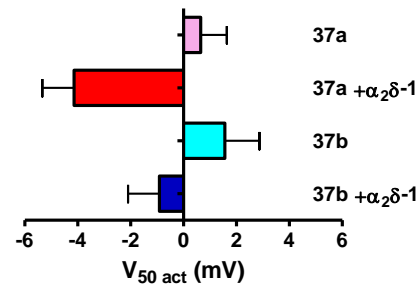
Figure 4.6 Whole-cell current of HA-Cav2.2e37 splice variants with and without α2δ-1.

(**a**) Average whole-cell current densities of Cav2.2 isoforms with and without $\alpha_2\delta$-1 in tsA-201 cells. Peak current density (pA/pF): e37b+α2δ-1 (blue), -204.5 ± 22.9 (+10mV, n=12); e37b (cyan), -41.7 ± 19.1 (+15mV, n=6); e37a+α2δ-1 (red), -323.0± 46.8 (+5mV, n=10); e37a (pink), -35.2 ± 10.0 (+15mV, n=6). (**b**) Conductance (G_{max}) and (**c**) Activation voltage ($V_{50,act}$). e37b+α2δ-1 (blue, n=12); e37b (cyan, n=6); e37a+α2δ-1 (red, n=10); e37a (pink, n=6). Mean ± SEM, *$P<0.05$, **$P<0.01$, ***$P<0.001$ (one-way ANOVA).

a
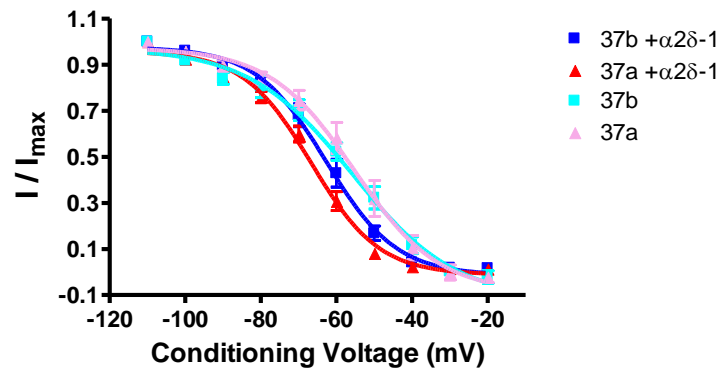
b
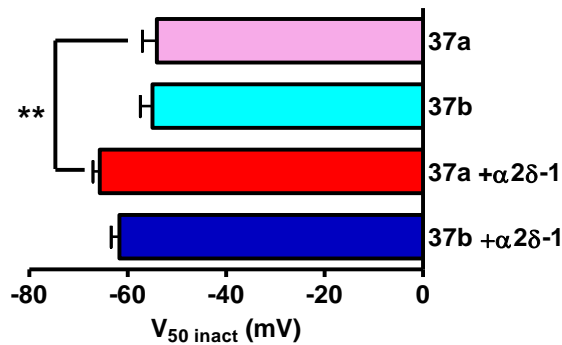
Figure 4.7 Inactivation of HA-Ca$_V$2.2e37 isoforms with and without α$_2$δ-1.

(a) The average relative currents of Ca$_V$2.2e37 isoforms with and without α$_2$δ-1 in tsA-201 cells, which were subjected to various conditioning voltages. In general, in the absence of α$_2$δ-1 the steady-state inactivation potentials of Ca$_V$2.2e37 isoforms were more depolarised.   (b) Mean inactivation voltages (V$_{50,inact}$) of Ca$_V$2.2e37 isoforms with and without α$_2$δ-1 from (a).   In the presence of α$_2$δ-1, the V$_{50,inact}$ is significantly more hyperpolarised. The difference in the average V$_{50,inact}$ between Ca$_V$2.2e37a and e37b was not statistically significant.   Ca$_V$2.2e37a (pink, n=6), Ca$_V$2.2e37b (cyan, n=4), Ca$_V$2.2e37a+α$_2$δ-1 (red, n=8), Ca$_V$2.2e37b+α$_2$δ-1 (blue, n=8)   **P<0.01 (one-way ANOVA).

4.6 Forward trafficking of Ca$_V$2.2 splice variants

To investigate the mechanism of differential Ca$_V$2.2 splice variant trafficking, BBS-tagged Ca$_V$2.2 constructs were expressed in N2a cells, to monitor the net appearance of the channels in the plasma membrane over time (Figure 4.8a). This protocol determines the net forward trafficking of Ca$_V$2.2, since the endocytosis of the labelled Ca$_V$2.2 channels at the cell surface occurs in this condition, as their endocytosis was not blocked.

The experiments showed that the average initial rate of appearance of Ca$_V$2.2e37a on the cell surface was significantly greater than for Ca$_V$2.2e37b, leading to a greater steady-state maximum cell surface expression level (Figure 4.8b, c). The appearance of the channel at the cell surface did not occur at 4 °C. The overall time constants determined from the fit of the single association exponential equation were not significantly different between these isoforms, however, it was difficult to interpret these values since the appearance of the channels at the cell surface is a product of multiple intracellular trafficking events. In any cases, these results imply that the increased presence of Ca$_V$2.2e37a on the cell surface is due to an increased trafficking from subcellular organelles to the plasma membrane.
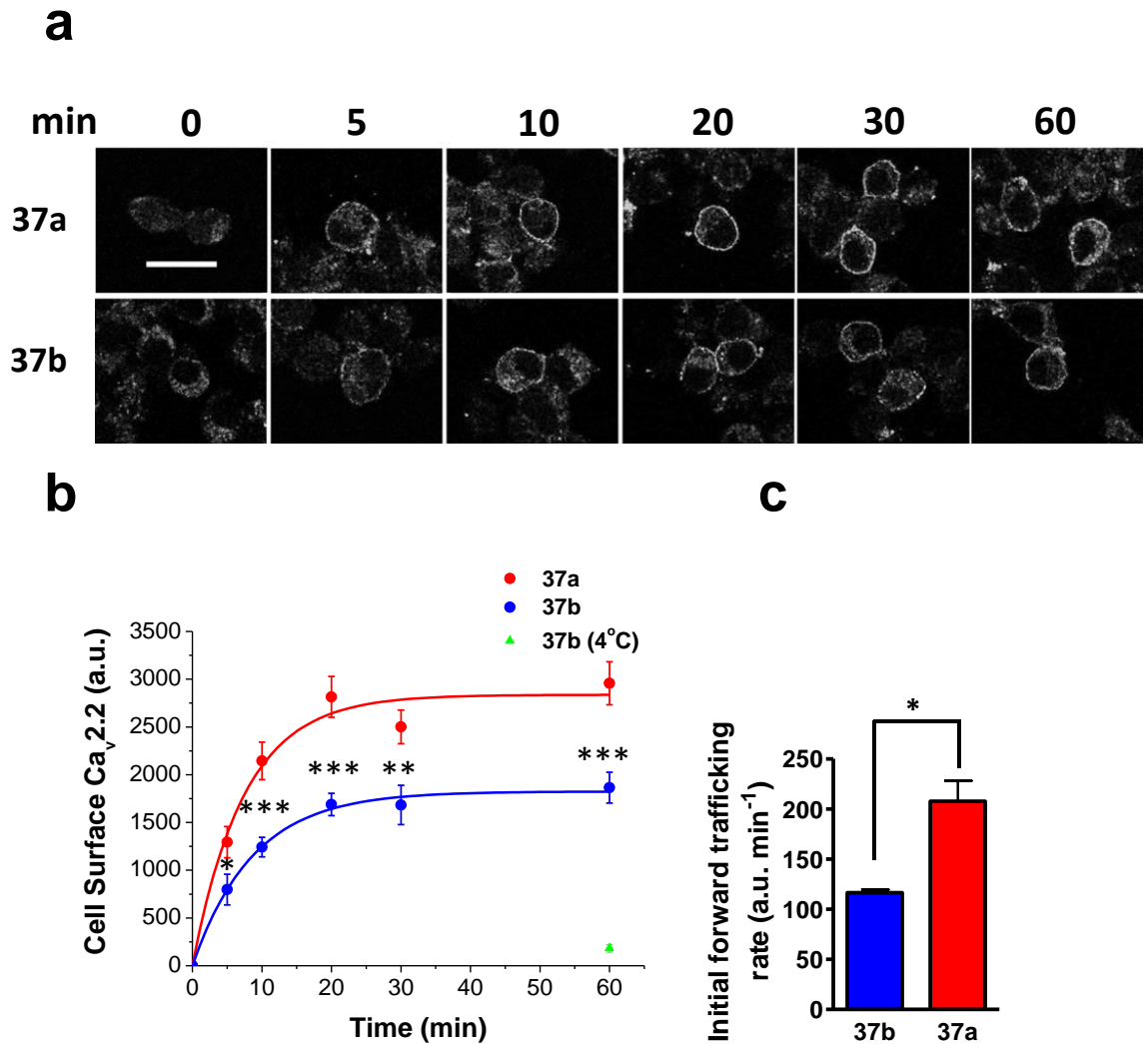
Figure 4.8 Net forward trafficking of BBS-tagged Ca$_V$2.2e37 splice variants.

(**a**) Representative confocal images of N2a expressing BBS-Ca$_V$2.2e37 isoforms at different time points after the start of the net forward trafficking assay, showing appearance of Ca$_V$2.2 at the cell surface by BTX-488 live labelling. Scale bar, 20 μm. (**b**) Kinetics of Ca$_V$2.2e37 isoform net forward trafficking. As a negative control (closed green triangle), Ca$_V$2.2e37b was kept at 4 °C after the start of the experiment. The kinetic curves were fitted to a single exponential to derive time constant τ (min). The rates of net forward trafficking ($1/\tau$, min^{-1}) were; Ca$_V$2.2e37a (closed red circle), 0.212 ± 0.027 (n=3); Ca$_V$2.2e37b (closed blue circle), 0.132 ± 0.036 (n=3). The data points in the graph contain all the cells analysed from the three separate experiments. (**c**) The initial rates of net forward trafficking. The gradient of linear regression was obtained as an initial average forward trafficking rate from each of 3 experiments, and summarised (in a.u./min). Ca$_V$2.2e37b (blue, n=3); Ca$_V$2.2e37a (red, n=3). *$P < 0.05$, **$P < 0.01$, ***$P < 0.001$ (Student's unpaired t-test).

4.7 Effect of Brefeldin A (BFA) on forward trafficking of Ca$_V$2.2 splice variants

4.7.1 Determining effective concentration of BFA

Transmembrane proteins at the cell surface originate from various cell organelles. The two main sources of transmembrane proteins inserted into the plasma membrane are; 1) newly synthesised proteins from the ER and the Golgi apparatus (for review see Guo et al., 2014), and 2) recycled proteins via recycling endosomes (Grant and Donaldson, 2009). Brefeldin A (BFA), which disrupts the structure of the Golgi apparatus and inhibits the translocation of proteins from the ER to the plasma membrane (Fujiwara et al., 1988; Lippincott-Schwartz et al., 1989), was then used to further elucidate the mechanism of differential Ca$_V$2.2e37a net forward trafficking.

Firstly, in order to determine the effective concentration of BFA, the cell surface expression of BBS-Ca$_V$2.2 isoforms was determined in the presence of 50, 200 and 500 ng/ ml BFA, applied 4 h prior to the start of the experiment and during the assay, and compared with the control condition with 0.4% DMSO (Figure 4.9). Both Ca$_V$2.2 isoforms were significantly reduced at the plasma membrane in 200 ng/ml BFA, therefore this concentration was used for the subsequent net forward trafficking experiments.
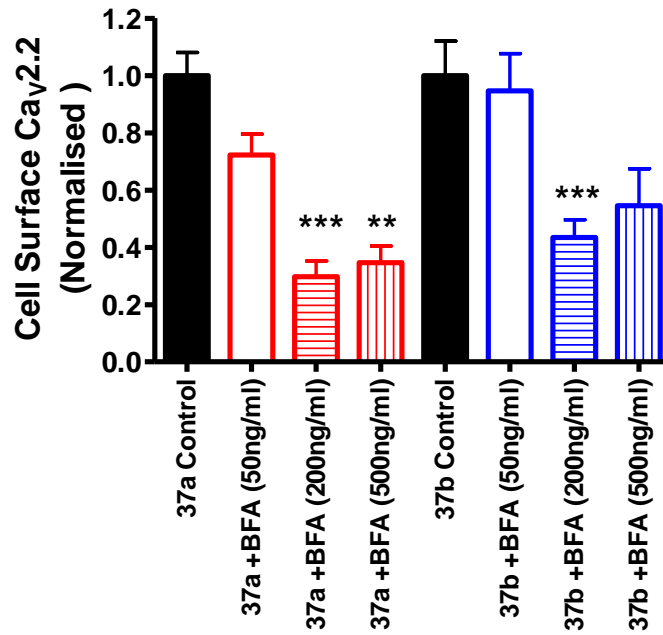
Figure 4.9 Effective concentration of BFA on reduction in HA-Ca$_V$2.2 on the cell surface.

Cell surface Ca$_V$2.2 was determined in the N2a cells expressing HA-Ca$_V$2.2, β1b and α$_2$δ-1 in the presence of 0, 50, 200 and 500 ng/ml BFA. The cells were pre-incubated with BFA 4 hours at 37 °C before the fixation with 4 % PFA. Cell surface HA fluorescence intensity was normalised to the control (0 ng/ml BFA) in each condition. 200 ng/ml of BFA was effective in reducing cell surface expression of both Ca$_V$2.2e37a and e37b. 37a control (n=68), 37a + 50 ng/ml BFA (n=52), 37a + 200 ng/ml BFA (n=33), 37a + 500 ng/ml BFA (n=14), 37a control (n=68), 37b + 50 ng/ml BFA (n=23), 37a + 200 ng/ml BFA (n=41), 37a + 500 ng/ml BFA (n=13). **$P<0.01$, ***$P<0.001$ (one-way ANOVA).

4.7.2 Effect of BFA on the net forward trafficking rate of Ca$_V$2.2 splice variants

In order to determine the rate of trafficking of Ca$_V$2.2e37 isoforms from the TGN to plasma membrane, the net forward trafficking experiments were performed as described previously in the presence of BFA, which blocks the trafficking from the TGN. In the presence of BFA, the maximum level of Ca$_V$2.2 splice variants appearing on the plasma membrane was markedly reduced compared to the control condition as expected (Figure 4.10a). This shows that approximately half of the channel population at the plasma membrane originated from the recycling endosomes within the duration of these experiments. Furthermore, in the presence of BFA the difference between Ca$_V$2.2e37a and Ca$_V$2.2e37b in the maximum cell surface level achieved was abolished. In addition, the kinetics of Ca$_V$2.2e37a net trafficking to the plasma membrane were markedly slowed compared to the absence of BFA (Figure 4.10b).

BFA inhibits Arf1, which is essential for the recruitment of AP-1, which mediates clathrin-dependent cargo sorting (Zhu et al., 1998; Ren et al., 2013). These observations raised the possibility that the greater forward trafficking and increased cell surface expression of Ca$_V$2.2e37a, relative to Ca$_V$2.2e37b, are due to differences in sequence of the proximal C-terminus of Ca$_V$2.2 as a result of alternative splicing, and that the underlying mechanism may involve AP-mediated sorting.
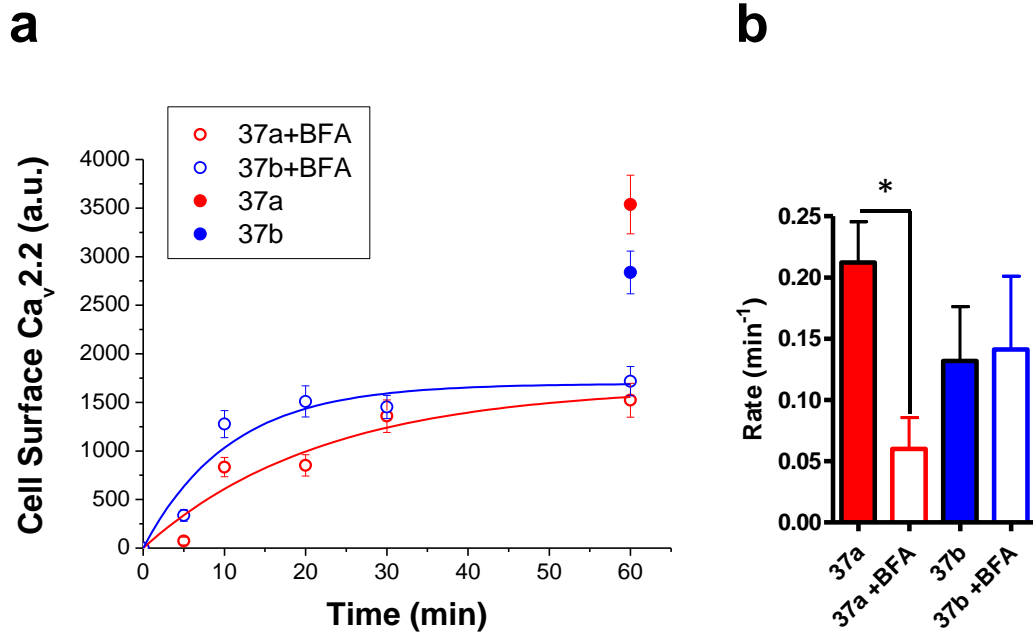
Figure 4.10 Effect of BFA on net forward trafficking of BBS-Ca$_V$2.2e37 isoforms.

(**a**) Kinetics of Ca$_V$2.2e37 isoform net forward trafficking in the presence of BFA. Ca$_V$2.2e37a+BFA (open red circle), $1/\tau = 0.060 \pm 0.021$ min^{-1}, n=3; Ca$_V$2.2e37b+BFA (open blue circle), 0.148 ± 0.049 min^{-1}, n=3. The cell surface level of Ca$_V$2.2 in the absence of BFA as a control is shown at t = 60 min (Ca$_V$2.2e37a, closed red circle and Ca$_V$2.2e37b, closed blue circle). The data points in the graph contain all the cells analysed from the three separate experiments. (**b**) Summary of the net forward trafficking rate of Ca$_V$2.2e37a isoforms with and without BFA. The rates of net forward trafficking from Figure 4.8b and Figure 4.10a are compared. Ca$_V$2.2e37a (red closed bar) n=3, Ca$_V$2.2e37a+BFA (red open bar) n=3, Ca$_V$2.2e37b (blue closed bar) n=3, Ca$_V$2.2e37b+BFA (blue open bar) n=3 ($P<0.05$, one-way ANOVA).

4.8 Endocytosis of Ca$_V$2.2 splice variants

The stability of Ca$_V$2.2 at the cell surface is another factor for determining the cell surface level of the channels. To determine if endocytosis rates of Ca$_V$2.2 isoforms are different, the disappearance of BBS-tagged Ca$_V$2.2 isoforms was determined. The endocytosis of the channels did not occur at 4 °C. Ca$_V$2.2e37a and Ca$_V$2.2e37b showed similar kinetics of internalisation, both reaching the same minimum cell surface level after 30 min (Figure 4.11). This result indicates that endocytosis did not contribute significantly to the observed differences in net forward trafficking. In addition, this implies that Ca$_V$2.2e37 isoforms were targeted equally by endocytic machineries for their basal endocytosis.
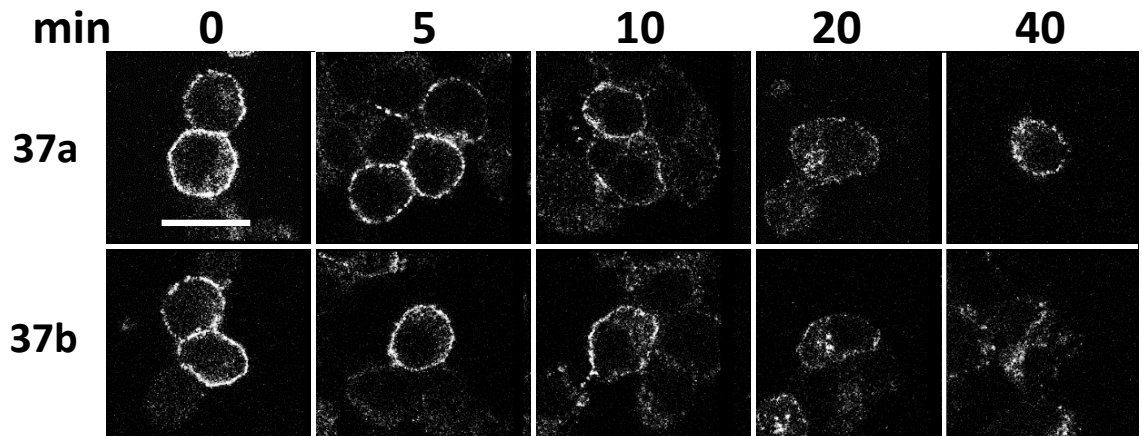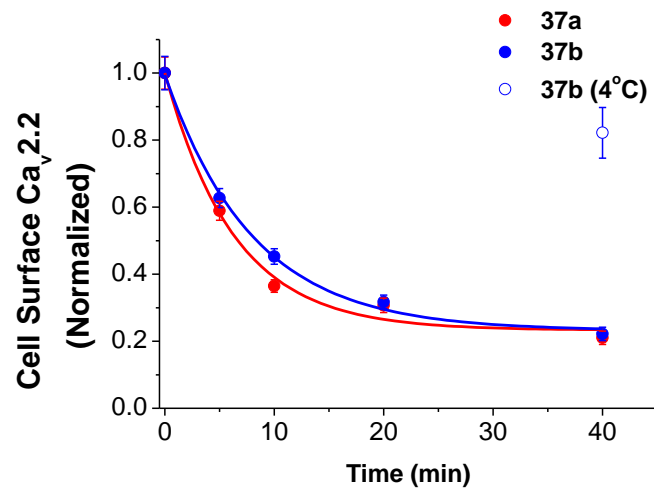
Figure 4.11 Endocytosis of Ca$_V$2.2e37 isoforms.

(**a**) Representative confocal images of N2a cells expressing BBS-tagged Ca$_V$2.2e37 isoforms at different time points after the start of an endocytosis assay shows the disappearance of BTX-488-labelled Ca$_V$2.2 from the cell surface (scale bar, 20 μm). (**b**) The endocytosis kinetics of Ca$_V$2.2e37 isoforms. The time constants (τ) from fitting a single exponential (min); Ca$_V$2.2e37a (red), 7.00 ± 1.23 (n=3); Ca$_V$2.2e37b (blue), 11.6 ± 3.53 (n=3). Ca$_V$2.2e37b (open blue circle) was kept at 4 °C as a negative control after the start of endocytosis experiment. The cell surface fluorescence was normalised to the average value at t=0 min for each isoform in the same experiment. The data points in the graph contain all the cells analysed from the three separate experiments.

4.9 Effect of AP-2 on the cell surface expression of $Ca_V2.2$ splice variants

The primary role of AP-2 is to mediate internalisation of transmembrane proteins by clathrin-dependent endocytosis. In order to determine whether AP-2 mediates internalisation of $Ca_V2.2$ splice variants and regulates the channel cell surface expression, $Ca_V2.2e37$ isoforms were co-expressed with the wild-type or mutant μ subunits of AP-2. The double mutation at F174 and D176 in the dominant-negative mutant, AP-2μ2 F174A/D176S has been shown to slow down the endocytosis from the plasma membrane by abolishing the interaction with YxxΦ motifs in the transmembrane cargo proteins (Motley et al., 2006).

4.9.1 Effect of AP-2 mutant on $Ca_V2.2$ cell surface expression

To investigate the role of AP-2 in trafficking of $Ca_V2.2e37$ splice variants, either the wild-type AP-2μ2 (WT) or dominant-negative mutant AP-2μ2 F174A/D176S were co-expressed with HA-tagged $Ca_V2.2e37$ isoforms, in the presence of $\alpha_2\delta$-1 and β1b in N2a cells. The cell surface expression of HA-$Ca_V2.2$ was examined as previously described against the control condition.

The previous reports on the effect of the AP-2μ2 F174A/D176S in reducing the rate of cargo endocytosis suggested that the cell surface expression of Cav2.2 isoforms was expected to increase in this condition. However, AP-2μ2 F174A/D176S and WT AP-2μ2 had no significant effect on the cell surface expression of $Ca_V2.2e37b$ (Figure 4.12). On the contrary, the cell surface expression of $Ca_V2.2e37a$ was significantly reduced in the presence of μ2 mutant. AP-2μ2 WT also reduced the cell surface expression of $Ca_V2.2e37a$, although this observation could be explained by the overexpression of AP-2μ2 causing increased recruitment of clathrin molecules and accelerating the rate of $Ca_V2.2$ endocytosis, which led to a reduction in channel cell surface expression.
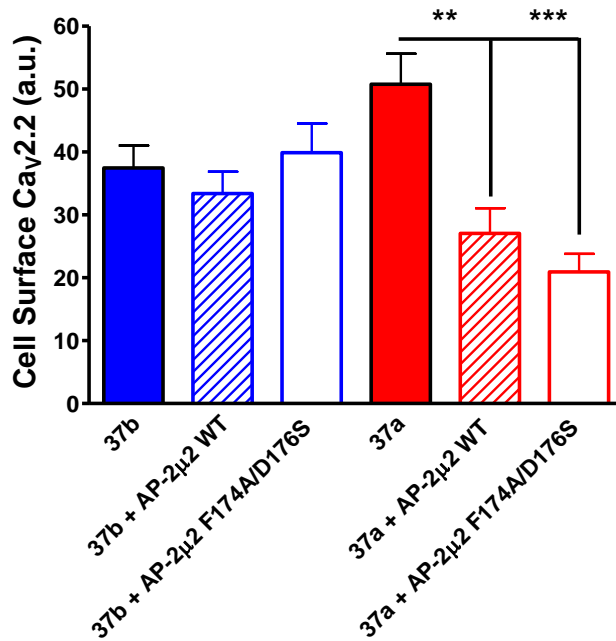
Figure 4.12 Effect of AP-2μ2 WT and F174A/D176S on cell surface expression of Ca$_V$2.2e37 isoforms.

HA-Ca$_V$2.2e37 isoforms were coexpressed with AP-2μ2 WT, dominant negative mutant AP-2μ2 F174A/D176S or blank pcDNA3 in the presence of β1b and α$_2$δ-1 in N2a. Both AP-2μ2 WT and F174A/D176S significantly reduced the cell surface expression of HA-Ca$_V$2.2e37a, but they had no effect on HA-Ca$_V$2.2e37b. 37b (n=95), 37b+AP-2μ2 WT (n=97), 37b+AP-2μ2 F174A/D176S (n=63), 37a (n=85), 37a+AP-2μ2 WT (n=49), 37a+AP-2μ2 F174A/D176S (n=74). $**P<0.01$, $***P<0.001$ (one-way ANOVA).

4.9.2 Effect of AP-2 mutant on Ca$_V$2.2 whole-cell current

To confirm the effect of AP-2 on Ca$_V$2.2e37 splice variant trafficking, the effect of AP-2 on whole-cell current of the Ca$_V$2.2 isoforms was investigated. Similarly to the immunocytochemistry experiments, HA-Ca$_V$2.2e37 isoforms were co-expressed with either AP-2µ2 WT or F174A/D176S in tsA-201 cells. The whole-cell current densities were determined as previously described.

AP-2µ2 F174A/D176S reduced the whole-cell current density of Ca$_V$2.2e37a by almost 50% (Figure 4.13a), which validated the observation from the cell surface labelling experiments in N2a cells (Figure 4.12). AP-2µ2 WT caused non-significant reduction in the Ca$_V$2.2e37a whole-cell current density, unlike in the previous cell surface labelling assays. In Ca$_V$2.2e37b on the other hand, AP-2µ2 F174A/D176S increased the whole-cell current density, whereas AP-2µ2 WT decreased the Ca$_V$2.2e37b current (Figure 4.13b).

The opposing effects of AP-2µ2 F174A/D176S on the whole-cell current of Ca$_V$2.2e37 isoforms were striking, and similar effects were also observed in their cell surface expression. The much smaller stabilising effect of AP-2µ2 F174A/D176S on Ca$_V$2.2e37b cell surface expression compared the whole-cell current was probably due to the difference in endogenous protein expression in the two different cell lines. This could be determined by a western blot against the endogenous AP-2µ2 with a specific antibody.

The marked effect of AP-2µ2 F174A/D176S on Ca$_V$2.2e37a cell surface expression and whole-cell current suggested that the amino acid sequence in the exon 37 contains AP interaction motifs and mediates trafficking. Nonetheless, the role of AP-2 is predominantly reported to be on endocytosis, and not on trafficking to the plasma membrane. Therefore, I decided to further examine the effect of AP-1 instead of AP-2 on the channel trafficking, since AP-1 plays a key role in trafficking from the TGN in various cell types and also interacts with its cargos through the same motifs (YxxΦ and [DE]xxxL[LI]) (Bonifacino and Traub, 2003).

a
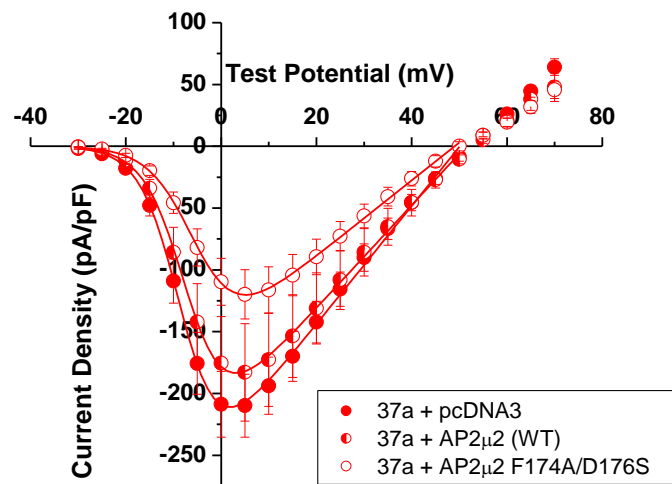
b
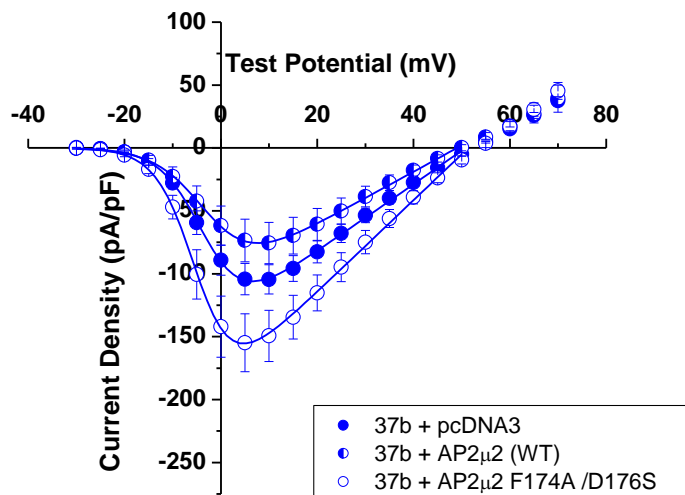
Figure 4.13 Effect of AP-2μ2 WT and F174A/D176S on whole-cell current density of Ca$_V$2.2e37 splice variants.

HA-Ca$_V$2.2e37 isoforms were coexpressed with AP-2μ2 WT, dominant negative mutant AP-2μ2F174A/D176S or blank pcDNA3 in the presence of β1b and α$_2$δ-1 in tsA-201. (**a**) Whole-cell current densities of Ca$_V$2.2e37a. Peak current density (at 5mV): +pcDNA3, -209.9 ± 25.4 pA/pF (n=26); +AP2μ2 WT, -183.0 ± 39.4 pA/pF (n=7); +AP2μ2 F174A/D176S, -154.8 ± 23.1 pA/pF (n=18). (**b**) Whole-cell current densities of Ca$_V$2.2e37b. Peak current density (at 10mV): +pcDNA3, -104.5 ± 11.7 pA/pF (n=39); +AP2μ2 WT, -75.5 ± 16.4 pA/pF (n=8); +AP2μ2 F174A/D176S, -149.4 ± 20.3 pA/pF (n=26). The differences in the peak current densities were not significantly different in one-way ANOVA.

4.9.3 Effect of AP-2 mutant on Ca$_V$2.2 endocytosis

Since AP-2μ2 F174A/D176A dominant negative mutant increased both the cell surface expression and the whole-cell current of Ca$_V$2.2e37b, the effect of this mutant AP-2 on the endocytosis of BBS-Ca$_V$2.2e37b was also assessed. The cell surface expression of BBS-Ca$_V$2.2e37b with the AP-2 mutant was greater than that with the control condition (pcDNA3) throughout the course of the experiment (Figure 4.14), as predicted from the previous immunocytochemistry experiment (Figure 4.12). However, the rate of endocytosis was not significantly different from the control condition (Figure 4.14). This may imply that clathrin-independent endocytic proteins such as caveolin can also mediate the internalisation of Ca$_V$2.2 channels in N2a cells .
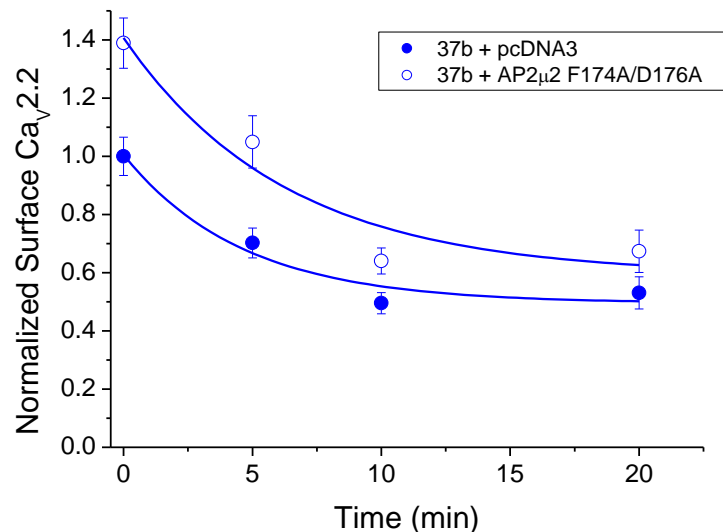
Figure 4.14 Effect of AP-2μ2 F174A/D176S on Ca$_V$2.2 endocytosis.

BBS-Ca$_V$2.2e37b was coexpressed with dominant negative mutant AP-2μ2F174A/D176S or blank pcDNA3 in the presence of β1b and α$_2$δ-1 in N2a. The cell surface BBS-Ca$_V$2.2e37b was normalised to the cell surface fluorescence density of the control condition with pcDNA3 at t=0 in each experiment. The rate of endocytosis (τ, min) was: e37b + pcDNA3 (blue, n=2) 4.61 ± 4.12, 37b + AP2μ2 F174A/D176A (blue open circle, n=2) 6.28 ± 3.81. The cell surface fluorescence was normalised to the average value of 37b + pcDNA3 at t=0 min in the same experiment. The data points in the graph contain all the cells analysed from the two separate experiments.

4.10 Effect of AP-1γ knockdown on trafficking of Ca$_V$2.2 splice variants

AP-1 mediates cargo sorting in the Golgi apparatus, via interaction with YxxΦ and [DE]xxxL[LI] motifs in the cargo. I noted that both these canonical motifs are present in the e37a sequence DMYSLL (Figure 1.8), supporting the possibility of interaction with AP-1. Interestingly, Ca$_V$2.2e37a contains both motifs in an overlapping manner, whereas Ca$_V$2.2e37b contains only a non-canonical [DE]xxxL[LI] motif where LL is substituted by ML (Hofmann et al., 1999; Motta et al., 1995). BFA disrupts AP-1-mediated sorting in the Golgi, and the reduction in the maximum level of Ca$_V$2.2 detected at the plasma membrane in the presence of BFA (Figure 4.10) implicated a role for AP-1 in Ca$_V$2.2 trafficking from the TGN to the plasma membrane.

To examine the involvement of AP-1 in Ca$_V$2.2 trafficking, AP-1γ shRNA was co-expressed with HA-tagged Ca$_V$2.2e37 isoforms to knockdown the expression of the key AP-1 subunit for interaction with [DE]xxxL[LI] (Cheung and Cousin, 2012). AP-1 1a shRNA is specific to AP-1γ sequence that is conserved in human, mouse and rat, while AP-1 1b shRNA is specific to the rat sequence only. These shRNAs inhibited reserve pool replenishment from bulk endosomes. Both AP-1γ shRNAs reduced intracellular AP-1γ (or γ-adaptin) expression level significantly by approximately 40-50% of the control scrambled AP-1γ shRNA in N2a cells (Figure 4.15). Subsequently, the effect of AP-1 1a shRNA on Ca$_V$2.2 cell surface expression was examined. Knockdown of AP-1 caused a modest, but significant reduction in the cell surface expression of both Ca$_V$2.2e37 isoforms (Figure 4.16), despite the partial reduction in the endogenous AP-1γ. These experiments demonstrate that AP-1 mediates trafficking of both Ca$_V$2.2e37 splice variants, and modulates cell surface expression.
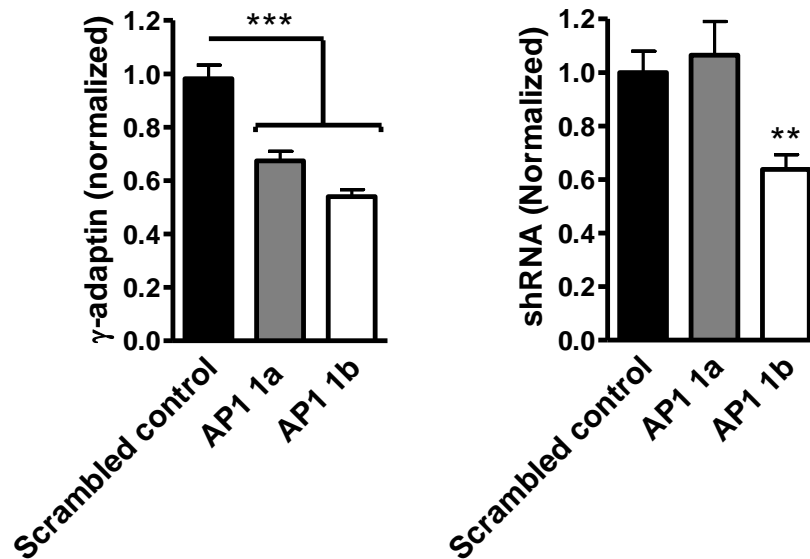
Figure 4.15 Effect of AP-1 knockdown by AP-1 shRNA on γ adaptin levels

Scrambled shRNA control, AP-1γ 1a shRNA or AP-1γ 1b shRNA were expressed in N2a. (Left) The γ adaptin expression was determined by immunostaining, and the expression levels were normalised to the cells expressing the scrambled control. Both AP-1γ shRNA 1a and 1b against AP-1γ subunit significantly reduces the expression of γ adaptin. (Right) The expression level of AP-1γ shRNAs were determined from mCerulean fluorescence, the shRNA expression levels were normalised to the cells expressing the scrambled control. AP-1γ 1b was not expressed as well as other shRNAs. Scrambled shRNA control (black), n=75; AP-1 1a (grey), n=44; AP-1 1b (white), n=83. **$P<0.01$, ***$P<0.001$ (one-way ANOVA).
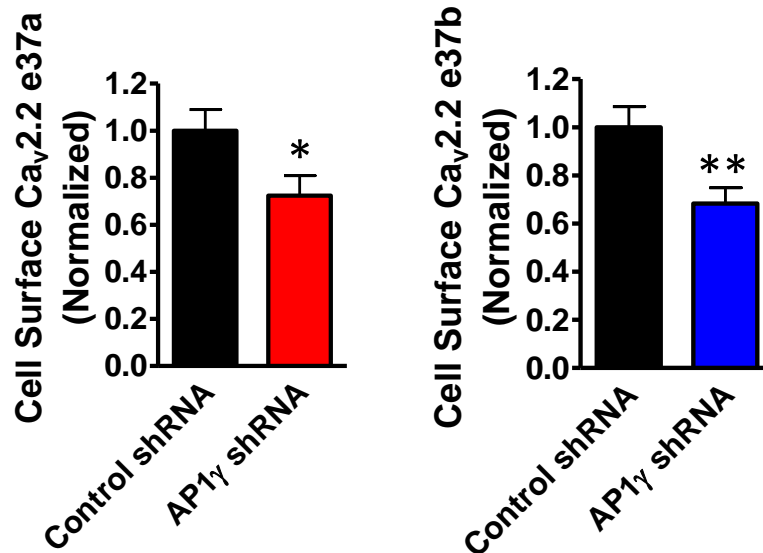
Figure 4.16 Effect of AP-1 knockdown on cell surface expression level of Ca$_V$2.2e37 isoforms.

HA-Ca$_V$2.2e37 isoforms were coexpressed with scrambled shRNA control or AP-1γ 1a shRNA in the presence of β1b and α$_2$δ-1 in N2a. The cell surface HA-Ca$_V$2.2 was normalised to the cells expressing scrambled control. AP-1γ shRNA significantly reduced cell surface expression of both Ca$_V$2.2e37 isoforms. Cell surface Ca$_V$2.2 was normalized to the scrambled AP-1 shRNA control condition in each experiment. The expression of shRNA detected by mCerulean was comparable in all conditions. Ca$_V$2.2e37a+control shRNA (closed bar, n=62); Ca$_V$2.2e37a+AP-1 shRNA (red, n=72). Ca$_V$2.2e37b+control shRNA (closed bar, n=92); Ca$_V$2.2e37b+AP-1 shRNA (blue, n=76). *$P<0.05$, **$P<0.01$ (Student's unpaired t-test).

4.11 Effect of dominant-negative AP-1σ mutant overexpression on trafficking of Ca$_V$2.2 splice variants

To confirm the importance of the interaction between AP-1 and Ca$_V$2.2 for the channel trafficking, the dominant-negative mutant of the σ subunit of AP-1 (AP-1σ V98S) was co-expressed with the Ca$_V$2.2e37 isoforms in N2a cells, in order to impair the interaction with [DE]xxxL[LI]. This construct has been shown to disrupt the somatodendritic trafficking of the copper transporter ATP7B in hippocampal neurons (Jain et al., 2015). AP-1σ V98S significantly reduced the cell surface expression of both Ca$_V$2.2e37 isoforms by approximately 50%, elative to those that were co-expressed with the wild type AP-1σ (Figure 4.17), validating the effect of AP-1γ knockdown. The disrupted trafficking of both Ca$_V$2.2 isoforms, as a result of the impairment of AP-1 function suggests that trafficking of both isoforms was mediated by AP-1 and that the non-canonical DxxxML motif in Ca$_V$2.2e37b may also function as an AP-1 binding motif and mediate trafficking to the plasma membrane.

a
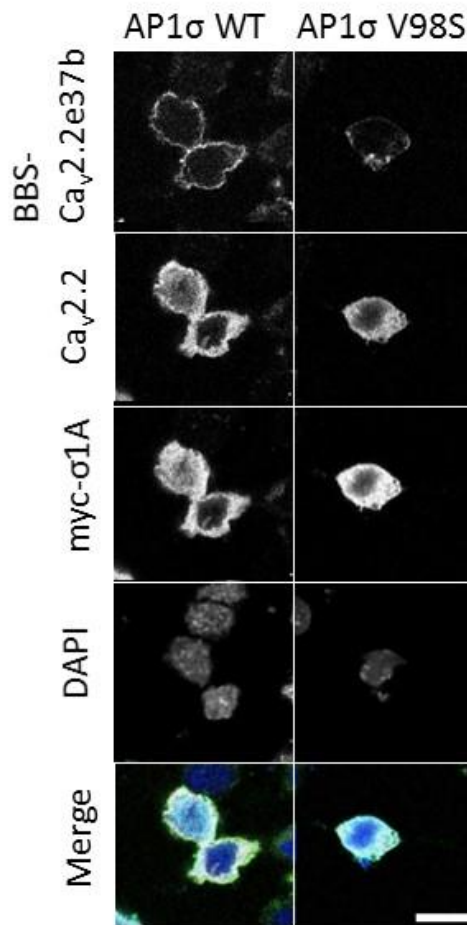
b
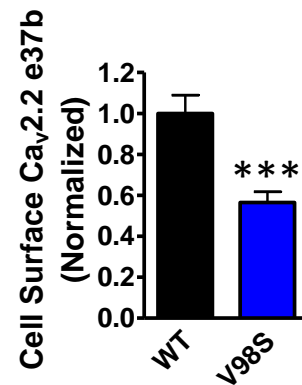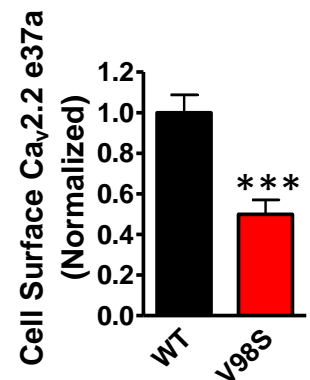
Figure 4.17 Effect of AP-1σ V98S on cell surface expression of Ca$_V$2.2e37 isoforms.

(**a**) Confocal images of BBS-tagged Ca$_V$2.2e37b, showing reduced cell surface expression (second panel) in the presence of AP-1σ V98S, compared to WT (scale bar, 20 μm). (**b**) Dominant-negative AP-1σ V98S mutant significantly reduced cell surface expression of both Ca$_V$2.2e37 isoforms. Cell surface Ca$_V$2.2 was normalized to the wild-type AP-1σ control condition in each experiment. The expression level of myc-tagged AP-1σ detected by anti-myc antibody was comparable in all conditions. (Left) Ca$_V$2.2e37a+AP-1σ WT (closed bar, n=44); Ca$_V$2.2e37a+AP-1σ V98S (red, n=41). (Right) Ca$_V$2.2e37b+AP-1σ WT (closed bar, n=47), Ca$_V$2.2e37b+AP-1σ V98S (blue, n=46). ***$P < 0.001$ (Student's unpaired t-test).

4.12 Adaptor protein interaction motifs in Ca$_V$2.2 splice variants

Since the Ca$_V$2.2e37a sequence contains both YxxΦ and [DE]xxxL[LI] motifs, key residues in wild-type (WT) DMYSLL were mutated to identify which motif is important in AP-1 interaction, and to elucidate the mechanism of Ca$_V$2.2 channel trafficking. In total 4 Ca$_V$2.2e37a mutants were created, mutating DMYSLL to DMASLL (Y/A), DMYSAL (L/A), DMYSAA (LL/AA) and DMASAA (YSLL/ASAA) (Table 4.1). The L/A mutant is only able to interact with AP-1μ, and the Y/A mutant can only interact with AP-1γσ, whereas the LL/AA and YSLL/ASAA mutants completely abolish the interaction with AP-1 via these motifs.

Table 4.1 AP binding motif mutants of Ca$_V$2.2e37a.

		Interaction with:	
Name	Motif	μ1	γ-σ1
WT	DMYSLL	√	√
L / A	DMYSAL	√	
LL / AA	DMYSAA		
Y / A	DMASLL		√
YSLL/YSAA	DMASAA		

4.12.1 Whole-cell expression of Ca$_V$2.2e37a AP binding motif mutants

In order to confirm that Ca$_V$2.2e37a AP binding motif mutants are expressed to the same extent as the WT Ca$_V$2.2, they were co-expressed with α$_2$δ-1 and β1b in tsA-201 cells to determine their whole-cell expression levels against the WT. All mutants were expressed at full length, and no truncated proteins were detected (Figure 4.18). The whole-cell expression levels of the mutants were similar with each other but slightly reduced compared to the WT, particularly for the YSLL/ASAA mutant.
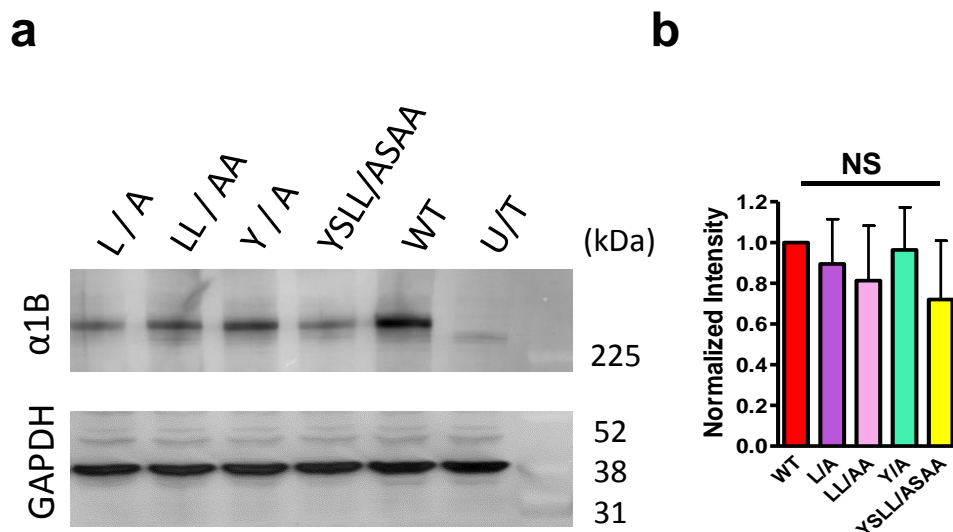
Figure 4.18 Western blot analysis of Ca$_V$2.2e37a AP binding motif mutants.

(**a**) The exemplary western blot showing full length Ca$_V$2.2 channels detected in the whole cell lysates (20 μg per lane) of tsA-201 expressing AP-binding motif mutants with α$_2$δ-1 and β1b. In the untransfected negative control (U/T), cells were transfected with GFP. GAPDH staining shows equal protein loading in all lanes. (**b**) The whole-cell expression levels of Ca$_V$2.2 channels were not significantly different (n=4, one-way ANOVA).

4.12.2 Cell surface expression of Ca$_V$2.2e37a AP binding motif mutants

The cell surface and whole-cell expression levels of these 4 mutants and the WT Ca$_V$2.2e37a were determined by immunocytochemistry (Figure 4.19a). The plasma membrane expression levels of the L/A and Y/A mutants were approximately 50 % of the WT, and the LL/AA and YSLL/ASAA mutants were almost undetectable at the cell surface (Figure 4.19b), despite the intracellular expression levels of all mutants showing no significant difference relative to the WT Ca$_V$2.2e37a (Figure 4.19b). This may reflect the smaller number of cells in which intracellular Ca$_V$2.2 expression was detected, particularly for the YSLL/ASAA mutant, as mutations in these motifs can lead to mis-sorting of the proteins, which are then degraded (Braulke and Bonifacino, 2009). I therefore took the L/A, Y/A and LL/AA mutants forward to further investigate the function and trafficking of these mutants.

a

WT
DMYSLL

L / A
DMYS**A**L

HA-Ca_v2.2
Ca_v2.2

LL / AA
DMYS**AA**

Y / A
DM**A**SLL
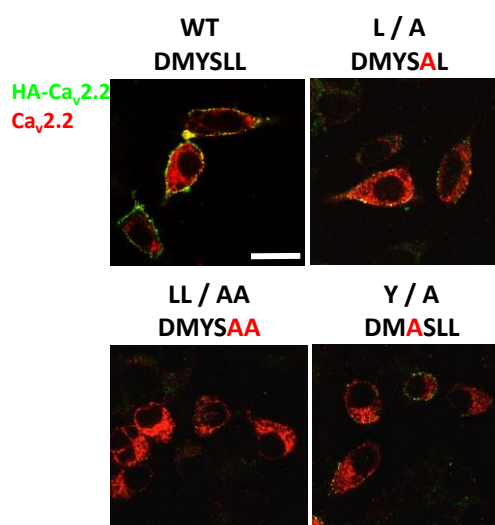
b
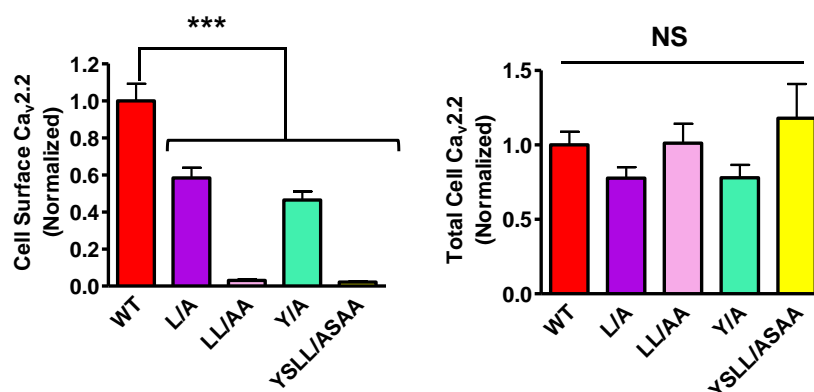
Figure 4.19 Cell surface expression of Cav**2.2e37a AP binding motif mutants.**

(**a**) Confocal images showing N2a expressing HA-tagged AP binding motif mutants (scale bar, 20 μm). (**b**) Cell surface expression of AP binding motif mutants. The values were normalised to the average HA fluorescence intensity of wild-type Ca_v2.2e37a from each experiment. (Left) cell surface: WT (red, n=64); L/A (purple, n=82); LL/AA (pink, n=43); Y/A (green, n=94); YSLL/ASAA (yellow, n=7). (Right) total Ca_v2.2 levels were not significantly different all conditions. Only few cells that were expressing Ca_v2.2 from YSLL/ASAA mutation were detected, due to a very low expression of Ca_v2.2. Mean ± SEM, ***$P < 0.001$ (one-way ANOVA).

4.12.3 Biophysical properties of Ca$_V$2.2e37a AP binding motif mutants

To investigate whether the reduced plasma membrane expression of these Ca$_V$2.2 mutants leads to a parallel reduction in function, the whole-cell current of the L/A, Y/A and LL/AA mutants expressed in tsA-201 cells were recorded in the presence of $\alpha_2\delta$-1 and β1b. No current was detected from the LL/AA mutant (Figure 4.20a), as predicted from the imaging experiments (Figure 4.19b). The L/A and Y/A mutations caused the Ca$_V$2.2 peak currents and G_{max} to be significantly reduced, compared to the WT Ca$_V$2.2e37a (Figure 4.20b). The V_{50} activation voltages were not altered for these mutants (Figure 4.20c).

Furthermore, inactivation properties of the AP binding motif mutant channels were also investigated. Inactivation kinetics (τ) were determined from the decay phase of the current traces at various activation voltages (Figure 4.21a). The inactivation profiles of the WT and L/A mutant were not significantly different, while the inactivation of the Y/L mutant at 0 mV was significantly faster than WT (Figure 4.21b). In addition, steady-state inactivation of the AP binding mutants was not significantly different (Figure 4.21c).

These results demonstrate that AP interaction is involved in the trafficking of Ca$_V$2.2e37a to the cell surface in the presence of the auxiliary subunits, and the reduced cell current density is due to the lower density of channels in the plasma membrane.
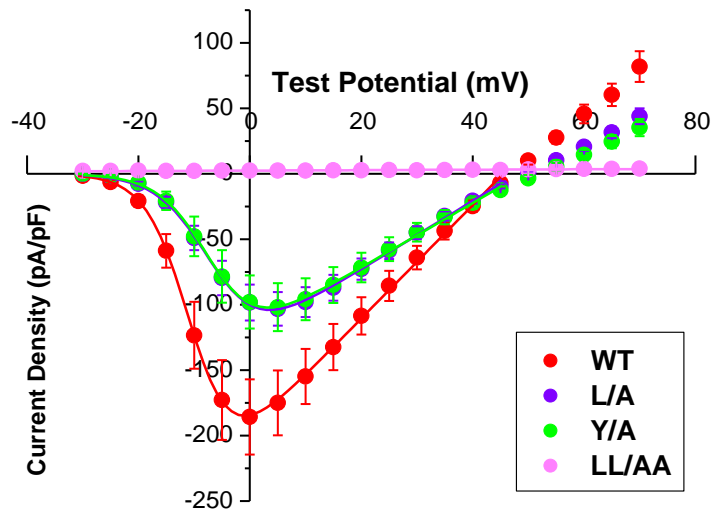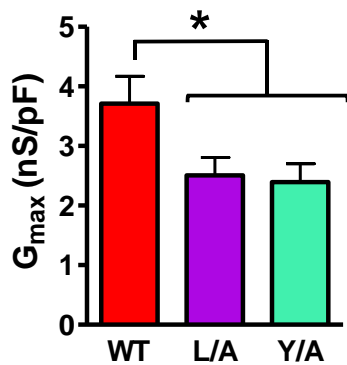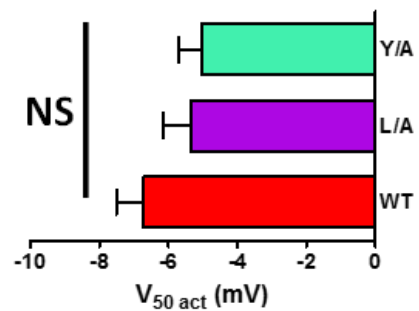
Figure 4.20 Whole-cell current density of Ca$_V$2.2e37a AP binding motif mutants.

(**a**) Whole-cell current density of HA-Ca$_V$2.2e37a AP-binding motif mutants. The current density of HA-Ca$_V$2.2e37b is shown in Figure 3.17. The peak current densities at +0 mV (pA/pF); WT (red), -185.7 ± 28.7 (n=24); L/A (purple), -103.2 ± 12.8 (n=27); Y/A (green), -101.9 ± 18.3 (n=30); LL/AA (pink), 2.44 ± 0.34 (n=4). (**b**) Conductance (G$_{max}$) values. WT (red, n=24); L/A (purple, n=27); Y/A (green, n=30). (**c**) Activation voltages (V$_{50,act}$) are not significantly different. WT (red, n=22); L/A (purple, n=27); Y/A (green, n=30). *P*= 0.27. Mean ± SEM, **P*< 0.05 (one-way ANOVA).
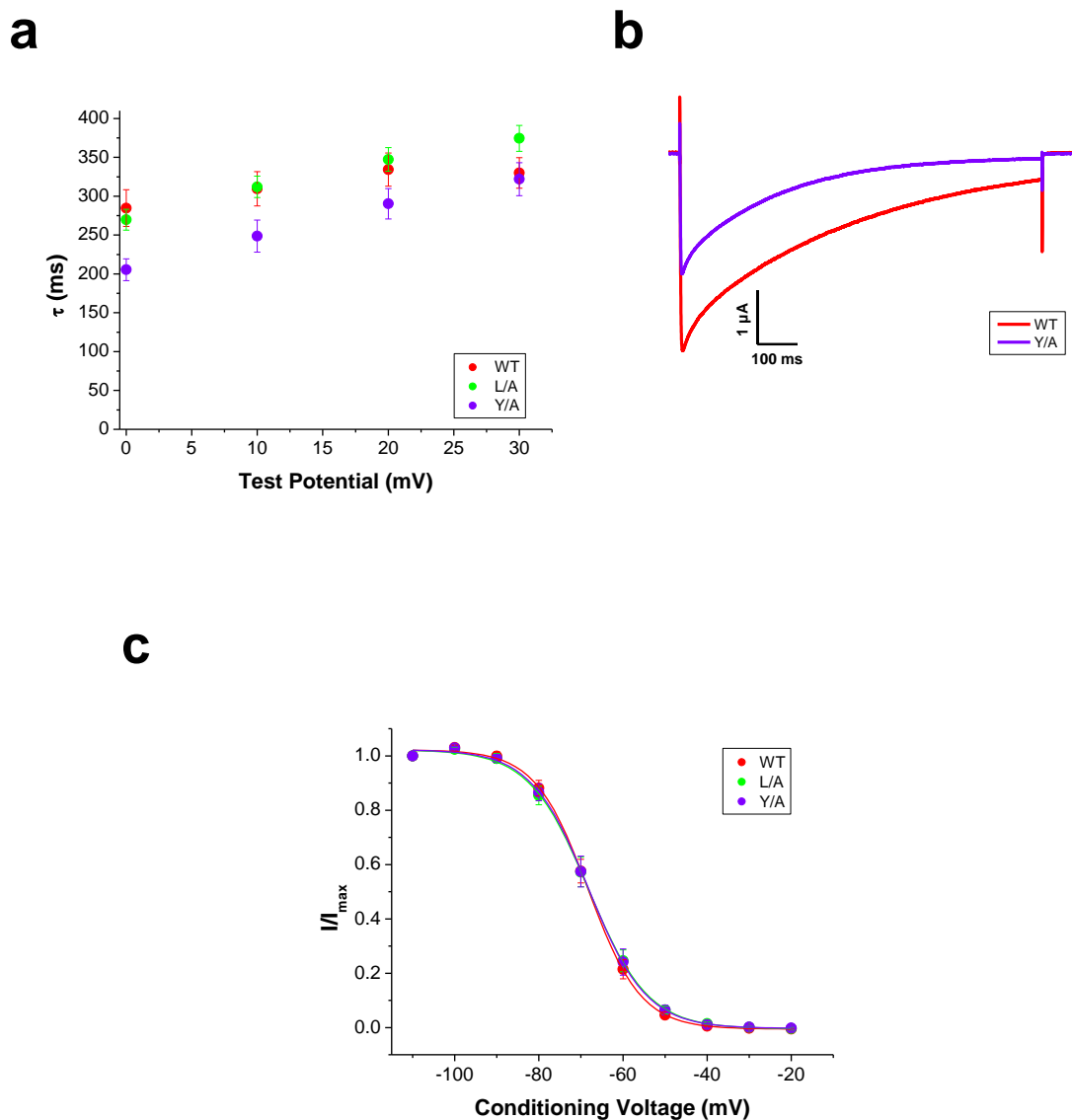
Figure 4.21 Inactivation of Cav2.2e37a AP binding motif mutants.

(**a**) Inactivation kinetics (τ) of WT and AP binding motif mutant Cav2.2e37a at 0, 10, 20 and 30 mV. Current decay of Y/A at 0 mV were significantly smaller than WT and L/A (*P*<0.05, one-way ANOVA). All other values were not significantly different from each other. (**b**) Representative current traces of WT and Y/A with a 0 mV long pulse. The holding potential was -90 mV. (**c**) Steady-state inactivation of the AP binding mutants were not significantly different from WT.

4.13 Expression and cellular localisation of Ca$_V$2.2e37a AP binding mutants in DRG neurons

4.13.1 Cell surface expression of Ca$_V$2.2e37a AP interaction mutants in the cell bodies of DRG neurons

In order to validate that the mutations in the AP-1 binding motifs at the proximal C-terminus of Ca$_V$2.2 have an effect on channel trafficking in neurons, these mutant Ca$_V$2.2 channels were also tagged with GFP at the N-terminus and expressed in DRG neurons, in the presence of α$_2$δ-1 and β1b (Figure 4.22a). Immunostaining for HA revealed that in the cell body of DRG neurons, expression of all mutants at the plasma membrane was reduced, particularly for the LL/AA mutant, without significantly affecting the total expression levels of the channels (Figure 4.22b), similarly to the findings in N2a cells.

4.13.2 Expression of Ca$_V$2.2e37a AP interaction mutants in the neurites of DRG neurons

To determine whether the AP binding motifs mediate Ca$_V$2.2 trafficking to neuronal processes, expression levels of Ca$_V$2.2e37 mutants in the neurites were determined by measuring fluorescence intensities of the GFP-tag. A significantly lower level of these mutants was observed in the neurite compartment (Figure 4.23a), without affecting the expression level of free mCherry as an expression marker (Figure 4.23b). This suggests that these motifs are also crucial for Ca$_V$2.2 trafficking along the neurites.
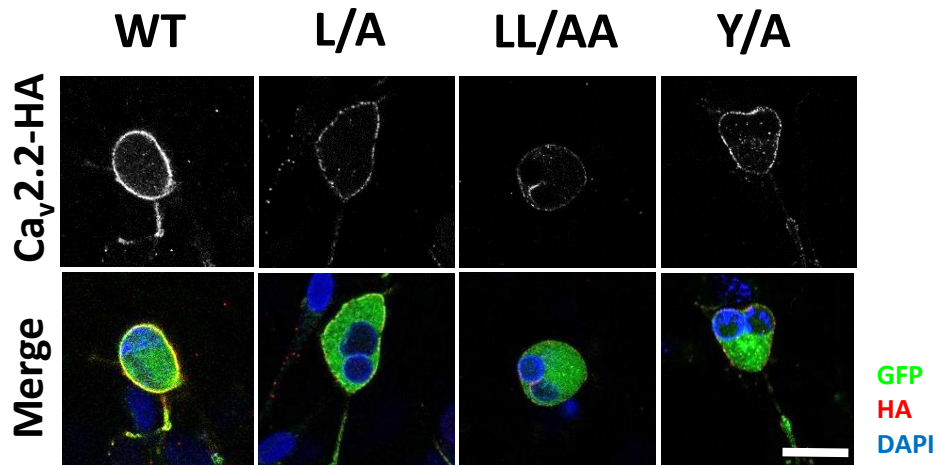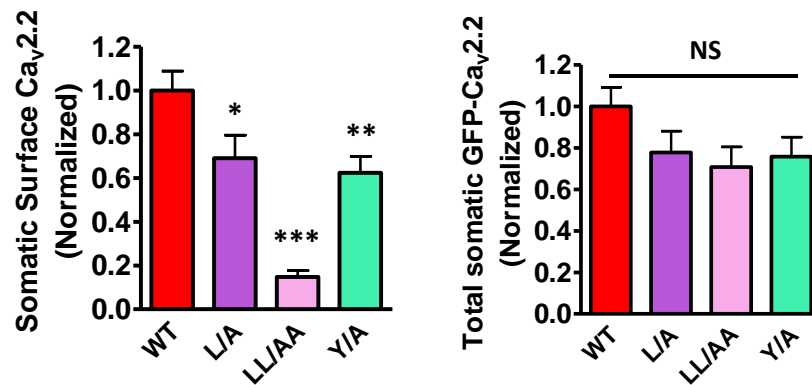
Figure 4.22 Ca$_V$2.2 AP binding motif mutants exhibit reduced trafficking to the cell surface of DRG soma.

(**a**) Confocal images of DRG somata expressing GFP-HA-tagged Ca$_V$2.2e37a AP-binding mutants (scale bar, 20 μm). (**b**) Cell surface expression of AP binding mutants. The values were normalised to the average HA fluorescence intensity of wild-type Ca$_V$2.2e37a from each experiment. Cell surface: WT (red, n=58); L/A (purple, n=34); LL/AA (pink, n=17); Y/A (green, n=43). *$P <$ 0.05, **$P <$ 0.01, ***$P <$ 0.001 (one-way ANOVA).
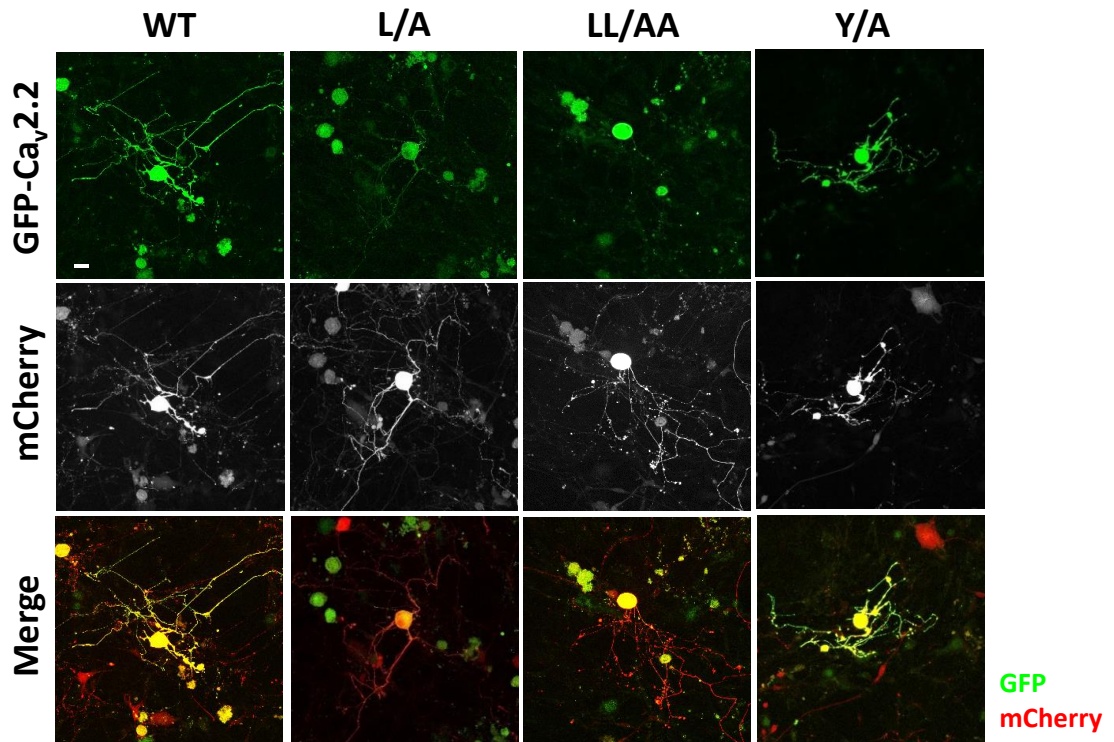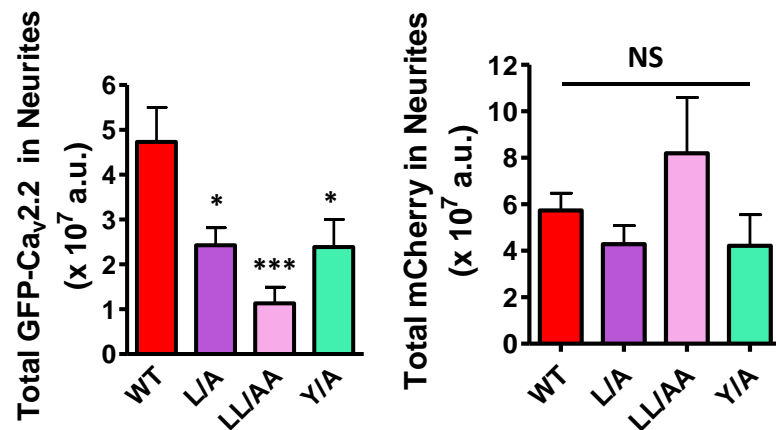
Figure 4.23 Ca$_V$2.2 AP binding motif mutants reduce trafficking to DRG neurites.

(**a**) Confocal images of DRG neurons expressing GFP-HA-tagged Ca$_V$2.2e37a AP-binding mutants (green) with free mCherry (red) in the neuronal processes (scale bar, 20 μm). GFP is also expressed in some non-neuronal cells. (**b**) Total fluorescence of Ca$_V$2.2 AP-binding mutants and free mCherry in the DRG neurites (in x10^7 a.u.). Total: WT (red, n=19); L/A (purple, n=18); LL/AA (pink, n=23); Y/A (green, n=16). The total mCherry fluorescence values in the neurites were not significantly different. *P< 0.05, **P< 0.01, ***P< 0.001 (one-way ANOVA).

4.14 Effect of AP binding mutation on Ca$_V$2.2 intracellular trafficking

4.14.1 Net forward trafficking of Ca$_V$2.2e37a AP binding motif mutants

The L/A and Y/A mutants were also tagged with the exofacial BBS-tag to investigate how these mutations affect intracellular trafficking of Ca$_V$2.2e37a. The appearance of the AP binding motif mutant channels on the plasma membrane was significantly slower than for WT Ca$_V$2.2e37a, leading to a reduction in the maximum fluorescence density of cell surface channels (Figure 4.24a). There was no significant difference between L/A and Y/A in terms of the rate of trafficking nor the maximum cell surface level. The slower overall rates of forward trafficking kinetics for these mutants, compared to WT Ca$_V$2.2e37a (Figure 4.24b), were similar to that for WT Ca$_V$2.2e37a in the presence of BFA (Figure 4.10).

4.14.2 Endocytosis of Ca$_V$2.2e37a AP binding mutants

Since the AP-binding motifs in the Ca$_V$2.2e37 isoforms are also recognised by AP-2 involved in endocytosis, the basal rate of endocytosis of the two isoforms and the Ca$_V$2.2e37a mutants were compared (Figure 4.25a). The average time constant for endocytosis was approximately doubled for the Ca$_V$2.2e37a L/A mutant, and more than tripled for the Y/A mutant, compared to WT Ca$_V$2.2e37a (Figure 4.25b). This observation could be explained by the action of AP-2 interacting with either YxxΦ or [DE]xxxL[LI], which mediates clathrin-dependent endocytosis (Nesterov et al., 1999; Motley et al., 2003). Slower internalisation of the Y/A mutant channels suggests that the YxxΦ motif plays a more dominant role than the [DE]xxxL[LI] motif in AP-2-mediated endocytosis of Ca$_V$2.2e37a.

a
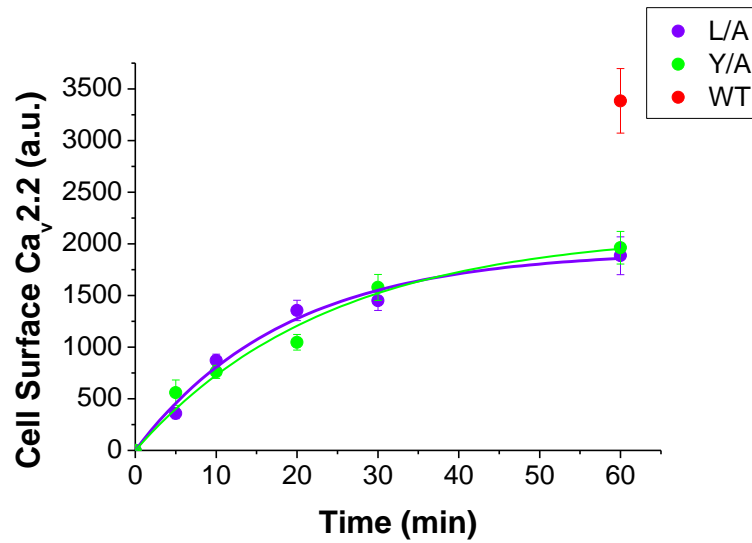
b
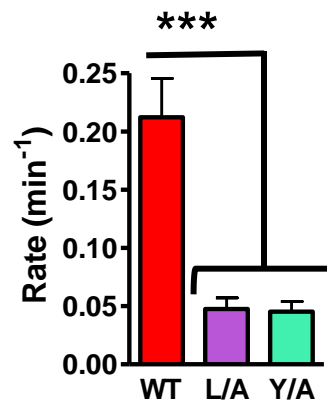
Figure 4.24 The net forward trafficking kinetics of Ca$_v$2.2e37a AP binding motif mutants.

(**a**) Net forward trafficking kinetics of AP binding motif mutants. L/A (purple), Y/A (green). Cell surface Cav2.2 of WT (red) was determined at t=60min as a control. The data points in the graph contain all the cells analysed from the 3-5 separate experiments. (**b**) Net forward trafficking rates 1/τ (min^{-1}): WT (red), 0.212 ± 0.027 (n=3, from Figure 4.10); L/A (purple), 0.048 ± 0.009 (n=5); Y/A (green) 0.045 ± 0.008 (n=4). Mean ± SEM, ***P< 0.001 (one-way ANOVA).

a
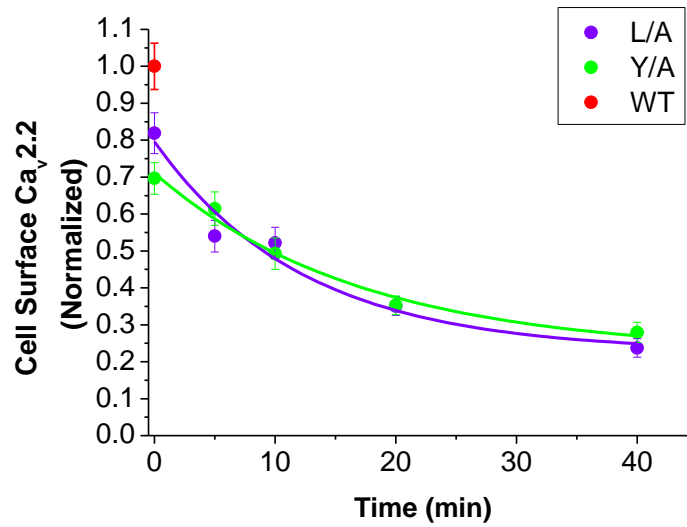
b
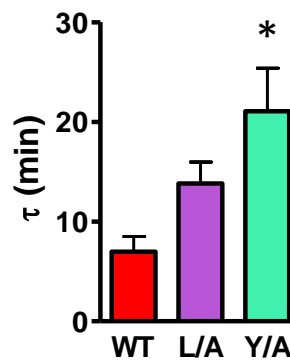
Figure 4.25 Endocytosis of Ca$_V$2.2e37a AP binding motif mutants.

(**a**) Endocytosis kinetics of Ca$_V$2.2e37a AP binding motif mutants. L/A (purple) and Y/A (green). WT as a control at t=0min (red). All plasma membrane fluorescence densities were normalised to average value of the WT at t=0 min. The data points in the graph contain all the cells analysed from the 3-4 separate experiments. (**b**) Rate of endocytosis expressed as time constants τ (min); WT (red), 7.00 ± 1.23 (n=3, from Figure 4.11); L/A (purple), 13.8 ± 1.85 (n=4); Y/A (green), 21.1 ± 3.53 (n=3). Mean ± SEM, *$P<$ 0.05 (one-way ANOVA).

4.15 Summary and Discussion

Using the tagged $Ca_V2.2$ constructs, I demonstrate enhanced trafficking of $Ca_V2.2e37a$ compared to the e37b splice variant, both to the plasma membrane and to neuronal processes of DRG neurons where these channels are physiologically important. The cell surface expression of $Ca_V2.2e37$ splice variants and mutants in transfected tsA-201, N2a and DRG neurons showed good correlations, demonstrating that these cells lines are suitable models to study $Ca_V2.2$ trafficking. The only exception is when these splice variants were expressed in the absence of $\alpha_2\delta$-1 (Figure 4.4, Figure 4.5), where N2a showed that the cell surface expression of $Ca_V2.2e37b$ was greater than e37a without $\alpha_2\delta$-1 (although this difference was not statistically significant in one-way ANOVA), whereas the average whole-cell currents of the two splice variants without $\alpha_2\delta$-1 in tsA-201 were identical. Neither cell lines express endogenous $\alpha_2\delta$ subunits (Cassidy et al., 2014), and the source of this difference is unknown.

The 37a exon contains interaction motifs for both the μ1 subunit and γ-σ1 hemicomplex of AP-1, which are overlapping (DMYSLL). The complete abolition of both motifs by mutating the motif to DMYSAA or DMASAA severely disrupted the trafficking of $Ca_V2.2e37a$ to the cell membrane and to DRG neurites, demonstrating the importance of these AP-1 interaction sites in the proximal C-terminus of $Ca_V2.2$. Furthermore, [DE]xxxL[LI] is also present in other voltage-gated calcium channels such as $Ca_V1.3$, 1.4 and $Ca_V2.1$(e37a) in the proximal C-terminus (Table 4.2), which may indicate an importance of this motif in trafficking of VGCCs. On the other hand, the $Ca_V2.2e37b$ splice variant has a non-canonical [DE]xxxL[LI] motif, where L[LI] is substituted by ML (DMEFML), which is indicated to be a less efficient signal compared with the canonical motif (Motta et al., 1995; Hofmann et al., 1999). In addition, the e37b sequence lacks YxxΦ. This may explain why $Ca_V2.2e37b$ channels are less efficiently trafficked to the plasma membrane and to the DRG neurites, compared to $Ca_V2.2e37a$, which contains two strong signals for binding to AP-1 in this exon.

The proximity of these motifs in the C-terminus of $Ca_V2.2$ to the membrane may also create a favourable site for AP-1 interaction. This has been demonstrated for AP-2 which is recruited to the plasma membrane via

PtdIns4,5P$_2$ interaction. This causes AP-2 to undergo a "locked" to "open" conformational change which exposes its motif-binding sites (Jackson et al., 2010). Although phosphoinositides such as PtdIns4P, that are prevalent in the Golgi, are alone insufficient for the recruitment of AP-1, the close proximity of these motifs to the membrane is probably important, as membrane-associated Arf1 brings AP-1 close to the Golgi membrane, where it unlocks the AP-1 conformation to allow for cooperative binding of the cargo and PtdIns4P (Ren et al., 2013; Stamnes and Rothman, 1993; Crottet et al., 2002).

The overlapping nature of the AP-1 binding motifs in Ca$_V$2.2e37a is unprecedented, but the AP-1 complex would be unable to bind both simultaneously due to conformational constraints (Heldwein et al., 2004; Ren et al., 2013). However, abolishing either one of the binding sites for AP-1µ1 and γ-σ1 in Ca$_V$2.2e37a, by mutating the key amino acids, led to a partial loss of cell surface expression and trafficking to the DRG neurites in this study. This indicates that both of the AP-1 subunits separately have the ability to interact with the overlapping motif in e37a, and are able to partially compensate for the trafficking defect in the e37a single mutants, when only one of the potential binding sites is available. However, when both motifs are available for interaction, one of the AP-1 subunits may have a higher affinity than the other towards its corresponding motif, to mediate more efficient trafficking in a native state. The binding affinity of AP-1 to these motifs has not been reported so far, but AP-2 has shown approximately 10-times greater affinity for YxxΦ than [DE]xxxL[LI] in recombinant proteins (Höning et al., 2005).

Other intracellular regions of Ca$_V$2.2 also contain possible interaction sites for APs. For example, there is one YxxΦ motif in the N-terminus (Y59), and two in the II-III loop (Y811 and Y1154), whereas there is only one other [DE]xxxL[LI] site in the distal C-terminus (E2256) in Ca$_V$2.2 (Figure 1.11), and all of these sites are conserved in human, mouse, rat, rabbit and chicken Ca$_V$2.2 sequences (available from database of National Center for Biotechnology Information (NCBI), U.S. National Library of Medicine). In the case of AP-2, binding to [DE]xxxL[LI], YxxΦ and PtdIns4,5P$_2$ is essential for ensuring its high affinity for the cargo in the membrane (Jackson et al., 2010). Ca$_V$2.2e37a may be able to present both motifs in the e37a sequence to the AP-1 complex studied here, and as a result the AP-1 complex is able to interact

with the conformationally most favourable counterpart motif for mediating effective trafficking. No mutational or interaction studies have been conducted on the other sites in Cav2.2 so far, and it will now be important to investigate the involvement of these sites in AP-mediated trafficking.

Although it is not clear which AP-1 subunit mediates trafficking more effectively in the native state, it has been shown for AP-2 that it interacts with YxxΦ with a higher affinity than [DE]xxxL[LI] (Jackson et al., 2010). This was also found in our experiments where Cav2.2e37a Y/A mutant showed a markedly slower endocytosis rate, indicating that the YxxΦ motif may also interact with AP-2μ2 subunits which are involved predominantly in clathrin-mediated endocytosis (Nesterov et al., 1999). Our findings suggest that in the case of endocytosis, YxxΦ may play a more important role than [DE]xxxL[LI] in mediating Cav2.2 internalisation.

Both shRNA knockdown of AP-1γ and expression of the dominant-negative AP-1σ mutant V98S reduced trafficking of both isoforms to the plasma membrane. This provides direct evidence for AP-1 mediating trafficking for both isoforms of Cav2.2, e37a and e37b. Nevertheless, incomplete inhibition suggests that Cav2.2 trafficking may also involve non-clathrin-mediated mechanisms, such as lipid raft and caveolae-mediated trafficking (Le Roy and Wrana, 2005; Parton and Simons, 2007). Indeed, Cav2 channels co-localise with caveolin and flotillin-1 in the presence of β and α2δ subunits, and are present in lipid rafts (Davies et al., 2006; Robinson et al., 2010). Overexpression studies of AP-1 dominant-negative mutants have previously indicated that AP-1 mediates somatodendritic trafficking of transmembrane receptors in the central neurons such as hippocampal neurons (Farías et al., 2012; Jain et al., 2015). Cav2.2e37a AP-1 binding site mutants demonstrate that AP-1 may also play an important role in axonal trafficking in DRG neurons, since these are pseudo-unipolar neurons that do not form dendrites, therefore binding of AP-1 to these sites may modulate the presence of these channels at the presynaptic membrane (Figure 4.26).

Throughout this study, cell surface expression levels of Cav2.2e37 splice variants and AP-binding mutants were carefully quantified and compared, by ensuring that the whole-cell expression levels of these α subunits were not significantly different between different conditions, thus the differences

observed at the cell surface were due to trafficking, and not due to the increased protein expression. Since the auxiliary subunits $\alpha_2\delta$-1 and β1b co-transfected in these experiments did not contain expression markers indicating their expression in the same cells, immunostaining for α subunits was crucial as smaller subunits such as $\alpha_2\delta$-1 and β1b are likely to be present if a very large subunit such as Ca$_V$2.2 α subunits is present. In the case of quadruple expression with AP-1 shRNAs and AP-1σ subunits, the cells for analysis were selected based on Ca$_V$2.2 α expression as well as the expression markers on these RNAs and proteins to ensure their presence.

In summary, this study provides an important insight into a novel Ca$_V$2.2 trafficking mechanism, which is modulated by alternative splicing, and mediated by AP-1. In the future studies, how the disruption of AP-1-mediated Ca$_V$2.2 trafficking affects Ca^{2+} influx at the presynaptic terminals should be measured by genetically-encoded Ca^{2+} indicator GCaMP (Tian et al., 2009; Akerboom et al., 2012) in functional synapses. Furthermore, how trafficking of Ca$_V$2.2 influences exocytosis from presynaptic terminals upon depolarisation, which likely to represent neurotransmitter release, could also be determined by electrophysiological methods examining evoked postsynaptic current, or presynaptically expressing VGlut1 tagged with pH-sensitive indicators such as mOrange or pHluorin (Hoppa et al., 2012; Ferron et al., 2014; Kavalali and Jorgensen, 2014).

Table 4.2 [DE]xxxL[LI] and YxxΦ motifs in the C-terminus of VGCCs.

Ca$_V$1.2	GRIKHL**D**VVT**LL**RRIQ
Ca$_V$1.3	GRIKHL**D**VVT**LL**RRIQ
Ca$_V$2.1 (e37a)	GRIHYK**DMY**S**LL**RVIS
Ca$_V$2.1 (e37b)	GRMPYL**DMY**Q**ML**RHMS
Ca$_V$2.2 (e37a)	CRIHYK**DMY**S**LL**RCIA
Ca$_V$2.2 (e37b)	GRISYN**D**MFE**ML**KHMS
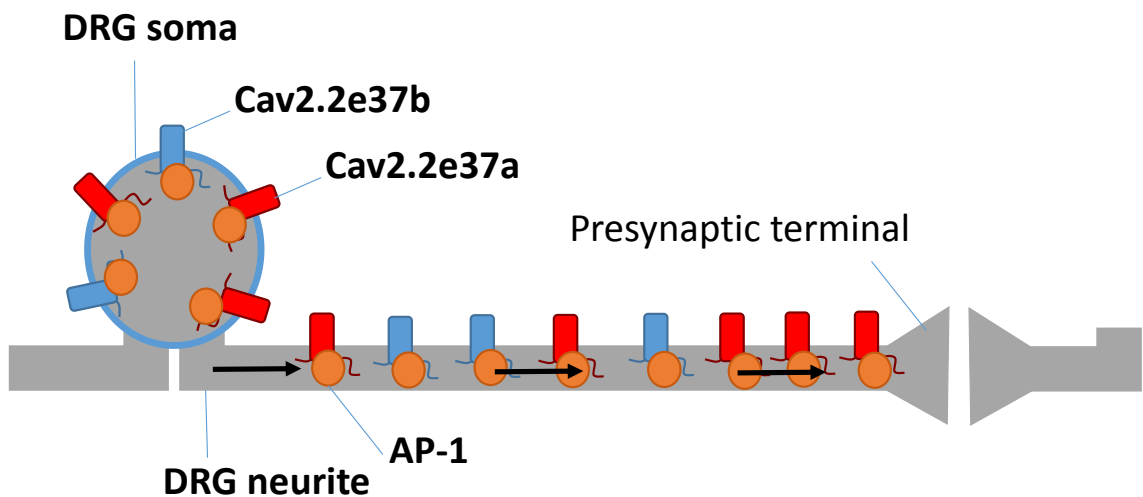
Figure 4.26 Trafficking of Ca$_V$2.2 splice variants in DRG neurons.

Schematic diagram of Ca$_V$2.2e37a (red) and e37b (blue) trafficking mediated by AP-1 (orange) to the plasma membrane of DRG soma and along the axon, as a result of alternative splicing.

Chapter 5 Effect of G protein-coupled receptors on calcium channel trafficking

5.1 Introduction

Previous studies have demonstrated that both D1 and D2 dopamine receptors directly interact with Ca$_V$2.2 via intracellular regions to modulate the channel properties, cell surface expression and internalisation (Kisilevsky et al., 2008; Kisilevsky and Zamponi, 2008). Nevertheless, the effect of GPCRs on trafficking of Ca$_V$2.2 splice variants has not been examined to this date. As described previously, Ca$_V$2.2e37 isoforms exhibit differential voltage-dependence of their G protein-mediated inhibition (Raingo et al., 2007; Andrade et al., 2010). The key amino acid residue involved in the voltage-independent inhibition of Ca$_V$2.2e37a was found to be the tyrosine residue in the YxxΦ motif (Raingo et al., 2007), which is involved in the AP-mediated channel trafficking as described in Chapter 4. This suggested a possible link between the G protein-mediated voltage-independent inhibition and trafficking of Ca$_V$2.2 isoforms. Here, the effect of D2R activation on Ca$_V$2.2e37 splice variant trafficking was extensively examined, using cell surface immunocytochemistry, electrophysiology and live cell labelling.

5.2 Effect of D2R on Ca$_V$2.2 trafficking

First, Ca$_V$2.2e37 isoforms (with α$_2$δ-1 and β1b) were co-expressed with D2R in N2a cells to determine the effect of D2R on cell surface expression the isoform channels without receptor activation. D2R had no effect on the cell surface expression of Ca$_V$2.2e37a, and modestly enhanced the cell surface expression of Ca$_V$2.2e37b (Figure 5.1). The effect on Ca$_V$2.2e37a was
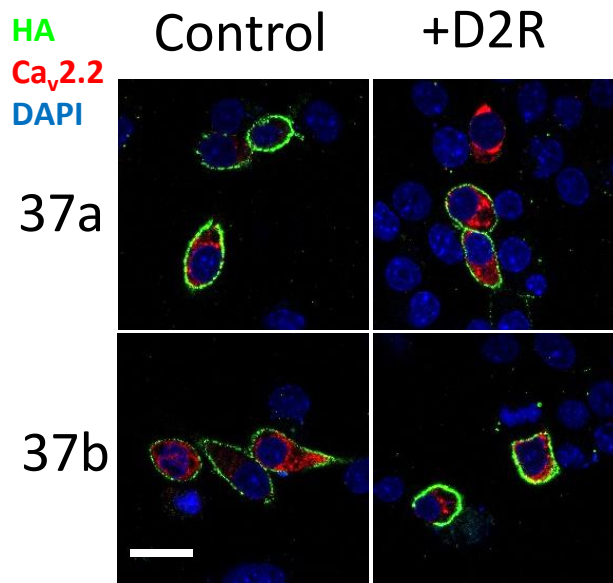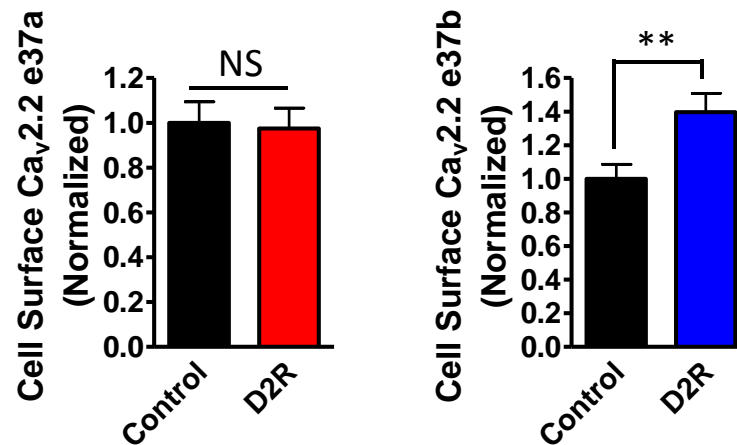
Figure 5.1 Effect of D2R expression on cell surface Ca$_V$2.2e37 isoforms.

(**a**) Confocal images of N2a cells expressing HA-tagged Ca$_V$2.2 with or without D2R (scale bar, 20 μm), in the presence of β1b and α$_2$δ-1. (**b**) Cell surface Ca$_V$2.2 with D2R is normalised to the control condition expressing empty vector in each experiment: Ca$_V$2.2e37a (closed bar, n=117); Ca$_V$2.2e37a+D2R (red, n=136); Ca$_V$2.2e37b (closed bar, n=133); Ca$_V$2.2e37b+D2R (blue, n=153). **P$<$0.01 (Student's unpaired t-test).

unexpected, as it has previously been reported that both D1R and D2R greatly enhance Ca$_V$2.2e37b expression at the plasma membrane (Kisilevsky and Zamponi, 2008; Kisilevsky et al., 2008). This observation suggests that Ca$_V$2.2e37 isoforms are differentially modulated by D2R.

5.3 Co-localisation between Ca$_V$2.2 splice variants and D2R at the cell surface

It has previously been reported that Ca$_V$2.2 and D2R directly interact and co-localise in both neurons and in expression system (Kisilevsky and Zamponi, 2008), but it is not clear whether these two species interact at the cell surface. To demonstrate the cell surface localisation of D2R, 3xFLAG tag was inserted at the end of the N-terminus of D2R, which is the extracellular domain in the native receptor. FLAG-tagged D2R and HA-Ca$_V$2.2 splice variants were co-expressed in N2a cells and extracellularly immunostained simultaneously post-fixation (Figure 5.2a). Confocal images revealed that D2R and Ca$_V$2.2 co-localise to some extent (Figure 5.2b). In order to analyse the co-localisation further, the images were analysed using a co-localisation analysis plugin in ImageJ. Pearson's correlation coefficient (r_P) indicated a low level of pairing in the distributions of the signals from D2R and Ca$_V$2.2, particularly for Ca$_V$2.2e37b (Figure 5.3a). The overlapping coefficient (r), which is an improved representation of the co-localisation between the two signals, indicated that approximately half of the total signals co-localise with the counterpart (Figure 5.3b). Both splice variants co-localised with D2R to a similar extent. Manders' coefficients (M_1 and M_2) are useful when the two images to be compared contain unequal numbers of objects, which is the likely case in most biological systems (Manders et al., 1993). M_1 indicates the proportion of FLAG-D2R co-localising with HA-Ca$_V$2.2 (Figure 5.3c left), and M_2 indicates the proportion of HA-Ca$_V$2.2 co-localising with FLAG-D2R (Figure 5.3c, right). For all of these co-localisation coefficients, the value would be 0 if the distribution was completely random and there were no overlaps of the two objects. If the two objects had the identical distribution, then these co-localisation coefficients would be 1 (Manders et al., 1993). In the M_1 analysis, Ca$_V$2.2e37b showed a significantly lower co-localisation compared to e37a, however, the M2 analysis

demonstrated an opposite trend for M$_1$. This could be due to the fact that many of the images for Ca$_V$2.2e37b in these experiments contained a higher background FLAG signal relative to e37a, which may have confounded the results. The source of the high FLAG noise is unknown, however, the three different type of analysis implied that partial co-localisation between D2R and Ca$_V$2.2 occurs at the cell surface in this expression system.

a
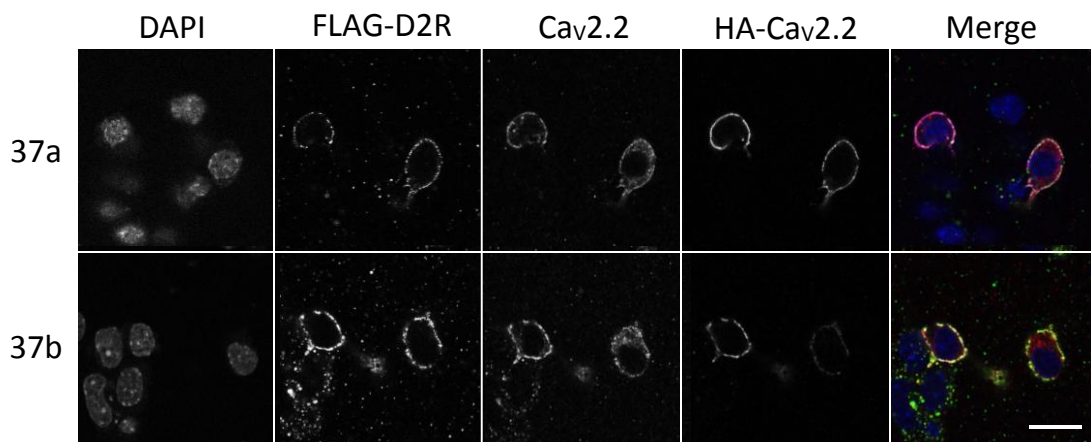
b
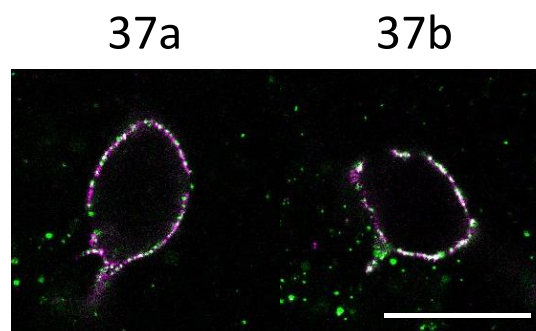
Figure 5.2 Co-localisation of D2R and Ca$_V$2.2 splice variants.

(**a**) Confocal images of N2a cells expressing 3xFLAG-D2R with HA-Ca$_V$2.2e37 (top) and HA-Ca$_V$2.2e37b (bottom). (**b**) Some co-localisation between D2R and Ca$_V$2.2 was observed at the plasma membrane. DAPI (blue), FLAG-D2R (green), CaV2.2 (red), HA-Ca$_V$2.2 (purple). White indicates the co-localisation between D1R and Ca$_V$2.2. Scale bar, 20 μm.
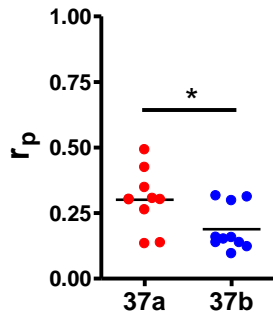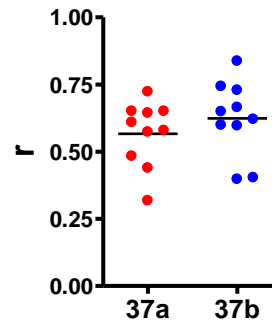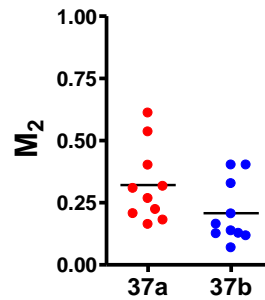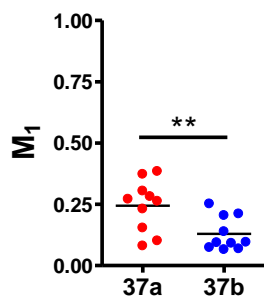
Figure 5.3 Co-localisation coefficients for D2R and Ca$_V$2.2 splice variants.

These co-localisation coefficients were determined using ImageJ plugin, JACoP. The value would be 0 if the distribution of HA-Ca$_V$2.2 and 3xFLAG-D2R in N2a cell surface is completely random and there are no overlaps of the two objects. If the two objects have the identical distribution, then these co-localisation coefficients would be 1. (**a**) Pearson's correlation coefficients (r_P), P=0.0201. (**b**) Overlapping coefficients (r), P=0.34. (**c**) Manders' co-localisation coefficient. M_1, P=0.0093. M_2, P=0.0832. Ca$_V$2.2e37a (red, n=10), Ca$_V$2.2e37b (blue, n=10).

5.4 Effect of D2R activation on cell surface $Ca_V2.2$ splice variants

5.4.1 Determining effective concentrations of quinpirole for $Ca_V2.2$ splice variant internalisation

Next, I examined whether $Ca_V2.2$ internalisation initiated by activation of GPCRs would be different for $Ca_V2.2e37$ isoforms. Upon D2R activation by the specific agonist Quin, the amount of both $Ca_V2.2e37$ isoforms on the cell surface was significantly reduced relative to the 0 nM Quin control after 30 min at 37 °C (Figure 5.4), which is likely to represent internalisation. The cell surface expression of $Ca_V2.2$ isoforms was dependent on the concentration of Quin, and was significantly reduced compared to the control at 100 nM, 300 nM and 1 µM. $Ca_V2.2e37a$ was more sensitive to a lower concentration of Quin, as the relative cell surface expression was significantly less at 30 nM Quin for $Ca_V2.2e37a$, but not for $Ca_V2.2e37b$. The relative reduction in amount of $Ca_V2.2$ at the cell surface in the presence of 100nM Quin was similar for both isoforms (Figure 5.5).

a

Cav2.2e37a

b
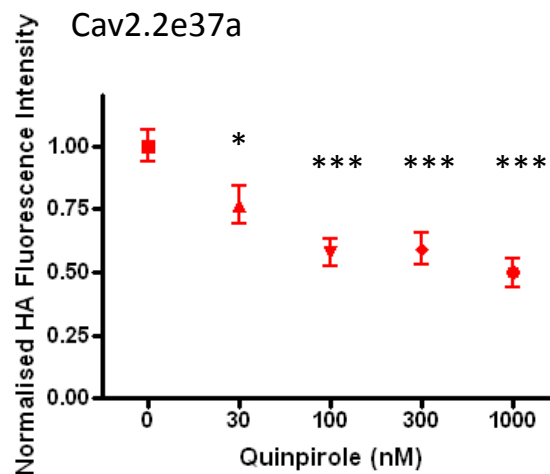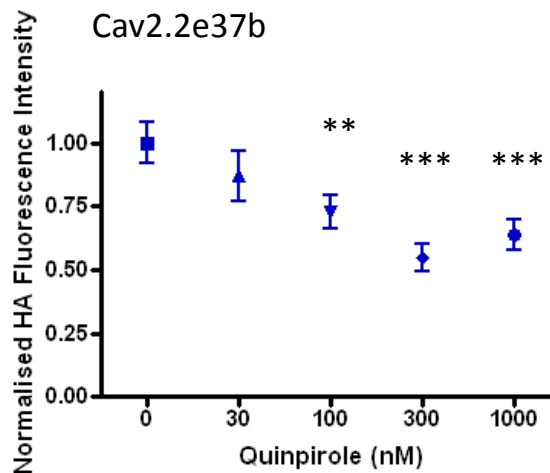
Cav2.2e37b

Figure 5.4 Dose-dependent effect of Quin on cell surface expression of Ca$_V$2.2e37 splice variants.

N2a cells co-expressing Ca$_V$2.2e37 isoforms and D2R were incubated with Quin at a range of concentrations for D2R activation. Relative cell surface Ca$_V$2.2e37a and e37b after 0, 30, 100, 300 and 1000 nM Quin application at 30 min at 37 °C. The cell surface florescence intensities of HA-Ca$_V$2.2 were normalised to the average value at t=0 min in each experiments. (**a**) Ca$_V$2.2e37a +0nM Quin (n=90), 30nM Quin (n=71), 100nM Quin (n=77), 300nM Quin (n=74), 1000nM Quin (n=51). (**b**) Ca$_V$2.2e37b +0nM Quin (n=80), 30nM Quin (n=76), 100nM Quin (n=76), 300nM Quin (n=89), 1000nM Quin (n=74) *$P<0.05$, **$P<0.01$, ***$P<0.001$ (one-way ANOVA).
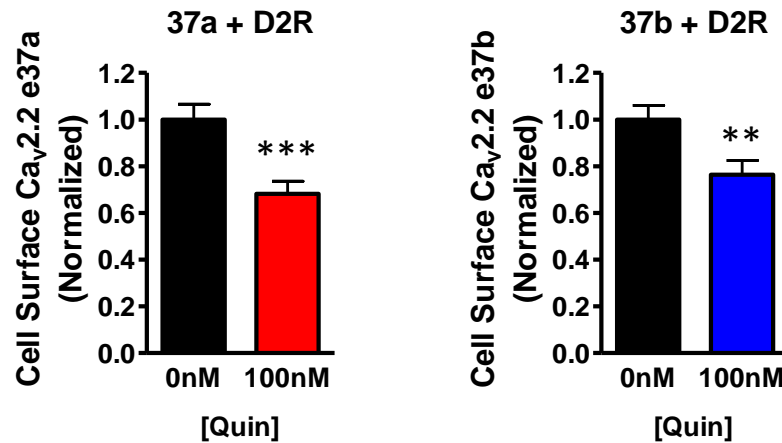
Figure 5.5 Effect of D2R activation on cell surface Ca$_V$2.2e37 splice variants.

Cell surface Ca$_V$2.2 in the presence of D2R, with or without 100nM Quin in N2a.   (Left) Ca$_V$2.2e37a (closed bar, n=98); Ca$_V$2.2e37a+Quin (red, n=99). (Right) Ca$_V$2.2e37b (closed bar, n=104); Ca$_V$2.2e37b+Quin (blue, n=91). **$P<0.01$, ***$P<0.001$ (Student's unpaired t-test).

5.4.2 Pertussis toxin is ineffective in blocking activated D2R-mediated Ca$_V$2.2 internalisation

In order to investigate further the mechanisms of D2R activity-mediated internalisation of Ca$_V$2.2, the cells expressing Ca$_V$2.2 splice variants and D2R were pre-treated with 500 ng/ml pertussis toxin (PTX) 16 h prior to the experiment to block any G protein-mediated action on Ca$_V$2.2. The activity of PTX was confirmed in the electrophysiological experiment, in which PTX blocks the G$\beta\gamma$-mediated voltage-dependent inhibition of Ca$_V$2.2 by Quin at this concentration (Figure 5.6).   However, the D2R activation-mediated internalisation of Ca$_V$2.2 splice variants was not blocked by pre-treatment with PTX under the same condition (Figure 5.7), indicating that D2R activity-mediated internalisation is independent of the direct action of G$\beta\gamma$ on Ca$_V$2.2.

a
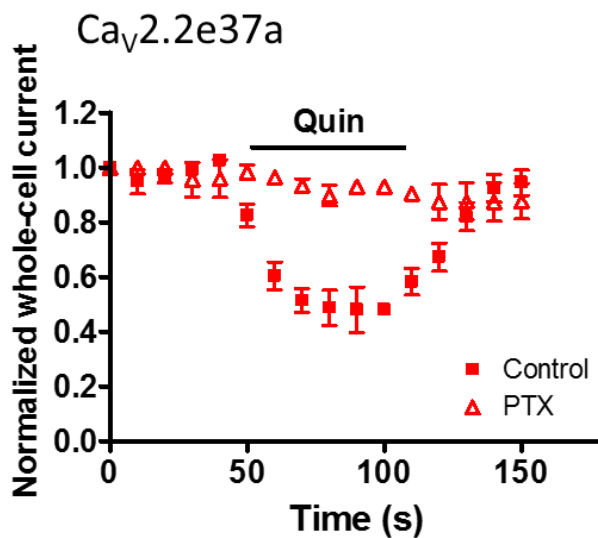
b
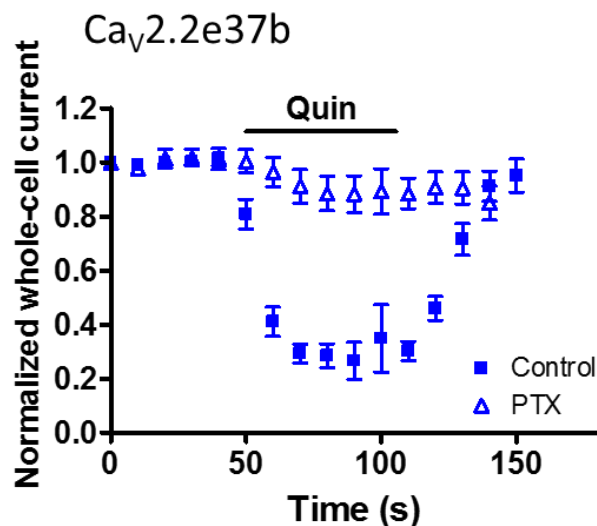
Figure 5.6 PTX blocks inhibition of Ca$_V$2.2 isoforms by D2R activation.

Whole-cell currents of Ca$_V$2.2e37 isoforms expressed in tsA-201 were normalised to the basal current at the beginning of the recording, prior to the addition of 300nM Quin. In the control condition, Quin application inhibits Ca$_V$2.2 current when the channels were activated at +5 mV. PTX pre-treated cells block this effect.   (**a**) Ca$_V$2.2e37a control (red closed squares), n=22; Ca$_V$2.2e37a control (red open triangles), n=3.   (**b**) Ca$_V$2.2e37b control (blue closed squares), n=23; Ca$_V$2.2e37b with PTX (blue open triangles), n=10.

5.4.3 AP-2 is involved in Ca$_V$2.2 internalisation triggered by D2R activation

Receptor sequestration has been reported for a number of GPCRs following activation, which is mediated by the recruitment of β-arrestin to the activated receptor (Krupnick and Benovic, 1998). β-arrestin targets GPCRs for clathrin-dependent internalisation by directly interacting with AP-2 (Goodman et al., 1996; Laporte et al., 1999; Zhang et al., 1996; Laporte et al., 2000). To test if blocking clathrin-mediated internalisation also inhibits D2R activation-induced Ca$_V$2.2 internalisation, the dominant-negative mutant of the AP-2 μ2 subunit F174A/D176S was co-expressed; this construct has been shown to impair transferrin endocytosis (Motley et al., 2006). In the presence of the AP-2μ2 mutant, Ca$_V$2.2 internalisation was not observed after Quin treatment (Figure 5.8). This suggests that functional AP-2 is essential for the internalisation of Ca$_V$2.2, triggered by D2R activation. All together, these data suggest that activation of the D2R cause both Ca$_V$2.2e37 isoforms to internalise via β-arrestin-mediated recruitment of clathrin, which requires functional AP-2.
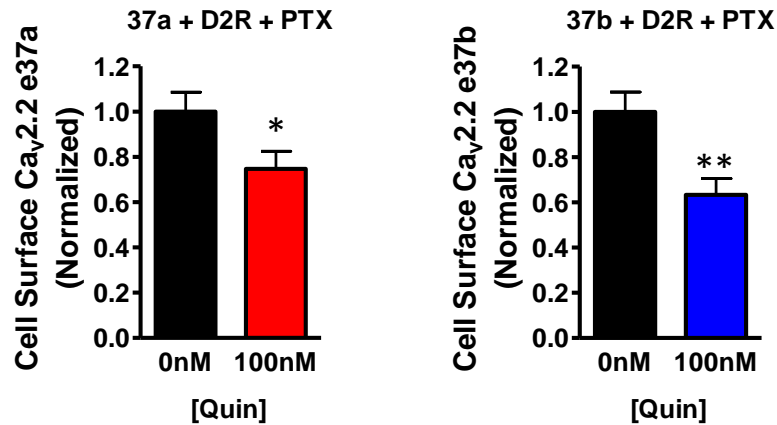
Figure 5.7 PTX does not block D2R activation-mediated internalisation of Ca$_V$2.2 splice variants.

Cell surface Ca$_V$2.2 in the presence of D2R in N2a, with or without 100nM Quin after PTX treatment. (Left) Ca$_V$2.2e37a (closed bar, n=72); Ca$_V$2.2e37a+Quin (red, n=76). (Right) Ca$_V$2.2e37b (closed bar, n=65); Ca$_V$2.2e37b+Quin (blue, n=55). *$P<0.05$, **$P<0.01$ (Student's unpaired t-test).
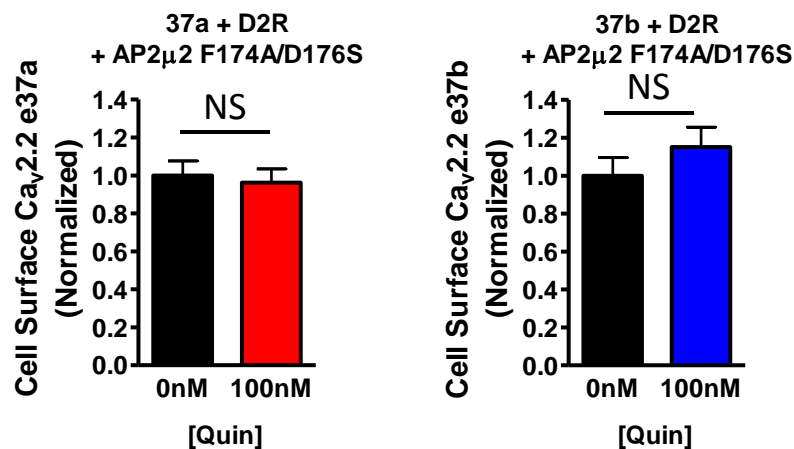
Figure 5.8 AP-2µ2 F174A/D176S blocks D2R activation-mediated internalisation of Ca$_V$2.2 splice variants.

Cell surface Ca$_V$2.2 in the presence of D2R and dominant-negative AP-2µ2 mutant F174A/D176S, with or without 100nM Quin. (Left) Ca$_V$2.2e37a (closed bar, n=70); Ca$_V$2.2e37a+Quin, AP-2µ2 F174A/D176S (red, n=57). (Right) Ca$_V$2.2e37b (closed bar, n=73); Ca$_V$2.2e37b+Quin (blue, n=71).

5.5 Effect of AP-2 and dynamin on voltage-dependent inhibition of Ca$_V$2.2 splice variants

As observed in 5.4.3, disruption of AP-2 interaction with Ca$_V$2.2 splice variants blocks internalisation of the channels, which is induced by D2R activation. I hypothesised that voltage-independent inhibition of Ca$_V$2.2 caused by G protein activation may be a result of, or partly mediated, by internalisation of the channels, based on the difference observed between Ca$_V$2.2e37a and e37b, both in the voltage-dependence of G protein mediated inhibition and the D2R-mediated internalisation of the channels. Thus, blocking internalisation may alter the voltage-dependency of G protein-mediated Ca$_V$2.2 inhibition.

In order to test this hypothesis, G protein-mediated voltage dependent inhibition of Ca$_V$2.2e37 isoforms was examined by activating the D2R with 300 nM Quin in a double-pulse protocol, as described in 3.5.3, with or without the endocytosis blockade. Dominant negative mutants of AP-2 µ2, F174A/D176S (Motley et al., 2006) and dynamin-1 K44R (Ruffieux-Daidié et al., 2008) were co-expressed with Ca$_V$2.2 splice variants and D2R, and the P2/P1 (relative current before and after the prepulse) was determined. If these proteins cause the inhibition to become more voltage-independent, the P2/P1 values are expected to decrease. AP-2 µ2 and dynamin wild-type proteins were also expressed as controls.

The P2/P1 values are summarised in Figure 5.9. In general, Ca$_V$2.2e37a showed smaller P2/P1 compared to Ca$_V$2.2e37b in any conditions tested, indicating the mode of G protein inhibition is more voltage-independent for Ca$_V$2.2e37a, which is in agreement with my previous observation (Figure 3.19), and the reports of others (Raingo et al., 2007; Andrade et al., 2010). However, AP-2 nor dynamin-1 did not have a significant effect on modulating the P2/P1, except for AP-2 WT which enhanced the difference in P2/P1 between Ca$_V$2.2e37a and 37b. Nevertheless, the lack of differences in P2/P1 between the control condition and the AP-2 or dynamin-1 (WT or dominant-negative mutant) conditions suggests it is unlikely that the clathrin-mediated endocytosis contributes to the voltage-independent component of Ca$_V$2.2 inhibition.
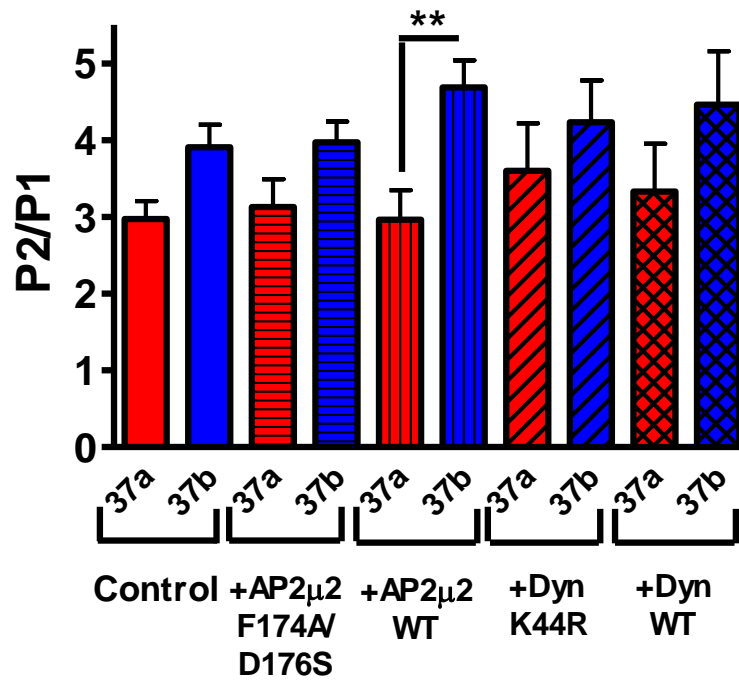
Figure 5.9 Effect of AP-2 and dynamin on G protein-mediated voltage-dependent inhibition.

Differences in the relative currents before and after a prepulse (P2/P1) in the presence of 300 nM Quin in tsA-201. In general, Ca$_V$2.2e37b showed a greater P2/P1 in all conditions, compared to Ca$_V$2.2e37a. There were no significant differences in P2/P1 among any conditions with AP-2 and dynamin proteins. Control: e37a (red, n=21), e37b (blue, n=24). +AP-2µ2 F174A/D176S: e37a (red border, n=15), e37b (blue border, n=28). +AP-2µ2 WT: e37a (red stripe, n=11), e37b (blue stripe, n=22). +dynamin-1 K44R: e37a (shaded red, n=4), e37b (shaded blue, n=4). +dynamin-1 WT: e37a (crossed red, n=6), e37b (crossed blue, n=8). **P<0.01 (one-way ANOVA).

5.6 Effect of D2R activation on Ca$_V$2.2 endocytosis

Since it was evident that D2R co-expression and activation affected the cell surface Ca$_V$2.2 levels, the effect of these events on Ca$_V$2.2 endocytosis was examined next. Using the endocytosis assay with BTX-labelling, the effect of 100nM Quin was determined on the endocytosis rate of BBS-tagged Ca$_V$2.2e37 isoforms, which were co-expressed with or without D2R. The endocytosis rate of Ca$_V$2.2e37b was significantly slowed by the presence of D2R (Figure 5.10a). Ca$_V$2.2e37b then internalised more rapidly in the presence of Quin, with a τ value similar to that determined for Ca$_V$2.2e37b alone (Figure 4.11, Figure 5.10). On the other hand, the basal endocytosis rate of Ca$_V$2.2e37a was not significantly affected by co-expression of D2R, compared to Ca$_V$2.2e37a alone (Figure 5.10b), as predicted from the previous comparison of cell surface expression levels. In contrast to the effect of Quin to reduce the overall cell surface expression of Ca$_V$2.2e37a channels (Figure 5.4), Quin treatment did not significantly accelerate Ca$_V$2.2e37a internalisation, possibly reflecting a minimum limit in the determination of endocytosis rate by this protocol.

5.6.1 Involvement of Ca$_V$2.2 AP binding motifs in D2R activation-mediated endocytosis of Ca$_V$2.2

To determine whether the AP interaction motifs in Ca$_V$2.2e37a were involved in the differential effect of the D2R to slow Ca$_V$2.2e37b internalisation, the effect of the Ca$_V$2.2e37a L/A and Y/A mutants were also examined (Figure 5.11a). Co-expression of D2R slowed the endocytosis of the L/A mutant, compared to the WT Ca$_V$2.2e37a with D2R (Figure 5.10b), with a time constant approaching that for Ca$_V$2.2e37b plus D2R (Figure 5.10a). In contrast, co-expression of D2R accelerated the endocytosis rate of the Y/A mutant, compared to its basal endocytosis rate, to a value similar to WT Ca$_V$2.2e37a plus D2R (Figure 5.11b). These results indicate that Ca$_V$2.2e37a internalisation can be both up- and down-regulated in association with the D2R, by the differential availability of the AP-binding motifs in its C-terminus. Quin treatment
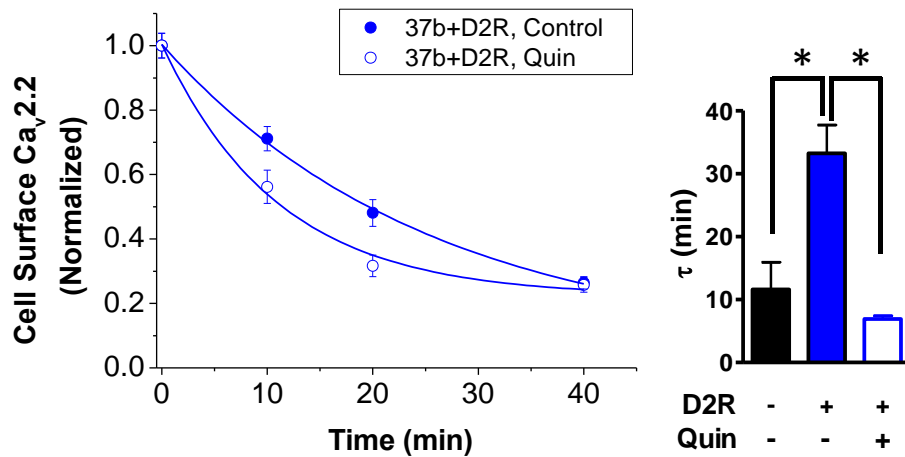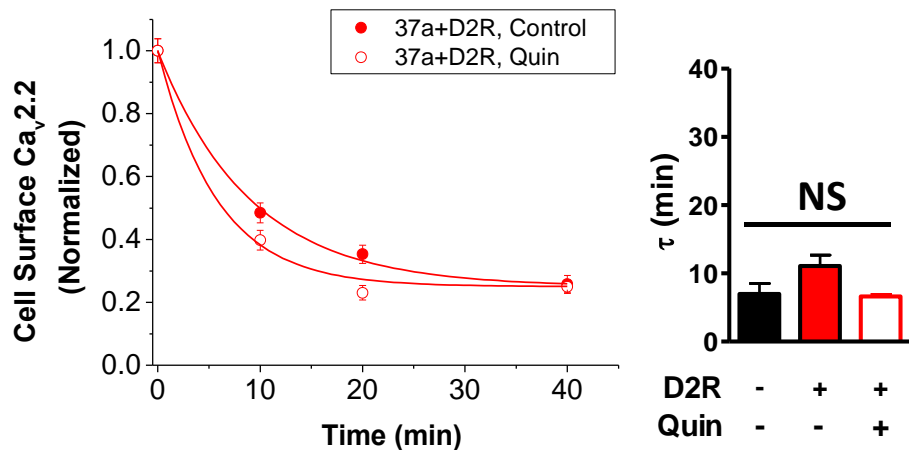
Figure 5.10 Effect of D2R activation on Ca$_V$2.2 endocytosis.

(**a**) (Left) Ca$_V$2.2e37b endocytosis rate was slowed by the presence of D2R, and accelerated by D2R activation. e37b+D2R (closed blue circle, n=4); e37b+D2R+Quin (open blue circle, n=3). (Right) The time constants for the endocytosis kinetics were (min); e37b (closed bar), 11.6 ± 3.53 (n=3, from Fig. 7B; e37b+D2R (closed blue bar), 29.0 ± 4.89 (n=4); e37b+D2R+Quin (open blue bar), 6.90 ± 0.36 (n=3). (**b**) (Left) e37a endocytosis was not significantly changed by the presence of D2R nor by D2R activation; e37a+D2R (closed red circle, n=5), e37a+D2R+Quin (open red circle, n=3). (Right) The time constants for the endocytosis kinetics were (min); e37a (closed bar), 7.00 ± 1.23 (n=3, from Fig. 7B); e37a+D2R (closed red bar), 11.1 ± 1.43 (n=5), e37a+D2R+Quin (open red bar) = 6.60 ± 0.22 (n=3). The cell surface fluorescence was normalised to the average value at t=0 min in each condition in the same experiment. The data points in the graph contain all the cells analysed from the 3-5 separate experiments. Mean ± SEM, *P< 0.05 (one-way ANOVA).

a
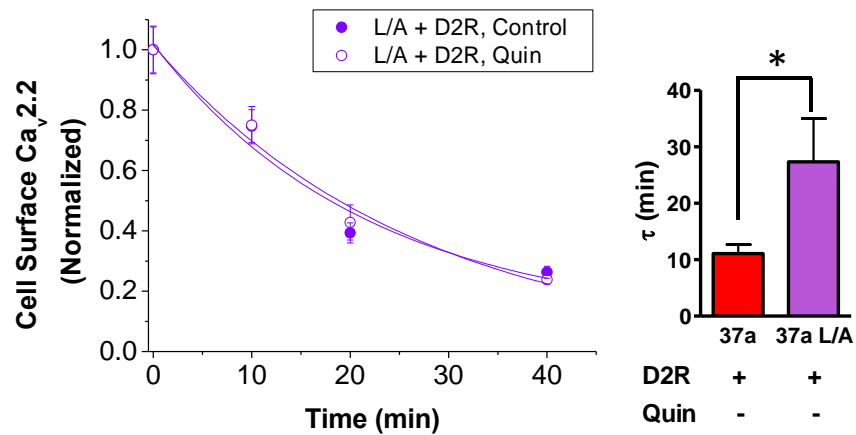
b
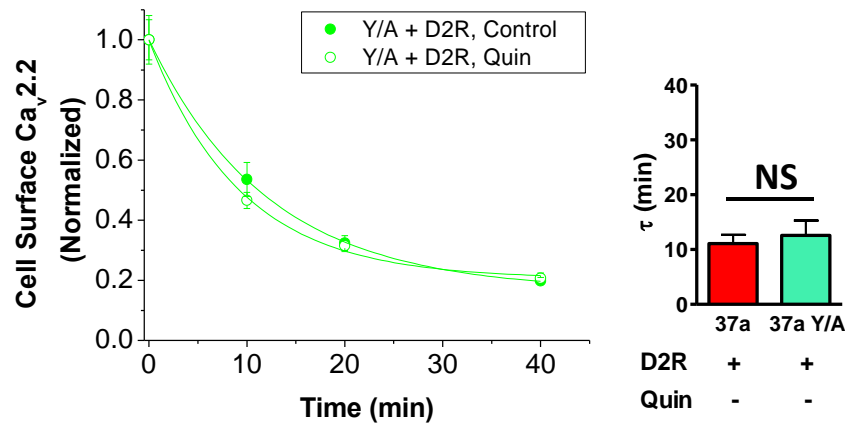
Figure 5.11 Mutation in AP binding motifs blocks D2R activation-mediated Ca$_V$2.2 endocytosis.

(**a**) (Left) Endocytosis of e37a L/A mutant was slowed by the presence of D2R, similarly to e37b, but was not accelerated by D2R activation. The time constants for the endocytosis kinetics were (min); L/A+D2R (closed purple circle), 27.3 ± 4.43 (n=3); L/A+D2R+Quin (open purple circle), 18.6 ± 1.62 (n=3). (Right) e37a+D2R (red, from Figure 5.10a), L/A+D2R (purple). (**b**) (Left) Endocytosis of Ca$_V$2.2e37a Y/A mutant was not changed by the presence of D2R, similarly to Ca$_V$2.2e37a, and was not accelerated by D2R activation. The time constants for the endocytosis kinetics were (min); Y/A+D2R (closed green circle), 12.6 ± 2.20 (n=3); Y/A+D2R+Quin (open green circle), 7.28 ± 0.90 (n=3). (Right) Ca$_V$2.2e37a+D2R (red, from Figure 5.10b), Y/A+D2R (green). The cell surface fluorescence was normalised to the average value at t=0 min in each condition in the same experiment. The data points in the graph contain all the cells analysed from the 3 separate experiments. Mean ± SEM, *P< 0.05 (one-way ANOVA).

did not alter the endocytosis of either mutant. These results indicate that disrupting the AP interaction motifs in Ca$_V$2.2e37 alters its interaction with the D2R and agonist-induced internalisation.

5.6.2 Interaction between Ca$_V$2.2 AP-binding motifs and D2R on whole-cell current

The endocytosis rates of Ca$_V$2.2 AP-binding mutants with and without the co-expression of D2R showed that L/A and Y/A mutants behave differently with D2R co-expression. While the endocytosis rate of the Y/A mutant was not affected by the presence of the D2R, the L/A mutant showed much slower endocytosis rate with D2R (Figure 5.11). To determine whether this difference in endocytosis rate leads to altered cell surface expression and the whole-cell current of the mutant channels, they were co-expressed with D2R in tsA-201 cells, in order to compare the whole-cell current densities, which is likely to represent the cell surface expression, according to the previous experiments (Figure 4.19, Figure 4.20).

To address whether the co-expression of D2R also affects the whole-cell current of these AP-binding mutants, the current densities were determined with co-expression of D2R in tsA-201 cells (Figure 5.12), and compared with those in the absence of D2R (Figure 4.20). Interestingly, the peak current density of the Y/A mutant with D2R was similar to that in the absence of D2R. Meanwhile, the peak current density of L/A with D2R increased, which was not significantly different from that of the WT Ca$_V$2.2e37a with D2R (Figure 5.13).
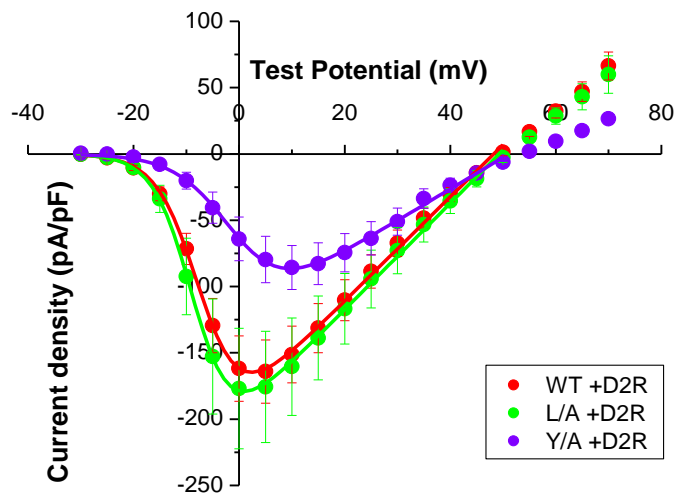
Figure 5.12 Whole-cell current densities of Ca$_V$2.2 AP-binding mutants in the presence of D2R.

Ca$_V$2.2e37a WT and AP-binding mutants were coexpressed with D2R, α$_2$δ-1 and β1b in tsA-201. In the presence of D2R, the peak current density of the Y/A mutant (purple) was significantly smaller than that of the WT (red) or the L/A mutant (green). Peak current density (pA/pF): Ca$_V$2.2e37a WT -164.1 ± 23.9 (n=19), L/A -175.7 ± 42.0 (n=6) at 5mV, Y/A -85.7 ± 16.6 (n=7) at 10 mV.
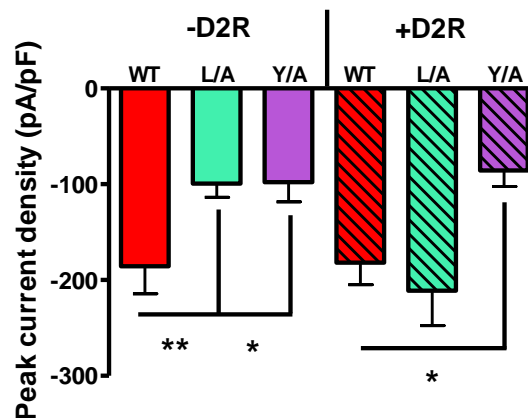
Figure 5.13 Summary graph of peak current densities of CaV2.2e37a AP-binding mutants with and without D2R.

The peak current densities of Ca$_V$2.2e37a WT and AP-binding mutants from Figure 4.20 (without D2R) and Figure 5.12 (with D2R) are summarised. The whole-cell current density of HA-Ca$_V$2.2e37b without D2R is shown in Figure 3.17. In the absence of D2R; Ca$_V$2.2e37a WT (red, n=24), L/A (green, n=27), Y/A (purple, n=30). In the presence of D2R; WT (shaded red, n=19), L/A (shaded green,n=6), Y/A (shaded purple, n=7). *P<0.05, **P<0.01 (one-way ANOVA).

5.7 Summary and Discussion

Direct interaction between $Ca_V2.2$ and dopamine receptors has been reported as an important event in regulating the surface expression of $Ca_V2.2$ (Kisilevsky et al., 2008; Kisilevsky and Zamponi, 2008), but the precise mechanisms for this trafficking have been poorly understood. In this study, differential effect of D2R co-expression on $Ca_V2.2$ splice variants was observed on their cell surface expression and endocytosis rates. In my experiments, co-expression of D2R does not increase the cell surface expression of $Ca_V2.2e37a$, and produces only a modest increase for $Ca_V2.2e37b$, whereas Kisilevsky and Zamponi (2008) reported a 2 to 3-fold increase in the cell surface expression of untagged and HA-tagged $Ca_V2.2e37b$ in the presence of D2R in tsA-201 cells (Kisilevsky and Zamponi, 2008). Nonetheless, this difference between the $Ca_V2.2$ isoforms may be due to the further observations in which the rate of endocytosis of $Ca_V2.2e37b$ is considerably slowed by the D2R, thus the channels are more stable and they accumulate at the cell surface. $Ca_V2.2e37a$, on the other hand, did not have this effect. This could be due to the lack of a canonical [DE]xxxL[LI] motif in $Ca_V2.2e37b$, since mutating this motif in $Ca_V2.2e37a$ (i.e. the L/A mutant) results in a larger whole-cell current in the presence of D2R, compared to the current in the absence of D2R, indicating an increase in the cell surface expression.

Interestingly, this stabilising effect at the plasma membrane diminishes upon D2R activation, and $Ca_V2.2e37b$ internalises at an increased rate similar to that for the channel expressed in the absence of the receptor. Upon D2R activation β-arrestin may be recruited to the activated D2R where it acts as an adaptor for AP-2-mediated internalisation (Goodman et al., 1996; Laporte et al., 2000, 2002; Lan et al., 2009). This recruitment of AP-2 to activated D2R via β-arrestin could occur without affecting the receptor coupling to G-proteins (Hausdorff et al., 1991). My study shows a new possible role of AP-2, mediated by β-arrestin recruitment to the receptor, which may also be important for the D2R activity-dependent $Ca_V2.2$ internalisation. This is supported by the results showing that disrupting the recruitment of functional AP-2 by overexpressing the dominant-negative mutant AP-2μ2 and mutations in [DE]xxxL[LI] and YxxΦ motifs inhibit $Ca_V2.2$ internalisation upon D2R activation, demonstrating that

functional AP-2 interaction is required for Ca$_V$2.2 internalisation mediated by D2R activation (Figure 5.14). It appears that Ca$_V$2.2e37a and 37b co-localise with D2R at the cell surface to a similar extent in the basal state. However, it is unclear whether Ca$_V$2.2 and D2R co-internalise together or they separate from each other and undergo internalisation pathway separately upon receptor activation.

Internalisation of Ca$_V$2.2 by activation of endogenous D2R has not previously been reported. Altier et al. (2006) showed ORL1 receptor-mediated internalisation of Ca$_V$2.2 upon chronic application of an ORL1 agonist, nociceptin in isolated DRG neurons by immunocytochemistry (Altier et al., 2006). However, this observation was not confirmed by the functional studies of Murali et al. (2012), where the prolonged (30 min) application of nociceptin did not decrease the Ca$_V$2.2 current in cell bodies of isolated small-diameter peptidergic DRG neurons, nor the post-synaptic current (Murali et al., 2012). The discrepancy between these studies could be explained by the difference in the subpopulation of the DRG neurons observed in the two studies. The difference in the expression patterns of Ca$_V$2.2 isoforms in peptidergic and non-peptidergic neurons has not been described, but this information may further elucidate the difference in the channel internalisation. Furthermore, the lack of decrease in Ca$_V$2.2 current upon prolonged ORL1 receptor activation could be explained by the balancing effect of increased *de novo* insertion of Ca$_V$2.2 into the plasma membrane. Further studies on the forward trafficking of BBS-Ca$_V$2.2 upon GPCR activation are required to validate this hypothesis.

In summary, this study provides a further insight into how D2R activities regulate Ca$_V$2.2 trafficking. The AP-binding motifs in the proximal C-terminus of Ca$_V$2.2 may be involved in the co-trafficking of Ca$_V$2.2 and D2R. Further investigations are required to determine two key mechanisms; how D2R enhance Ca$_V$2.2 cell surface expression, and how its activation causes Ca$_V$2.2 endocytosis. In addition, a future work on the D2R-mediated internalisation of Ca$_V$2.2 in neurons from regions of the brain rich in D2R expression such as the dorsal striatum and nucleus accumbens is also required to demonstrate the physiological significance of this phenomenon.
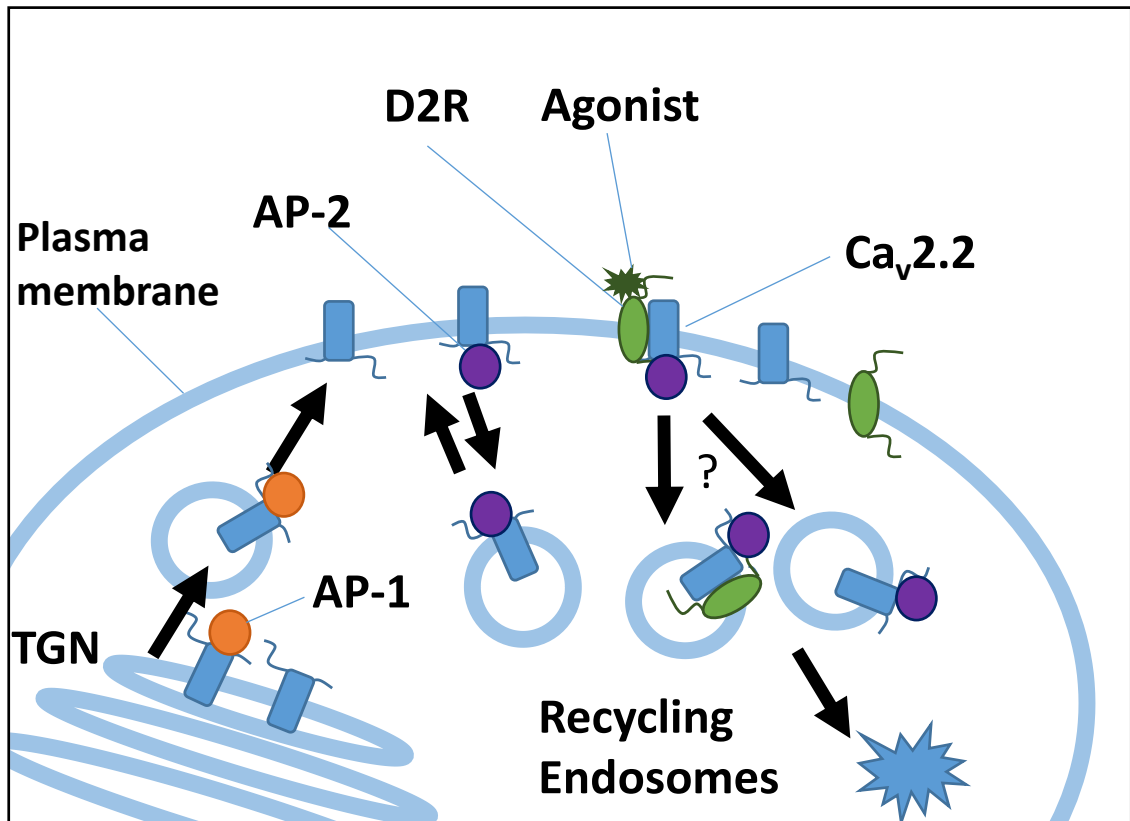
Figure 5.14 Possible mechanisms for AP-mediated trafficking of Ca$_V$2.2 and D2R.

Schematic diagram of Ca$_V$2.2 trafficking mediated by APs and D2R. Cell surface level of Ca$_V$2.2 (blue) is tightly regulated by AP-1 (orange) and AP-2 (purple). Additionally, D2R (green) activation controls the Ca$_V$2.2 at the cell surface, where the channel endocytosis is mediated by AP-2.

Chapter 6 General discussion and Conclusion

6.1 Co-trafficking of Ca$_V$2.2 and D2R

In Chapter 5, the stabilising effect of D2R co-expression on Ca$_V$2.2e37b at the plasma membrane was demonstrated, which diminished upon D2R activation, and the channel internalised at an increased rate similar to that for the channel expressed in the absence of the receptor. There are two possible explanations for this observation; 1) the activated D2R-Ca$_V$2.2 complex internalises together at an accelerated rate, 2) the activated D2R undergoes a conformational change and dissociates from Ca$_V$2.2 at the cell surface, and they internalise separately at their own native rates. How D2 receptors decrease the endocytosis rate of Ca$_V$2.2e37b channels is still not clear, however, the co-localisation of Ca$_V$2.2 and D2R via direct interaction of their intracellular regions suggested previously (Kisilevsky and Zamponi, 2008) implies that APs may be able to bind to the cargo motifs in Ca$_V$2.2 and D2R simultaneously to regulate their co-trafficking. Indeed, the D2R contains YxxΦ motifs in its intracellular loop 2 and 3 near the plasma membrane, but does not contain [DE]xxxL[LI] (Namkung and Sibley, 2004). This implies that an adaptor protein may potentially interact with Ca$_V$2.2 via [DE]xxxL[LI], and D2R via YxxΦ simultaneously if co-trafficking of Ca$_V$2.2 and D2R were to be mediated efficiently, similarly to the higher affinity of AP-2 shown in the presence of both motifs, compared to each single one separately (Jackson et al., 2010). The stabilising effect of Ca$_V$2.2e37b at the cell surface in the presence of D2R could be explained by this novel concept where the μ-subunit of AP-2 interacts with either of these YxxΦ motifs in D2R, while the α-σ2 hemicomplex interacts with the DxxxML motif in the e37b sequence, which may be inefficient for AP-2 mediated endocytosis in their co-internalisation from the cell surface, compared to Ca$_V$2.2e37a which contains a canonical motif, DxxxLL mediating efficient endocytosis. My data supports this mode of interaction, since mutating the DxxxLL motif in Ca$_V$2.2e37a to DxxxAL slows its endocytosis, only in the

additional presence of the D2R, but mutating YxxΦ motif in the C-terminus of Ca$_V$2.2e37a does not. All the rates of endocytosis of Ca$_V$2.2e37 isoforms and AP-binding mutants with or without D2R are summarised in Table 6.1.

It is still unclear where the interaction between Ca$_V$2.2 and D2R predominantly occurs. Co-localisation experiments here have shown that some interaction occurs at the plasma membrane. The previous report indicated an intracellular co-localisation (Kisilevsky and Zamponi, 2008), but this could mean either that they are co-trafficked to the plasma membrane together, or they internalise together from the cell surface. To address this question, it would be interesting to determine how co-expression of D2R affects the forward trafficking of Ca$_V$2.2, by monitoring the appearance of BBS-tagged channels. However, it is unlikely that the AP-binding motifs in Ca$_V$2.2 play a major role in forward trafficking of D2R-Ca$_V$2.2 complexes, since the whole-cell current of the AP-binding motif mutants remained the same, or rather increased in the presence of D2R, therefore these motifs may play more dominant role in endocytosis in the presence of D2R.

Since the use of BTX to track the internalised Ca$_V$2.2 was not sufficiently effective, improved fluorescent tags, for example using quantum dot (Qdot) technology, which has a greater tracking efficiency of transmembrane proteins (Groc et al., 2007) could prove useful. Qdot is brighter and more photostable than single dyes such as AF-488, and particularly useful in live-imaging experiments. This molecular tool may improve the monitoring of co-trafficking of Ca$_V$2.2 and D2R to and from the cell surface in future experiments. In addition, how the activities of D2R and other GPCRs affect trafficking of endogenous Ca$_V$2.2 has not been studied so far. Inserting the sequence for the exofacial tag such as HA and BBS or pHlourin into the same location as in the constructs used in this study within the Ca$_V$2.2-encoding gene of transgenic mice in order to generate the exofacial tag knock-in mice would create a powerful tool to further investigate the regulatory mechanisms of Ca$_V$2.2 trafficking in the native neurons. The exofacial tag knock-in mice may enable investigation into the developmental effect on Ca$_V$2.2 trafficking by comparing the Ca$_V$2.2 traffikcing in neurons of embryonic and adult mice. In addition, these transgenic mice may also allow one to investigate the effect of endogenous GPCR activation (such as D2, μ-opioid and GABA$_B$ receptors) on

Ca$_V$2.2 trafficking. If the approach for the exofocial tag knock-in into the Ca$_V$2.2-encoding sequence was proven successful, this technique could also be applied to the transgenic mice expressing only e37a (aa*) and 37b (b*b) (Andrade et al., 2010) to tag only the Ca$_V$2.2e37a or e37b isoforms to determine the endogenous trafficking and the effect of endogenous GPCR activation on the isoform trafficking in the neurons of these animals. Finally, these transgenic mice could potentially be useful tools to study the effect of various pharmacological drugs targeted to Ca$_V$2.2 on the channel trafficking.

Table 6.1 Effect of D2R activation on rate of endocytosis of Ca$_V$2.2e37 splice variants and mutants.

	τ (min)	
[Quin]	0 nM	100 nM
37a	7.00 ± 1.23	n/a
37a + D2R	11.1 ± 1.43	6.60 ± 0.22
37b	11.6 ± 3.53	n/a
37b + D2R	29.0 ± 4.89	6.90 ± 0.36
37a L/A	13.8 ± 1.85	n/a
37a L/A + D2R	27.3 ± 4.43	18.6 ± 1.62
37a Y/A	21.1 ± 3.53	n/a
37a Y/A + D2R	12.6 ± 2.20	7.28 ± 0.90

6.2 Alternative Ca$_V$2.2 trafficking mechanisms

In Chapter 4, the role of APs in the differential trafficking of isoforms to the plasma membrane and neurites was explored led to a conclusion that APs interact with the proximal C-mediate channel trafficking. Nevertheless, as summarised in

Figure 1.11, Ca$_V$2.2 contains a number of other potential AP-interaction sites which were not investigated in this study. These potential sites may be able to compensate for the interaction with APs when the motifs in exon 37 are mutated. Furthermore, these motifs that have not yet been studied could be used preferentially or have higher affinity for APs than the motifs in exon 37 explored in this study. Although the binding affinity of adaptor APs to these motifs has been reported to be relatively weak (Höning et al., 2005; Jackson et al., 2010), direct interaction of APs with these motifs in Ca$_V$2.2 could be assessed by surface plasmon resonance, as the dissociation constants (K_D) between AP-2 and the cargos were demonstrated to be approximated 1 µM (Jackson et al., 2010). The involvement of these potential AP-interaction sites (particularly those that are close to the plasma membrane), as well as the non-canonical DxxxML motif in exon 37b, in Ca$_V$2.2 trafficking also requires further investigation using site-directed mutagenesis to address this issue in the future. This could be assessed by the series of trafficking experiments demonstrated in this study, and in conjunction with the surface plasmon resonance experiments.

Some of the results in this study suggest that APs may not be the only determinants in Ca$_V$2.2 trafficking. Ubiquitination leading to proteasomal degradation has been reported to be greater in Ca$_V$2.2e37b than e37a (Marangoudakis et al., 2012), however, whole-cell expression levels of Ca$_V$2.2e37 isoforms in my study did not support this observation. Other possible trafficking mechanisms for Ca$_V$2.2 include protein sorting in caveolae, which is one of the most studied clathrin-independent sorting domains (Parton and Simons, 2007), although some reports suggest that clathrin-independent pathways have a minor role in endocytosis (Bitsikas et al., 2014). Both exocytosis and endocytosis take place in caveolae to control plasma membrane protein distribution (Parton and del Pozo, 2013). Moreover, a number of VGCCs, such as Ca$_V$1.2 (Balijepalli et al., 2006; Xia et al., 2007), Ca$_V$2.1 (Davies et al., 2006) and Ca$_V$2.2 (Xia et al., 2007; Robinson et al., 2010), are

present in lipid raft domains. Furthermore, α$_2$δ subunits are also present in lipid rafts / caveolae (Davies et al., 2006; Robinson et al., 2011). The mechanism by which α$_2$δ subunits regulate VGCC trafficking is still unclear; however, the Ca$_V$2.2e37a isoform requires the presence of α$_2$δ-1 for its greater cell surface expression compared to e37b, indicating that α$_2$δ-1 may promote Ca$_V$2.2e37a trafficking in caveolae. This could be confirmed by determining the protein levels of these splice variants in the lipid rafts with or without coexpression of α$_2$δ-1 with the methods previously used in this group, namely the detergent-resistance membrane (DRM) or Triton X-100 insoluble membrane fractions (Kadurin et al., 2012).

6.3 Possible consequences of Ca$_V$2.2 trafficking in diseases / treatments

The involvement of Ca$_V$2.2e37a in modulating neuropathic pain through morphine analgesia has already been implicated by other studies (Bell et al., 2004; Altier et al., 2007; Raingo et al., 2007; Andrade et al., 2010). The differential modulation of Ca$_V$2.2 isoform trafficking by α$_2$δ-1 described in this study could be a further link for Ca$_V$2.2e37a in neuropathic pain modulation. Firstly, α$_2$δ-1 is mainly expressed in the small-diameter nociceptive DRG neurons (Newton et al., 2001). In addition, at least 20 % of DRG neurons express Ca$_V$2.2e37a, and of these ~75 % are small-diameter nociceptive neurons, exhibiting a preferential expression (Bell et al., 2004). In sciatic nerve ligated rats, as an animal model of neuropathic pain, α$_2$δ-1 expression is increased in all DRG neurons in terms of the mRNA and protein level, regardless of their modalities and diameter (Bauer et al., 2009; Newton et al., 2001). Although a further investigation is required to understand how the α$_2$δ-1 level expressed in the heterologous system is correlated to the endogenous level in these DRG neurons, more Ca$_V$2.2e37a may be trafficked to the cell surface and to presynaptic terminals compared to e37b to increase the presynaptic Ca^{2+} currents upon up-regulation of α$_2$δ-1 in neuropathic pain states. Although Ca$_V$2.2e37a mRNA was downregulated in a neuropathic pain model, this reduction was in the total DRG RNA and there are no reports on

changes in Ca$_V$2.2e37a level specifically in the small-diameter neurons (Altier et al., 2007). In addition, even if there are less CaV2.2e37a channels present in nociceptive neurons during neuropathic pain, the up-regulated α$_2$δ-1 may potentially enhance the trafficking of these channels to the plasma membrane where they are active. Secondly, the voltage-dependence of Ca$_V$2.2e37a/b splice variants is also differentially modulated by α$_2$δ-1. In neuropathic pain conditions, the increased level of α2δ-1 may cause Ca$_V$2.2e37a to be activated at a more hyperpolarised potentials upon the arrival of action potentials, to release more neurotransmitter into the synaptic cleft. Finally, although there are some contradicting reports (Eroglu et al., 2009), neuropathic pain is thought to be alleviated by gabapentinoid drugs such as gabapentin and pregabalin which act by disrupting the trafficking of α$_2$δ-1 to the plasma membrane, and as a result reduce the Ca$_V$2 cell surface expression (Hendrich et al., 2008; Bauer et al., 2009). Since Ca$_V$2.2e37a may be more sensitive to α$_2$δ-1 level, the effect of the gabapentinoid drugs in trafficking of e37a may be greater, affecting the trafficking from Rab11-dependent recycling endosomes in particular, as shown previously for α$_2$δ-2 (Tran-Van-Minh and Dolphin, 2010).

Mutations in *AP1S2* which encodes for the brain isoform of AP-1σ1, σ1B, have been found in families with X-linked mental retardation (Tarpey et al., 2006). To elucidate the molecular basis for X-linked mental retardation, σ1B-knockout transgenic mice have been studied which causes ~ 50 % reduction in the synaptic vesicle (SV) density in the hippocampal synaptic boutons, demonstrating the crucial role of AP-1 in SV recycling (Glyvuk et al., 2010). However, as demonstrated in my study, disrupting interaction between AP-1 and Ca$_V$2.2 also leads to reduction in Ca$_V$2.2 trafficking to the synaptic terminals, which may also disturb the SV recycling by reducing Ca^{2+} flux upon depolarisation (Marks and McMahon, 1998). Furthermore, MEDNIK (mental retardation, enteropathy, deafness, neuropathy, ichthyosis and keratodermia) syndrome is caused by disruption in subcellular localisation of the Cu^{2+} transporters, ATP7A and ATP7B due to mutations in *AP1S1* that encode for another isoform AP-1 σ1A, leading to perturbation in Cu^{2+} metabolism (Montpetit et al., 2008; Martinelli et al., 2013; Jain et al., 2015). Although there are no reports on other proteins affected by this mutation *in vivo*, it demonstrates how mis-localisation of a protein due to malfunctioning of clathrin-mediated protein sorting can be the cause of pathological conditions.

Assessing the effect of these mutations on the subcellular localisation of $Ca_V2.2$ would give a further insight to the physiological relevance of my study in the role of AP-1 in $Ca_V2.2$ trafficking. Moreover, the protein expression and the role of AP-1 in the peripheral nervous system is still unknown, which should be investigated in the future using the σ1B-knockout in transgenic mice described by Glyvuk et al. (2010). Finally, development of specific pharmacological tools to disrupt the interaction between $Ca_V2.2$ and AP-1 would be of a great interest for a further investigation in modulating $Ca_V2.2$ activity at the presynaptic terminals.

6.4 Conclusion

This study presents novel evidence that $Ca_V2.2$ trafficking in cell lines and in cell bodies and neurites of DRG neurons is mediated by AP-1, and is fine-tuned by alternative splicing of exon 37. The difference in the trafficking of these splice variants originates in protein sorting in the Golgi network. Furthermore, alternative splicing of exon 37 also modulates the trafficking pattern of $Ca_V2.2$ resulting from D2R interaction and activation. Blocking the interaction of APs with the binding motif in the proximal C-terminus of $Ca_V2.2$ may modulate calcium entry into neuronal cells and its response to dopamine receptor activation. This study has provided a further insight, not only into how alternative splicing modulates ion channel trafficking, but also to the key mechanisms for $Ca_V2.2$ trafficking in neurons. My findings here potentially lead to new studies of AP-mediated trafficking of other VGCCs, as well as other ion channels and receptors that are essential for neurotransmission.

Appendix

Supplementary experiments

Appendix 1: Whole-cell current recordings from N2a cells

In this study, all the immunocytochemistry experiments and trafficking assays were carried out in N2a cells. However, the electrophysiological recordings were performed typically in transfected tsA-201 cells due to their robustness in whole-cell patch clamp. To validate the observations on the cell surface expression of $Ca_V2.2$ in these experiments, whole-cell current recording in N2a cells was performed in order to validate the results and circumvent possible differences in the endogenous protein expression in these two different cells lines, that might differentially affect the trafficking of $Ca_V2.2$.

N2a cells were transfected with mEos-$Ca_V2.2e37a/b$, $\alpha_2\delta$-1 and $\beta1b$, and whole-cell current recording was attempted under the same protocol for tsA-201 cells. The N2a cells expressing $Ca_V2.2$ were much more difficult to obtain current recordings in whole-cell patch clamp due to the poor seals obtained. Therefore, perforated whole-cell patch clamp was utilised using 200 µg/ml amphotericin B in 0.4 % DMSO in the internal electrode solution. The cell was held in the cell-attached mode for approximately 5 min until the whole-cell access was established by amphotericin B, and the cell capacitance and series resistance were compensated prior to the voltage clamp protocol.

The whole-cell current recordings were obtained, but less successfully compared to tsA-201 cells due to the higher series resistance that was not compensated sufficiently. Nevertheless, $Ca_V2.2e37a$ appeared to exhibit a greater whole-cell current density and hyperpolarised shift in its activation, compared to $Ca_V2.2e37b$ in N2a cells (Appendix Figure 1), however, it requires more experiments to confirm the electrophysiological properties in N2a cells.
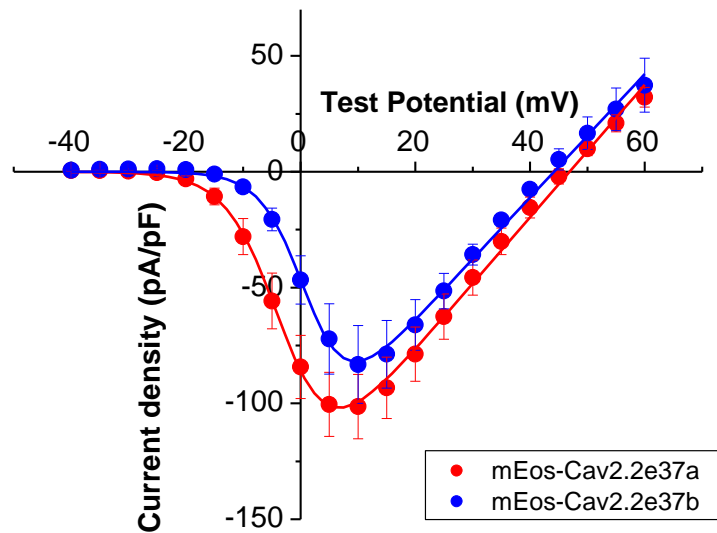
Appendix Figure 1: Perforated whole-cell patch clamp of N2a cells.

N2a cells expressing mEos-CaV2.2e37 isoforms show whole-cell current densities that are similar to those obtained from tsA-201. Peak current density (at -10 mV): mEos-Ca$_V$2.2e37a (red), -101.3 ± 13.9 pA/PF (n=10), mEos-Ca$_V$2.2e37b (blue), -83.2 ± 16.7 pA/PF (n=6). Mean ± SEM.

Bibliography

Akerboom, J., Chen, T.-W., Wardill, T.J., Tian, L., Marvin, J.S., Mutlu, S., Calderón, N.C., Esposti, F., Borghuis, B.G., Sun, X.R., et al. (2012). Optimization of a GCaMP Calcium Indicator for Neural Activity Imaging. J. Neurosci. *32*, 13819–13840.

Alberts, B., Johnson, A., Lewis, J., Raff, M., Roberts, K., and Walter, P. (2002). Molecular Biology of the Cell (Garland Science).

Alexopoulou, A.N., Couchman, J.R., and Whiteford, J.R. (2008). The CMV early enhancer/chicken β actin (CAG) promoter can be used to drive transgene expression during the differentiation of murine embryonic stem cells into vascular progenitors. BMC Cell Biol. *9*, 2.

Altier, C., Khosravani, H., Evans, R.M., Hameed, S., Peloquin, J.B., Vartian, B.A., Chen, L., Beedle, A.M., Ferguson, S.S.G., Mezghrani, A., et al. (2006). ORL1 receptor–mediated internalization of N-type calcium channels. Nat. Neurosci. *9*, 31–40.

Altier, C., Dale, C.S., Kisilevsky, A.E., Chapman, K., Castiglioni, A.J., Matthews, E.A., Evans, R.M., Dickenson, A.H., Lipscombe, D., Vergnolle, N., et al. (2007). Differential role of N-type calcium channel splice isoforms in pain. J. Neurosci. Off. J. Soc. Neurosci. *27*, 6363–6373.

Altier, C., Garcia-Caballero, A., Simms, B., You, H., Chen, L., Walcher, J., Tedford, H.W., Hermosilla, T., and Zamponi, G.W. (2011). The Cavβ subunit prevents RFP2-mediated ubiquitination and proteasomal degradation of L-type channels. Nat. Neurosci. *14*, 173–180.

Andrade, A., Denome, S., Jiang, Y.-Q., Marangoudakis, S., and Lipscombe, D. (2010). Opioid inhibition of N-type Ca2+ channels and spinal analgesia couple to alternative splicing. Nat. Neurosci. *13*, 1249–1256.

Aricescu, A.R., Lu, W., and Jones, E.Y. (2006). A time- and cost-efficient system for high-level protein production in mammalian cells. Acta Crystallogr. D Biol. Crystallogr. *62*, 1243–1250.

Arimura, N., and Kaibuchi, K. (2007). Neuronal polarity: from extracellular signals to intracellular mechanisms. Nat. Rev. Neurosci. *8*, 194–205.

Arimura, N., Hattori, A., Kimura, T., Nakamuta, S., Funahashi, Y., Hirotsune, S., Furuta, K., Urano, T., Toyoshima, Y.Y., and Kaibuchi, K. (2009). CRMP-2 directly binds to cytoplasmic dynein and interferes with its activity. J. Neurochem. *111*, 380–390.

Azizan, E.A.B., Poulsen, H., Tuluc, P., Zhou, J., Clausen, M.V., Lieb, A., Maniero, C., Garg, S., Bochukova, E.G., Zhao, W., et al. (2013). Somatic mutations in ATP1A1 and CACNA1D underlie a common subtype of adrenal hypertension. Nat. Genet. *45*, 1055–1060.

Baig, S.M., Koschak, A., Lieb, A., Gebhart, M., Dafinger, C., Nürnberg, G., Ali, A., Ahmad, I., Sinnegger-Brauns, M.J., Brandt, N., et al. (2011). Loss of Cav1.3 (CACNA1D) function in a human channelopathy with bradycardia and congenital deafness. Nat. Neurosci. *14*, 77–84.

Balijepalli, R.C., Foell, J.D., Hall, D.D., Hell, J.W., and Kamp, T.J. (2006). Localization of cardiac L-type Ca2+ channels to a caveolar macromolecular signaling complex is required for β2-adrenergic regulation. Proc. Natl. Acad. Sci. *103*, 7500–7505.

Barfield, R.M., Fromme, J.C., and Schekman, R. (2009). The Exomer Coat Complex Transports Fus1p to the Plasma Membrane via a Novel Plasma Membrane Sorting Signal in Yeast. Mol. Biol. Cell *20*, 4985–4996.

Basbaum, A.I., Bautista, D.M., Scherrer, G., and Julius, D. (2009). Cellular and Molecular Mechanisms of Pain. Cell *139*, 267–284.

Bats, C., Groc, L., and Choquet, D. (2007). The Interaction between Stargazin and PSD-95 Regulates AMPA Receptor Surface Trafficking. Neuron *53*, 719–734.

Bauer, C.S., Nieto-Rostro, M., Rahman, W., Tran-Van-Minh, A., Ferron, L., Douglas, L., Kadurin, I., Sri Ranjan, Y., Fernandez-Alacid, L., Millar, N.S., et al.

(2009). The increased trafficking of the calcium channel subunit alpha2delta-1 to presynaptic terminals in neuropathic pain is inhibited by the alpha2delta ligand pregabalin. J. Neurosci. Off. J. Soc. Neurosci. *29*, 4076–4088.

Bell, T.J., Thaler, C., Castiglioni, A.J., Helton, T.D., and Lipscombe, D. (2004). Cell-Specific Alternative Splicing Increases Calcium Channel Current Density in the Pain Pathway. Neuron *41*, 127–138.

Bernheim, L., Beech, D.J., and Hille, B. (1991). A diffusible second messenger mediates one of the pathways coupling receptors to calcium channels in rat sympathetic neurons. Neuron *6*, 859–867.

Bichet, D., Cornet, V., Geib, S., Carlier, E., Volsen, S., Hoshi, T., Mori, Y., and De Waard, M. (2000). The I-II loop of the Ca2+ channel alpha1 subunit contains an endoplasmic reticulum retention signal antagonized by the beta subunit. Neuron *25*, 177–190.

Bitsikas, V., Corrêa, I.R., and Nichols, B.J. (2014). Clathrin-independent pathways do not contribute significantly to endocytic flux. eLife e03970.

Boehm, M., and Bonifacino, J.S. (2001). Adaptins The Final Recount. Mol. Biol. Cell *12*, 2907–2920.

Bogdanov, Y., Michels, G., Armstrong-Gold, C., Haydon, P.G., Lindstrom, J., Pangalos, M., and Moss, S.J. (2006). Synaptic GABAA receptors are directly recruited from their extrasynaptic counterparts. EMBO J. *25*, 4381–4389.

Bolte, S., and Cordelières, F.P. (2006). A guided tour into subcellular colocalization analysis in light microscopy. J. Microsc. *224*, 213–232.

Bonifacino, J.S., and Traub, L.M. (2003). Signals for sorting of transmembrane proteins to endosomes and lysosomes. Annu. Rev. Biochem. *72*, 395–447.

Bourinet, E., Soong, T.W., Sutton, K., Slaymaker, S., Mathews, E., Monteil, A., Zamponi, G.W., Nargeot, J., and Snutch, T.P. (1999). Splicing of α1A subunit gene generates phenotypic variants of P- and Q-type calcium channels. Nat. Neurosci. *2*, 407–415.

Bowersox, S.S., Gadbois, T., Singh, T., Pettus, M., Wang, Y.X., and Luther, R.R. (1996). Selective N-type neuronal voltage-sensitive calcium channel

blocker, SNX-111, produces spinal antinociception in rat models of acute, persistent and neuropathic pain. J. Pharmacol. Exp. Ther. *279*, 1243–1249.

Braulke, T., and Bonifacino, J.S. (2009). Sorting of lysosomal proteins. Biochim. Biophys. Acta BBA - Mol. Cell Res. *1793*, 605–614.

Brittain, J.M., Piekarz, A.D., Wang, Y., Kondo, T., Cummins, T.R., and Khanna, R. (2009). An Atypical Role for Collapsin Response Mediator Protein 2 (CRMP-2) in Neurotransmitter Release via Interaction with Presynaptic Voltage-gated Calcium Channels. J. Biol. Chem. *284*, 31375–31390.

Brose, N., Petrenko, A.G., Südhof, T.C., and Jahn, R. (1992). Synaptotagmin: a calcium sensor on the synaptic vesicle surface. Science *256*, 1021–1025.

Buraei, Z., and Yang, J. (2010). The β Subunit of Voltage-Gated Ca2+ Channels. Physiol. Rev. *90*, 1461–1506.

Calderón-Rivera, A., Andrade, A., Hernández-Hernández, O., González-Ramírez, R., Sandoval, A., Rivera, M., Gomora, J.C., and Felix, R. (2012). Identification of a disulfide bridge essential for structure and function of the voltage-gated Ca2+ channel α2δ-1 auxiliary subunit. Cell Calcium *51*, 22–30.

Cantí, C., Davies, A., and Dolphin, A.C. (2003). Calcium Channel α2δ Subunits: Structure, Functions and Target Site for Drugs. Curr. Neuropharmacol. *1*, 209–217.

Cantí, C., Nieto-Rostro, M., Foucault, I., Heblich, F., Wratten, J., Richards, M.W., Hendrich, J., Douglas, L., Page, K.M., Davies, A., et al. (2005). The metal-ion-dependent adhesion site in the Von Willebrand factor-A domain of alpha2delta subunits is key to trafficking voltage-gated Ca2+ channels. Proc. Natl. Acad. Sci. U. S. A. *102*, 11230–11235.

Cantí, C., Page, K.M., Stephens, G.J., and Dolphin, A.C. (1999). Identification of Residues in the N Terminus of α1B Critical for Inhibition of the Voltage-Dependent Calcium Channel by Gβγ. J. Neurosci. *19*, 6855–6864.

Cassidy, J.S., Ferron, L., Kadurin, I., Pratt, W.S., and Dolphin, A.C. (2014). Functional exofacially tagged N-type calcium channels elucidate the interaction with auxiliary α2δ-1 subunits. Proc. Natl. Acad. Sci. 201403731.

Castiglioni, A.J., Raingo, J., and Lipscombe, D. (2006). Alternative splicing in the C-terminus of CaV2.2 controls expression and gating of N-type calcium channels. J. Physiol. *576*, 119–134.

Catterall, W.A. (2000). Structure and regulation of voltage-gated Ca2+ channels. Annu. Rev. Cell Dev. Biol. *16*, 521–555.

Catterall, W.A. (2011). Voltage-Gated Calcium Channels. Cold Spring Harb. Perspect. Biol. *3*, a003947.

Chaplan, S.R., Pogrel, J.W., and Yaksh, T.L. (1994). Role of voltage-dependent calcium channel subtypes in experimental tactile allodynia. J. Pharmacol. Exp. Ther. *269*, 1117–1123.

Chaudhuri, D., Chang, S.-Y., DeMaria, C.D., Alvania, R.S., Soong, T.W., and Yue, D.T. (2004). Alternative Splicing as a Molecular Switch for Ca2+/Calmodulin-Dependent Facilitation of P/Q-Type Ca2+ Channels. J. Neurosci. *24*, 6334–6342.

Chaudhuri, D., Alseikhan, B.A., Chang, S.Y., Soong, T.W., and Yue, D.T. (2005). Developmental Activation of Calmodulin-Dependent Facilitation of Cerebellar P-Type Ca2+ Current. J. Neurosci. *25*, 8282–8294.

Chen, Y.-H., Li, M.-H., Zhang, Y., He, L.-L., Yamada, Y., Fitzmaurice, A., Shen, Y., Zhang, H., Tong, L., and Yang, J. (2004). Structural basis of the alpha1-beta subunit interaction of voltage-gated Ca2+ channels. Nature *429*, 675–680.

Cheung, G., and Cousin, M.A. (2012). Adaptor Protein Complexes 1 and 3 Are Essential for Generation of Synaptic Vesicles from Activity-Dependent Bulk Endosomes. J. Neurosci. *32*, 6014–6023.

Chi, X.X., Schmutzler, B.S., Brittain, J.M., Wang, Y., Hingtgen, C.M., Nicol, G.D., and Khanna, R. (2009). Regulation of N-type voltage-gated calcium channels (Cav2.2) and transmitter release by collapsin response mediator protein-2 (CRMP-2) in sensory neurons. J. Cell Sci. *122*, 4351–4362.

Cornet, V., Bichet, D., Sandoz, G., Marty, I., Brocard, J., Bourinet, E., Mori, Y., Villaz, M., and De Waard, M. (2002). Multiple determinants in voltage-dependent P/Q calcium channels control their retention in the endoplasmic reticulum. Eur. J. Neurosci. *16*, 883–895.

Crottet, P., Meyer, D.M., Rohrer, J., and Spiess, M. (2002). ARF1·GTP, Tyrosine-based Signals, and Phosphatidylinositol 4,5-Bisphosphate Constitute a Minimal Machinery to Recruit the AP-1 Clathrin Adaptor to Membranes. Mol. Biol. Cell *13*, 3672–3682.

Davies, A., Douglas, L., Hendrich, J., Wratten, J., Tran Van Minh, A., Foucault, I., Koch, D., Pratt, W.S., Saibil, H.R., and Dolphin, A.C. (2006). The calcium channel alpha2delta-2 subunit partitions with CaV2.1 into lipid rafts in cerebellum: implications for localization and function. J. Neurosci. Off. J. Soc. Neurosci. *26*, 8748–8757.

Davies, A., Kadurin, I., Alvarez-Laviada, A., Douglas, L., Nieto-Rostro, M., Bauer, C.S., Pratt, W.S., and Dolphin, A.C. (2010). The alpha2delta subunits of voltage-gated calcium channels form GPI-anchored proteins, a posttranslational modification essential for function. Proc. Natl. Acad. Sci. U. S. A. *107*, 1654–1659.

Delmas, P., Coste, B., Gamper, N., and Shapiro, M.S. (2005). Phosphoinositide lipid second messengers: new paradigms for calcium channel modulation. Neuron *47*, 179–182.

De Waard, M., Pragnell, M., and Campbell, K.P. (1994). Ca2+ channel regulation by a conserved β subunit domain. Neuron *13*, 495–503.

Dolphin, A.C. (2003a). Beta subunits of voltage-gated calcium channels. J. Bioenerg. Biomembr. *35*, 599–620.

Dolphin, A.C. (2003b). G protein modulation of voltage-gated calcium channels. Pharmacol. Rev. *55*, 607–627.

Dolphin, A.C. (2012). Calcium channel auxiliary α2δ and β subunits: trafficking and one step beyond. Nat. Rev. Neurosci. *13*, 542–555.

Dolphin, A.C., and Scott, R.H. (1987). Calcium channel currents and their inhibition by (-)-baclofen in rat sensory neurones: modulation by guanine nucleotides. J. Physiol. *386*, 1–17.

Donato, R., Page, K.M., Koch, D., Nieto-Rostro, M., Foucault, I., Davies, A., Wilkinson, T., Rees, M., Edwards, F.A., and Dolphin, A.C. (2006). The ducky(2J) mutation in Cacna2d2 results in reduced spontaneous Purkinje cell

activity and altered gene expression. J. Neurosci. Off. J. Soc. Neurosci. *26*, 12576–12586.

Dubel, S.J., Starr, T.V., Hell, J., Ahlijanian, M.K., Enyeart, J.J., Catterall, W.A., and Snutch, T.P. (1992). Molecular cloning of the alpha-1 subunit of an omega-conotoxin-sensitive calcium channel. Proc. Natl. Acad. Sci. U. S. A. *89*, 5058–5062.

Dulubova, I. (1999). A conformational switch in syntaxin during exocytosis: role of munc18. EMBO J. *18*, 4372–4382.

Dunlap, K., and Fischbach, G.D. (1981). Neurotransmitters decrease the calcium conductance activated by depolarization of embryonic chick sensory neurones. J. Physiol. *317*, 519–535.

Eggermann, E., Bucurenciu, I., Goswami, S.P., and Jonas, P. (2012). Nanodomain coupling between Ca2+ channels and sensors of exocytosis at fast mammalian synapses. Nat. Rev. Neurosci. *13*, 7–21.

Eroglu, C., Allen, N.J., Susman, M.W., O'Rourke, N.A., Park, C.Y., Ozkan, E., Chakraborty, C., Mulinyawe, S.B., Annis, D.S., Huberman, A.D., et al. (2009). Gabapentin receptor alpha2delta-1 is a neuronal thrombospondin receptor responsible for excitatory CNS synaptogenesis. Cell *139*, 380–392.

Farías, G.G., Cuitino, L., Guo, X., Ren, X., Jarnik, M., Mattera, R., and Bonifacino, J.S. (2012). Signal-Mediated, AP-1/Clathrin-Dependent Sorting of Transmembrane Receptors to the Somatodendritic Domain of Hippocampal Neurons. Neuron *75*, 810–823.

Fernández-Chacón, R., Königstorfer, A., Gerber, S.H., García, J., Matos, M.F., Stevens, C.F., Brose, N., Rizo, J., Rosenmund, C., and Südhof, T.C. (2001). Synaptotagmin I functions as a calcium regulator of release probability. Nature *410*, 41–49.

Ferron, L., Nieto-Rostro, M., Cassidy, J.S., and Dolphin, A.C. (2014). Fragile X mental retardation protein controls synaptic vesicle exocytosis by modulating N-type calcium channel density. Nat. Commun. *5*.

Fesce, R., Grohovaz, F., Valtorta, F., and Meldolesi, J. (1994). Neurotransmitter release: fusion or "kiss-and-run"? Trends Cell Biol. *4*, 1–4.

Field, M.J., Cox, P.J., Stott, E., Melrose, H., Offord, J., Su, T.-Z., Bramwell, S., Corradini, L., England, S., Winks, J., et al. (2006). Identification of the alpha2-delta-1 subunit of voltage-dependent calcium channels as a molecular target for pain mediating the analgesic actions of pregabalin. Proc. Natl. Acad. Sci. U. S. A. *103*, 17537–17542.

Fujiwara, T., Oda, K., Yokota, S., Takatsuki, A., and Ikehara, Y. (1988). Brefeldin A causes disassembly of the Golgi complex and accumulation of secretory proteins in the endoplasmic reticulum. J. Biol. Chem. *263*, 18545–18552.

Gandini, M.A., Henríquez, D.R., Grimaldo, L., Sandoval, A., Altier, C., Zamponi, G.W., Felix, R., and González-Billault, C. (2014). CaV2.2 channel cell surface expression is regulated by the light chain 1 (LC1) of the microtubule-associated protein B (MAP1B) via UBE2L3-mediated ubiquitination and degradation. Pflüg. Arch. - Eur. J. Physiol. *466*, 2113–2126.

Gao, T., Bünemann, M., Gerhardstein, B.L., Ma, H., and Hosey, M.M. (2000). Role of the C terminus of the α1C(CaV1.2) Subunit in Membrane Targeting of Cardiac L-type Calcium Channels. J. Biol. Chem. *275*, 25436–25444.

Geppert, M., Goda, Y., Hammer, R.E., Li, C., Rosahl, T.W., Stevens, C.F., and Südhof, T.C. (1994). Synaptotagmin I: a major Ca2+ sensor for transmitter release at a central synapse. Cell *79*, 717–727.

Glebov, O.O., Bright, N.A., and Nichols, B.J. (2006). Flotillin-1 defines a clathrin-independent endocytic pathway in mammalian cells. Nat. Cell Biol. *8*, 46–54.

Glyvuk, N., Tsytsyura, Y., Geumann, C., D'Hooge, R., Hüve, J., Kratzke, M., Baltes, J., Böning, D., Klingauf, J., and Schu, P. (2010). AP-1/σ1B-adaptin mediates endosomal synaptic vesicle recycling, learning and memory. EMBO J. *29*, 1318–1330.

Goodman, O.B., Krupnick, J.G., Santini, F., Gurevich, V.V., Penn, R.B., Gagnon, A.W., Keen, J.H., and Benovic, J.L. (1996). β-Arrestin acts as a clathrin adaptor in endocytosis of the β2-adrenergic receptor. Nature *383*, 447–450.

Grant, B.D., and Donaldson, J.G. (2009). Pathways and mechanisms of endocytic recycling. Nat. Rev. Mol. Cell Biol. *10*, 597–608.

Groc, L., Lafourcade, M., Heine, M., Renner, M., Racine, V., Sibarita, J.-B., Lounis, B., Choquet, D., and Cognet, L. (2007). Surface Trafficking of Neurotransmitter Receptor: Comparison between Single-Molecule/Quantum Dot Strategies. J. Neurosci. *27*, 12433–12437.

Guo, Y., Sirkis, D.W., and Schekman, R. (2014). Protein Sorting at the trans-Golgi Network. Annu. Rev. Cell Dev. Biol. *30*, 169–206.

Gurnett, C.A., Felix, R., and Campbell, K.P. (1997). Extracellular interaction of the voltage-dependent Ca2+ channel alpha2delta and alpha1 subunits. J. Biol. Chem. *272*, 18508–18512.

Hall, D.D., Dai, S., Tseng, P.-Y., Malik, Z., Nguyen, M., Matt, L., Schnizler, K., Shephard, A., Mohapatra, D.P., Tsuruta, F., et al. (2013). Competition between α-actinin and Ca2+-Calmodulin Controls Surface Retention of the L-type Ca2+ Channel CaV1.2. Neuron *78*, 483–497.

Han, Y., Kaeser, P.S., Südhof, T.C., and Schneggenburger, R. (2011). RIM Determines Ca2+ Channel Density and Vesicle Docking at the Presynaptic Active Zone. Neuron *69*, 304–316.

Hanson, P.I., Roth, R., Morisaki, H., Jahn, R., and Heuser, J.E. (1997). Structure and conformational changes in NSF and its membrane receptor complexes visualized by quick-freeze/deep-etch electron microscopy. Cell *90*, 523–535.

Hata, Y., Slaughter, C.A., and Südhof, T.C. (1993). Synaptic vesicle fusion complex contains unc-18 homologue bound to syntaxin. Nature *366*, 347–351.

Hatakeyama, S., Wakamori, M., Ino, M., Miyamoto, N., Takahashi, E., Yoshinaga, T., Sawada, K., Imoto, K., Tanaka, I., Yoshizawa, T., et al. (2001). Differential nociceptive responses in mice lacking the alpha(1B) subunit of N-type Ca(2+) channels. Neuroreport *12*, 2423–2427.

Hausdorff, W.P., Campbell, P.T., Ostrowski, J., Yu, S.S., Caron, M.G., and Lefkowitz, R.J. (1991). A small region of the beta-adrenergic receptor is

selectively involved in its rapid regulation. Proc. Natl. Acad. Sci. U. S. A. *88*, 2979–2983.

Heldwein, E.E., Macia, E., Wang, J., Yin, H.L., Kirchhausen, T., and Harrison, S.C. (2004). Crystal structure of the clathrin adaptor protein 1 core. Proc. Natl. Acad. Sci. U. S. A. *101*, 14108–14113.

Hendrich, J., Van Minh, A.T., Heblich, F., Nieto-Rostro, M., Watschinger, K., Striessnig, J., Wratten, J., Davies, A., and Dolphin, A.C. (2008). Pharmacological disruption of calcium channel trafficking by the alpha2delta ligand gabapentin. Proc. Natl. Acad. Sci. U. S. A. *105*, 3628–3633.

Hendrich, J., Bauer, C.S., and Dolphin, A.C. (2012). Chronic pregabalin inhibits synaptic transmission between rat dorsal root ganglion and dorsal horn neurons in culture. Channels *6*, 124–132.

Herculano-Houzel, S. (2009). The human brain in numbers: a linearly scaled-up primate brain. Front. Hum. Neurosci. *3*, 31.

Herlitze, S., Garcia, D.E., Mackie, K., Hille, B., Scheuer, T., and Catterall, W.A. (1996). Modulation of Ca2+ channels βγ G-protein py subunits. Nature *380*, 258–262.

Hibino, H., Pironkova, R., Onwumere, O., Vologodskaia, M., Hudspeth, A.J., and Lesage, F. (2002). RIM - binding proteins (RBPs) couple Rab3 - interacting molecules (RIMs) to voltage - gated Ca2+ channels. Neuron *34*, 411–423.

Hille, B. (2001). Ion Channels of Excitable Membranes.

Hirning, L.D., Fox, A.P., McCleskey, E.W., Olivera, B.M., Thayer, S.A., Miller, R.J., and Tsien, R.W. (1988). Dominant role of N-type Ca2+ channels in evoked release of norepinephrine from sympathetic neurons. Science *239*, 57–61.

Hirst, J., Sahlender, D.A., Choma, M., Sinka, R., Harbour, M.E., Parkinson, M., and Robinson, M.S. (2009). Spatial and functional relationship of GGAs and AP-1 in Drosophila and HeLa cells. Traffic Cph. Den. *10*, 1696–1710.

Hirst, J., D. Barlow, L., Francisco, G.C., Sahlender, D.A., Seaman, M.N.J., Dacks, J.B., and Robinson, M.S. (2011). The Fifth Adaptor Protein Complex. PLoS Biol *9*, e1001170.

Hirst, J., Borner, G.H.H., Antrobus, R., Peden, A.A., Hodson, N.A., Sahlender, D.A., and Robinson, M.S. (2012). Distinct and overlapping roles for AP-1 and GGAs revealed by the "knocksideways" system. Curr. Biol. CB *22*, 1711–1716.

Hodgkin, A.L., and Huxley, A.F. (1952). A quantitative description of membrane current and its application to conduction and excitation in nerve. J. Physiol. *117*, 500–544.

Hofmann, M.W., Höning, S., Rodionov, D., Dobberstein, B., Figura, K. von, and Bakke, O. (1999). The Leucine-based Sorting Motifs in the Cytoplasmic Domain of the Invariant Chain Are Recognized by the Clathrin Adaptors AP1 and AP2 and their Medium Chains. J. Biol. Chem. *274*, 36153–36158.

Höning, S., Ricotta, D., Krauss, M., Späte, K., Spolaore, B., Motley, A., Robinson, M., Robinson, C., Haucke, V., and Owen, D.J. (2005). Phosphatidylinositol-(4,5)-Bisphosphate Regulates Sorting Signal Recognition by the Clathrin-Associated Adaptor Complex AP2. Mol. Cell *18*, 519–531.

Hoppa, M.B., Lana, B., Margas, W., Dolphin, A.C., and Ryan, T.A. (2012). α2δ expression sets presynaptic calcium channel abundance and release probability. Nature *486*, 122–125.

Ikeda, S.R. (1991). Double-pulse calcium channel current facilitation in adult rat sympathetic neurones. J. Physiol. *439*, 181–214.

Ikeda, S.R. (1996). Voltage-dependent modulation of N-type calcium channels by G-protein β γsubunits. Nature *380*, 255–258.

Jackson, L.P., Kelly, B.T., McCoy, A.J., Gaffry, T., James, L.C., Collins, B.M., Höning, S., Evans, P.R., and Owen, D.J. (2010). A large-scale conformational change couples membrane recruitment to cargo binding in the AP2 clathrin adaptor complex. Cell *141*, 1220–1229.

Jain, S., Farías, G.G., and Bonifacino, J.S. (2015). Polarized sorting of the copper transporter ATP7B in neurons mediated by recognition of a dileucine signal by AP-1. Mol. Biol. Cell *26*, 218–228.

Jay, S.D., Sharp, A.H., Kahl, S.D., Vedvick, T.S., Harpold, M.M., and Campbell, K.P. (1991). Structural characterization of the dihydropyridine-sensitive calcium

channel alpha 2-subunit and the associated delta peptides. J. Biol. Chem. *266*, 3287–3293.

Jiang, Y.-Q., Andrade, A., and Lipscombe, D. (2013). Spinal morphine but not ziconotide or gabapentin analgesia is affected by alternative splicing of voltage-gated calcium channel CaV2.2 pre-mRNA. Mol. Pain *9*, 67.

Jones, L.P., Patil, P.G., Snutch, T.P., and Yue, D.T. (1997). G-protein modulation of N-type calcium channel gating current in human embryonic kidney cells (HEK 293). J. Physiol. *498*, 601–610.

Ju, W., Morishita, W., Tsui, J., Gaietta, G., Deerinck, T.J., Adams, S.R., Garner, C.C., Tsien, R.Y., Ellisman, M.H., and Malenka, R.C. (2004). Activity-dependent regulation of dendritic synthesis and trafficking of AMPA receptors. Nat. Neurosci. *7*, 244–253.

Kadurin, I., Alvarez-Laviada, A., Ng, S.F.J., Walker-Gray, R., D'Arco, M., Fadel, M.G., Pratt, W.S., and Dolphin, A.C. (2012). Calcium Currents Are Enhanced by α2δ-1 Lacking Its Membrane Anchor. J. Biol. Chem. *287*, 33554–33566.

Kaeser, P.S., Deng, L., Wang, Y., Dulubova, I., Liu, X., Rizo, J., and Südhof, T.C. (2011). RIM proteins tether Ca2+ channels to presynaptic active zones via a direct PDZ-domain interaction. Cell *144*, 282–295.

Kaneko, S. (2003). Alternative splicing of Cav2 genes and their functional significance. Nihon Yakurigaku Zasshi Folia Pharmacol. Jpn. *121*, 233–240.

Kaneko, S., Cooper, C.B., Nishioka, N., Yamasaki, H., Suzuki, A., Jarvis, S.E., Akaike, A., Satoh, M., and Zamponi, G.W. (2002). Identification and characterization of novel human Ca(v)2.2 (alpha 1B) calcium channel variants lacking the synaptic protein interaction site. J. Neurosci. Off. J. Soc. Neurosci. *22*, 82–92.

Katz, B., and Miledi, R. (1965). The Effect of Calcium on Acetylcholine Release from Motor Nerve Terminals. Proc. R. Soc. Lond. B Biol. Sci. *161*, 496–503.

Kavalali, E.T., and Jorgensen, E.M. (2014). Visualizing presynaptic function. Nat. Neurosci. *17*, 10–16.

Kepplinger, K.J.F., Kahr, H., Förstner, G., Sonnleitner, M., Schindler, H., Schmidt, T., Groschner, K., Soldatov, N.M., and Romanin, C. (2000). A sequence in the carboxy-terminus of the α1C subunit important for targeting, conductance and open probability of L-type Ca2+ channels. FEBS Lett. *477*, 161–169.

Kim, C., Jun, K., Lee, T., Kim, S.S., McEnery, M.W., Chin, H., Kim, H.L., Park, J.M., Kim, D.K., Jung, S.J., et al. (2001). Altered nociceptive response in mice deficient in the alpha(1B) subunit of the voltage-dependent calcium channel. Mol. Cell. Neurosci. *18*, 235–245.

Kirchhausen, T. (1999). Adaptors for Clathrin-Mediated Traffic. Annu. Rev. Cell Dev. Biol. *15*, 705–732.

Kirchhausen, T. (2000). Clathrin. Annu. Rev. Biochem. *69*, 699–727.

Kisilevsky, A.E., and Zamponi, G.W. (2008). D2 dopamine receptors interact directly with N-type calcium channels and regulate channel surface expression levels. Channels *2*, 269–277.

Kisilevsky, A.E., Mulligan, S.J., Altier, C., Iftinca, M.C., Varela, D., Tai, C., Chen, L., Hameed, S., Hamid, J., Macvicar, B.A., et al. (2008). D1 receptors physically interact with N-type calcium channels to regulate channel distribution and dendritic calcium entry. Neuron *58*, 557–570.

Klumperman, J. (2011). Architecture of the Mammalian Golgi. Cold Spring Harb. Perspect. Biol. *3*, a005181.

Krovetz, H.S., Helton, T.D., Crews, A.L., and Horne, W.A. (2000). C-Terminal Alternative Splicing Changes the Gating Properties of a Human Spinal Cord Calcium Channel α1A Subunit. J. Neurosci. *20*, 7564–7570.

Krupnick, J.G., and Benovic, J.L. (1998). The Role of Receptor Kinases and Arrestins in G Protein–Coupled Receptor Regulation. Annu. Rev. Pharmacol. Toxicol. *38*, 289–319.

Lan, H., Teeter, M.M., Gurevich, V.V., and Neve, K.A. (2009). An Intracellular Loop 2 Amino Acid Residue Determines Differential Binding of Arrestin to the Dopamine D2 and D3 Receptors. Mol. Pharmacol. *75*, 19–26.

Laporte, S.A., Oakley, R.H., Zhang, J., Holt, J.A., Ferguson, S.S.G., Caron, M.G., and Barak, L.S. (1999). The β2-adrenergic receptor/βarrestin complex recruits the clathrin adaptor AP-2 during endocytosis. Proc. Natl. Acad. Sci. *96*, 3712–3717.

Laporte, S.A., Oakley, R.H., Holt, J.A., Barak, L.S., and Caron, M.G. (2000). The Interaction of β-Arrestin with the AP-2 Adaptor Is Required for the Clustering of β2-Adrenergic Receptor into Clathrin-coated Pits. J. Biol. Chem. *275*, 23120–23126.

Laporte, S.A., Miller, W.E., Kim, K.-M., and Caron, M.G. (2002). β-Arrestin/AP-2 Interaction in G Protein-coupled Receptor Internalization: identification of a β-arrestin binding site in β2-adaptin. J. Biol. Chem. *277*, 9247–9254.

Lau, C.G., and Zukin, R.S. (2007). NMDA receptor trafficking in synaptic plasticity and neuropsychiatric disorders. Nat. Rev. Neurosci. *8*, 413–426.

Leenders, A.G.M., Lin, L., Huang, L.-D., Gerwin, C., Lu, P.-H., and Sheng, Z.-H. (2008). The role of MAP1A light chain 2 in synaptic surface retention of Cav2.2 channels in hippocampal neurons. J. Neurosci. Off. J. Soc. Neurosci. *28*, 11333–11346.

Le Roy, C., and Wrana, J.L. (2005). Clathrin- and non-clathrin-mediated endocytic regulation of cell signalling. Nat. Rev. Mol. Cell Biol. *6*, 112–126.

Li, B., Zhong, H., Scheuer, T., and Catterall, W.A. (2004). Functional Role of a C-Terminal Gβγ-Binding Domain of Cav2.2 Channels. Mol. Pharmacol. *66*, 761–769.

Liao, P., Zhang, H.Y., and Soong, T.W. (2009). Alternative splicing of voltage-gated calcium channels: from molecular biology to disease. Pflüg. Arch. - Eur. J. Physiol. *458*, 481–487.

Lin, Z., Haus, S., Edgerton, J., and Lipscombe, D. (1997). Identification of Functionally Distinct Isoforms of the N-Type Ca2+ Channel in Rat Sympathetic Ganglia and Brain. Neuron *18*, 153–166.

Lin, Z., Lin, Y., Schorge, S., Pan, J.Q., Beierlein, M., and Lipscombe, D. (1999). Alternative Splicing of a Short Cassette Exon in α1B Generates Functionally

Distinct N-Type Calcium Channels in Central and Peripheral Neurons. J. Neurosci. *19*, 5322–5331.

Lippincott-Schwartz, J., Yuan, L.C., Bonifacino, J.S., and Klausner, R.D. (1989). Rapid redistribution of Golgi proteins into the ER in cells treated with brefeldin A: Evidence for membrane cycling from Golgi to ER. Cell *56*, 801–813.

Lipscombe, D., Pan, J.Q., and Gray, A.C. (2002). Functional diversity in neuronal voltage-gated calcium channels by alternative splicing of Cavα1. Mol. Neurobiol. *26*, 21–44.

Lipscombe, D., Andrade, A., and Allen, S.E. (2013). Alternative splicing: Functional diversity among voltage-gated calcium channels and behavioral consequences. Biochim. Biophys. Acta BBA - Biomembr. *1828*, 1522–1529.

Manders, E.M.M., Verbeek, F.J., and Aten, J.A. (1993). Measurement of co-localization of objects in dual-colour confocal images. J. Microsc. *169*, 375–382.

Marangoudakis, S., Andrade, A., Helton, T.D., Denome, S., Castiglioni, A.J., and Lipscombe, D. (2012). Differential Ubiquitination and Proteasome Regulation of CaV2.2 N-Type Channel Splice Isoforms. J. Neurosci. *32*, 10365–10369.

Marks, B., and McMahon, H.T. (1998). Calcium triggers calcineurin-dependent synaptic vesicle recycling in mammalian nerve terminals. Curr. Biol. *8*, 740–749.

Martinelli, D., Travaglini, L., Drouin, C.A., Ceballos-Picot, I., Rizza, T., Bertini, E., Carrozzo, R., Petrini, S., Lonlay, P. de, Hachem, M.E., et al. (2013). MEDNIK syndrome: a novel defect of copper metabolism treatable by zinc acetate therapy. Brain *136*, 872–881.

Matlin, A.J., Clark, F., and Smith, C.W.J. (2005). Understanding alternative splicing: towards a cellular code. Nat. Rev. Mol. Cell Biol. *6*, 386–398.

Maxfield, F.R., and McGraw, T.E. (2004). Endocytic recycling. Nat. Rev. Mol. Cell Biol. *5*, 121–132.

Maximov, A., and Bezprozvanny, I. (2002). Synaptic targeting of N-type calcium channels in hippocampal neurons. J. Neurosci. Off. J. Soc. Neurosci. *22*, 6939–6952.

Mayor, S., and Pagano, R.E. (2007). Pathways of clathrin-independent endocytosis. Nat. Rev. Mol. Cell Biol. *8*, 603–612.

McCleskey, E.W., Fox, A.P., Feldman, D.H., Cruz, L.J., Olivera, B.M., Tsien, R.W., and Yoshikami, D. (1987). Omega-conotoxin: direct and persistent blockade of specific types of calcium channels in neurons but not muscle. Proc. Natl. Acad. Sci. U. S. A. *84*, 4327–4331.

McEnery, M.W., Snowman, A.M., Sharp, A.H., Adams, M.E., and Snyder, S.H. (1991). Purified omega-conotoxin GVIA receptor of rat brain resembles a dihydropyridine-sensitive L-type calcium channel. Proc. Natl. Acad. Sci. U. S. A. *88*, 11095–11099.

McKinney, S.A., Murphy, C.S., Hazelwood, K.L., Davidson, M.W., and Looger, L.L. (2009). A bright and photostable photoconvertible fluorescent protein. Nat. Methods *6*, 131–133.

McMahon, H.T., Missler, M., Li, C., and Südhof, T.C. (1995). Complexins: cytosolic proteins that regulate SNAP receptor function. Cell *83*, 111–119.

Miller, T.M., and Heuser, J.E. (1984). Endocytosis of synaptic vesicle membrane at the frog neuromuscular junction. J. Cell Biol. *98*, 685–698.

Montpetit, A., Côté, S., Brustein, E., Drouin, C.A., Lapointe, L., Boudreau, M., Meloche, C., Drouin, R., Hudson, T.J., Drapeau, P., et al. (2008). Disruption of AP1S1, Causing a Novel Neurocutaneous Syndrome, Perturbs Development of the Skin and Spinal Cord. PLoS Genet *4*, e1000296.

Mori, Y., Friedrich, T., Kim, M.-S., Mikami, A., Nakai, J., Ruth, P., Bosse, E., Hofmann, F., Flockerzi, V., Furuichi, T., et al. (1991). Primary structure and functional expression from complementary DNA of a brain calcium channel. Nature *350*, 398–402.

Motley, A., Bright, N.A., Seaman, M.N.J., and Robinson, M.S. (2003). Clathrin-mediated endocytosis in AP-2-depleted cells. J. Cell Biol. *162*, 909–918.

Motley, A.M., Berg, N., Taylor, M.J., Sahlender, D.A., Hirst, J., Owen, D.J., and Robinson, M.S. (2006). Functional analysis of AP-2 alpha and mu2 subunits. Mol. Biol. Cell *17*, 5298–5308.

Motta, A., Bremnes, B., Morelli, M.A.C., Frank, R.W., Saviano, G., and Bakke, O. (1995). Structure-Activity Relationship of the Leucine-based Sorting Motifs in the Cytosolic Tail of the Major Histocompatibility Complex-associated Invariant Chain. J. Biol. Chem. *270*, 27165–27171.

Murali, S.S., Napier, I.A., Rycroft, B.K., and Christie, M.J. (2012). Opioid-related (ORL1) receptors are enriched in a subpopulation of sensory neurons and prolonged activation produces no functional loss of surface N-type calcium channels. J. Physiol. *590*, 1655–1667.

Namkung, Y., and Sibley, D.R. (2004). Protein Kinase C Mediates Phosphorylation, Desensitization, and Trafficking of the D2 Dopamine Receptor. J. Biol. Chem. *279*, 49533–49541.

Narahashi, T., Moore, J.W., and Scott, W.R. (1964). Tetrodotoxin Blockage of Sodium Conductance Increase in Lobster Giant Axons. J. Gen. Physiol. *47*, 965–974.

Nesterov, A., Carter, R.E., Sorkina, T., Gill, G.N., and Sorkin, A. (1999). Inhibition of the receptor-binding function of clathrin adaptor protein AP-2 by dominant-negative mutant mu2 subunit and its effects on endocytosis. EMBO J. *18*, 2489–2499.

Newton, R.A., Bingham, S., Case, P.C., Sanger, G.J., and Lawson, S.N. (2001). Dorsal root ganglion neurons show increased expression of the calcium channel alpha2delta-1 subunit following partial sciatic nerve injury. Brain Res. Mol. Brain Res. *95*, 1–8.

Nowycky, M.C., Fox, A.P., and Tsien, R.W. (1985). Three types of neuronal calcium channel with different calcium agonist sensitivity. Nature *316*, 440–443.

Opatowsky, Y., Chen, C.-C., Campbell, K.P., and Hirsch, J.A. (2004). Structural analysis of the voltage-dependent calcium channel beta subunit functional core and its complex with the alpha 1 interaction domain. Neuron *42*, 387–399.

Owen, D.J., Collins, B.M., and Evans, P.R. (2004). Adaptors for clathrin coats: structure and function. Annu. Rev. Cell Dev. Biol. *20*, 153–191.

Paez-Segala, M.G., Sun, M.G., Shtengel, G., Viswanathan, S., Baird, M.A., Macklin, J.J., Patel, R., Allen, J.R., Howe, E.S., Piszczek, G., et al. (2015).

Fixation-resistant photoactivatable fluorescent proteins for CLEM. Nat. Methods *12*, 215–218.

Page, K.M., Cantí, C., Stephens, G.J., Berrow, N.S., and Dolphin, A.C. (1998). Identification of the Amino Terminus of Neuronal Ca2+ Channel α1 Subunits α1B and α1E as an Essential Determinant of G-Protein Modulation. J. Neurosci. *18*, 4815–4824.

Pan, J.Q., and Lipscombe, D. (2000). Alternative Splicing in the Cytoplasmic II–III Loop of the N-Type Ca Channel α1B Subunit: Functional Differences Are β Subunit-Specific. J. Neurosci. *20*, 4769–4775.

Pang, Z.P., Shin, O.-H., Meyer, A.C., Rosenmund, C., and Südhof, T.C. (2006). A Gain-of-Function Mutation in Synaptotagmin-1 Reveals a Critical Role of Ca2+-Dependent Soluble N-Ethylmaleimide-Sensitive Factor Attachment Protein Receptor Complex Binding in Synaptic Exocytosis. J. Neurosci. *26*, 12556–12565.

Parton, R.G., and del Pozo, M.A. (2013). Caveolae as plasma membrane sensors, protectors and organizers. Nat. Rev. Mol. Cell Biol. *14*, 98–112.

Parton, R.G., and Simons, K. (2007). The multiple faces of caveolae. Nat. Rev. Mol. Cell Biol. *8*, 185–194.

Perin, M.S., Fried, V.A., Mignery, G.A., Jahn, R., and Südhof, T.C. (1990). Phospholipid binding by a synaptic vesicle protein homologous to the regulatory region of protein kinase C. Nature *345*, 260–263.

Raghib, A., Bertaso, F., Davies, A., Page, K.M., Meir, A., Bogdanov, Y., and Dolphin, A.C. (2001). Dominant-negative synthesis suppression of voltage-gated calcium channel Cav2.2 induced by truncated constructs. J. Neurosci. Off. J. Soc. Neurosci. *21*, 8495–8504.

Rahajeng, J., Giridharan, S.S.P., Naslavsky, N., and Caplan, S. (2010). Collapsin Response Mediator Protein-2 (Crmp2) Regulates Trafficking by Linking Endocytic Regulatory Proteins to Dynein Motors. J. Biol. Chem. *285*, 31918–31922.

Raingo, J., Castiglioni, A.J., and Lipscombe, D. (2007). Alternative splicing controls G protein-dependent inhibition of N-type calcium channels in nociceptors. Nat. Neurosci. *10*, 285–292.

Ren, X., Farías, G.G., Canagarajah, B.J., Bonifacino, J.S., and Hurley, J.H. (2013). Structural basis for recruitment and activation of the AP-1 clathrin adaptor complex by Arf1. Cell *152*, 755–767.

Reynolds, I.J., Wagner, J.A., Snyder, S.H., Thayer, S.A., Olivera, B.M., and Miller, R.J. (1986). Brain voltage-sensitive calcium channel subtypes differentiated by omega-conotoxin fraction GVIA. Proc. Natl. Acad. Sci. U. S. A. *83*, 8804–8807.

Richards, D.A., Guatimosim, C., and Betz, W.J. (2000). Two Endocytic Recycling Routes Selectively Fill Two Vesicle Pools in Frog Motor Nerve Terminals. Neuron *27*, 551–559.

Robinson, M.S. (2004). Adaptable adaptors for coated vesicles. Trends Cell Biol. *14*, 167–174.

Robinson, P., Etheridge, S., Song, L., Armenise, P., Jones, O.T., and Fitzgerald, E.M. (2010). Formation of N-type (Cav2.2) voltage-gated calcium channel membrane microdomains: Lipid raft association and clustering. Cell Calcium *48*, 183–194.

Robinson, P., Etheridge, S., Song, L., Shah, R., Fitzgerald, E.M., and Jones, O.T. (2011). Targeting of Voltage-Gated Calcium Channel α2δ-1 Subunit to Lipid Rafts Is Independent from a GPI-Anchoring Motif. PLoS ONE *6*, e19802.

Ruffieux-Daidié, D., Poirot, O., Boulkroun, S., Verrey, F., Kellenberger, S., and Staub, O. (2008). Deubiquitylation Regulates Activation and Proteolytic Cleavage of ENaC. J. Am. Soc. Nephrol. JASN *19*, 2170–2180.

Saegusa, H., Kurihara, T., Zong, S., Kazuno, A., Matsuda, Y., Nonaka, T., Han, W., Toriyama, H., and Tanabe, T. (2001). Suppression of inflammatory and neuropathic pain symptoms in mice lacking the N-type Ca2+ channel. EMBO J. *20*, 2349–2356.

Sakurai, T., Hell, J.W., Woppmann, A., Miljanich, G.P., and Catterall, W.A. (1995). Immunochemical Identification and Differential Phosphorylation of

Alternatively Spliced Forms of the α1A Subunit of Brain Calcium Channels. J. Biol. Chem. *270*, 21234–21242.

Salvaterra, P.M., and Mahler, H.R. (1976). Nicotinic acetylcholine receptor from rat brain. Solubilization, partial purification, and characterization. J. Biol. Chem. *251*, 6327–6334.

Sandoz, G., Bichet, D., Cornet, V., Mori, Y., Felix, R., and De Waard, M. (2001). Distinct properties and differential β subunit regulation of two C-terminal isoforms of the P/Q-type Ca2+-channel α1A subunit. Eur. J. Neurosci. *14*, 987–997.

Scott, R.H., and Dolphin, A.C. (1987). Activation of a G protein promotes agonist responses to calcium channel ligands. Nature *330*, 760–762.

Scott, V.E.S., Felix, R., Arikkath, J., and Campbell, K.P. (1998). Evidence for a 95 kDa Short Form of the α1A Subunit Associated with the ω-Conotoxin MVIIC Receptor of the P/Q-type Ca2+ Channels. J. Neurosci. *18*, 641–647.

Sekine-Aizawa, Y., and Huganir, R.L. (2004). Imaging of receptor trafficking by using α-bungarotoxin-binding-site-tagged receptors. Proc. Natl. Acad. Sci. U. S. A. *101*, 17114–17119.

Snider, W.D., and McMahon, S.B. (1998). Tackling Pain at the Source: New Ideas about Nociceptors. Neuron *20*, 629–632.

Söllner, T., Whiteheart, S.W., Brunner, M., Erdjument-Bromage, H., Geromanos, S., Tempst, P., and Rothman, J.E. (1993). SNAP receptors implicated in vesicle targeting and fusion. Nature *362*, 318–324.

Sørensen, J.B., Fernández-Chacón, R., Südhof, T.C., and Neher, E. (2003). Examining Synaptotagmin 1 Function in Dense Core Vesicle Exocytosis under Direct Control of Ca2+. J. Gen. Physiol. *122*, 265–276.

Splawski, I., Timothy, K.W., Sharpe, L.M., Decher, N., Kumar, P., Bloise, R., Napolitano, C., Schwartz, P.J., Joseph, R.M., Condouris, K., et al. (2004). CaV1.2 Calcium Channel Dysfunction Causes a Multisystem Disorder Including Arrhythmia and Autism. Cell *119*, 19–31.

Stamnes, M.A., and Rothman, J.E. (1993). The binding of AP-1 clathrin adaptor particles to Golgi membranes requires ADP-ribosylation factor, a small GTP-binding protein. Cell *73*, 999–1005.

Stenmark, H. (2009). Rab GTPases as coordinators of vesicle traffic. Nat. Rev. Mol. Cell Biol. *10*, 513–525.

Südhof, T.C. (2012). The Presynaptic Active Zone. Neuron *75*, 11–25.

Südhof, T.C. (2013). Neurotransmitter Release: The Last Millisecond in the Life of a Synaptic Vesicle. Neuron *80*, 675–690.

Takahashi, M., Seagar, M.J., Jones, J.F., Reber, B.F., and Catterall, W.A. (1987). Subunit structure of dihydropyridine-sensitive calcium channels from skeletal muscle. Proc. Natl. Acad. Sci. U. S. A. *84*, 5478–5482.

Tarpey, P.S., Stevens, C., Teague, J., Edkins, S., O'Meara, S., Avis, T., Barthorpe, S., Buck, G., Butler, A., Cole, J., et al. (2006). Mutations in the Gene Encoding the Sigma 2 Subunit of the Adaptor Protein 1 Complex, AP1S2, Cause X-Linked Mental Retardation. Am. J. Hum. Genet. *79*, 1119–1124.

Tedford, H.W., and Zamponi, G.W. (2006). Direct G protein modulation of Cav2 calcium channels. Pharmacol. Rev. *58*, 837–862.

Tian, L., Hires, S.A., Mao, T., Huber, D., Chiappe, M.E., Chalasani, S.H., Petreanu, L., Akerboom, J., McKinney, S.A., Schreiter, E.R., et al. (2009). Imaging neural activity in worms, flies and mice with improved GCaMP calcium indicators. Nat. Methods *6*, 875–881.

Todd, A.J., Hughes, D.I., Polgár, E., Nagy, G.G., Mackie, M., Ottersen, O.P., and Maxwell, D.J. (2003). The expression of vesicular glutamate transporters VGLUT1 and VGLUT2 in neurochemically defined axonal populations in the rat spinal cord with emphasis on the dorsal horn. Eur. J. Neurosci. *17*, 13–27.

Tran-Van-Minh, A., and Dolphin, A.C. (2010). The α2δ Ligand Gabapentin Inhibits the Rab11-Dependent Recycling of the Calcium Channel Subunit α2δ-2. J. Neurosci. *30*, 12856–12867.

Tsuruta, K., Frey, E.A., Grewe, C.W., Cote, T.E., Eskay, R.L., and Kebabian, J.W. (1981). Evidence that LY-141865 specifically stimulates the D-2 dopamine receptor. Nature *292*, 463–465.

Tzartos, S.J., and Changeux, J.P. (1983). High affinity binding of alpha-bungarotoxin to the purified alpha-subunit and to its 27,000-dalton proteolytic peptide from Torpedo marmorata acetylcholine receptor. Requirement for sodium dodecyl sulfate. EMBO J. *2*, 381–387.

Van Petegem, F., Clark, K.A., Chatelain, F.C., and Minor, D.L., Jr (2004). Structure of a complex between a voltage-gated calcium channel beta-subunit and an alpha-subunit domain. Nature *429*, 671–675.

Vigues, S., Gastaldi, M., Massacrier, A., Cau, P., and Valmier, J. (2002). The α1A subunits of rat brain calcium channels are developmentally regulated by alternative RNA splicing. Neuroscience *113*, 509–517.

Waithe, D., Ferron, L., Page, K.M., Chaggar, K., and Dolphin, A.C. (2011). Beta-subunits promote the expression of CaV2.2 channels by reducing their proteasomal degradation. J. Biol. Chem. *286*, 9598–9611.

Wang, C.-W., Hamamoto, S., Orci, L., and Schekman, R. (2006). Exomer: a coat complex for transport of select membrane proteins from the trans-Golgi network to the plasma membrane in yeast. J. Cell Biol. *174*, 973–983.

Watanabe, S. (2015). Slow or fast? A tale of synaptic vesicle recycling. Science *350*, 46–47.

Watanabe, H., Yamashita, T., Saitoh, N., Kiyonaka, S., Iwamatsu, A., Campbell, K.P., Mori, Y., and Takahashi, T. (2010). Involvement of Ca2+ Channel Synprint Site in Synaptic Vesicle Endocytosis. J. Neurosci. *30*, 655–660.

Watanabe, S., Rost, B.R., Camacho-Pérez, M., Davis, M.W., Söhl-Kielczynski, B., Rosenmund, C., and Jorgensen, E.M. (2013). Ultrafast endocytosis at mouse hippocampal synapses. Nature *504*, 242–247.

Watanabe, S., Trimbuch, T., Camacho-Pérez, M., Rost, B.R., Brokowski, B., Söhl-Kielczynski, B., Felies, A., Davis, M.W., Rosenmund, C., and Jorgensen, E.M. (2014). Clathrin regenerates synaptic vesicles from endosomes. Nature *515*, 228–233.

Wenningmann, I., and Dilger, J.P. (2001). The Kinetics of Inhibition of Nicotinic Acetylcholine Receptors by (+)-Tubocurarine and Pancuronium. Mol. Pharmacol. *60*, 790–796.

Wijetunge, S., Dolphin, A.C., and Hughes, A.D. (2002). Tyrosine kinases act directly on the alpha1 subunit to modulate Cav2.2 calcium channels. Biochem. Biophys. Res. Commun. *290*, 1246–1249.

Wilkins, M.E., Li, X., and Smart, T.G. (2008). Tracking Cell Surface GABAB Receptors Using an α-Bungarotoxin Tag. J. Biol. Chem. *283*, 34745–34752.

Williams, M.E., Brust, P.F., Feldman, D.H., Patthi, S., Simerson, S., Maroufi, A., McCue, A.F., Velicelebi, G., Ellis, S.B., and Harpold, M.M. (1992). Structure and functional expression of an omega-conotoxin-sensitive human N-type calcium channel. Science *257*, 389–395.

Xia, F., Leung, Y.M., Gaisano, G., Gao, X., Chen, Y., Manning Fox, J.E., Bhattacharjee, A., Wheeler, M.B., Gaisano, H.Y., and Tsushima, R.G. (2007). Targeting of Voltage-Gated K+ and Ca2+ Channels and Soluble N-Ethylmaleimide-Sensitive Factor Attachment Protein Receptor Proteins to Cholesterol-Rich Lipid Rafts in Pancreatic α-Cells: Effects on Glucagon Stimulus-Secretion Coupling. Endocrinology *148*, 2157–2167.

Zamponi, G.W., Bourinet, E., Nelson, D., Nargeot, J., and Snutch, T.P. (1997). Crosstalk between G proteins and protein kinase C mediated by the calcium channel α1 subunit. Nature *385*, 442–446.

Zhang, J., Ferguson, S.S.G., Barak, L.S., Ménard, L., and Caron, M.G. (1996). Dynamin and β-Arrestin Reveal Distinct Mechanisms for G Protein-coupled Receptor Internalization. J. Biol. Chem. *271*, 18302–18305.

Zhang, M., Chang, H., Zhang, Y., Yu, J., Wu, L., Ji, W., Chen, J., Liu, B., Lu, J., Liu, Y., et al. (2012). Rational design of true monomeric and bright photoactivatable fluorescent proteins. Nat. Methods *9*, 727–729.

Zhang, Y., Helm, J.S., Senatore, A., Spafford, J.D., Kaczmarek, L.K., and Jonas, E.A. (2008). PKC-Induced Intracellular Trafficking of CaV2 Precedes Its Rapid Recruitment to the Plasma Membrane. J. Neurosci. *28*, 2601–2612.

Zhu, Y., Traub, L.M., and Kornfeld, S. (1998). ADP-Ribosylation Factor 1 Transiently Activates High-Affinity Adaptor Protein Complex AP-1 Binding Sites On Golgi Membranes. Mol. Biol. Cell *9,* 1323–1337.

Zhuchenko, O., Bailey, J., Bonnen, P., Ashizawa, T., Stockton, D.W., Amos, C., Dobyns, W.B., Subramony, S.H., Zoghbi, H.Y., and Lee, C.C. (1997). Autosomal dominant cerebellar ataxia (SCA6) associated with small polyglutamine expansions in the α1A-voltage-dependent calcium channel. Nat. Genet. *15*, 62–69.